ENERGY LABORATORY

MASSACHUSETTS INSTITUTE
OF TECHNOLOGY

GROUND-LEVEL OZONE IN EASTERN NORTH AMERICA: ITS FORMATION AND TRANSPORT

by
Stephen G. Zemba,
Jay A. Fay
and
Daniel S. Golomb

Energy Laboratory Report No. MIT-EL 90-002
October 1990

GROUND-LEVEL OZONE IN EASTERN NORTH AMERICA: ITS FORMATION AND TRANSPORT

by
Stephen G. Zemba,
Jay A. Fay
and
Daniel S. Golomb

Final Report For the Project Entitled "Long Range Oxidant Model"

Prepared for

Consolidated Edison Company of New York
and
New England Power Service Company

Energy Laboratory Report No. MIT-EL 90-002
October 1990

FOREWORD

The research project entitled "Long Range Oxidant Model" was an outgrowth of earlier MIT research on "Acid Rain Modeling and Source Apportionment," and it was carried out under the supervision of Professor James A. Fay and Dr. Daniel Golomb. The principal author of this Final Report, Stephen G. Zemba, submitted a dissertation entitled "A Seasonally Averaged Model of Boundary Layer Ozone for Eastern North America" in partial fulfillment of the requirement for a Ph.D. degree. His dissertation has been used unchanged as the body of this report, but the Appendices (which add more than 50% to the volume of the report) have been omitted. While the report makes frequent references to these Appendices, they are not essential for comprehension of the text. The reader requiring access to these Appendices is referred to the MIT Library Microreproduction Laboratory*, whence a hard copy or microfiche version of the entire dissertation may be purchased.

An Executive Summary, prepared by Drs. Daniel Golomb and Derek Teare, with the assistance of Ms. Nancy Stauffer, has been added as part of the conversion of the dissertation into a project Final Report.

---

* Order Department, MIT Library Microreproduction Laboratory, Building 14-0551, Cambridge, MA 02139. Telephone number: (617) 253-5668.

Table of Contents

Chapter 1 Introduction

GROUND-LEVEL OZONE IN EASTERN NORTH AMERICA: ITS FORMATION AND TRANSPORT

Abstract

Ozone (O_3), a natural component of the troposphere, is augmented by photochemical processes involving manmade emissions of nitrogen oxides (NO_x) and volatile organic compounds (VOCs). Sufficiently high concentrations of ozone are detrimental to the respiratory system. Ozone exposure also reduces crop yields and damages forests. This study attempts to explain the underlying factors which contribute to observed ozone levels.

Long range transport models of three species - NO_x, VOCs and ozone - are developed for eastern North America. The seasonally averaged models include the essential physical and chemical processes in a relatively simple framework. NO_x and VOCs are treated as primary species, i.e., they are modeled from their introduction into the atmosphere to their point of removal. Detailed emission inventories serve as input to the precursor models. Ozone is considered a secondary species because it is not directly emitted. Rather, its production is assumed to be a function of ambient NO_x and VOCs levels.

Measured concentrations, available for NO_2 and ozone, are compared with model predictions and aid in determining adjustable model parameters. Predicted NO_x concentrations are consistent with rural observations but underestimate sites influenced by nearby sources at which the long range assumptions break down. Local models which properly treat proximate sources account for the discrepancy. The VOCs model, having no measurements for verification, adopts parameters consistent with the NO_x model and known chemical properties. Both biogenic and manmade emissions contribute to ambient VOCs levels. Biogenic emissions are found to be more important over most of ENA; anthropogenic sources of VOCs are dominant only in urban areas.

Consistent with empirical patterns, the ozone model predicts small regional gradients and hence a limited dependence on NO_x and VOCs precursors. The natural background component is determined to be two-thirds of average ozone levels. Regional transport is significant; ozone lifetimes are estimated to be of the order of a day. The high background level and insensitivity to precursors suggests that significant reductions of average ozone concentrations will be difficult to achieve.

GROUND-LEVEL OZONE IN EASTERN NORTH AMERICA: ITS FORMATION AND TRANSPORT

Executive Summary

Ground-level ozone poses a risk to human health and to the ecology. On many summer afternoons, peak ozone concentrations are high enough to threaten the respiratory systems of humans. Persistently high average concentrations over the growing season are deleterious to crops and forests, and published estimates of the value of crop losses in the United States resulting from long-term exposure to ozone are in the range $2-3 billion per year.

Ground-level ozone is formed by solar-driven reactions in the atmosphere between two precursors: nitrogen oxides (NO_x), which are emitted from fossil fuel combustion, and volatile organic compounds (VOCs), which are produced by industrial and transportation activities, and by natural sources such as trees and vegetation. Computer models are frequently used to predict the reductions of precursor emissions that would be required to bring peak ozone concentrations down to acceptable levels. The "traditional" ozone models try to predict the build-up of summertime peaks by simulating all the ozone-related chemical reactions that would occur within a few days and within a single city or other limited area. These models work reasonably well for estimating peak concentrations, but no validated model exists that predicts seasonal average concentrations of ozone over wide regions, such as eastern North America.

If more effective regional ozone-control strategies are to be devised, there is need for a better understanding of ozone formation and transport over long distances. Under the research project summarized in this report the objective was to develop a model that would be chemically simple but which could, given known precursor emissions, predict ozone concentrations that had actually been measured at various sites throughout eastern North America, averaged over a six-month period. The modeling discussed in this report draws heavily on previous experience - and success - in calculation of acid deposition, specifically the calculation of wet sulfate deposition from knowledge of SO_2 emissions, and of NO_3 precipitation from an assessment of anthropogenic nitrogen oxides production.

Thus the new ozone model considers a single layer of atmosphere with a constant height, seasonally averaged wind field and dispersion characteristics, and regionally averaged transformation and deposition rates. Emissions of NO_x and VOC including biogenic emissions are taken for 7000 emission cells, 40 x 40 km wide, as obtained from the National Acid Precipitation Assessment Program. Model parameters are optimized ("tuned") so as to obtain the best match with observed seasonally averaged NO_x, VOC and O_3 concentrations.

The modeled ozone concentrations are not very sensitive to the selected parameters of the model. Most important, as Figure S-1 demonstrates, there is a surprising lack of gradients in average ozone concentrations over eastern North America. The contour lines suggest a smooth variation over the entire region, and all levels are quite high.

The current standards for *peak* levels state that the daily maximum hourly concentration should not exceed 240 micrograms per cubic meter more than three times in three years. With average concentrations typically a fourth of that peak standard, it is not surprising that violations occur frequently, in rural as well as urban settings.

Two factors lead to the generally elevated average levels. First, any ozone present in the atmosphere can be carried long distances by the wind. Thus, urban-generated ozone readily spreads to rural areas. The precursors (especially the naturally produced VOCs) are similarly dispersed, so that production of ozone occurs not only near emissions sources but throughout the region, even over water. Thus, long-range transport of ozone and precursors is significant.

The second factor pushing up average levels is relatively high concentration of naturally occurring ("background") ozone. According to the model, as much as half of the average ozone measured at the ground consists of ozone that has either diffused down from the stratosphere or has formed in the troposphere (within about 15 km of the earth's surface) from naturally produced precursors. That estimate is consistent with the findings of investigators who measured the natural ozone "background" in remote regions, away from anthropogenic emission sources.

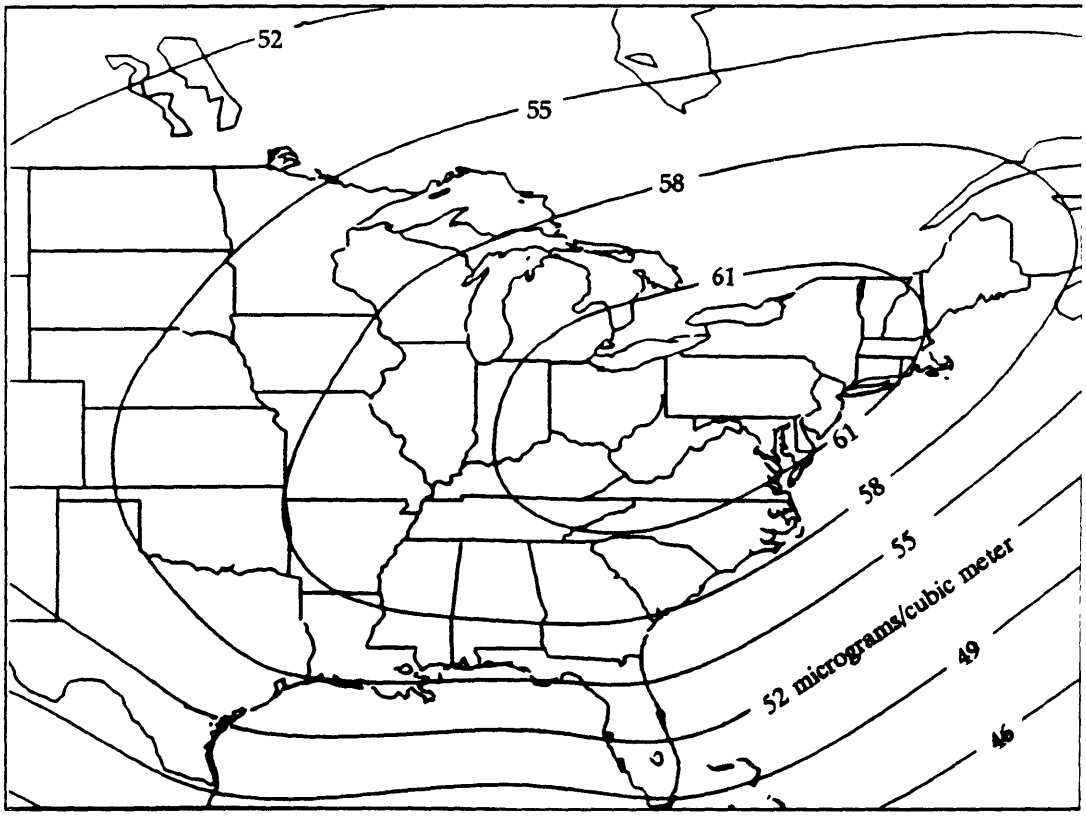

Figure S-1. Average ozone concentrations between April and September in eastern North America, as estimated by the model described in this report. Units are $\mu g/m^3$. 1 $\mu g/m^3$ is approximately equal to 0.5 parts per billion by volume (ppbv).

The implications of this finding for environmental policymaking are significant. A major fraction of the ozone at ground level will remain unaffected by changes of anthropogenic emissions. Also, the amount of ozone formed does not vary in direct proportion to the amount of precursor emissions. Thus, a reduction of precursor emission may not accomplish a proportionate reduction of seasonally and regionally averaged ozone concentrations. Finally, the data show that in some areas the naturally produced VOCs may be more abundant than the anthropogenic VOCs. In general, anthropogenic sources contribute about a fifth of the average VOC concentration, but in some urban areas that fraction may exceed a half. Those findings mean that control strategies aimed at reducing anthropogenic VOC concentrations may be effective only in or near urban areas.

Interesting results are obtained when the new model is used to calculate the reductions in precursor and ozone levels that can be expected from selected reductions in emissions. The analysis shows that halving anthropogenic NO_x emissions across eastern North America would also halve average NO_x levels in the atmosphere. But halving anthropogenic VOCs emissions would reduce average VOCs levels by only 10-20%. Reducing both NO_x and VOCs emissions by 50% would reduce seasonally averaged ozone by less than 10%.

For ozone the connection between concentration levels and the amounts of its precursors, NO_x and VOCs, is not as clearcut as was found for $SO_4^=$ and NO_3^- in precipitation. The connection is complicated by the fact that the intrusion of tropospheric ozone into the atmospheric boundary layer is about equally important as the production there of ozone from precursors emitted from ground level sources. Also, the photochemistry of ozone production is distinctly more complex than that of SO_2 or NO_x oxidation. Finally, emissions of VOCs from natural sources, in amounts that are not well documented, are comparable to anthropogenic emissions in aggregate amounts, and most likely are more important in rural regions. Taken together, these effects add greater uncertainty to the ozone modeling than was found for the MIT acid deposition model.

It must be emphasized that the new model is preliminary: in its present form, it contains too many uncertainties to be used in devising control strategies for achieving specific ozone standards. Reducing those uncertainties requires work on several fronts. First, given the potential importance of VOCs as an ozone precursor, the details of the VOCs-related chemical reactions must be better understood. Second, more VOCs monitors should be set up throughout the region, and more ozone monitors in rural areas. (Most ozone monitors are now in or near metropolitan areas.) A larger, more representative data base would contribute to better estimates of anthropogenic versus natural ozone, which would in turn help clarify the relationship between ground-level ozone and its precursors.

Chapter 1

Introduction

1.1 Importance and Effects of Ozone

Ozone is ubiquitous. This simple statement, borrowed from a now forgotten reference, reflects the fact that ozone (chemically, O_3) is a pervasive atmospheric constituent. Its presence in the stratosphere creates a shield which screens a large portion of the ultraviolet radiation from the sun, and there is presently concern over whether this layer is being depleted and what potential effects the change may have on human health and welfare.

This dissertation, however, is concerned with boundary layer ozone. Found in the lower troposphere, its abundance is approximately one-tenth as large as in the stratospheric layer [1]. Unlike other pollutants such as oxides of sulfur and nitrogen, ozone is not directly emitted into the atmosphere. Rather, it is produced photochemically and is an important oxidant in atmospheric chemistry. The amount present is influenced by many factors, including insolation, intrusion from the stratosphere, synoptic weather conditions, atmospheric composition, and the concentrations and emissions of its chemical precursors. The most important precursors are oxides of nitrogen (NO_x) and volatile organic compounds (VOCs). It is worthy to note that ozone is a component of an unpolluted atmosphere as there exist natural sources of its precursors. However, anthropogenic precursor emissions serve to create ozone in excess of natural background levels. Manmade NO_x sources, generated as a byproduct of combustion processes, far exceed natural sources in the United States. VOCs have significant manmade and biogenic sources. A significant portion of the fast reacting species (believed to be the most important to ozone production) are thought to originate from natural sources such as forests.

Boundary layer ozone affects the environment and humankind in various ways. Long term exposures to excessively high concentrations of one part per million cause irreversible damage to the pulmonary function of test animals [2]. Effects on human health continue to be extensively investigated. Documented consequences of acute ozone exposure include coughing, shortness of breath, and irritation to the respiratory tract. Symptoms are strongest for individuals engaged in strenuous exercise and are exhibited at concentration levels as low as 180 parts per billion (ppb) [3]. Once believed to be most dangerous to groups such as the elderly and asthmatics, ozone is now thought to be detrimental to all categories of people, although there are general differences in the manner of affectation [3,4]. Other aspects of health effects require more research, however. Unresolved is the importance of integrated dose (as compared with acute exposure to elevated concentrations). Potential chronic effects are just beginning to be investigated. Continuous exposure is hypothesized to decrease resistance to infection and also to structually alter the gas exchange region of the lungs [3].

Ozone also affects plant vegetation. Numerous studies have shown that ozone exposure reduces crop yield. The National Crop Loss Assessment Network (NCLAN) centrally stores data from crop loss experiments due to pollution exposure [5]. Collective results are being used in an effort to quantify the relationship between ozone and plant growth. No single quantitative measure has been identified as significant for all crops, but there is growing evidence that for individual species either peak concentrations or integrated doses can be the important variable [6,7]. Typical annual reductions in crop yield caused by ozone are estimated to be 0-20% [8]. Adams and Crocker estimate the cost of these losses to be $2-3 billion per year [9]. Additionally, ozone is thought to damage forests. The difficulty in isolating its effects from other environmental factors has complicated research efforts to quantify ozone devastation. A recent study examining Jeffrey Pine trees has correlated visible ozone injury with a reduction in growth. Control and test areas were distinguished by measured regional ozone exposure [10]. Another investigation supports a positive relationship between ozone exposure and susceptibility to frost.

Because of its hazard to human health ozone is regulated by the United States Environmental Protection Agency (EPA) as a criteria pollutant. The primary standard for ozone is currently 120 parts per billion (ppb); a violation occurs if the daily maximum hourly concentration exceeds the standard more than once in a year. A secondary standard geared toward improving crop and forest conditions is in the early stage of discussion.

EPA's implementation of the Clean Air Act divides the United States into air quality regions which roughly follow the boundaries of major metropolitan areas. The states developed EPA approved State Implementation Plans (SIPs) designed to reduce ozone precursor levels to the degree necessary to meet the standard in each nonattainment region by the end of 1987. Unfortunately, more than 60 metropolitan areas failed to meet the primary standard [11], and the situation worsened in the unusually hot summer of 1988.

The failure to reduce ozone levels presents EPA with a puzzling dilemma. Since SIPs were constructed with state of the art knowledge and modeling techniques their ineffectiveness raises serious concerns. The regulatory approach in urban areas has emphasized control of anthropogenic VOCs. Ozone insensitivity to significant decreases in estimated VOC emissions has spurred doubts as to the appropriateness of EPA control strategies [12].

Is our knowledge of atmospheric processes inadequate? Are atmospheric chemistry and pollutant dispersion too complex to understand? Have the prescribed control plans been correctly applied and monitored? Are we undertaking sufficient and properly directed research? Must we resign and accept the present ozone problem simply as one of the consequences of our urbanized society?

It is probably somewhat premature to adopt the latter approach of desperation. Ozone research is a young field and a great deal has been learned in a relatively short period of time. Control efforts have had some success, most notably in southern California, where mobile source controls of precursors have achieved significant reductions in ozone levels. However, exceedances are still frequent. Is it possible to meet the ozone standard? The simple but probably impractical answer is yes, as elimination of all anthropogenic emissions would revert environmental concentrations to background values, which, at an annual average of 20-40 ppb, are within the EPA standard. The fact that the standard, at 120 ppb, is only several times greater than the background suggests that significant measures will need to be taken to ensure compliance. The ultimate question, which incorporates socioeconomic as well as scientific issues, is "To what degree, considering all costs and issues involved, are we willing to change the way we interact with the environment to achieve healthful air quality?". Further research, appropriately applied, will do more to aid in addressing this question.

1.2 Basic Atmospheric Chemistry and Modeling

The state of the art knowledge of atmospheric chemistry is developed to the degree where the major processes responsible for ozone production are well established. Smog chamber experiments, in which a known mixture of gases is irradiated and the time-evolving constituents measured, has been the principal tool used to infer reaction pathways. Since most of the trials simulated highly polluted conditions, the processes governing moderately and slightly polluted atmospheres may not be as well understood. Much contemporary research is being devoted to the study of the fast reacting, short lived radical species which govern oxidation rates. A second area of concentrated effort is the effort to unravel the complex oxidation sequences of organic compounds.

Although atmospheric chemistry is complicated, the basics of ozone production are straightforward. Nitrogen dioxide (NO_2) is photolyzed to produce nitrous oxide (NO) and an excited oxygen atom; the latter usually combines with diatomic oxygen to produce an ozone molecule. The overall reaction can be written:

$$NO_2 + O_2 + h\nu \rightarrow NO + O_3 \tag{1.1}$$

Once created, the products may simply recombine in the reverse reaction.

$$NO + O_3 \rightarrow NO_2 + O_2 \tag{1.2}$$

The combination of eqns. (1.1) and (1.2) generally produces no net ozone over a diurnal period. There can be temporal variation, however, as the photolysis rate depends on the hour of the day and the recombination is not instantaneous. Normally, however, the cessation of reaction (1.1) after sunset permits sufficient time during the nocturnal period for all of the photolyzed NO_2 to regenerate via eqn. (1.2) and O_3 will return to its initial value by sunrise.

Net ozone production occurs because a pathway exists which competes with eqn. (1.2) for the NO molecule and converts it to NO_2 without consuming the newly formed O_3 molecule. The oxidation is accomplished by a peroxyl radical (which can either be hydroperoxyl (HO_2) or an organic peroxyl (RO_2).

$$RO_2 + NO \rightarrow RO + NO_2 \tag{1.3}$$

The amount of ozone produced by this simple mechanism depends on the rates of reaction and the concentrations of the the reactants. Typical polluted atmospheric compositions are such that both pathways in eqns. (1.2) and (1.3) are significant recyclers of NO. Assuming that some fraction of the peroxyls are of organic origin, it can be seen that both precursors, NO_x and VOCs, are important to produce net ozone. Although complete atmospheric chemistry involves many more reactions, eqns. (1.1)-(1.3) are the essential mechanism through which ozone is produced in the troposphere [1].

Once produced, ozone becomes an important oxidant in the atmosphere. It can react with NO_2 to form a nitrate radical. More importantly, ozone itself can be photolyzed to generate an excited oxygen atom. About 1% of the excited oxygen reacts with water molecules to form a pair of hydroxyl radicals. The latter are important oxidizing agents in many atmospheric processes [1]. The rate of ozone destruction by these two pathways is rather slow; net ozone, once generated via eqns. (1.1)-(1.3), can have chemical lifetimes of several days in the summer, and several months in the winter (when photolysis is reduced). Adding surface deposition as another sink, the summer lifetime of ozone in the troposphere is thought to be about two days. [13]

Various models to predict ozone concentrations are either available or in the process of development. In general, models have become more sophisticated with the increased understanding of ozone generation and dispersion. Most models are "episodic"; they are designed to make predictions over periods of several days during which ozone concentrations are elevated to high levels. These events are usually associated with the movement of high pressure weather systems [14]. The goal of episodic modeling is to simulate conditions which lead to buildup of ozone during which standards are frequently exceeded. Early efforts, such as the original EKMA model, are based almost principally on chemical mechanisms as they are designed to reproduce smog chamber measurements [15]. Gradually, improvements have evolved in two general areas. First, the chemical mechanisms have become more detailed and accurate as they incorporate discoveries in atmospheric chemistry. Second, the regional dependence of ozone and its precursors has been identified, and the importance of convective and dispersive processes requires the tracking of each species in both time and space.

Ozone models differ in spatial and temporal resolution, number of vertical layers, extent and refinement of the modeling domain, and sophistication and composition of their chemical mechanisms. Typical regional models employ grid cells tens of kilometers on a side and embody a few hundred reactions. Given this complexity, the computational demands of some models stress the most powerful computers, thereby limiting the number of scenarios that can be investigated. An even greater constraint on episodic models is the amount of input they require; typically needed are are temporally resolved wind fields, emission estimates (both anthropogenic and biogenic) of relevant chemical species, and initial species concentrations. Assemblage of these can be a monumental task!

The results of a limited number of model simulations have been published. Perhaps the most extensive example of an applied episodic model is that of M. Liu et al. [16] who used a mesoscale photochemical model named RTM-III to simulate an eight day pollution period which occured in July 1978. Chemistry is modeled via the carbon bond mechanism developed for enhanced versions of the EKMA model. Numerical grid cells of 80 x 80 km covered an area 2080 x 1840 km over the northeastern United States. They achieved good correlation with measurements of ozone made at nine rural locations. Residuals were typically 25-50% of observed values, indicative of a fair amount of scatter. However, predictions of NO and NO_2 showed no correlation with measured values, and residuals were of the same magnitude as the measurements.

The combination of good agreement with ozone but less than satisfactory agreement with NO_x is puzzling as NO_x is a fundamental precursor of ozone. One explanation is that chemical mechanism of Liu et al. is relatively insensitive to NO_x and the successful ozone correlation is a consequence of other factors. A second possible explanation is that Liu et al. were successful in predicting the average daily spatial pattern of NO_x (notwithstanding absolute levels or hourly temporal evolution). Accurate ozone prediction, an integrated product of NO_2 photolysis, could have been the result of a sufficiently compensating dissociation rate. A third potential source of error is uncertain NO_x observations. NO_2 and NO are difficult to measure at the low levels typical at remote locations.

The emphasis of EPA efforts has shifted from a city-specific EKMA approach to regional modeling of urban airsheds. The Regional Oxidant Model, currently under development, is a comprehensive time-dependent Eulerian model. Numerical grid resolution is $\frac{1}{4}^\circ$ longitude by $\frac{1}{6}^\circ$ latitude within the $3\frac{1}{2}$ layer model. Separate processors handle inputs of air quality, meteorology, emissions, cloud cover, land use, initial and boundary conditions, and topography. The meteorological module interpolates nondeterministic wind fields from irregularly spaced measurements. A stochastic approach is employed in which multiple flow field realizations are analyzed. The chemical mechanism calculates concentrations at thirty minute intervals for each individual realization and the results are ultimately combined to provide probability distributions of each species in space and time. The overall algorithm is intended to simulate events lasting several days [17].

1.3 Approach and Aims of this Dissertation

A perfect representation of reality is virtually impossible to achieve. In general models should incorporate the essential physics and chemistry of the problem. Further refinement can approximate the physical world better and better, but there is a point of diminishing returns where the extension of the model places too large a burden on its capacity to be solved. Episodic models are a very useful scientific tool as they are our best representation of the atmosphere. Often, their failures indicate critical areas which need further research. Much has been and will continue to be learned from episodic models. However, their complexity does limit the number of times they can be applied. It is most unlikely that these models will be able to simulate periods as long as several months duration. Thus, they are limited in the amount of information they can provide. Careful planning is essential if episodic models are to be used efficiently.

Ozone models will likely be the central tool used to devise future control strategies. The critical need, from the perspective of the EPA, is to reduce peak ozone levels to meet the ambient standard in areas of noncompliance. There may be additional considerations in the future; a secondary standard could be implemented to limit total ozone exposure to crops and forests. Models will have to predict the effects of future emission scenarios so that regulatory decisions can be promulgated. It is likely that these decisions will be based on only a limited number of studies if computationally restrictive episodic models are used. Thus, there is a danger that complex episodic models may not be able to provide sufficient information for decisionmakers.

This thesis proposes the alternate viewpoint that a much simpler model can yield important information about regional ozone. The working hypothesis is that seasonally averaged pollutant concentrations can be modeled considering only the essential and basic atmospheric processes. Fay et al. [18,19] successfully applied this approach to model the wet deposition of sulfate and nitrate in eastern North America. Their model of primary and secondary species concentrations is based on an analytical solution of coupled advection- diffusion equations whose source (sink) term contains linear parameterizations of chemical transformation and deposition, both wet and dry. Inputs to the model are a set of nine physicochemical parameters and a limited number of emission sources of the primary species; output permits the estimation of concentrations at an arbitrary receptor field. Applications to wet sulfate and nitrate depositions produced annual and seasonal models which predict observations to within 20%. The linear model permits the calculation of source-receptor transfer coefficients thereby facilitating the investigation of a multitude of future emission scenarios. The chief advantage of the Fay et al. models is their simplicity; they incorporate the key processes which influence the pollutant from its origin to its deposition while consuming very limited computational resources.

This study extends the simplified modeling approach to ozone. There are two major factors which distinguish ozone modeling from sulfate and nitrate deposition modeling. First, ozone is an ambient airborne pollutant, not an ionic component of rainwater. Although this doesn't affect the form of the transport terms, it does shift the modeling emphasis from rainwater scavenging to the analysis of airborne concentrations. Second, its chemical origination is quite different. Sulfate and nitrate have direct anthropogenic sources which are oxidized by the atmosphere. Ozone, however, lacks a direct source. Its production depends on many factors, though the key chemical precursors are NO_x and VOCs. The ozone production function is not amenable to the linear hypothesis and thus the analytical solution of Fay et al. is inapplicable.

A gridded numerical approach is employed in this thesis to allow an arbitrary nonlinear source function for ozone. Another advantage of a numerical approach is the ability to vary the model parameters spatially within the modeling domain. Although this option is not explored in this work it may be useful in future endeavours. The production of ozone is assumed to be proportional to a function of NO_x and VOCs concentrations. Other effects, such as insolation, average temperature, etc., are taken to be of secondary importance and are assumed spatially constant. The ozone model necessitates that ambient VOCs and NO_x levels be known throughout the computational region. As a "precursor" to ozone, VOCs and NO_x models are developed. These species each have direct emissions. Although the analytical solution technique is viable for these precursors, a numerical approach is adopted for these species to conform with gridded emission inventories and subsequent ozone analyses. Thus, the complete ozone model consists of three numerical solutions; one for each of the two precursors, NO_x and VOCs, and the third for ozone which uses the output of the two precursor solutions.

The seasonally averaged approach of Fay et al. is maintained for ozone. The model predicts average levels of ozone throughout eastern North America. Ozone has both a significant "background" (produced from natural precursors and intrusion from the stratosphere) and a strong diurnal pattern. The modeled seasonal averages must be carefully interpreted in lieu of these effects. The relationship between average and peak values is of importance because of the regulatory constraints placed on ozone exceedances. Empirical data is analyzed to investigate the validity of using averaged concentrations as a surrogate for peak values.

The model results are compared to measured ozone and NO_2 values (averaged seasonal VOC measurements could not be found). The parameters governing the model are chosen to provide the most satisfactory agreement with observed values. The range of possible values for each parameter is constrained by reasonable physical limits as deduced from the literature.

Ozone and NO_2 are monitored at several hundred stations across the eastern United States. Because monitors are frequently situated such that they measure the highest ambient concentrations within a region, most of the stations are located in urban areas near significant sources of ozone precursors. As a result, these sites are not evenly distributed throughout the region. The models developed predict regional concentrations for all of eastern North America, a significant portion of which is inadequately monitored. Ambient measurements need to be prudently analyzed in developing representative regional models.

The initial part of the second chapter presents and discusses the NO_x and VOCs emission inventories utilized as input to the modeling studies of their respective species. The larger portion of this chapter is devoted to the presentation and analysis of ozone and NO_2 measurements. Significant knowledge may be garnished solely from the observations. Regional patterns, if apparent, can be helpful in model formulation. As both the NO_x and ozone models are tuned by comparison with observations these data are vital to this dissertation. Especially important to ozone are the interelationships between average, peak, and other temporally defined variables. There exists a number of monitors where ozone and NO_2 are simultaneously measured; these can be used to search for an empirical relationship between the two species.

The third chapter describes in detail the numerical methodology used by this work. Presented are the model equations and the techniques by which they are solved. The fourth chapter applies the methodology to develop models of the precursors NO_x and VOCs. The fifth chapter, and core of this dissertation, describes the development of a regional ozone model to predict seasonally averaged ozone levels in eastern North America. The sixth and final chapter discusses and summarizes this work.

Chapter 2

Emissions and Measurements

This chapter describes two important databases utilized by this thesis - emission inventories and ambient measured concentrations. Emissions are used as the source input to the transport models of NO_x and VOCs. Measurements of ozone and NO_x are used for comparison with model results and, in an iterative manner, to determine some of the empirical constants embodied by the models.

The value of emission and measurement data is not limited to model development. They are an autonomous source of information which can illuminate basic patterns of pollutant distribution. The combination of emissions and measurements can be used to infer atmospheric processes such as dispersion, transport, creation and removal. Their importance warrants the detailed treatment they receive in this chapter.

2.1 Emission Inventories

Emission inventories attempt to identify the spatial (and possibly temporal) distribution of sources which release pollutants into the atmosphere. Generally, emitters are categorized as either point or area sources. A point source is a fixed location emitter; most inventories maintain a threshold size criterion for inclusion in this category. Area sources are the sum of all other emissions within a given geographic region. This includes small point sources, mobile sources such as automobiles, and emissions which occur over large regions such as a field or forest.

Comprehensive emission inventories are necessary to quantitatively understand the underlying causes of pollution. Construction of a regional inventory is not a trivial matter. Uncertainties are inherent in identifying all sources (completeness) and in the calculation of actual emissions, which for combustion sources are usually based on estimations of fuel usage and emission factors (the rate of emission per unit fuel consumed). Several detailed emission inventories have been or are being developed for the United States and Canada. During the course of this work two were available for use. The first is constructed by the Department of Energy (DOE) [20]; the second by the National Acid Precipitation Assessment Program (NAPAP) [21]. Both are annual estimates for the 1980 calendar year. Recently two other inventories have been released. The Electric Power Research Institute (EPRI) has constructed a 1982 inventory [22]; NAPAP, a 1985 inventory. Unfortunately, these latter two inventories were released too late to be included as part of this work. As the more recent inventories are purportedly of higher quality, they may provide fruitful opportunities for extension of this modeling study.

The versions of the DOE and NAPAP inventories received on magnetic tape cover anthropogenic emissions in the United States. As shown in Table 2.1, the DOE inventory is somewhat coarser and contains a significantly smaller number of distinguished point sources. Aggregate totals are presented for both VOCs and NO_2, the latter including NO emissions (reported as NO_2. Total NO_2 emissions are comparable for the two inventories, with the NAPAP total being 7% greater than the DOE sum. Spatial distributions of NO_2 are similar, with the densest emission regions centered about major metropolitan areas. Patterns of VOCs emissions also exhibit urban clustering in both inventories. The geographic similarity of NO_2 and VOCs emissions is not merely coincidence; it reflects the fact that the two pollutants share common sources. There is, however, a significant difference in aggregate VOCs emissions between the two inventories. The summed NAPAP inventory is more than a factor of three higher than the DOE total (Table 2.1). This is a consequence of DOE inventory failing to include all sources of anthropogenic VOCs.

The NAPAP inventory is chosen for use in the precursor modeling studies in the fourth chapter because of its finer detail and more complete VOCs estimates. Table 2.2 provides a more detailed summary of the NAPAP inventory. Area sources comprise the majority of both anthropogenic NO_2 and VOCs. A secondary breakdown by source category distinguishes mobile and stationary sources. The former result from transportation activities and the latter includes utility and industrial emissions. Both categories are significant sources of VOCs and NO_2. This poses serious implications for designing control strategies to curb ozone precursors, which will be discussed in more detail in the conluding chapter.

Although a component of the complete NAPAP emission inventory, the majority of Canadian NO_x and VOCs emissions are obtained separately from Environment Canada [23]. (Emissions of three provinces - Alberta. British Columbia and Saskatchewan - are taken from NAPAP [1]). Table 2.3 presents the distribution of stationary and mobile source totals for each province. Aggregate Canadian emission estimates are much smaller than their U.S. counterparts. Only provincial totals are available for area sources. They are subsequently allocated to a number of individual subsources of size one degree latitude by one degree longitude for use in modeling NO_x and VOCs. The share of the total area source distributed to each subsource is based roughly on the population density of the province.

Emission density maps of the combined NAPAP and Canadian anthropogenic NO_2 and VOCs inventories are shown in Figs. 2.1 and 2.2. Each figure presents two projections which correspond to the numerical domains used in modeling. Units for the plots are kg $km^{-2}s^{-1}$. The upper plot aggregates emissions to cells roughly 160 km on a side, the lower plot to 40 km cells. (These also correspond to the numerical model discretization). The use of larger cells smoothes the emission field, reflected by the reduced scale of upper plots. Densities are generally higher in eastern North America. As discussed above, the geographic similarity of the two inventories is apparent, as well as the pattern of urban emission concentration. The contrast between urban and remote emission densities is somewhat stronger for NO_2.

Biogenic emissions of VOCs have been identified as a significant source. Lamb et al. [24] have developed a biogenic emission inventory for the continental United

States. They estimate the aggregate mass of biogenic VOCs to be 30.7 teragrams, significantly larger than the anthropogenic total (Table 2.1). Fig. 2.3 is a gridded map of biogenic VOC emission density in kg $km^{-2}s^{-1}$. Estimates of Canadian emissions are extrapolated from border values in the northern U.S., with emissions at the northernmost latitudes reduced to simulate decreased biogenic activity. Similarly, Mexican emission densities are extrapolated from border southwestern U.S. values. Comparing Figs. 2.2 and 2.3, regions of high biogenic and anthropogenic VOCs differ significantly. Biogenic VOCs are more regionally uniform, exhibiting smaller local intensification. Values in the southern U.S. are comparatively higher in the biogenic distribution. Both sources of VOCs are believed to contribute to ozone formation and are considered in the formulation of the VOCs model in chapter four.

2.2 Measurements

The initial goal of most models is to generate results which are in consonance with observed concentration patterns. Failure to achieve such agreement can challenge the legitimacy of a model. Measurements are thus a means of verifying the the model's consistency. Generally, the better a model matches observations, the more confidence can be attributed to its reliability in predicting future scenarios.

As the models developed in this thesis contain adjustable empirical constants, observations are used not only for comparison but also to determine some of the model parameters. Thus, measurements are of great importance to this work.

Because ozone and NO_2 are regulated by the EPA under the Clean Air Act, extensive efforts have been made to monitor their ground level concentrations. A nationwide network of hourly measurements is compiled and stored by the EPA in a centralized database at Research Triangle Park, North Carolina [25]. VOCs concentrations are not measured as they are not a criteria pollutant. Monitoring of this important ozone precursor is just beginning to gain momentum.

In addition to collecting and archiving the ambient air pollution database, the EPA publishes Air Quality Data Reports each year which summarize and compile measurements made throughout the United States. Frequency distributions provide a statistical profile of each criteria pollutant subject to regulation. A second section provides information about averages and peak values. The compiled data primarily addresses the question of whether or not federal air pollution limits have been exceeded. Thus, because the standard for NO_2 is prescribed as an annual average, all one-hour measurements are included in the statistical analysis, and the supplementary published data is in the form of a yearly average. The ozone standard, however, is based on a one-hour peak concentration; if the ambient concentration exceeds the permissible limit of 120 parts per billion at any hour during the day, an exceedance is incurred. Prior to 1982, statistical ozone summaries include all one-hour concentrations taken in the calendar year. Since then the amount of data incorporated in the summaries has been limited. A reporting period for ozone is defined individually for each station on the basis of when exceedances occur or are anticipated. A typical ozone season runs from April through October. Furthermore, the analysis has been revised to include only the single peak concentration from each day during the season. Distributions and averages of peak values are thought to provide information in better consonance with the form of the federal standard.

The regional models developed in this thesis are for average pollutant levels over a season extending from April through September. Initial work attempted to use the data from the published Air Quality Reports surrogately for seasonal averages. As this eventually proved less than satisfactory, raw data was twice obtained from the EPA in order to develop averages consistent with the modeling studies. The first installment provided quarterly summaries of NO_2 and ozone for the year 1980 [26]. This permitted construction of seasonal NO_2 concentrations. Ozone quarterly summaries, however, were based on averages of daily peak values, consistent with the post 1982 EPA reporting philosophy.

A second, more extensive excursion into the database was necessary to obtain the proper information to construct seasonally averaged ozone concentrations [27]. A further consideration arose as to the selection of the year for which raw one-hour measurements were obtained. The consistent approach would choose 1980 as it coincides with the base year of the emission inventory. Unfortunately, data was obtained for 1985 in anticipation of the release of the new NAPAP inventory which, because of delays, was not available in time for use in this work. This is not a serious problem, however, as emissions of ozone precursors are not believed to have varied greatly over the five year period. NAPAP estimates that aggregate anthropogenic NO_x emissions decreased 2% from 1980 to 1985 [1]. This difference is well within the uncertainties inherent in the inventories themselves.

It is conceivable, though, that differences may be significant in certain geographic regions. Given the compounding uncertainties of other aspects of this modeling, a detailed analysis of this effect is not worthwhile. Year to year variability in measurements is caused by interannual meteorological fluctuations. The optimal approach would be the construction of multi-year averages of measurements to provide robust estimates of typical conditions across the monitoring network. Such an effort is precluded, however, by the vast amount of data handling and analysis necessary to accomplish the task.

Thus a temporal composite of data is utilized in this work. Modeling results are compared to both 1980 and 1985 measurements averaged appropriately over the April to September season whenever possible. All presentations of data are clearly annotated. The philosophy adhered to by this work, however, is that the choice of year does not significantly bias comparison of model results and observations.

An additional caveat with regard to the monitoring network should be noted. Typically, measurements are made in or near heavily polluted urban areas where exceedances are anticipated. This presents two problems with regard to their use in model development. First, the urban bias compromises their regional representativeness. Second, they are often situated to measure fine scale differences over distances smaller than the numerical grid scale lengths used by the model. Thus, a given measurement may not even be locally representative in terms of a regional scale model. Monitoring stations are distinguished by land usage as either urban (city center), suburban, or rural. These classifications make no attempt to characterize nearby sources. Thus, a site designated as rural may be much closer to large pollution sources than is an urban monitor situated in a small town. Caution is necessary when interpreting ambient data and using it in model development.

2.2.1 Diurnal Patterns of NO_2 and Ozone

Ambient NO_2 and ozone concentrations follow characteristic diurnal cycles which are to a degree interdependent. Although this thesis models seasonally averaged quantities, the nature of the daily cycle has important implications. Generally, NO_x (the sum of NO_2 and NO) is emitted continuously in urban areas with temporal fluctuations such as "rush hour" peaks and late night lulls. NO_2 concentrations reflect local emissions but also depend on atmospheric chemistry and transport from outside the region. Photolytic activity depresses NO_2 concentrations during daylight hours while simultaneously raising ozone and NO levels. Both NO_2 and ozone are deposited at night in the stable boundary layer thereby reducing ground level concentrations with respect to values in the air column above. The onset of heating in the early morning hours remixes the boundary layer, increasing ground level concentrations simply through fumigation of more polluted air from aloft. Ozone concentrations contain a background component notwithstanding the amount produced by local photochemistry. Averaged ground level measurements incorporate all of these effects; they are not true averages over the boundary layer air column. Modeling in this work, described in detail in chapter three, assumes a constant height mixed layer. A key assumption of this thesis is that these ground level averages can be used as surrogates for boundary layer averages, implying that the relationship between the two is more or less similar over the monitoring network. A second assumption is that NO_2 is an appropriate surrogate for NO_x, implying network consistency in the ratios of NO_2 to NO. These assumptions are not directly confirmable due to a lack of the necessary data. However, comparison with model results in chapters four and five provides information as to their validity.

Figs. 2.4-2.9 are included as examples of the diurnal nature of NO_2 and ozone. The concentration units of each plot are parts per billion (ppb). Plotted in the lower portion of each figure are one-hour concentrations of 1985 data averaged over the April to September season. Vertical bars indicate the standard deviation of each one-hour average. The upper portion records the frequency with which the maximum daily concentration occurred within each hour. The plots are paired to present NO_2 and ozone concentrations concurrently at the same location. The three sites - one from each of the main classifications - are chosen randomly from the database. They are not selected as representative of their respective groups. Rather, they serve to emphasize the uniqueness associated with each monitoring location.

Figs. 2.4-2.5 are plots of observations at Denver, Colorado, a site classified as urban. NO_2 concentrations (Fig. 2.4) begin to rise in the morning hours, probably as a consequence of fumigation of the air above. Concentrations continue to build - most likely enhanced by local emissions - until a late morning peak. Levels fall during the afternoon as photolysis converts some of the NO_2 to NO. A second peak occurs in the late afternoon, possibly attributable to a surge in emissions and the recombination of ozone and NO. Levels generally fall during the night as NO_2 is deposited and converted to nitric acid. Dual peaks in the maximum distribution also suggest the importance of local emissions. The corresponding ozone plot (Fig.

2.5) also exhibits early morning deposition. The initial rise in concentration is probably due to fumigation, and levels continue to increase as photolysis produces ozone. An early afternoon peak is eroded as ozone is scavenged, possibly by fresh NO emissions as well as NO already present. The general decrease of ozone into the night probably results from recombination and by deposition to the ground. The rise at 0300 may be the result of nightime transport.

Figs. 2.6-2.7 show a similar pair of plots at a suburban monitor in Decatur, Georgia. The sharp rise in NO_2 (Fig. 2.6) in the morning hours probably results from fumigation and in situ emissions. Depressed daytime levels indicate photolytic effects. The greater relative magnitude of the depression compared to Fig. 2.4 may reflect a more continuous emission and scavenging mechanism at the Colorado site. The secondary peak in the late evening probably reflects the recombination of ozone and NO, and nightime decreases indicate deposition and nitric acid formation. Ozone concentrations (Fig. 2.7) suggest a high degree of photochemical production, and the peak value occurs later in the day than it does at the urban Colorado site. While the evening decline results partly from recombination, it cannot account for all of the decline; the ozone produced is probably being transported away from the site.

The final example, Figs. 2.8-2.9, show diurnal concentration at a rural monitor in Michigan. The NO_2 plot (Fig. 2.8) shows the effects of early morning fumigation and daytime photolysis. The nightime peaks are possibly the result of transport into the region. This is further supported by the frequency of daily peaks which occur at night. The ozone plot (Fig. 2.9) is flatter than for the urban and suburban sites, probably caused by lower photolytic production due to lower NO_2 levels. Nightime concentrations decrease steadily, indicative of deposition or scavenging.

Figs. 2.4-2.9 are both typical of and different from NO_2 and ozone profiles at other monitors. Generally, the consequences of daytime photolysis - enhanced ozone and depressed NO_2 - are seen at all sites. Each station is unique, however, as the factors that contribute to the diurnal cycle vary. Although a site is presented from each of the urban, suburban and rural categories, their concentration patterns cannot be called typical of the entire class. Urban monitors can be found that possess rural characteristics, rural sites can seem suburban in nature, etc. There is also no algorithm for discerning the characteristics of a monitoring station from its concentration profiles as increases or decreases can often be attributed to more than one cause. Although future data plots are usually separated into categories, they should not be construed to truly reflect the implied meanings of the classifications. The division of stations is simply a convenience to reduce the amount of data which appears in a single plot.

2.2.2 Seasonal and Night/Day Differences in NO_2 and Ozone

Both NO_2 and ozone exhibit seasonal and diurnal variability, but the differences are accentuated for the latter species. The effects are the result of photolytic activity which produces ozone in the daylight hours at the expense of dissociated NO_2 concentrations. The difference in daytime/nightime levels is greater during the summer months when photolytic activity is higher.

Figs. 2.10-2.13, in units of ppb, graphically illustrate these points. Selected from the 1985 EPA database are 122 NO_2 monitors (40 urban, 55 suburban, 23 rural and 4 unclassified) and 250 ozone sites (46 urban, 126 suburban, 63 rural and 15 unclassified) . All possess a 75% minimum coverage for half-day periods in both the summer and winter. Daytime is defined from 8:00 AM to 7:00 PM, nightime from 8:00 PM to 7:00 AM. The summer season is defined from April through September, the winter noncontiguously from October through March. Figs. 2.10 and 2.11 plot daytime vs nightime NO_2 concentrations. Generally, daytime levels are lower than nightime levels. The suppression is magnified during the summer season when photolysis is more prevalent. On average, levels of summer NO_2 are slightly lower than wintertime values, confirmed by average daily means of 18.8 and 20.3 ppb, respectively. Taken as a whole, NO_2 day and night concentrations corrlelate well, with correlation coefficients of 0.93 and 0.96 for the summer and winter plots. Rural measurements tend to lie at the lower end of the plot and suggest the possibility of a categorical distinction from the suburban and urban monitors.

Larger diurnal and seasonal effects are present for ozone. Figs. 2.12 and 2.13 show average summer levels of 31.5 ppb and average winter levels of 18.6 ppb. The diurnal trend is even more dramatic, with the difference between daytime and nightime levels being 20.4 ppb and 7.6 ppb, respectively, in the summer and winter seasons. The latter differences are significantly greater than those seen in NO_2 concentrations, suggestive of ozone production which exceeds the level of diurnal NO_2 variation. More scatter between day and night concentrations is evident for ozone, reflected by correlation coefficients of 0.52 for summer and 0.76 for winter. This scatter is probably a function of photolysis conditions which differ amongst individual monitors. Urban, suburban and rural monitors overlap extensively and make it difficult to identify any categorical distinctions.

2.2.3 Spatial Measurement Patterns

Monitoring sites are not evenly distributed throughout the United States. Urban clustering can place several monitors within the confines of a single grid cell, while the paucity of rural data leaves large areas barren of data. Comparison of a set of measurements with modeling results of a finite difference solution is biased and can potentially be misrepresentative of the true regional distribution. The scale length over which ambient concentrations vary is typically smaller than the size of grid cells used in model calculations. This fine scale variation is sensitive to local source distributions which, for practical considerations, must be integrally averaged over grid cells by regional modeling. Direct comparison of model results with a network of measurements incorporates two effects which influence scatter and uncertainty. Firstly, if several measurements occur within a single grid cell, a range of measured values, representing local scatter, is compared to a single modeled value. If the set of measurements is randomly distributed within a cell, their average may be appropriately used for model comparison. Secondly, sparsely sampled areas are inherently uncertain because a single value, subject to stochastic fine scale variation, is treated as being representative of the regional average. Thus, caution is necessary in interpreting model results with respect to the data from ambient measurement networks.

The regional distributions of NO_2 and ozone concentrations which follow are presented in two forms. The first are maps of the actual measurements. Clustering of monitors makes some of these maps difficult to read, but they importantly emphasize spatial sampling patterns and give a flavor for areawide trends and variation. Three techniques are employed to make the distributions more comprehensible. As discussed previously, the data are presented in three separate categories. The superposed numbers are kept small to further reduce crowding. Finally, each map is accompanied by an expanded center section to further elucidate the measurement pattern.

Still, portions of the figures are cluttered and spatial patterns difficult to discern. The second presentation of each data field averages proximate measurements to produce a simplified spatial distribution. All measurements are sorted to bins 4° longitude by 3° latitude and averaged to their centroidal coordinates. Contours are added to the smoothed maps to facilitate their interpretation. The reduced fields no longer represent measured data. Rather, they are a massaged dataset designed to identify large scale trends. Their construction is sensitive to bin size, the latter being judgmentally selected to produce lucid distributions which maintain the character of the original measurement pattern. The number of datapoints represented by each box average varies due to the irregularities of the original distribution. (Appendix I includes maps the number of points used to construct each average). Implications drawn from the averaged plots need to be cautiously considered. Nonetheless, they can be useful in highlighting large scale features which can be obscured by the irregular distribution of the original data. They also can be used to compare with model results in an effort to reduce the scatter present in the original data and to eliminate multiple observations within grid cells.

NO_2 Regional Distributions

Plots of ambient NO_2 concentrations averaged over April through September 1980 are shown in Figs. 2.14-2.17 for monitoring sites classified as urban, suburban, rural and other (unclassified). Units of the plot, as for all other regional distribution plots, are $\mu g\, m^{-3}$. The number of stations in each classification is 183, 192, 70 and 16, respectively. The data are calculated as the arithmetic mean of quarterly averages. The sites selected possess a minimum of 75% coverage of the available measurements for each quarterly period. Metropolitan clustering of sites is apparent from the location of the data. Even a number of the stations designated as rural are actually near groups of urban and suburban monitors, reflective of intentional siting practices which concentrate in areas of dense source emission to capture high pollutant levels. Proximate concentrations vary significantly making it difficult to identify regional patterns. Peripheral values in the northwest and southeast tend to be lower on average than central values. Rural measurements (Fig. 2.16) tend to be lower on average than other categories.

Fig. 2.18 is a smoothed map of the combined seasonal 1980 NO_2 data shown in Figs. 2.14-2.17. The condensation process reduces the number of datapoints from 461 to 40. Several local peaks are apparent, two of which occur around the Chicago and New York metropolitan areas. A third peak in eastern Tennessee is composed of only a few datapoints. A band of lower concentrations extends from Florida to the northwest, separating elevated regions in Texas and the northeast. (This same pattern is reflected by the emission density distribution shown in Fig 2.1). A scatter plot of each raw concentration compared with its corresponding averaged value is shown in Fig. 2.19. Symbols distinguish the four classes of monitors. The range of averaged values is about 70% of the range of the original concentrations. The correlation coefficient of the plot is 0.68, indicating a good relationship between the two variables. Some box averages are constructed over ranges in excess of 80 $\mu g\, m^{-3}$! Note that a pair of raw measurments exceed the federal NO_2 standard of 100 $\mu g\, m^{-3}$.

Several plots contained in Appendix I supplement the 1980 averaged NO_2 dataplots. The uneven distribution of points which comprise the box averages of Fig. 2.18 is demonstrated. Scatter plots similar to Fig. 2.19 but separated by class emphasize the lower values of NO_2 observed at rural sites.

A second series of plots is displayed for 1985 averaged NO_2 concentrations for the April to September season. Figs. 2.20-2.23 map the distribution of 44 urban, 65 suburban, 29 rural and 5 unclassified monitoring sites, respectively. The data are constructed from raw one-hour concentrations provided by the EPA and a 75% minimum data capture is used to screen stations. Note that the number of sites is smaller for each category than for the 1980 data; this occurs for two reasons. First, a portion of the 1980 monitors are 24-hour integrated measurements, and their counterparts are not part of the 1985 hourly data received. Second, the number of NO_2 monitors has declined as the ambient standard has generally been achieved throughout the region. There is some overlap between the 1980 and 1985 measuring sites but the two datasets are geographically unique. The distributions are similar to their 1980 counterparts, supporting the assertion that a difference between the 1980 and 1985 seasons is difficult to detect. The class of rural monitors once again appears to exhibit lower measured values than the other site groupings. (This observation is supported by additional Figs. in Appendix I).

A smoothed map of the combined 1985 NO_2 data is shown in Fig. 2.24. The condensed dataset eliminates 114 monitors through averaging, reducing the total number of points from 143 to 29. The contour pattern is similar to the 1980 plot (Fig. 2.18), highlighting a concentration trough between elevated regions in the southwestern and northeastern United States. The corresponding scatter plot of raw concentrations vs. box averaged values is shown in Fig. 2.25. Smoothing lessens the range of values from roughly 90 to 50 ppb. A correlation coefficient of 0.64 confirms a reasonable relationship between raw and averaged concentrations.

Ozone Regional Distributions

This section presents plots of 1985 ozone averaged over the April-September half-year. As for NO_2, a 75% coverage criterion is used to screen valid sites. Distributions of raw data are presented in Figs. 2.26-2.29, which map 76, 201, 116, and 28 averages at monitors from urban, suburban, rural and other site classifications. Visual examination of these plots suggests little difference between site categories. Variation between proximate observations is present, but its magnitude is not as great as in the NO_2 distributions. Significant geographic gradients are not apparent in the data netwroks.

This observation is reinforced by Fig. 2.30 which maps box averages of the combined 1985 ozone data. Ozone values are generally 50-70 $\mu g\,m^{-3}$ over most of the region, with a few local peaks and lows. Contours indicate a possible gradient in the southern U.S. caused mainly by lower Florida measurements. Fig. 2.31 plots the box averages against their corresponding raw values. Each box average is constructed over a fair range of raw ozone values, indicative of the local variation in measurements. The overall range of box averaged data is about 40 $\mu g\,m^{-3}$ compared with 70 $\mu g\,m^{-3}$ for the raw averages. The correlation coefficient of 0.60 reflects the general but scattered relationship between the two variables. A breakdown of Fig. 2.31 by class and state is included in Appendix I and serves to emphasize the apparent randomness of the dataset.

The failure of ozone to exhibit geographic differences is in itself significant. (The recent NAPAP interim summary notes a similar observation [1]). If Fig. 2.30 is an accurate portrayal of regional ozone, it implies a regional independence over most of the eastern United States. A quasi-uniform ozone distribution has further implications in regional modeling, discussed extensively in subsequent chapters.

Fig. 2.32 is a box average plot constructed on a finer scale ($\frac{10}{6}^{\circ} \times \frac{10}{4}^{\circ}$) than Fig. 2.30. The plot serves two purposes. First, it shows the effect of including fewer points in the box averages; regional scatter is greater and it is more difficult to deduce overall patterns. Basic contour patterns and levels are similar. The second purpose of this data is to provide a reasonably sized box average dataset for modeling applications in the fifth chapter. Supporting plots for Fig. 2.32 are contained in Appendix I.

Both Figs. 2.30 and 2.32 are constructed on scales larger than that used in the numerical modeling studies. Thus, averaging is performed over several grid cells. Appendix II addresses the issue of proximate receptors with respect to the numerical grid discretization.

There is a distinct possibility that the measurements in Figs. 2.26-2.29 are not regionally representative. Other researchers, asserting that remote sites reflect mixed air masses and are thus a better measure of regional ozone levels, have laboriously attempted to distinguish remote monitoring sites which are not affected by local sources [28,29]. Identification of truly remote sites is useful because they provide a measure of concentrations free from the effects of local anthropogenic sources. A subset of the monitors shown in Figs. 2.26-2.29 have been identified by Meyer [28] as sites unaffected by local sources. The nineteen sites which qualify are plotted in Fig. 2.33. The nonuniform distribution and sparseness of sites precludes the identification of spatial patterns.

Ozone concentrations have been measured at a network of national park monitors. Mapped in Fig. 2.34 are 1979 annual average concentrations at five sites [30]. Although limited in number and not consistent with the seasonal focus of this thesis, they nevertheless represent rural locale and thus are presented for reference. Small but significant geographic differences are visible. The sparseness of the data, however, precludes generalizations and limits its usefulness.

The remote sites identified in Figs. 2.33 and 2.34 are compared separately with ozone model results. They address the question of whether or not there is a difference in remote monitors that the model is able to detect.

2.2.4 Ozone Averages

This dissertation models seasonally averaged ozone, a measure of the integrated dose experienced at a monitoring station. As discussed in the previous chapter, seasonal averages may have a direct bearing on crop loss and forest damage. The regulatory focus, however, has thus far concentrated only on acute health effects where the appropriate variable is peak concentrations. A model which predicts average levels cannot be directly used to estimate peak values. However, if a relationship exists between average and peak concentrations, the results of a seasonally averaged model may be extrapolated to infer peak concentrations.

This section examines the empirical relationship between average and peak levels for the ozone data presented in Figs. 2.26-2.29. Three variables are defined to examine peak levels during the 1985 April-September season. The first is the average daily maximum, computed as the mean of the single highest concentration observed each day. The second measure is the growing season average, defined as the average of concentration between the hours of 9:00 AM and 4:00 PM (which generally corresponds to the period of elevated ozone). The third measure is the average of the three highest one-hour concentrations observed during the season.

Plots of each of the three variables versus the 24 hour seasonal averages are shown in Figs. 2.35-2.37. Units are $\mu g\, m^{-3}$, and symbols distinguish categories of receptors. Generally, the relationships are good, though scatter is present in each plot. Correlation coefficients for the three plots are 0.69 , 0.76, and 0.21, respectively. Monitoring categories overlap offering little distinction between urban, suburban and rural sites. The weakest of the relationships is between the seasonal average and the average of three highest concentrations (Fig. 2.37), where the correlation breaks down at high values of the latter variable. The latter correlation is significantly weakened by the outlying points whose mean of three highest concentrations exceeds 250 $\mu g\,m^{-3}$. Unlike Figs 2.35 and 2.36, there is a tendency for the extreme points to be from the suburban and urban categories. The average of the three highest concentrations can be highly influenced by singular episodes whose stochastic nature is not amenable to statistical predicitions. Thus, a seasonally averaged model is probably not the appropriate tool to predict the absolute highest concentrations at an individual receptor.

The daily maxima and growing season averages do relate fairly well to the complete seasonal average. The relationships shown in Figs. 2.35 and 2.36 can be approximated by the following equations.

$$\text{Average Daily Maxima} = 1.9 \times \text{Seasonal Average} \tag{2.1}$$

$$\text{Growing Season Average} = 1.4 \times \text{Seasonal Average} \tag{2.2}$$

These empirical relationships can be used to reasonably estimate average daily maxima and growing season averages from seasonal averages. However, the scatter present in the relationships means that significant variation is possible at individual receptors. Versions of Figs. 2.35-2.37 separated geographically by state and supplementary plots relating the measures of maximum concentration to each other are contained in Appendix III. There is evidence of some geographic similarities in small subgroups of monitors.

The ozone averages mapped in Figs. 2.26-2.29 mask the diurnal variation evident in the individual profiles shown in Figs. 2.5, 2.7 and 2.9. Plots of standard deviation versus mean values is shown in Figs. 2.38 and 2.39 for the seasonal averages of the 1985 April-September season. Plot 2.38 is separated by site classification and Fig. 2.39 identifies sites by state abbreviations. The average standard deviation (39 $\mu g\,m^{-3}$) is almost two-thirds the mean of the concentration averages (60 $\mu g\,m^{-3}$). Some stations actually have higher standard deviations than averages! Figs. 2.38 and 2.39 emphasizes the uniqueness of individual stations, as average levels can have a range of standard deviations, hence varying overall distributions. The geographic distribution of Fig. 2.39 is essentially random, though a few subclusters of monitors are apparent.

2.2.5 Empirical Relation of NO_2 and Ozone Concentrations

The introductory discussion emphasized the importance of NO_x as a precursor to ozone production. Assuming NO_2 concentrations proportional to NO_x, one might expect a relationship to exist between measured NO_2 and ozone concentrations. Such a relationship has been difficult to establish. Recently, Buhr et al. found that ozone production, measured as the late afternoon concentration minus a relatively constant morning value, is proportional to ambient NO_x concentration at remote sites in Colorado and Pennsylvania [31]. Most monitoring stations, however, are impacted by significant anthropogenic sources of pollution. As the surroundings of each monitor are unique, the NO_x- ozone relationship is site dependent. For example, a measuring station in close proximity to a highway or combustion point source is likely to show low ozone levels in spite of very high NO_x concentrations because the majority of NO_x is emitted as NO, a scavenger of ozone. A monitor downwind might show elevated levels of both ozone NO_x as the latter, mostly oxidized to NO_2, is able to serve as the photochemical production fuel for ozone. A measuring site located far downwind of an urban plume may exhibit high ozone and low NO_x, as the former is transported over greater distances prior to being removed from the atmosphere. The NO_x-ozone relationship is affected by other variables as well. VOC concentrations, winds, temperature, and insolation also have major impacts on ozone production.

A total of 137 sites monitored both NO_2 and ozone for various lengths during the 1985 April-September period. At any given site, daily averages of ozone and NO_2 are in general unrelated in a strictly statistical sense. At some sites, the pattern seems random. At others, some mild trends are evident, though each station is unique. A flavor of the variability among monitors is illustrated in Figs. 2.40-2.45, which plot average daily NO_2 concentrations vs. average daily ozone. Two examples are included from each of the urban, suburban and rural classifications. Each "x" corresponds to a single day, while the triangle represents the average of all days. Fig. 2.40 shows a positive correlation of NO_2 and ozone at an urban site in Houston, TX. Mean NO_2 and ozone levels are each about 25 ppb. This is the strongest relationship of the 137 sites with a correlation coefficient of 0.62. This may reflect in situ ozone production not strongly affected by other variables. A negative correlation exists at another urban site in Colorado Springs, CO, plotted in Fig. 2.41. The combination of lower NO_2 and relatively higher ozone is more typical of monitors in the network. The negative correlation could be the result of ozone scavenging by fresh local emissions of NO. A pair of suburban monitors in Massachusetts and Florida are shown in Figs. 2.42 and 2.43. Both show positive correlations, though the degree of scatter is large. The level of ozone is similar at the two sites but the Chelsea, MA station (Fig. 2.42) has much higher NO_2 levels than does the Florida monitor (Fig. 2.43). Two sites designated as rural are plotted in Figs. 2.44 and 2.45. Both exhibit negative correlations and typically large scatter. The significance of the correlation at the Oklahoma site is rather weak (Fig. 2.44), and too few data points at the Maryland site (Fig. 2.45) limits the usefulness of its information. These six stations, selected at random, confirm the site specific nature of the NO_2-ozone relationship and emphasize the importance of other ozone influencing variables which contribute to the scatter seen in the plots.

There seems little hope for a direct relationship between seasonally averaged ozone and NO_2 concentrations, as the regional maps of NO_2 show significant gradients and source effects and those of ozone relatively constant levels. This hypothesis is supported by Figs. 2.46 and 2.47 which plots measurements of ozone and NO_2 at common monitors. Each datapoint is averaged over the 1985 April-September period, and a 75% data coverage requirement yields ninety-four valid sites. Symbols separate Fig. 2.46 into the urban, suburban, rural, and unknown site classifications while Fig. 2.47 is an identical plot denoted with state abbreviations. An overall correlation coefficient of -0.35 implies an inverse relationship, though statistical significance is overwhelmed by scatter. All three major site categories contribute to the inverse, and no distinct geographic tendencies are apparent.

The difficulty in establishing an empirical NO_2-ozone relationship within the 1985 data reinforces the individual uniqueness of each monitor. The combination of the weak inverse relationship between NO_2 (Figs. 2.46 and 2.47) and the apparent lack of gradients in ozone distributions (Figs. 2.26-2.30) suggest that modeling the network of ozone concentrations as a function of precursor concentrations may be difficult.

Regional models can predict changes only over scale lengths characteristic of their spatial refinement. The regional models developed in chapters four and five have grid cell sizes of 40 km on a side. They are thus inappropriate models to examine the fine scale variations exhibited at monitor clusters within the measuring networks. Direct comparison of model results with the ambient concentrations presented in this chapter will exhibit a great amount of scatter. The issue addressed by this thesis in subsequent chapters is to see how well the model results correlate with the measured values on an average basis.

Note: 1 teragram = 1 million metric tons

Inventory	Total Number of Sources	Area Source Description	Total emissions (teragrams)	
			NO_2	VOCs
DOE (U.S.)	17165	County Totals	18.8	6.4
NAPAP (U.S.)	70390	Gridded $\frac{1}{4}^\circ$ by $\frac{1}{6}^\circ$	20.2	21.0
Biogenic	3081	County Totals	-	30.7
Canadian	287	Province Totals	1.8	2.7

Table 2.1: Comparison of Emission Inventories

NAPAP Inventory	Point	Area	Total	Mobile	Stationary	Other
Number of Sources	50159	20231	70390	-	-	-
NO_2 (teragrams)	8.7	11.5	20.2	8.4	10.3	1.5
VOCs (teragrams)	3.7	17.3	21.0	9.3	6.6	5.1

Table 2.2: NAPAP Inventory Breakdown

Province	Total emissions (teragrams)			
	NO_2		VOCs	
	Area	Point	Area	Point
Alberta	0.33	0.11	0.49	0.13
British Columbia	0.18	0.01	0.24	0.02
Manitoba	0.09	-	0.20	0.01
New Brunswick	0.03	0.02	0.04	0.01
Newfoundland	0.03	-	0.02	-
Nova Scotia	0.04	0.03	0.06	0.01
Ontario	0.39	0.13	0.58	0.09
Prince Edward Island	0.01	-	0.01	-
Quebec	0.27	0.02	0.29	0.06
Saskatchewan	0.15	0.01	0.45	0.01
Total	1.52	0.33	2.38	0.35

Table 2.3: Canadian Emissions by Province

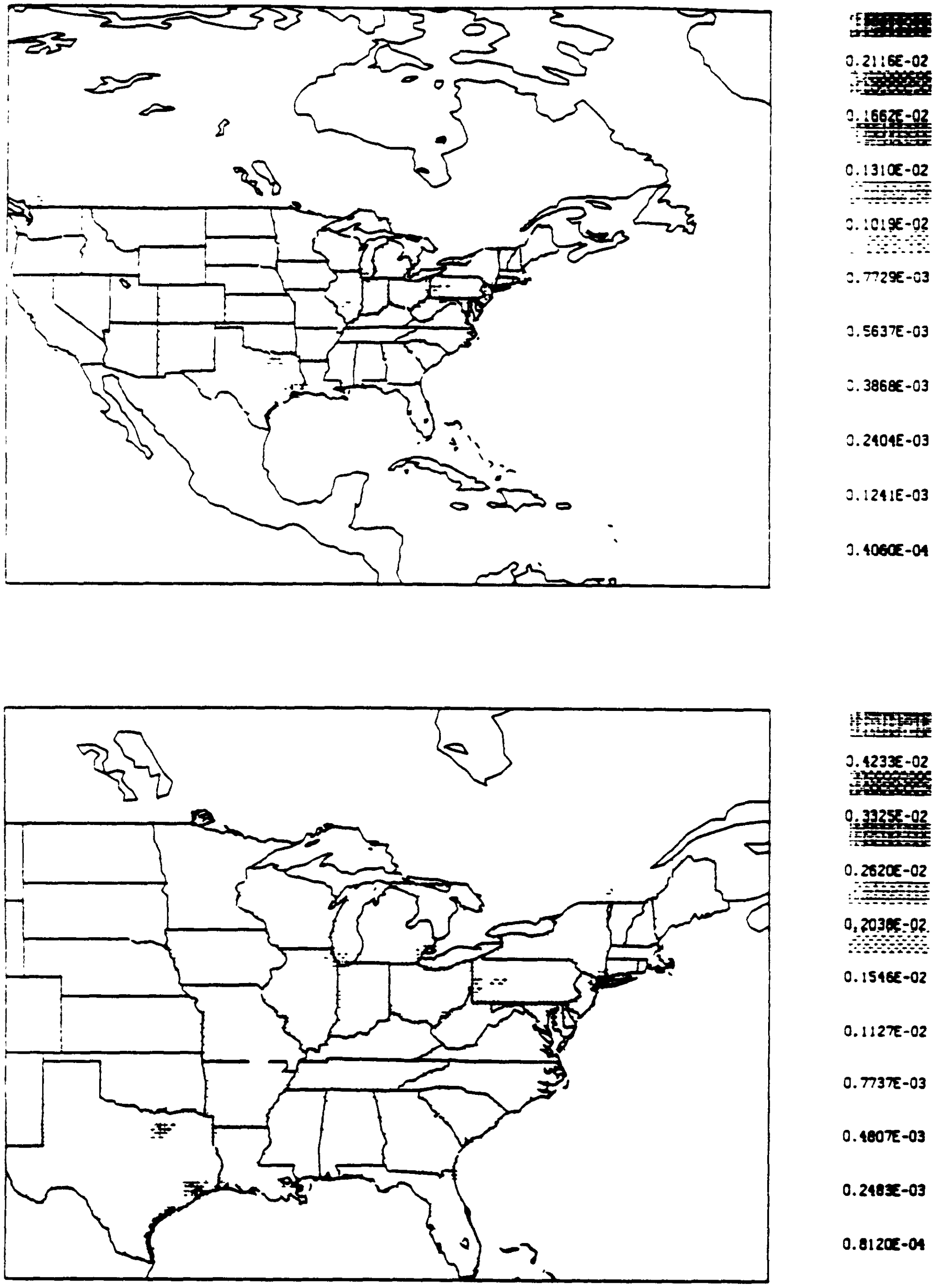

Fig. 2.1 NO$_x$ Emission Flux (kg km^{-2}s^{-1}). The upper map corresponds to the outer numerical projection, the lower map the inner projection.

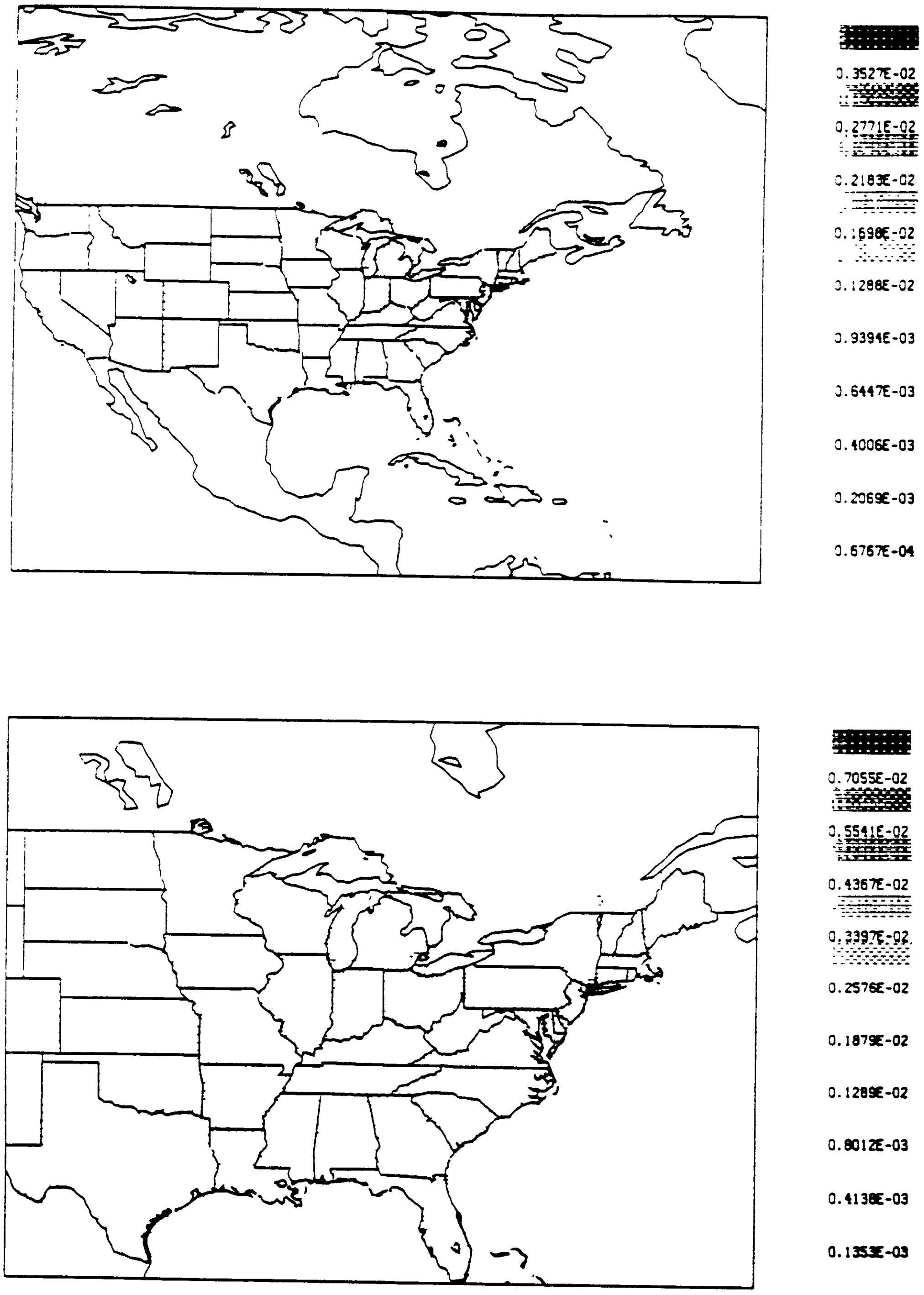

Fig. 2.2 Anthropogenic VOCs Emission Flux (kg km^{-2}s^{-1}). The upper map corresponds to the outer numerical projection, the lower map the inner projection.

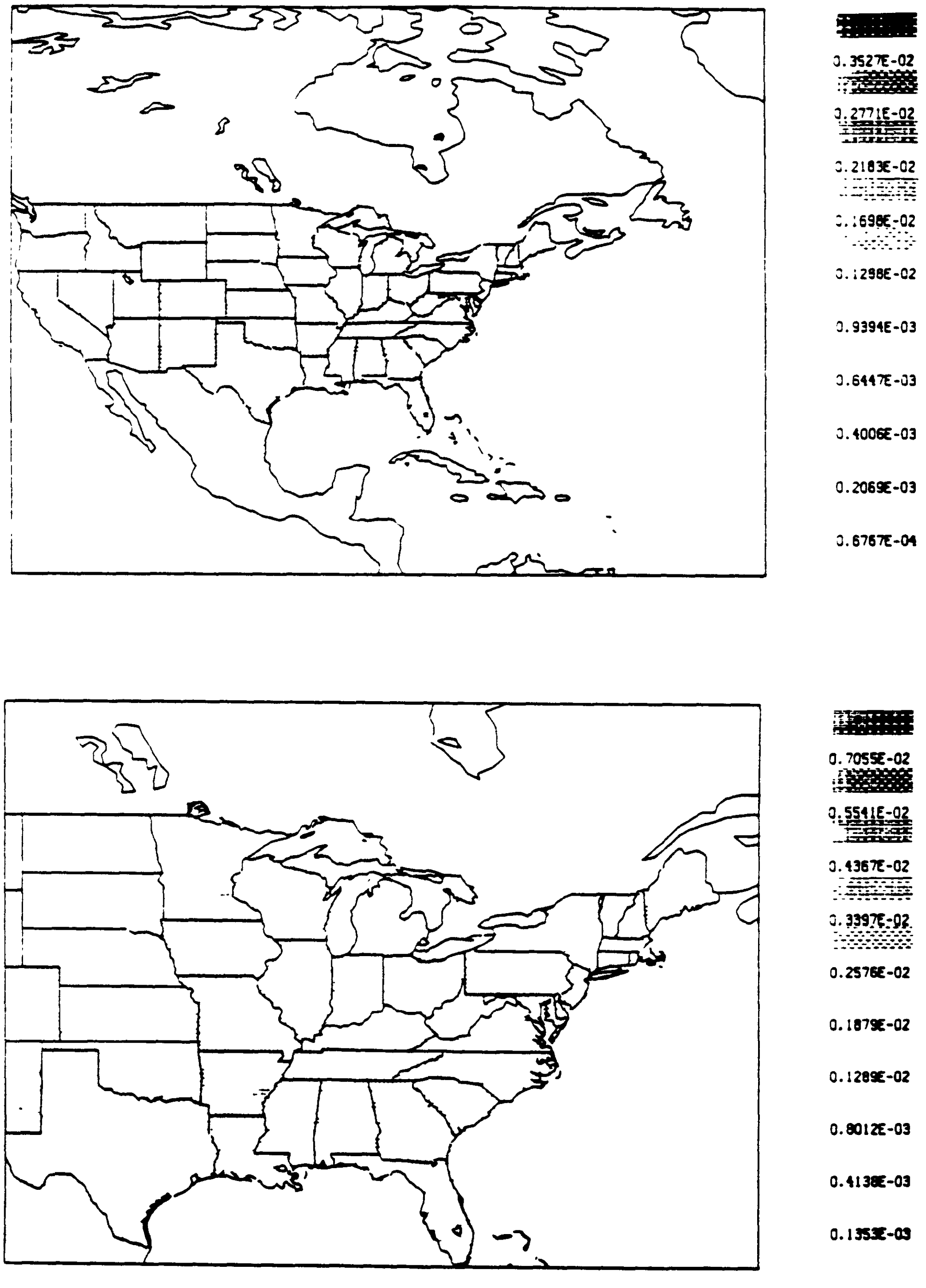

Fig. 2.3 Biogenic VOCs Emission Flux (kg $km^{-2}s^{-1}$). The upper map corresponds to the outer numerical projection, the lower map the inner projection.

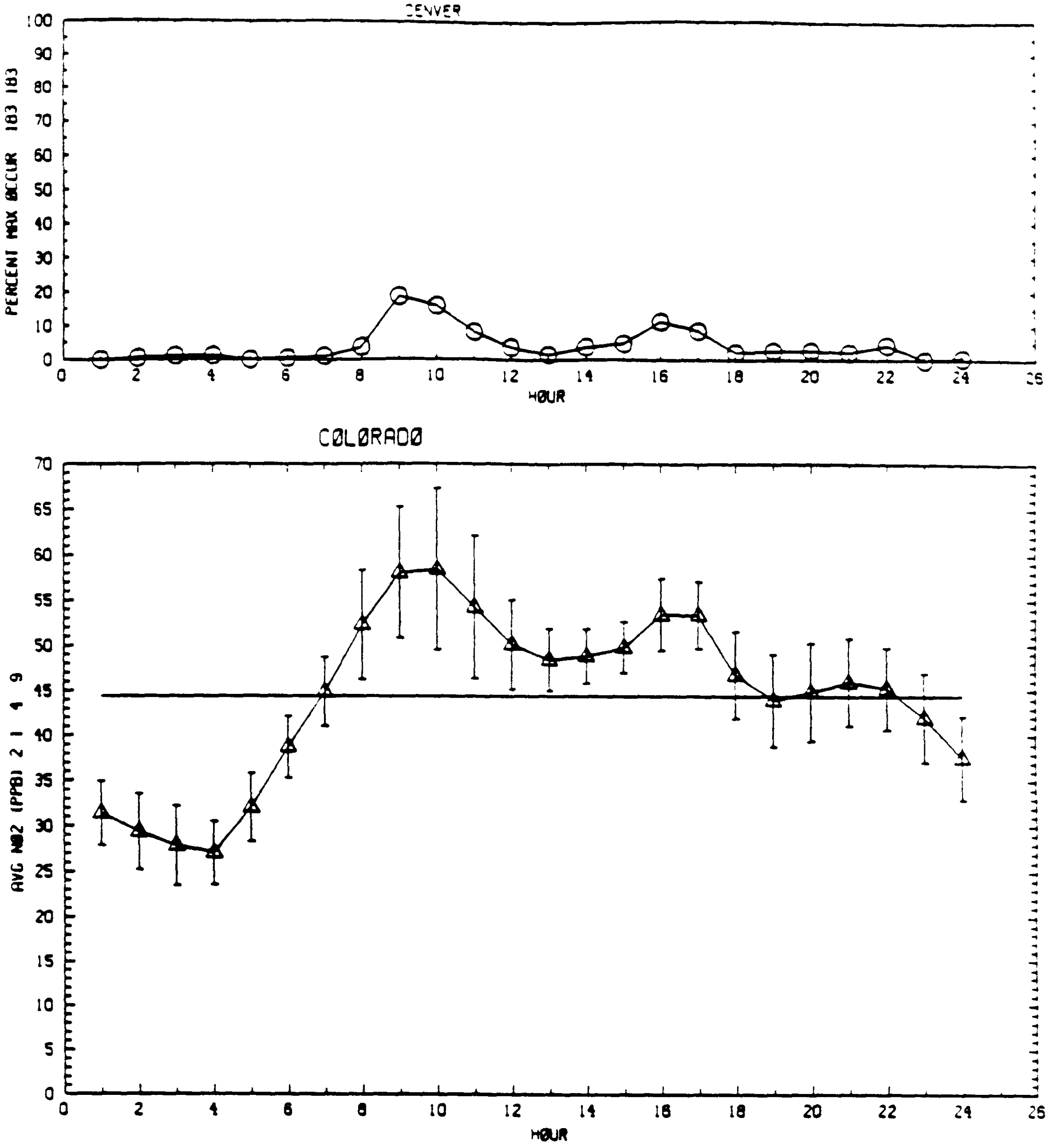

Fig. 2.4 Measured NO_2 at an urban site in Denver, CO over the April-September 1985 season. Upper section shows the frequency (%) that the daily maximum occurs in each hour. The lower section plots average concentrations (ppb). Vertical bars signify the standard deviation of each hourly mean, and the horizontal line indicates the overall average concentration.

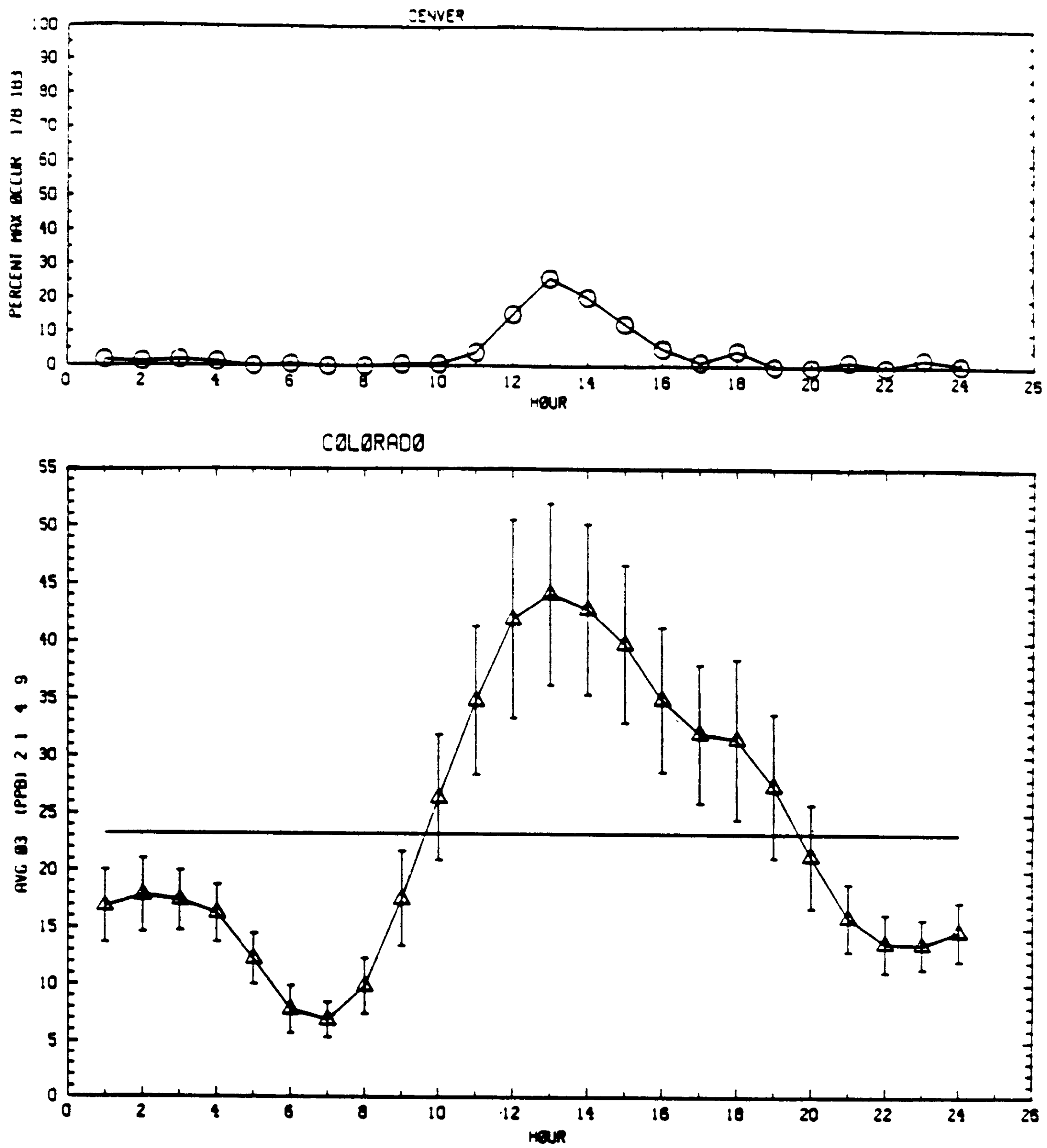

Fig. 2.5 Measured ozone at an urban site in Denver, CO over the April-September 1985 season. Upper section shows the frequency (%) that the daily maximum occurs in each hour. The lower section plots average concentrations (ppb). Vertical bars signify the standard deviation of each hourly mean, and the horizontal line indicates the overall average concentration.

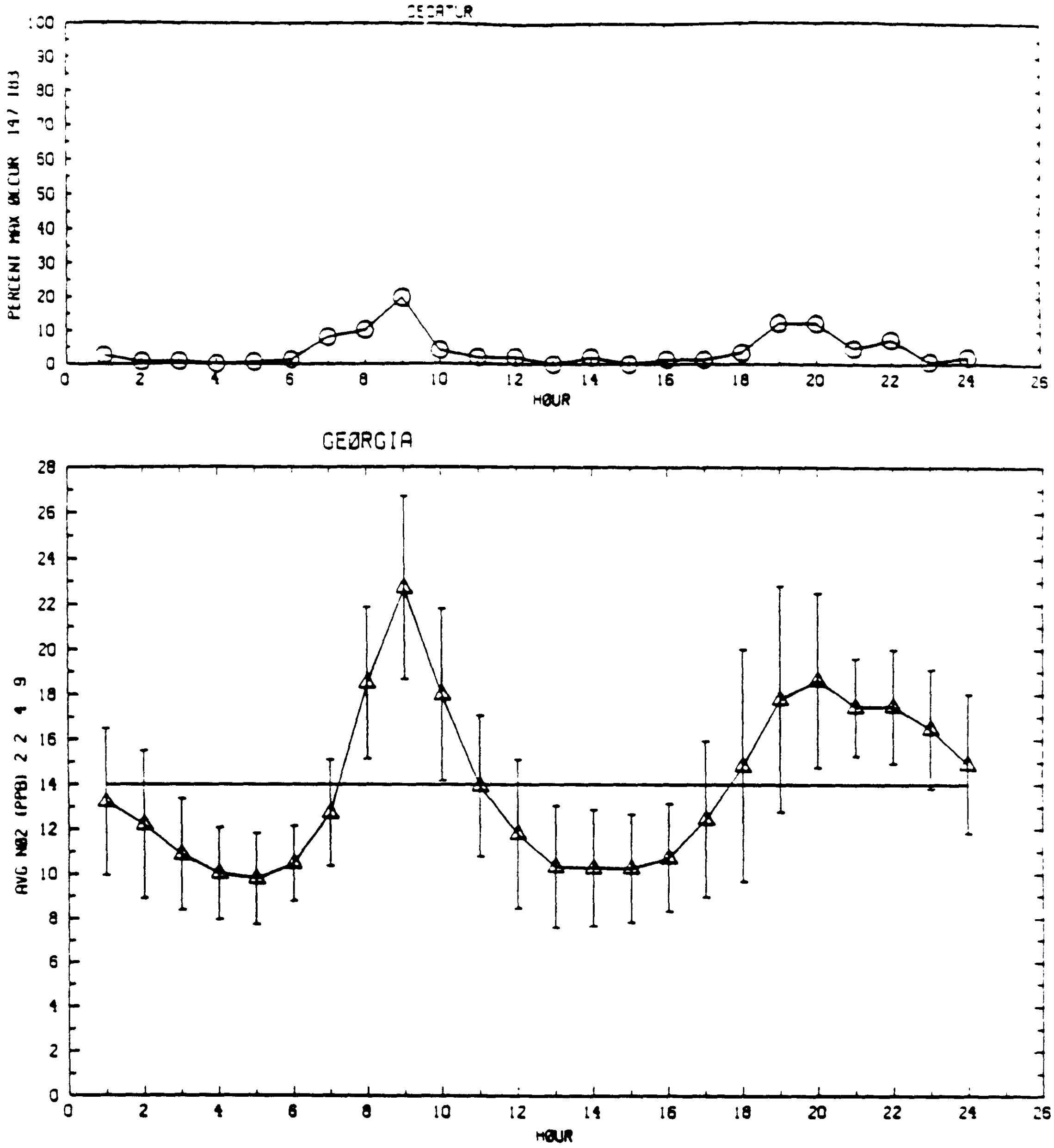

Fig. 2.6 Measured NO_2 at a suburban site in Decatur, GA over the April-September 1985 season. Upper section shows the frequency (%) that the daily maximum occurs in each hour. The lower section plots average concentrations (ppb). Vertical bars signify the standard deviation of each hourly mean, and the horizontal line indicates the overall average concentration.

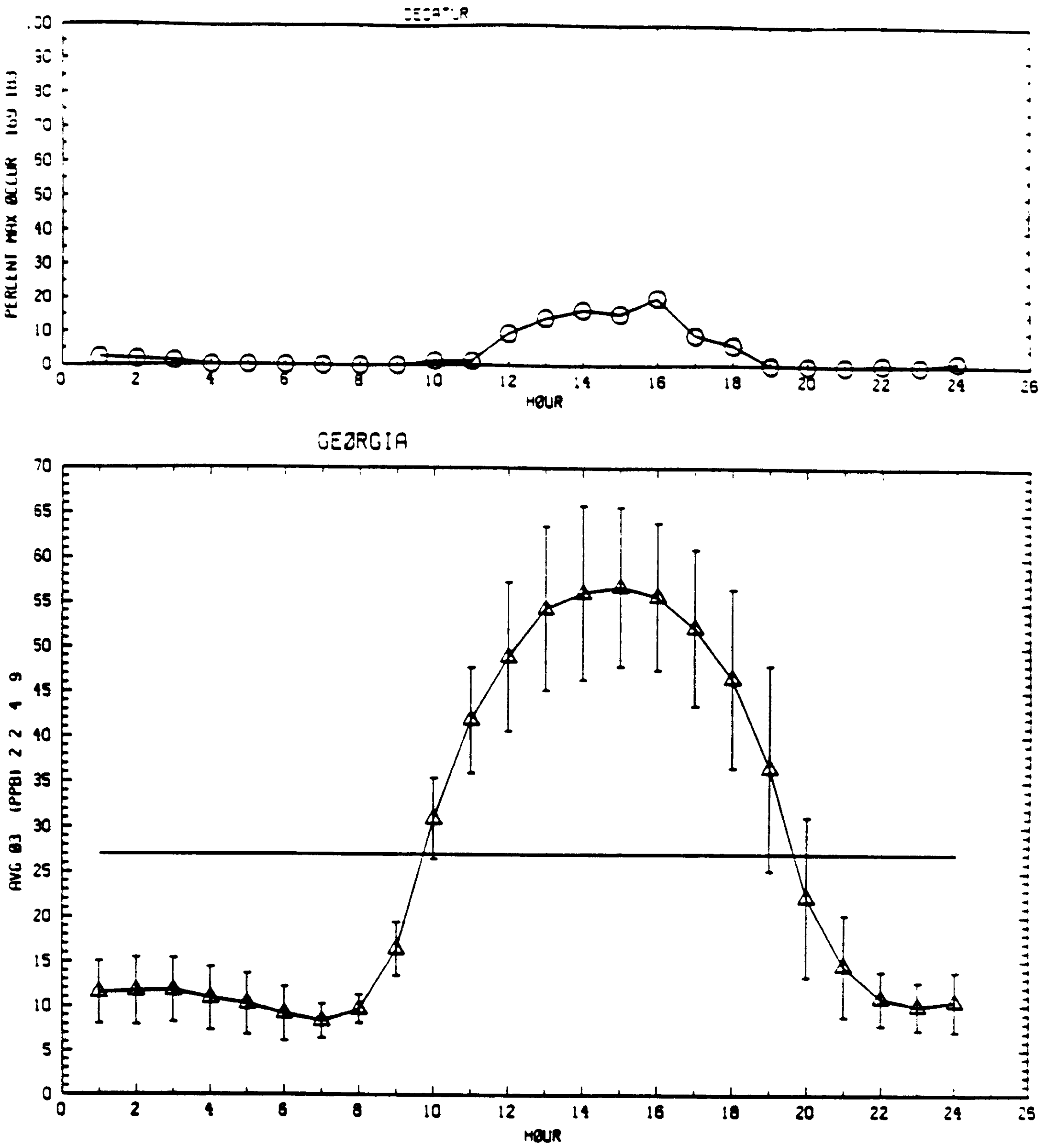

Fig. 2.7 Measured ozone at a suburban site in Decatur, GA over the April-September 1985 season. Upper section shows the frequency (%) that the daily maximum occurs in each hour. The lower section plots average concentrations (ppb). Vertical bars signify the standard deviation of each hourly mean, and the horizontal line indicates the overall average concentration.

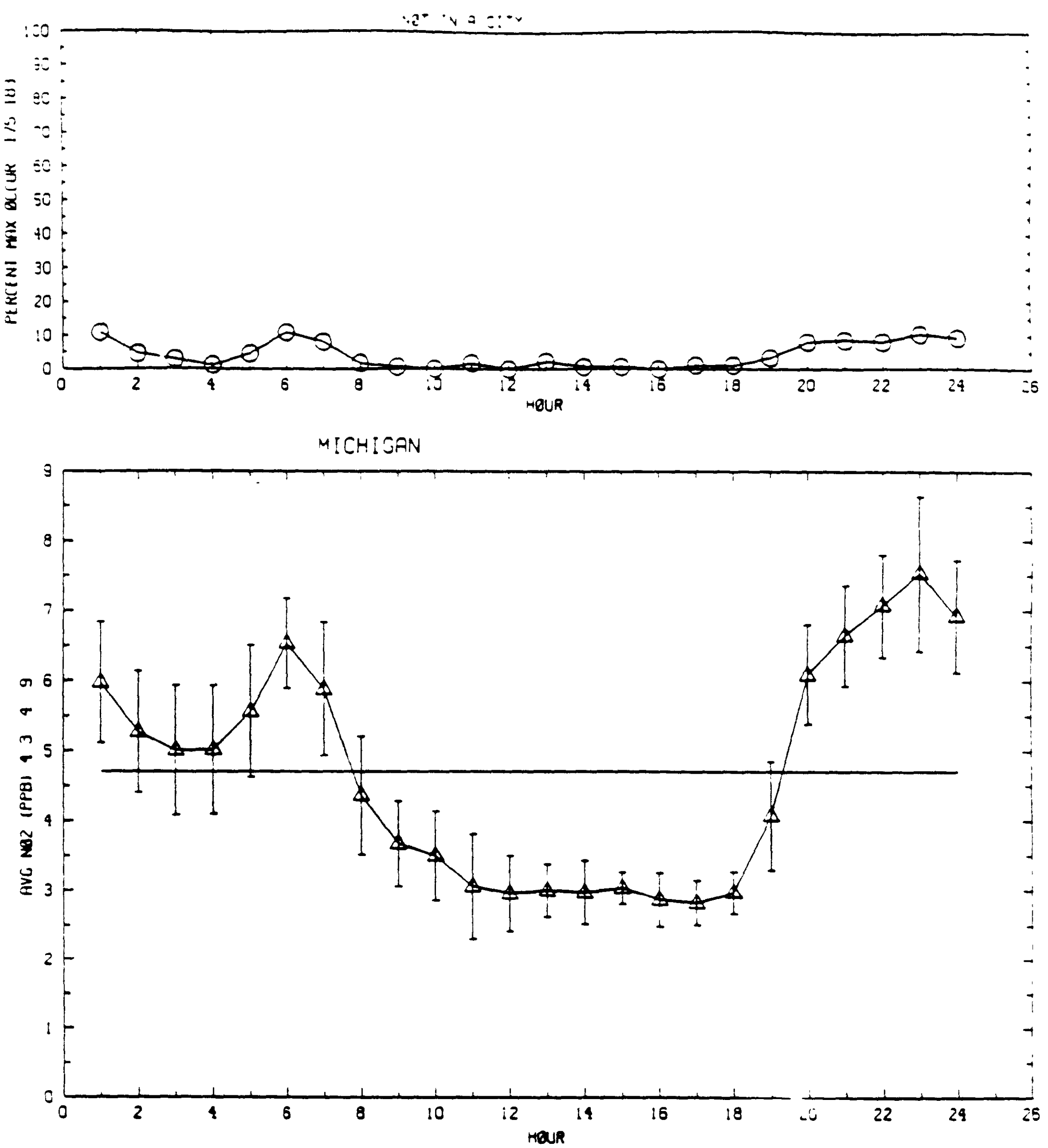

Fig. 2.8 Measured NO_2 at a rural site in Michigan over the April-September 1985 season. Upper section shows the frequency (%) that the daily maximum occurs in each hour. The lower section plots average concentrations (ppb). Vertical bars signify the standard deviation of each hourly mean, and the horizontal line indicates the overall average concentration.

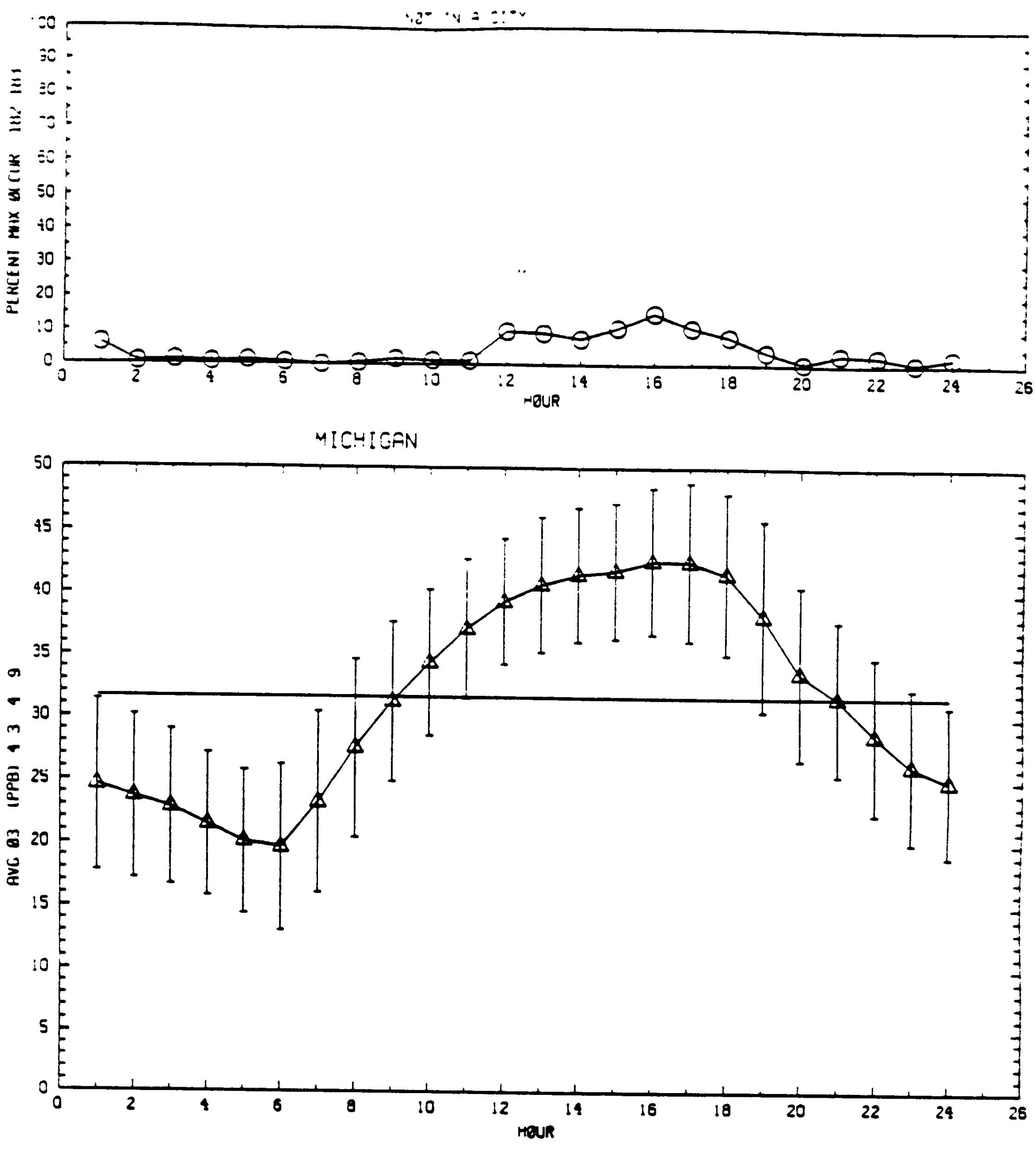

Fig. 2.9 Measured ozone at a rural site in Michigan over the April-September 1985 season. Upper section shows the frequency (%) that the daily maximum occurs in each hour. The lower section plots average concentrations (ppb). Vertical bars signify the standard deviation of each hourly mean, and the horizontal line indicates the overall average concentration.

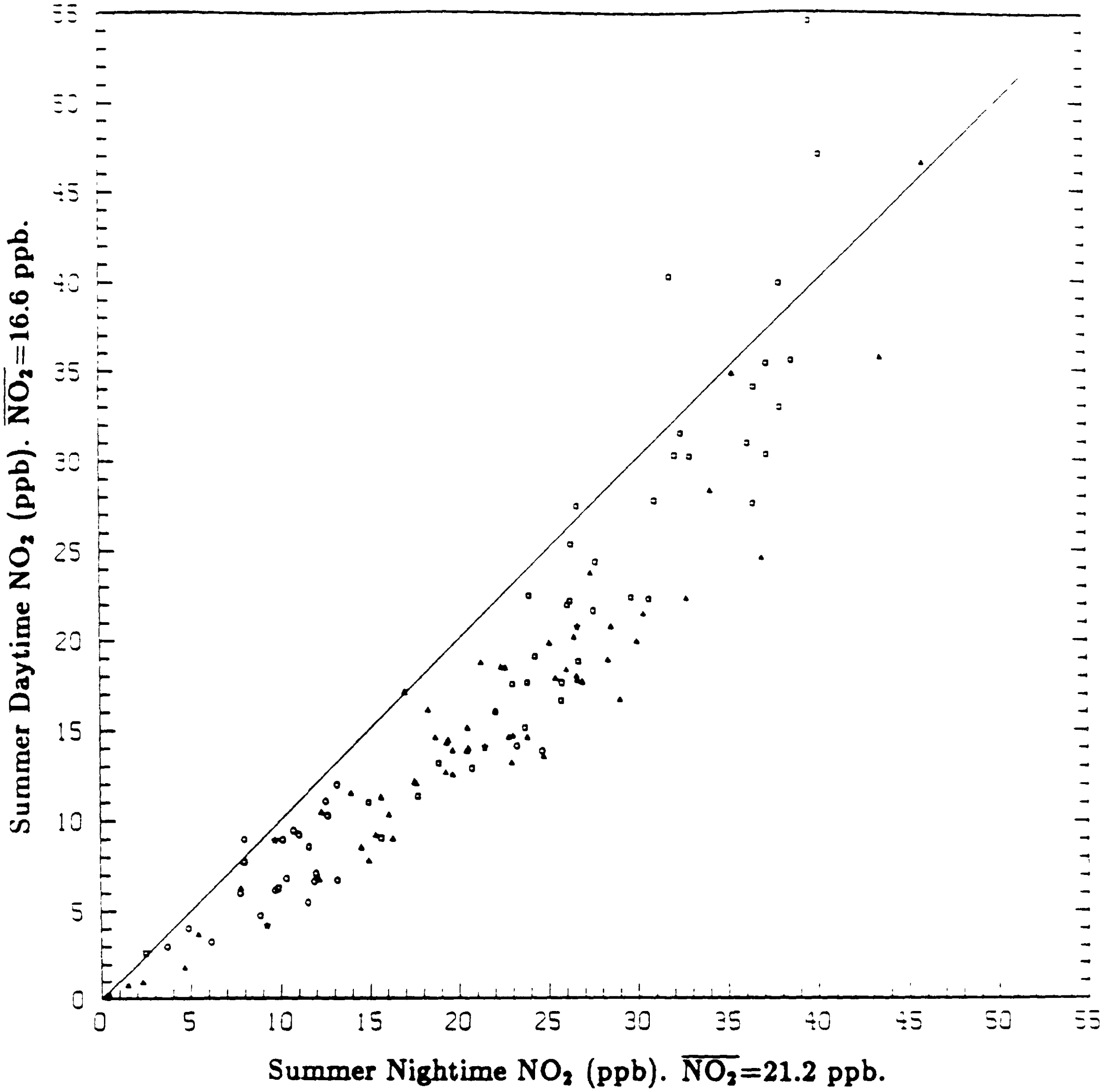

Fig. 2.10 Average Summer Daytime NO_2 vs. Average Summer Nightime NO_2. Units are parts per billion (ppb). Square, triangle, circle, and star symbols designate urban, suburban, rural, and unknown site classes. Daytime is defined from 7:00 AM to 7:00 PM, nightime from 7:00 PM to 7:00 AM. Correlation coefficient r=0.93. 1985 April to September data.

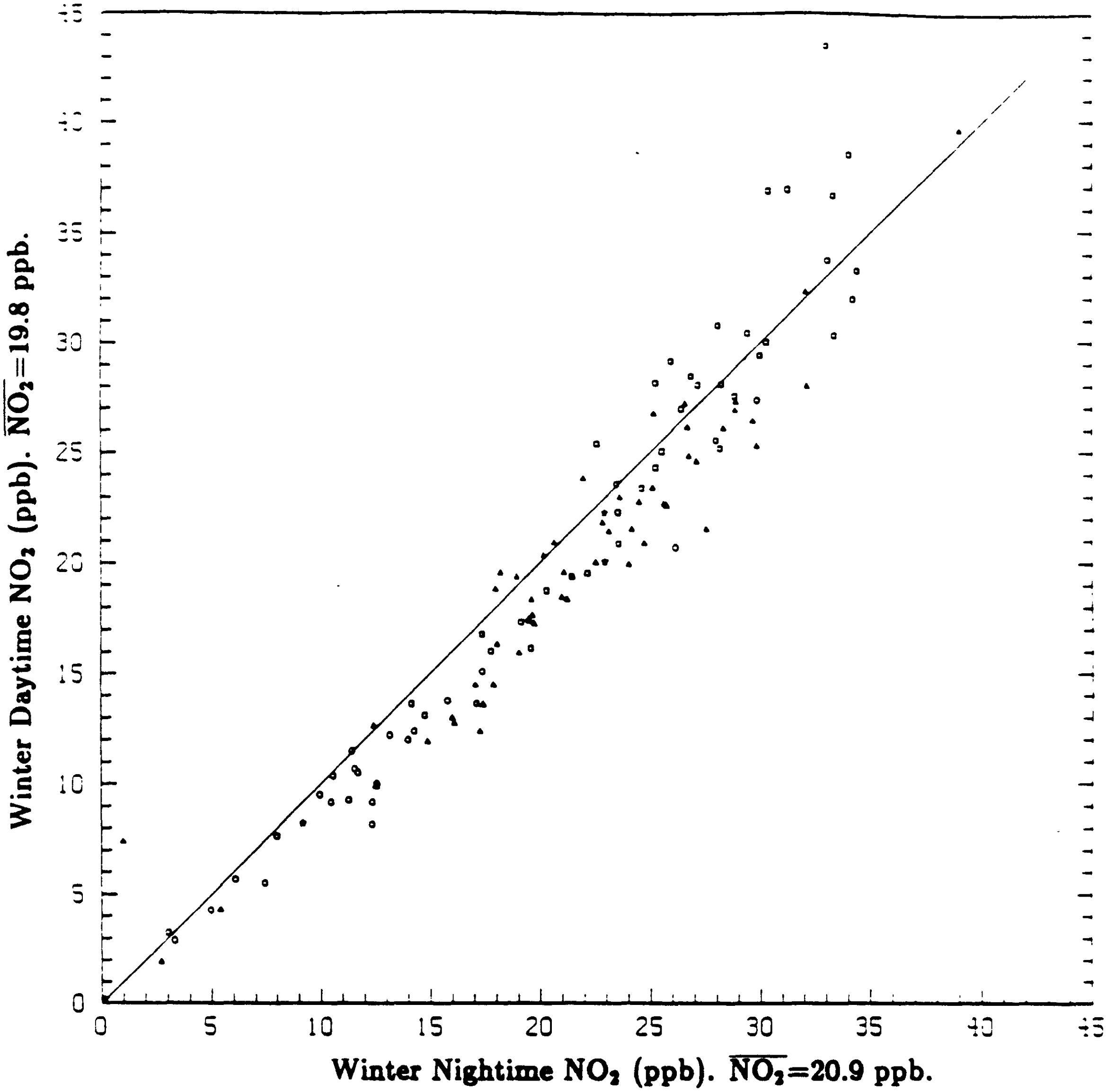

Fig. 2.11 Average Winter Daytime NO_2 vs. Average Winter Nightime NO_2. Units are parts per billion (ppb). Square, triangle, circle, and star symbols designate urban, suburban, rural, and unknown site classes. Daytime is defined from 7:00 AM to 7:00 PM, nightime from 7:00 PM to 7:00 AM. Correlation coefficient r=0.96. 1985 January to March, October to November data.

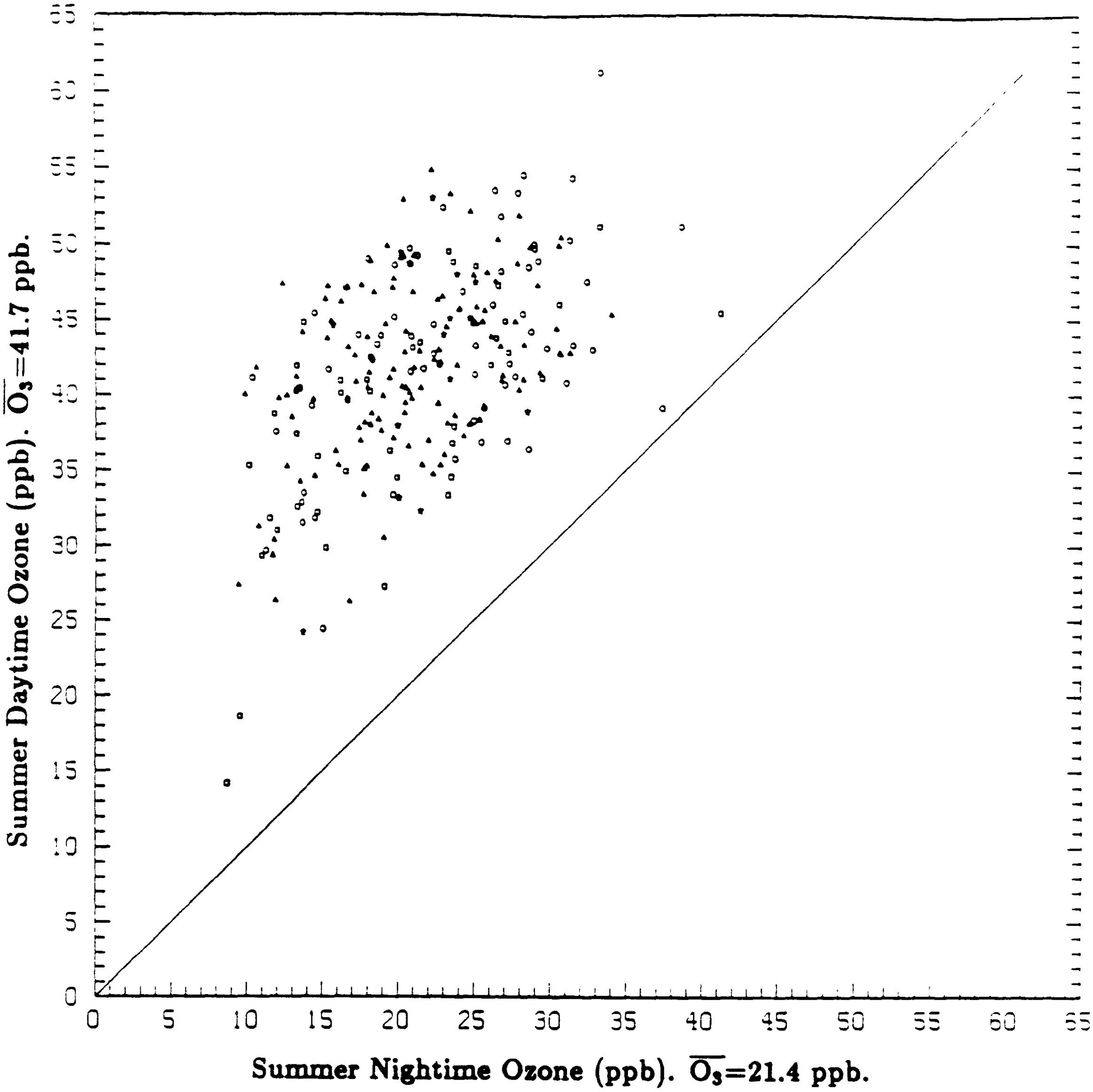

Fig. 2.12 Average Summer Daytime Ozone vs. Average Summer Nightime Ozone. Units are parts per billion (ppb). Square, triangle, circle, and star symbols designate urban, suburban, rural, and unknown site classes. Daytime is defined from 7:00 AM to 7:00 PM, nightime from 7:00 PM to 7:00 AM. Correlation coefficient r=0.52. 1985 April to September data.

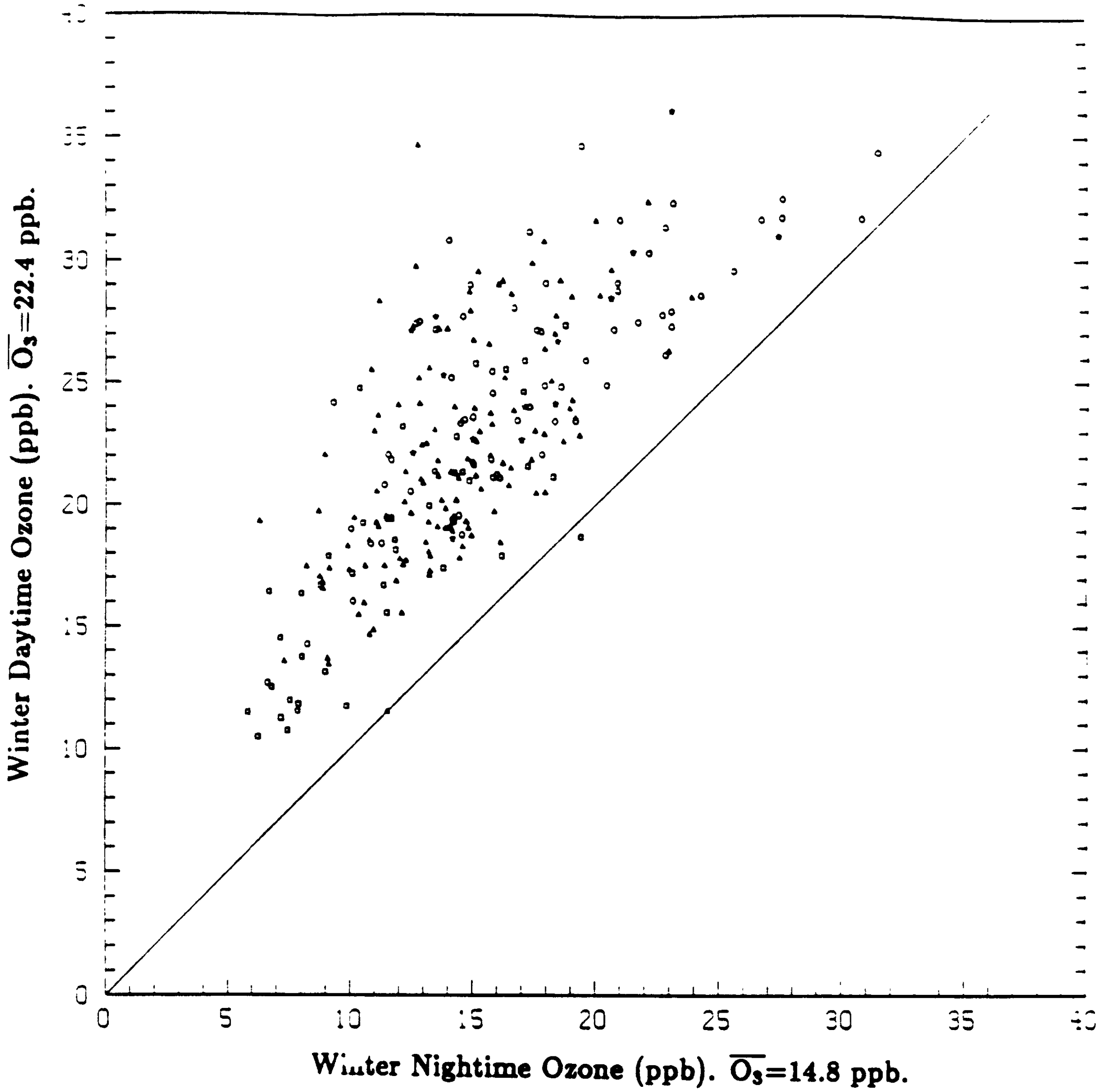

Fig. 2.13 Average Winter Daytime Ozone vs. Average Winter Nightime Ozone. Units are parts per billion (ppb). Square, triangle, circle, and star symbols designate urban, suburban, rural, and unknown site classes. Daytime is defined from 7:00 AM to 7:00 PM, nightime from 7:00 PM to 7:00 AM. Correlation coefficient r=0.76. 1985 January to March, October to November data.

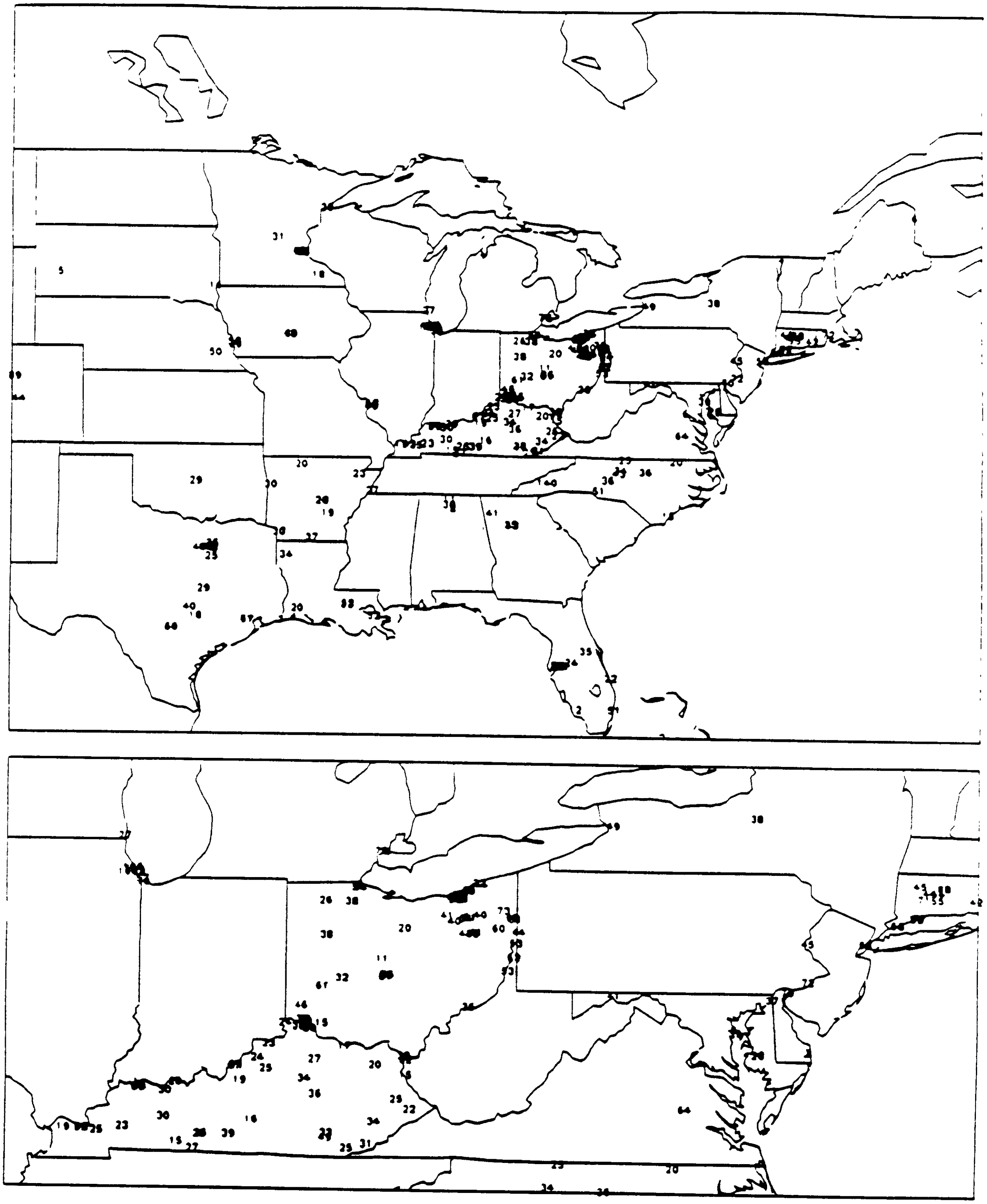

Fig. 2.14 1980 Seasonal Average NO_2 Concentrations at Urban Monitoring Sites ($\mu g\ m^{-3}$).

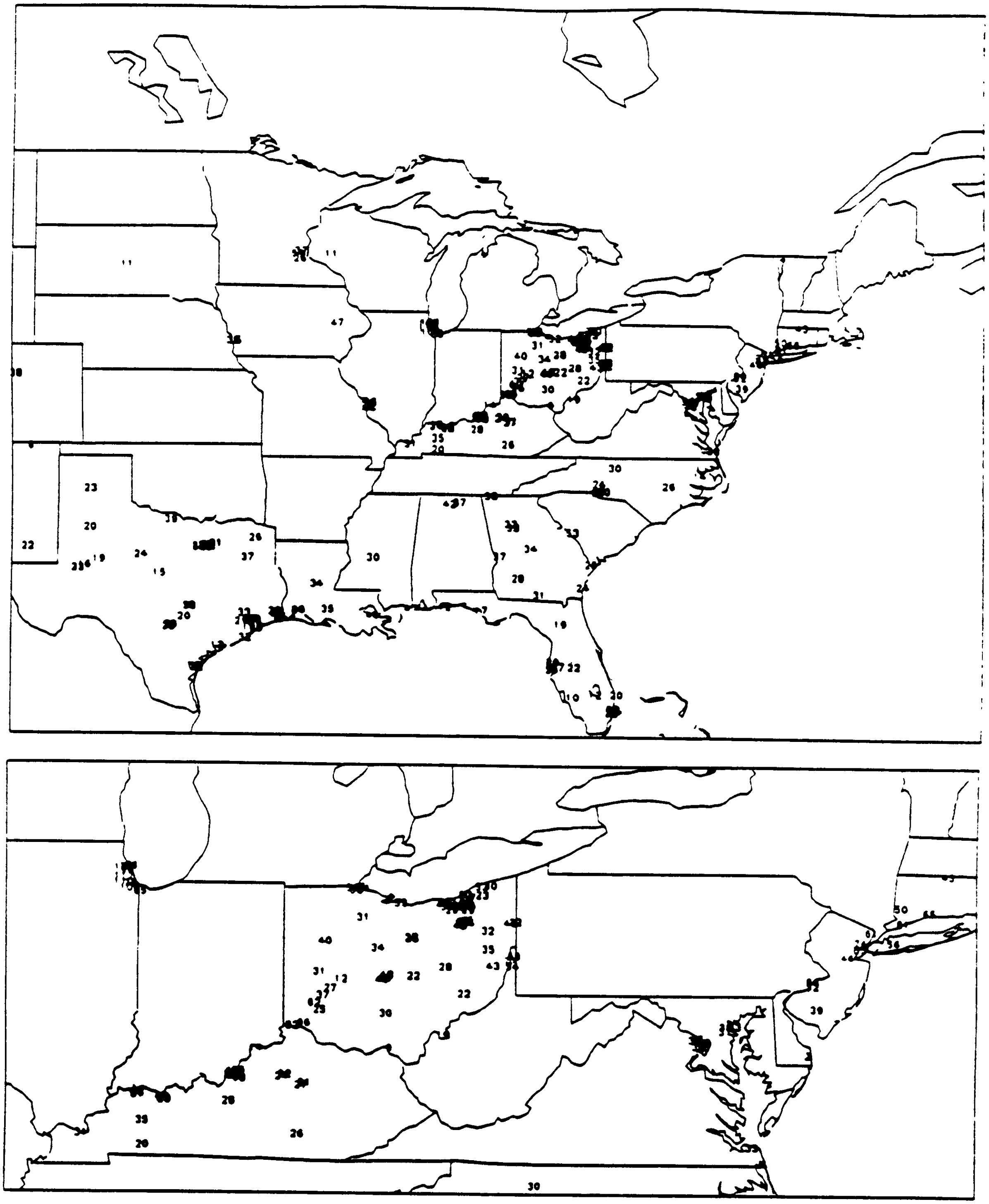

Fig. 2.15 1980 Seasonal Average NO_2 Concentrations at Suburban Monitoring Sites ($\mu g\,m^{-3}$).

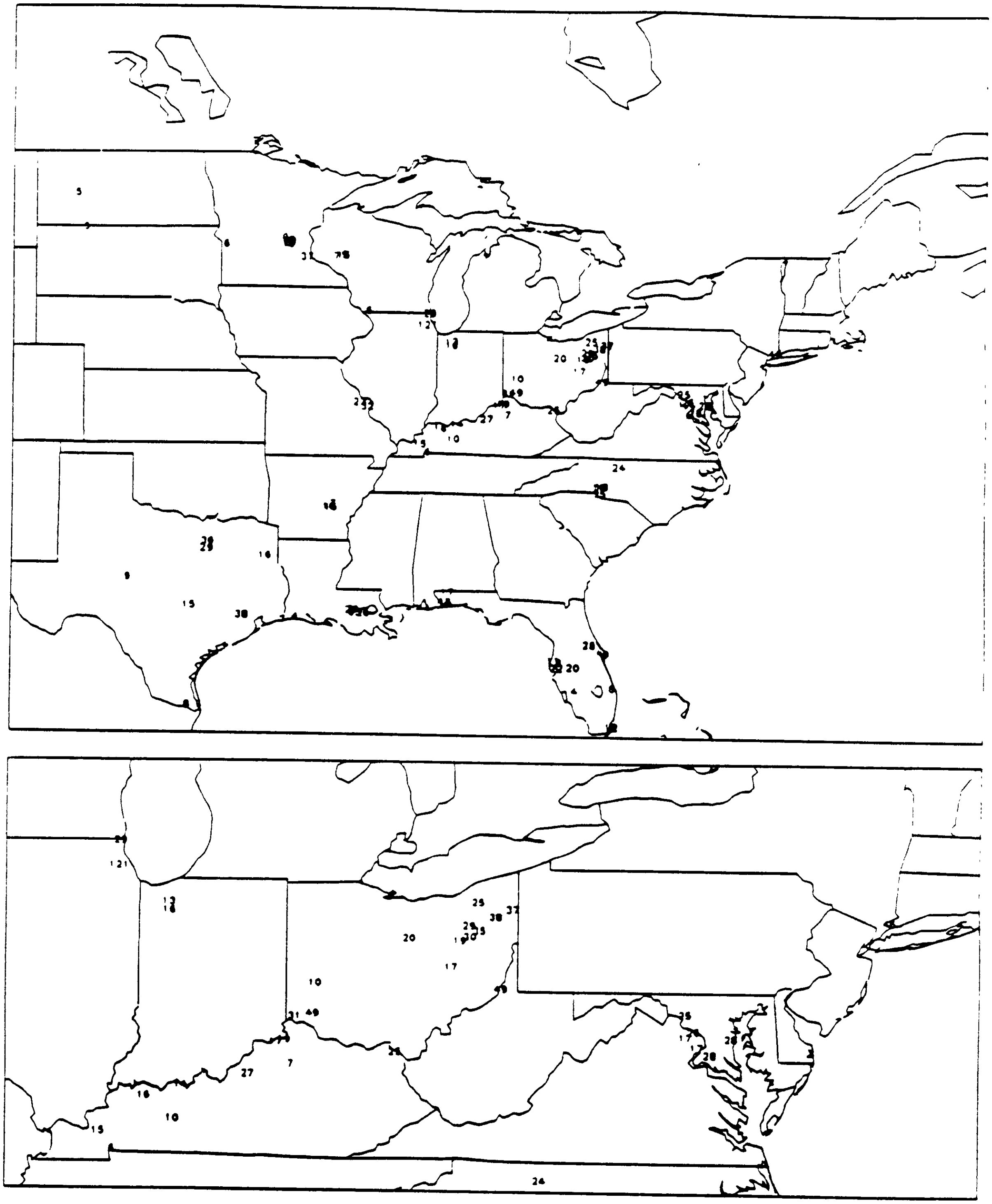

Fig. 2.16 1980 Seasonal Average NO_2 Concentrations at Rural Monitoring Sites ($\mu g\ m^{-3}$).

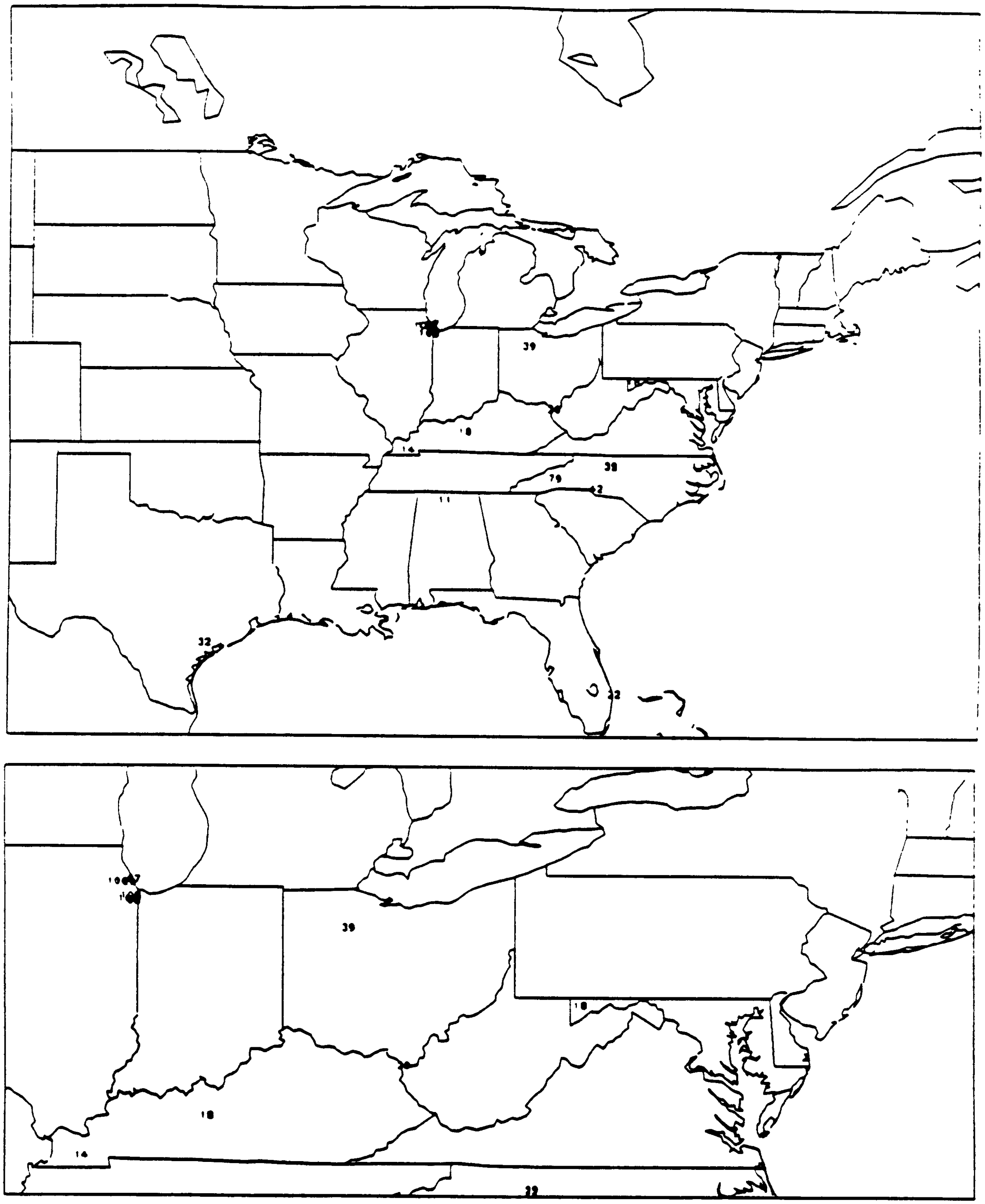

Fig. 2.17 1980 Seasonal Average NO_2 Concentrations at Unclassified Monitoring Sites ($\mu g\ m^{-3}$).

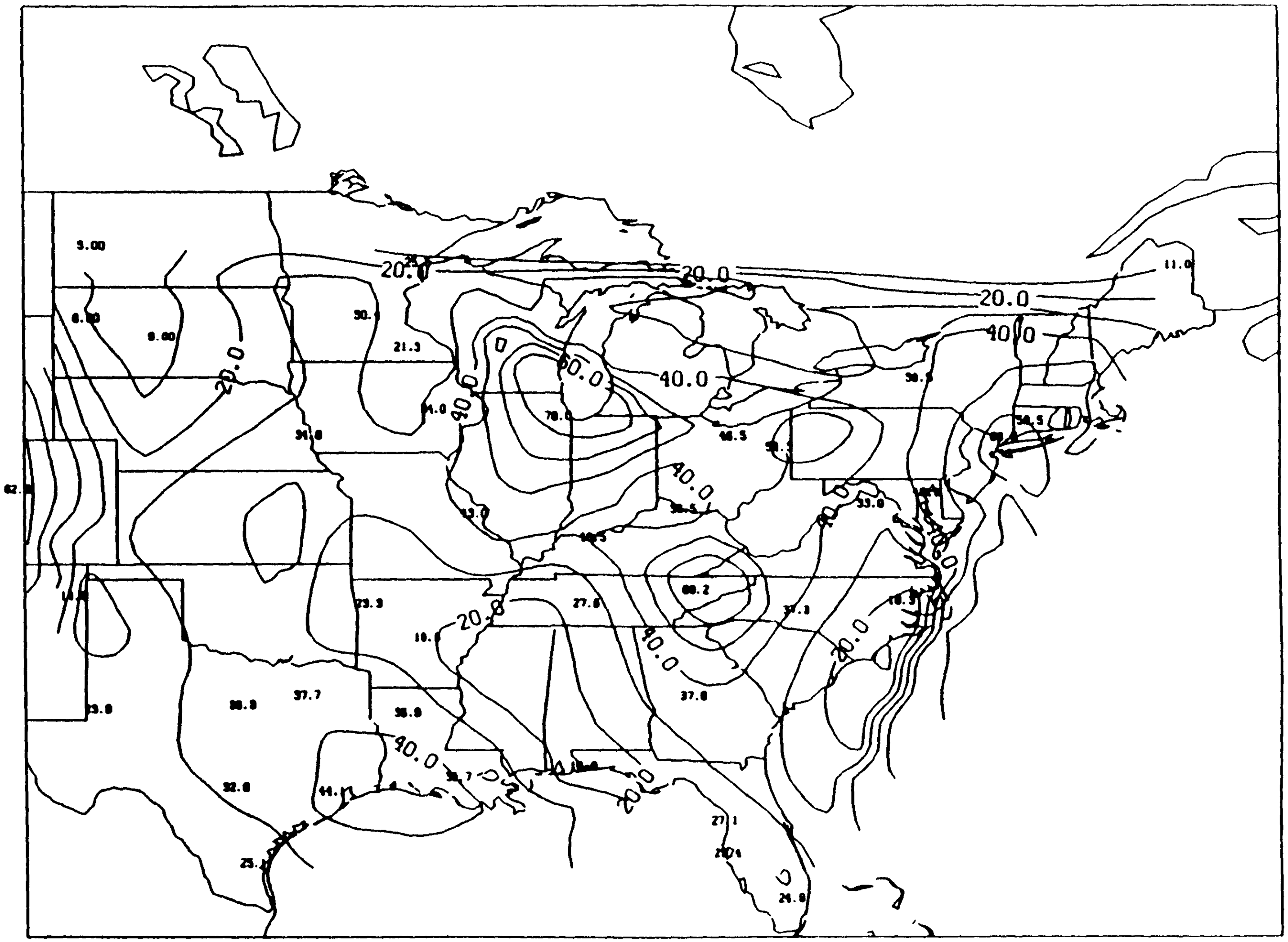

Fig. 2.18 1980 Seasonal Box Average NO_2 Concentrations ($\mu g\ m^{-3}$). Box size 4° longitude by 3° latitude. Contours from 10 to 70 ($\mu g\ m^{-3}$) by 10 ($\mu g\ m^{-3}$).

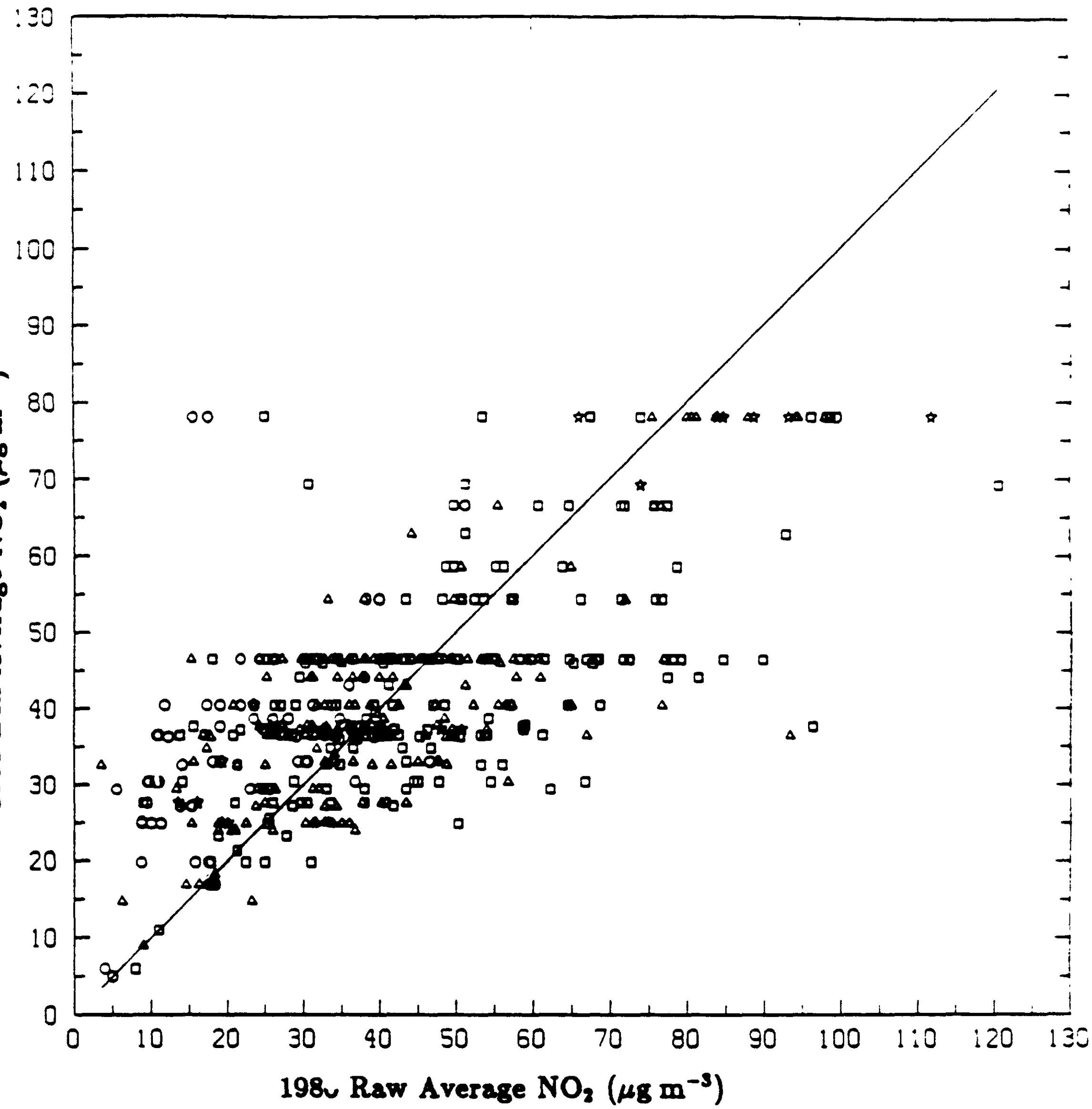

Fig. 2.19 1980 Seasonal Box Average NO_2 vs. Raw Average NO_2 Concentrations ($\mu g\ m^{-3}$). Square, triangle, circle and star symbols denote urban, suburban, rural, and unclassified monitors. Correlation coefficient r=0.68.

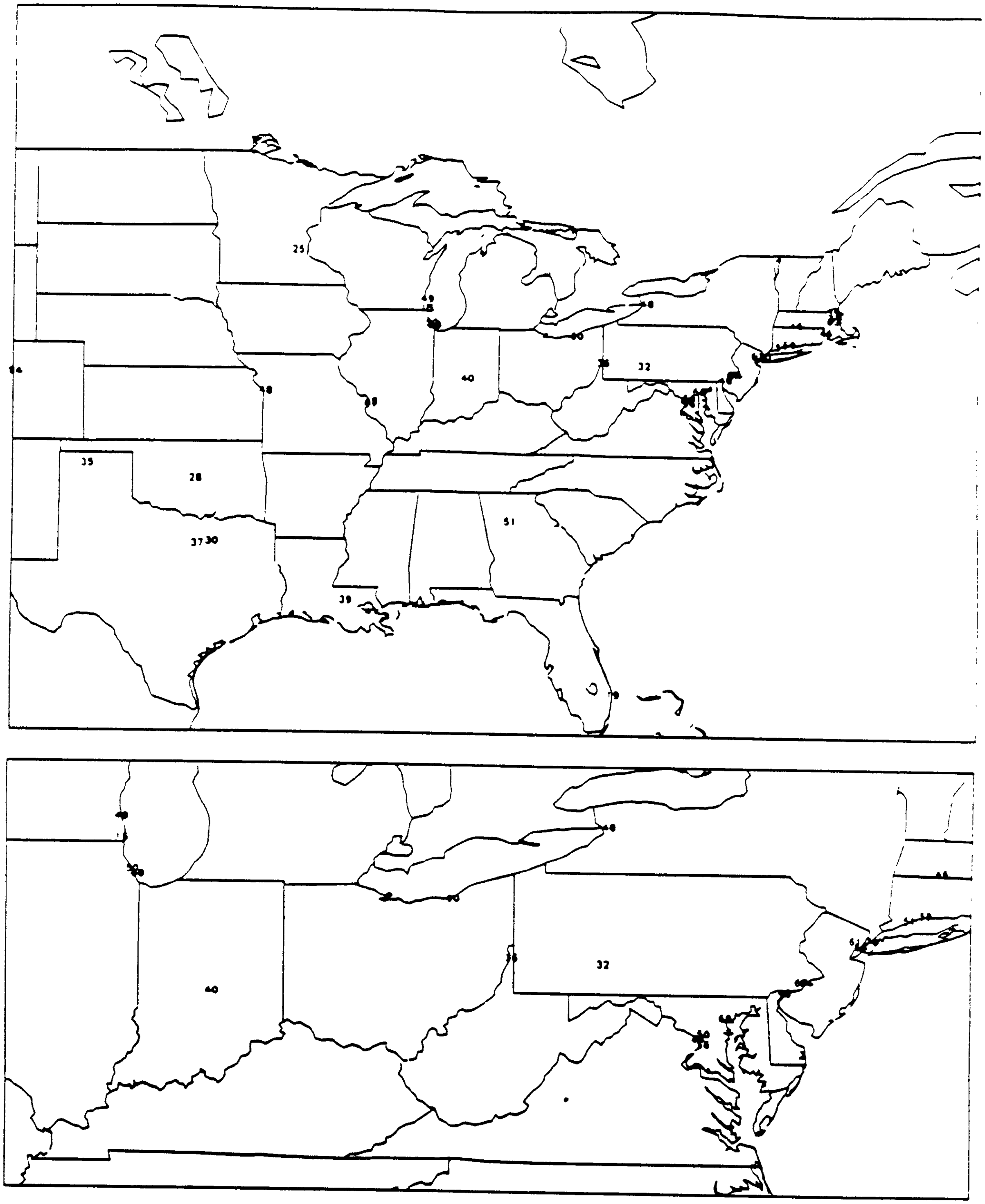

Fig. 2.20 1985 Seasonal Average NO_2 Concentrations at Urban Monitoring Sites ($\mu g\,m^{-3}$).

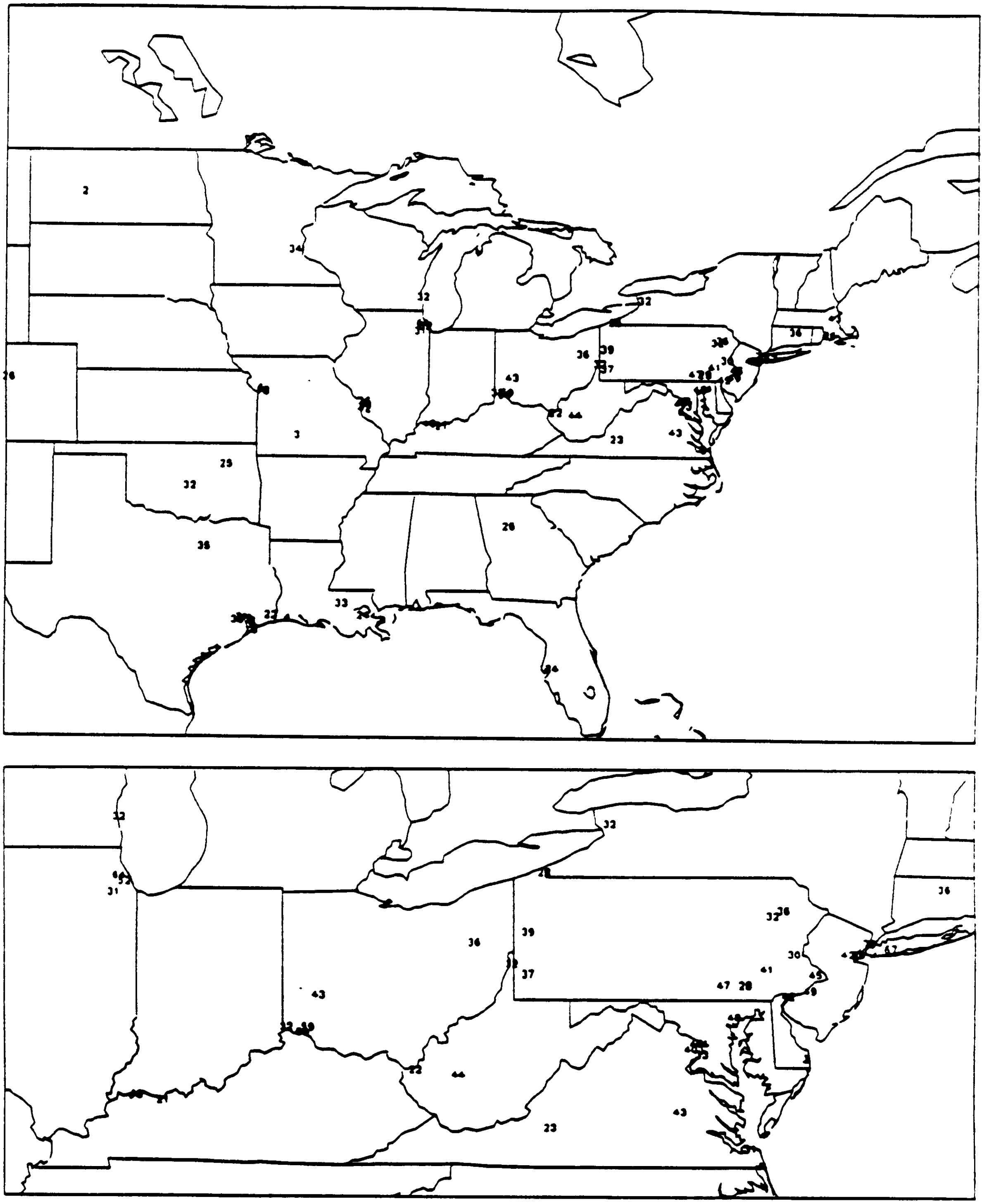

Fig. 2.21 1985 Seasonal Average NO_2 Concentrations at Suburban Monitoring Sites ($\mu g\ m^{-3}$).

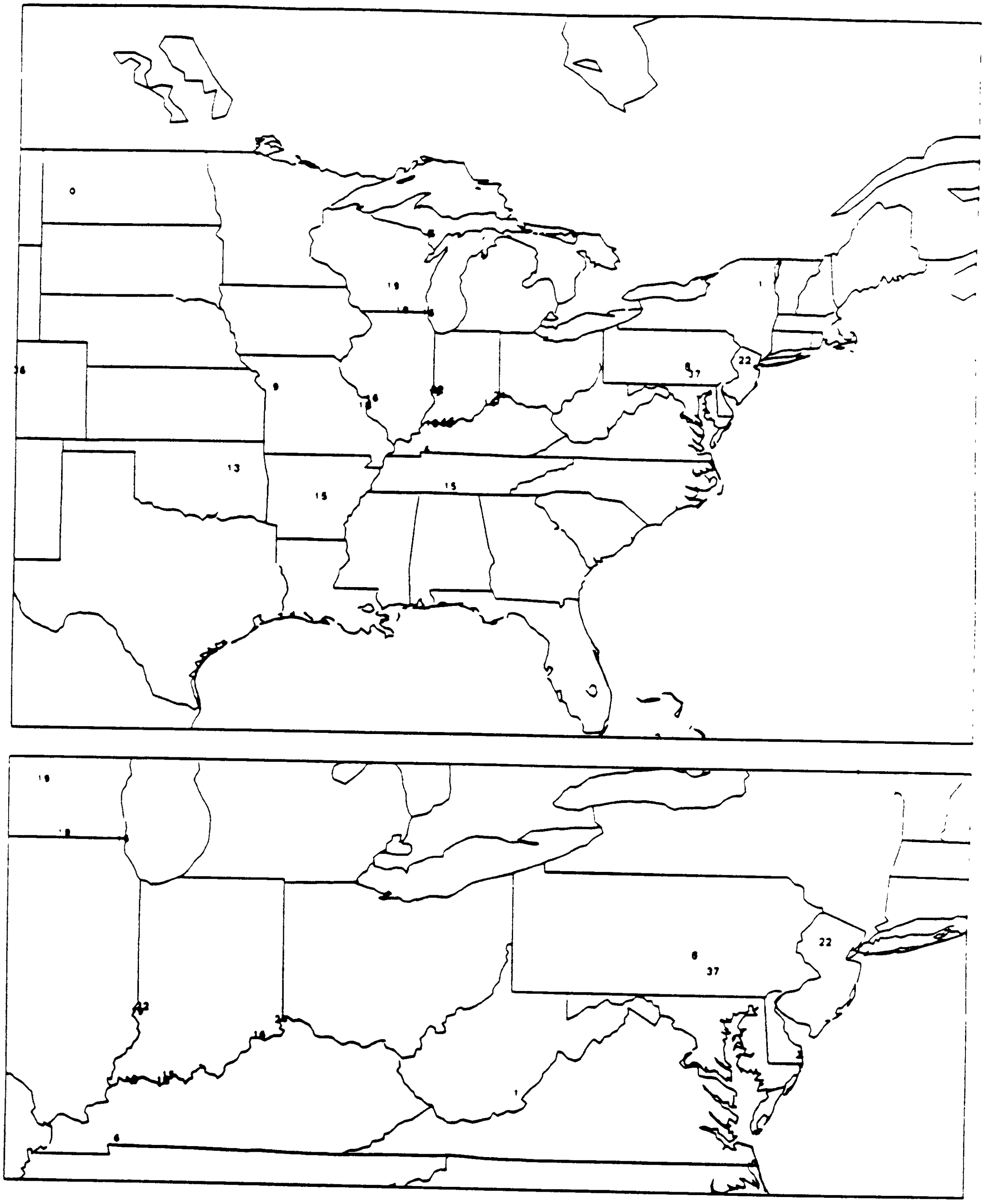

Fig. 2.22 1985 Seasonal Average NO_2 Concentrations at Rural Monitoring Sites ($\mu g\ m^{-3}$).

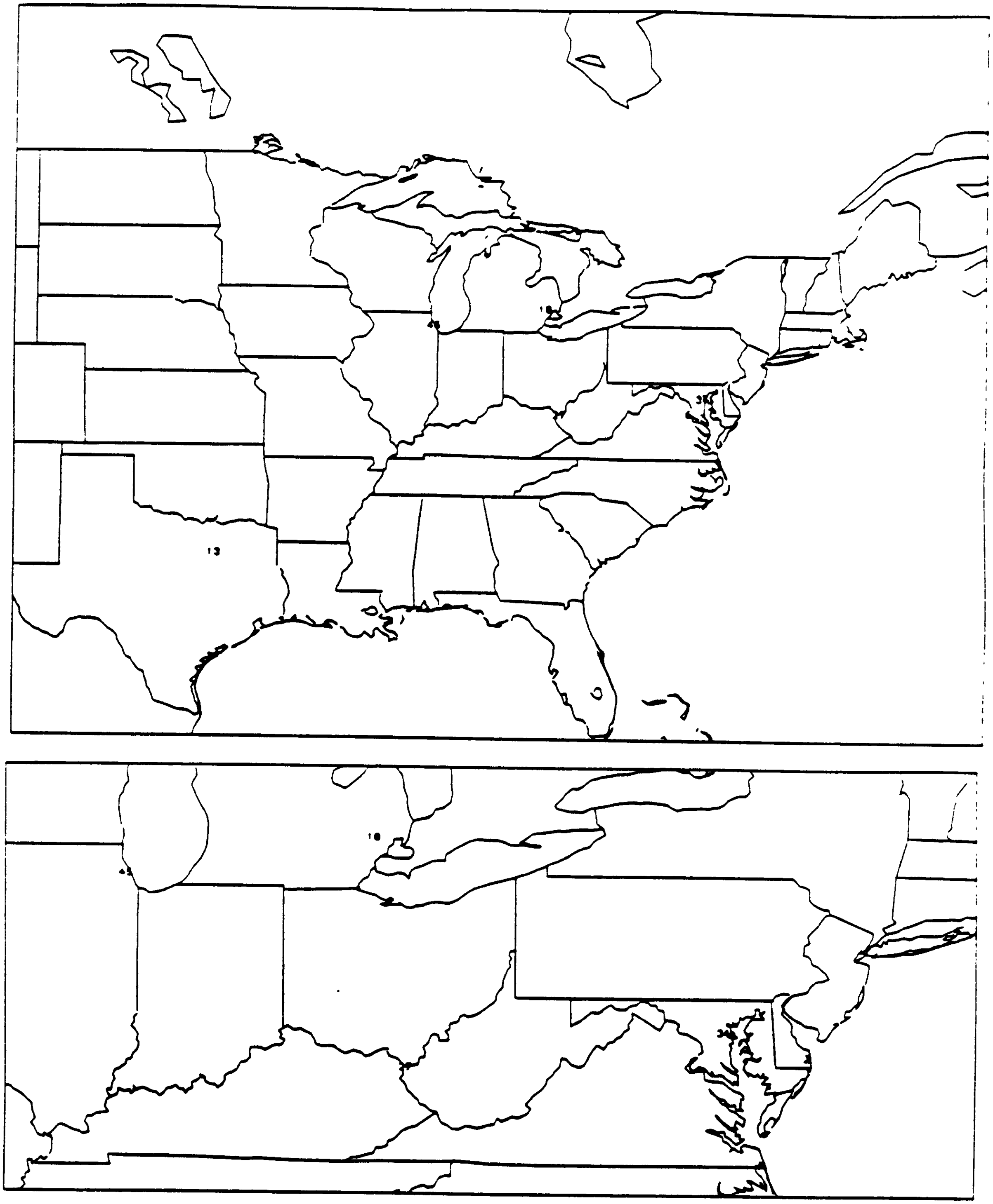

Fig. 2.23 1985 Seasonal Average NO_2 Concentrations at Unclassified Monitoring Sites ($\mu g\, m^{-3}$).

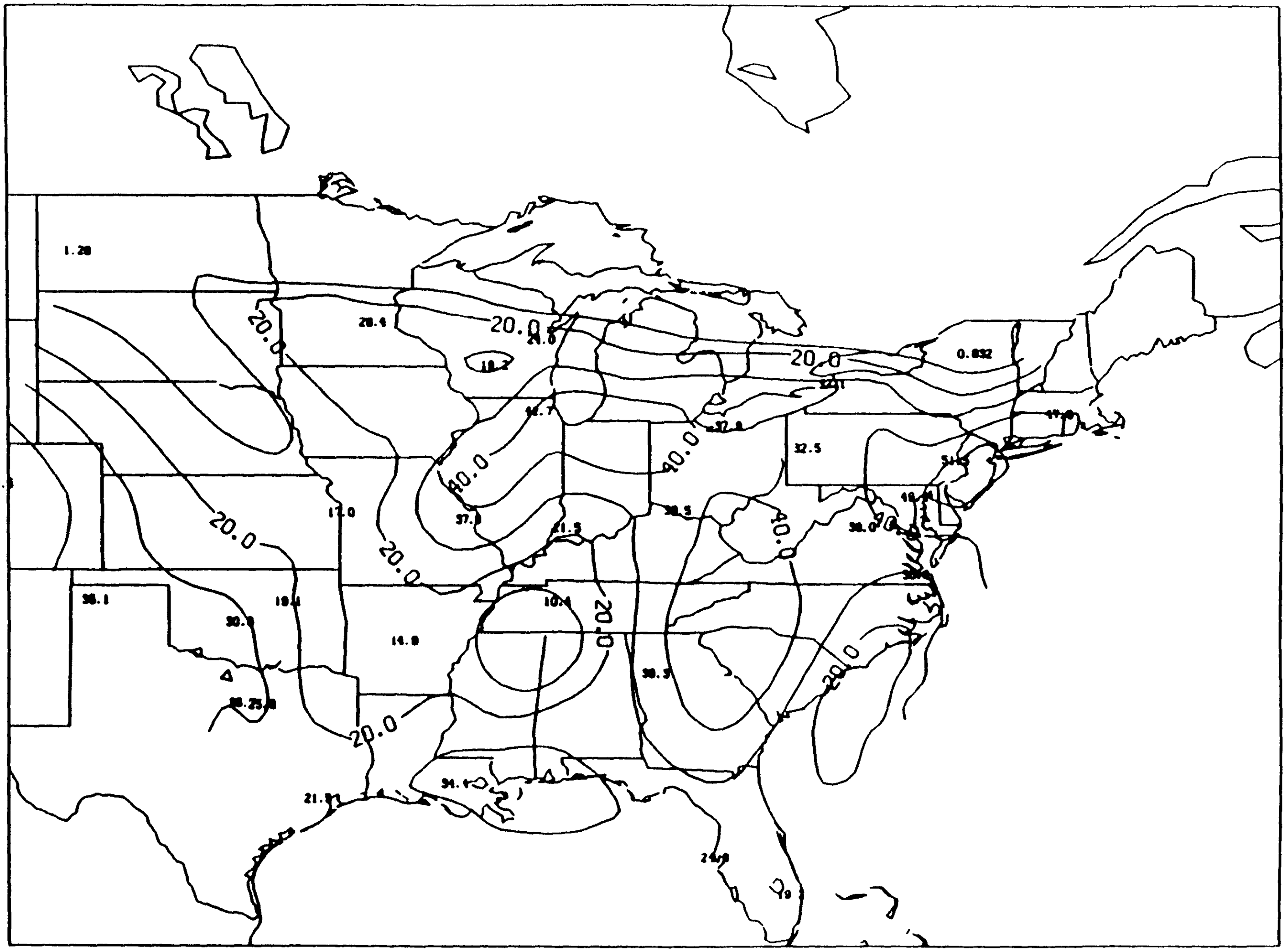

Fig. 2.24 1985 Seasonal Box Average NO_2 Concentrations ($\mu g\ m^{-3}$). Box size 4° longitude by 3° latitude. Contours from 10 to 50 $\mu g\ m^{-3}$ by 10 $\mu g\ m^{-3}$.

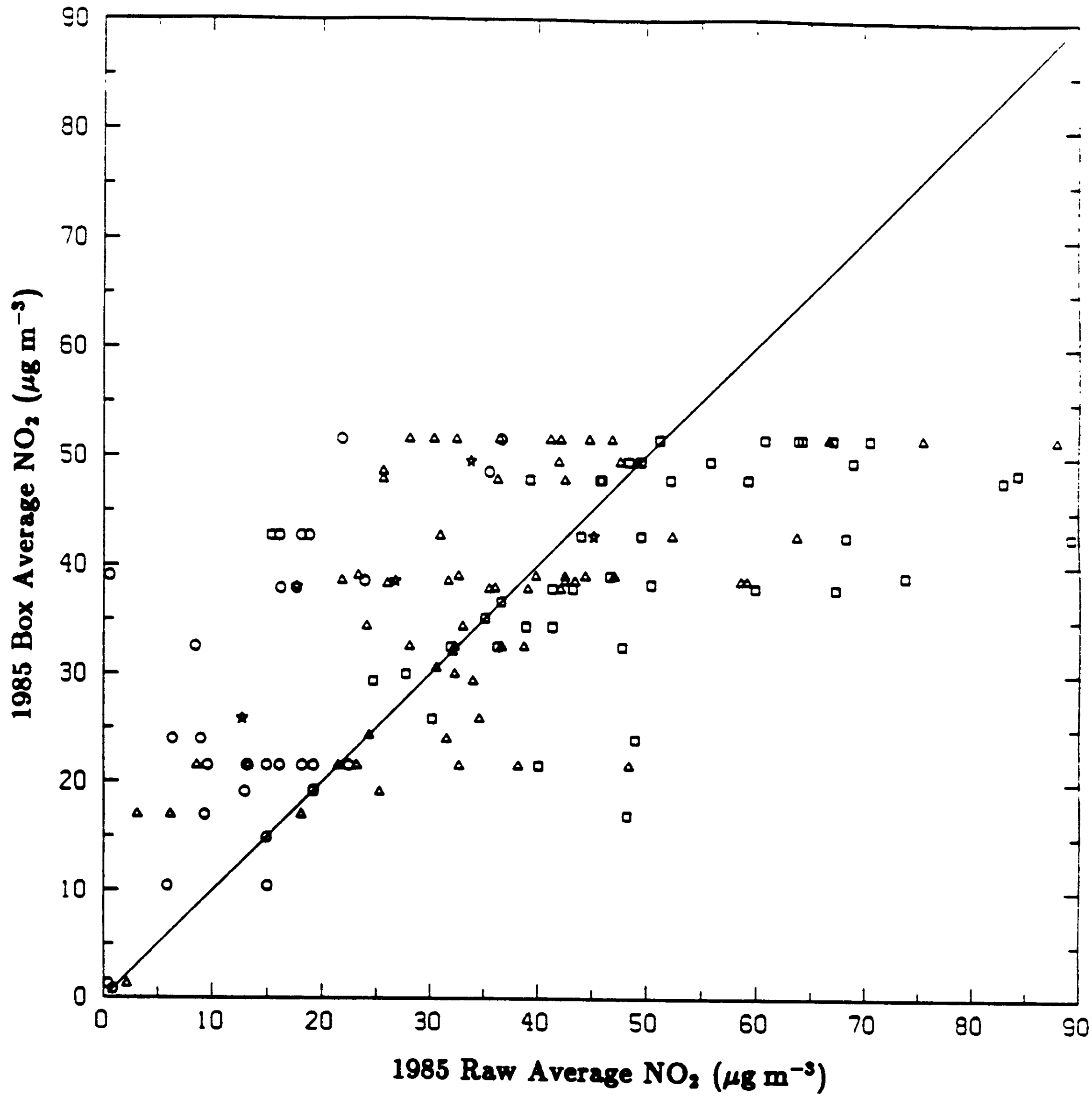

Fig. 2.25 1985 Seasonal Box Average NO_2 vs. Raw Average NO_2 ($\mu g\, m^{-3}$). Square, triangle, circle and star symbols denote urban, suburban, rural, and unclassified monitors. Correlation coefficient r=0.65.

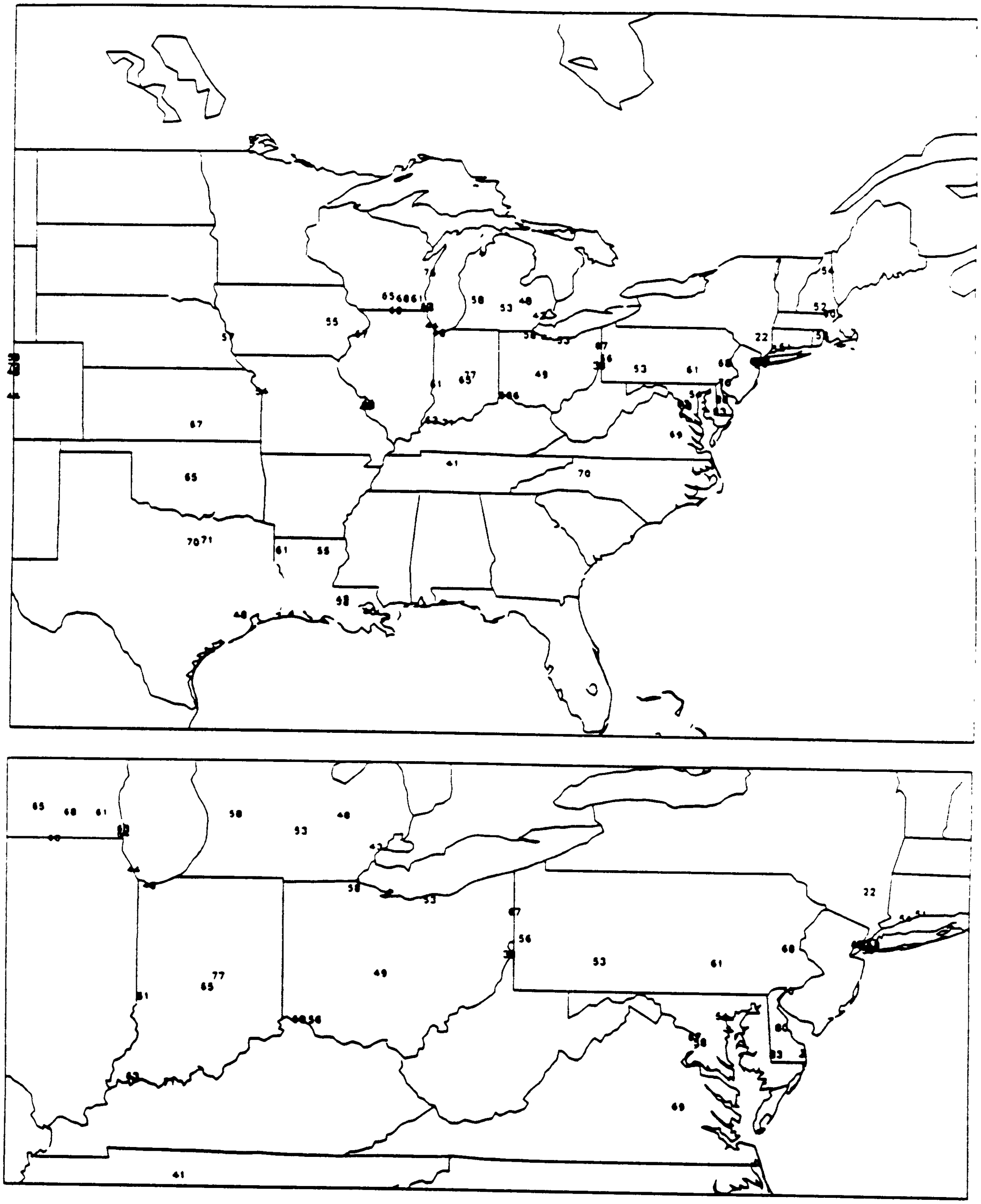

Fig. 2.26 1985 Seasonal Average Ozone Concentrations at Urban Monitoring Sites ($\mu g\ m^{-3}$).

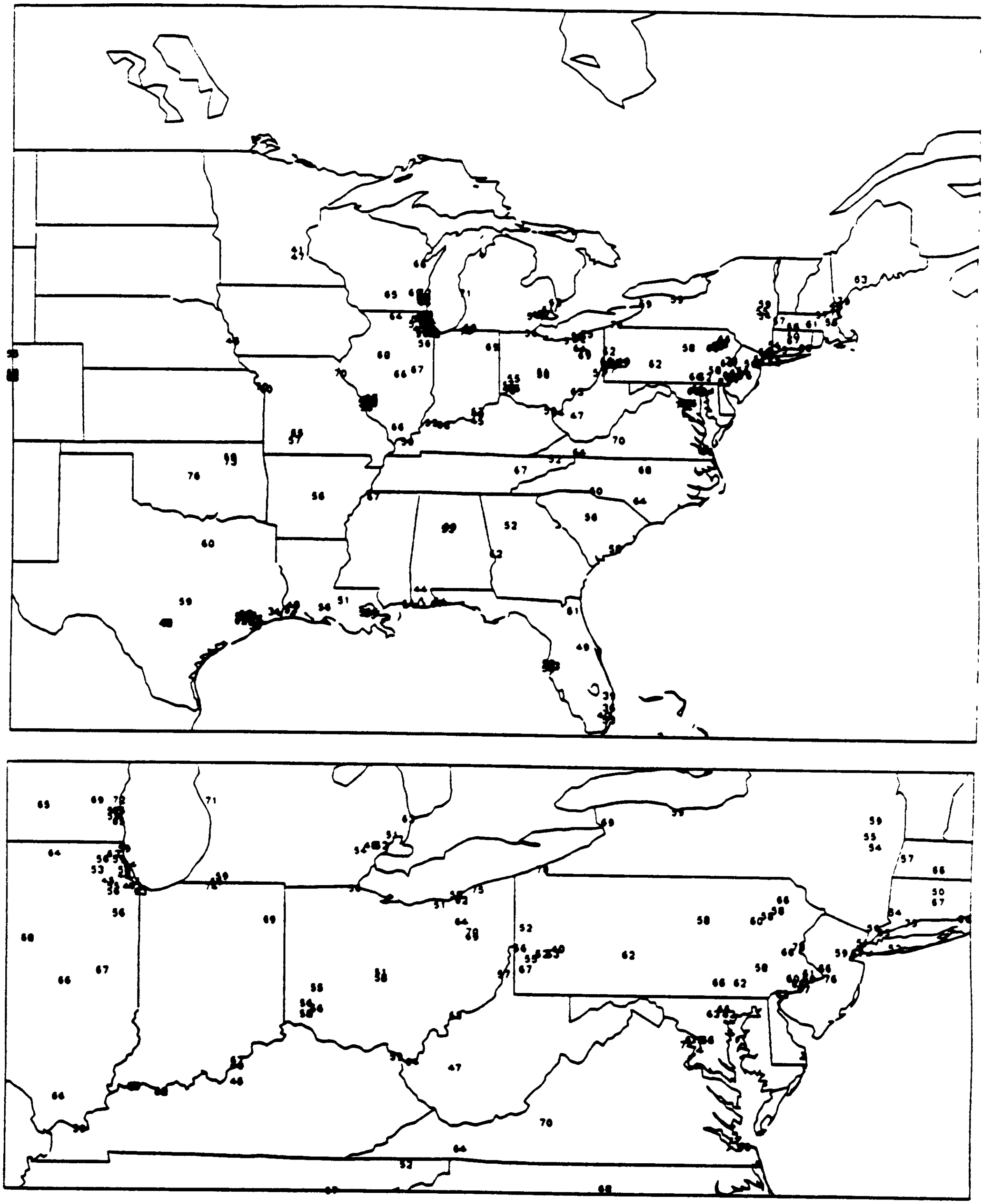

Fig. 2.27 1985 Seasonal Average Ozone Concentrations at Suburban Monitoring Sites ($\mu g\ m^{-3}$).

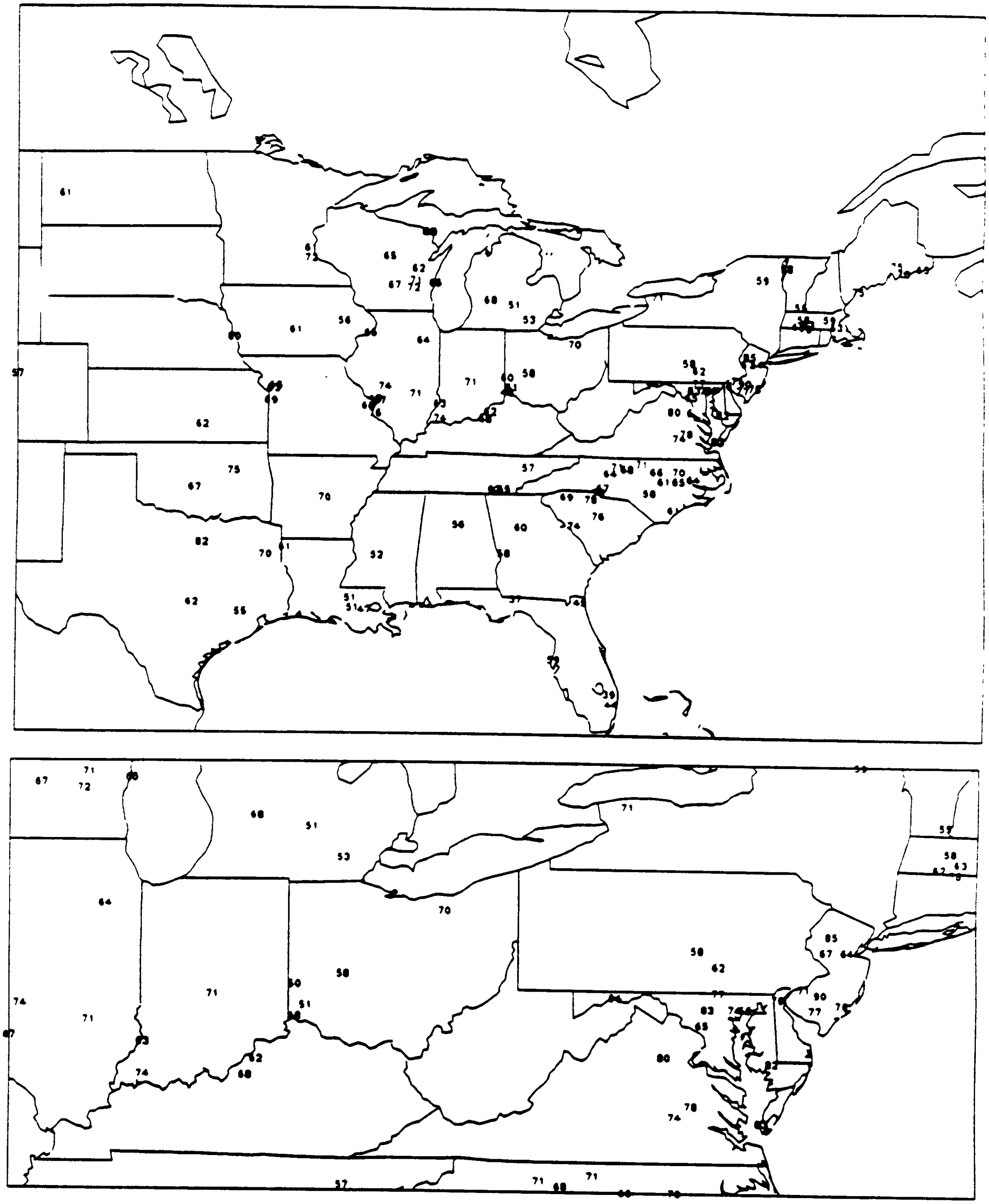

Fig. 2.28 1985 Seasonal Average Ozone Concentrations at Rural Monitoring Sites ($\mu g\ m^{-3}$).

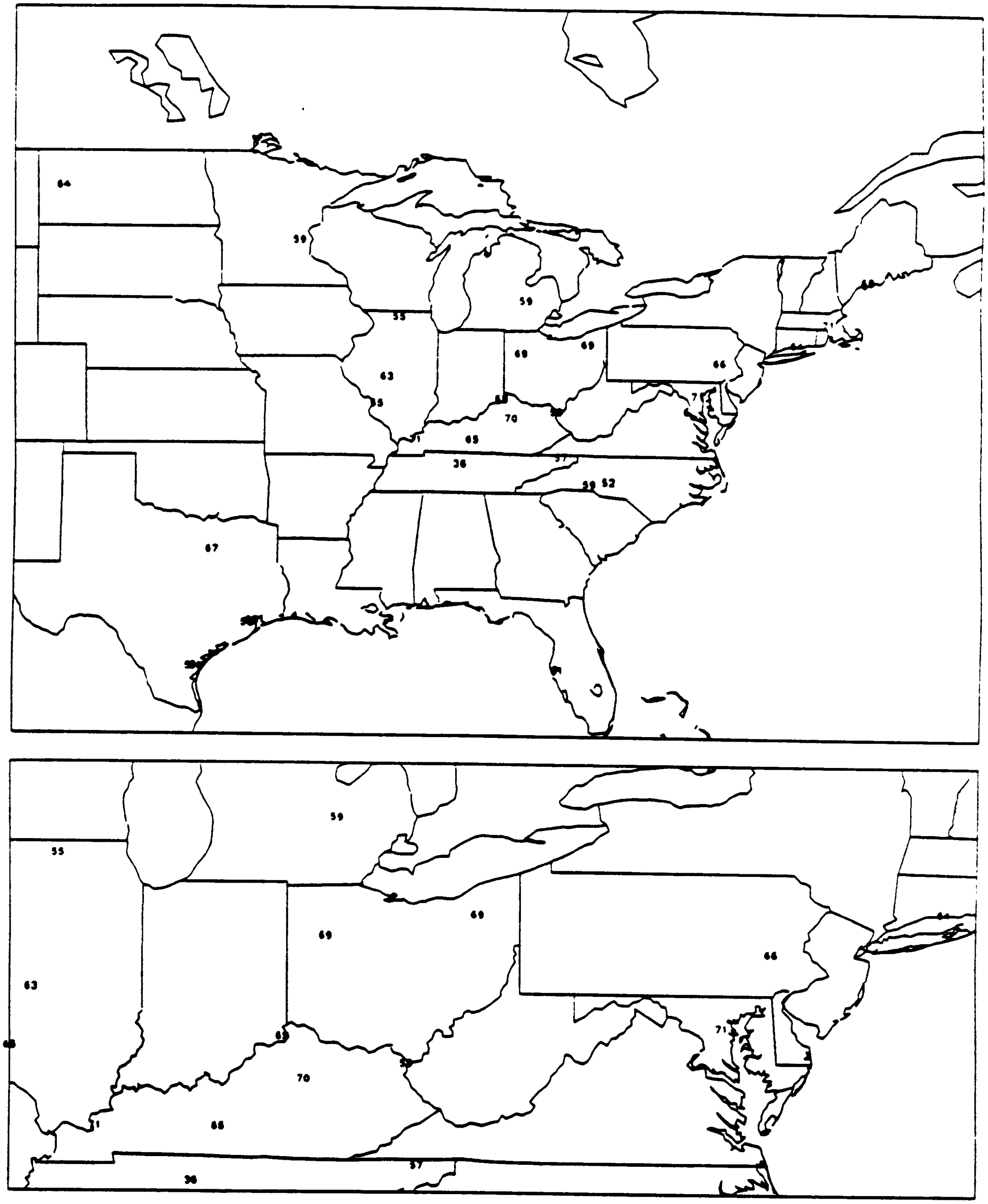

Fig. 2.29 1985 Seasonal Average Ozone Concentrations at Unclassified Monitoring Sites ($\mu g\, m^{-3}$).

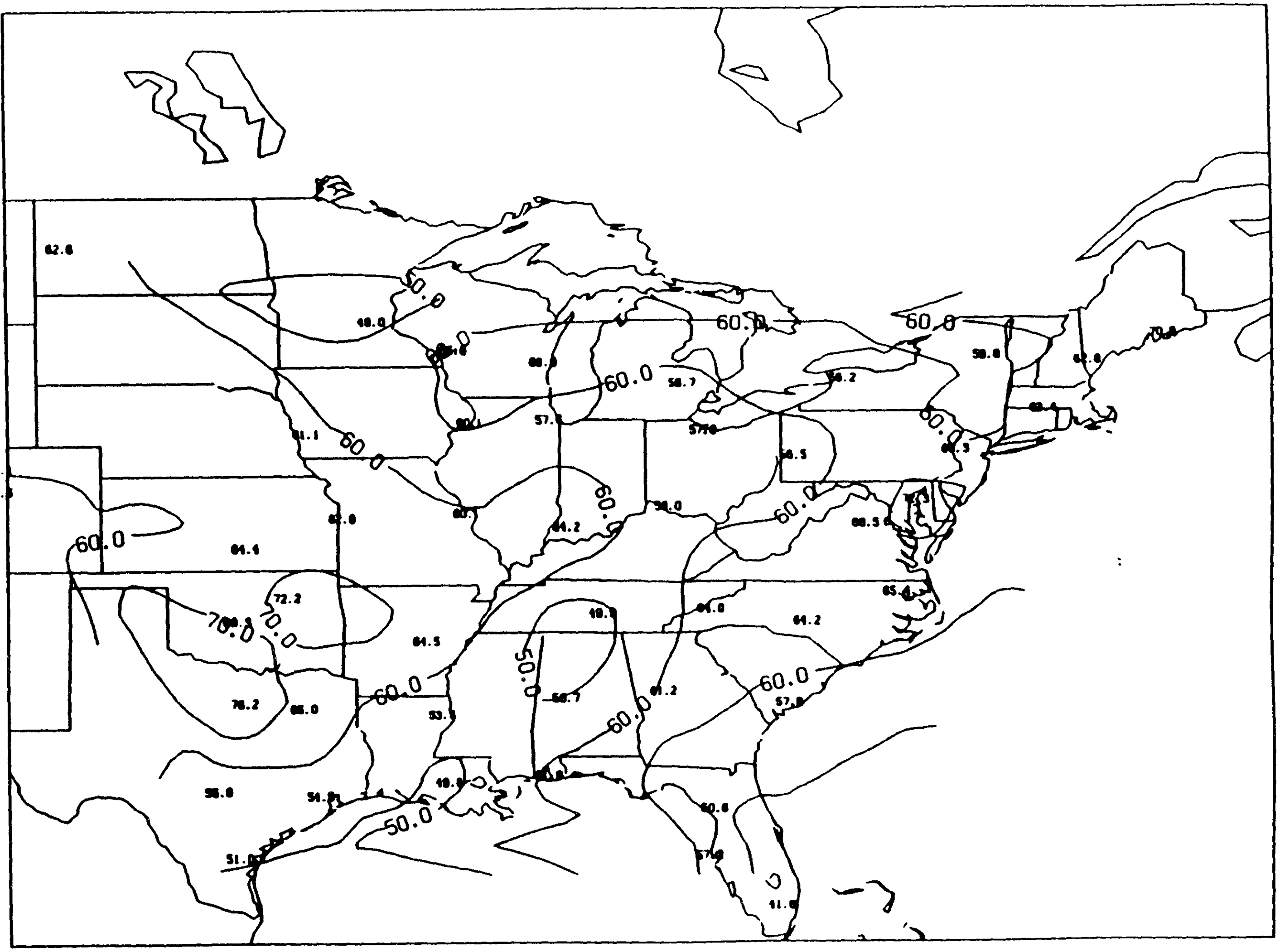

Fig. 2.30 1985 Seasonal Box Average Ozone Concentrations ($\mu g\, m^{-3}$). Box size 4° longitude by 3° latitude. Contours from 50 to 70 $\mu g\, m^{-3}$ by 10 $\mu g\, m^{-3}$.

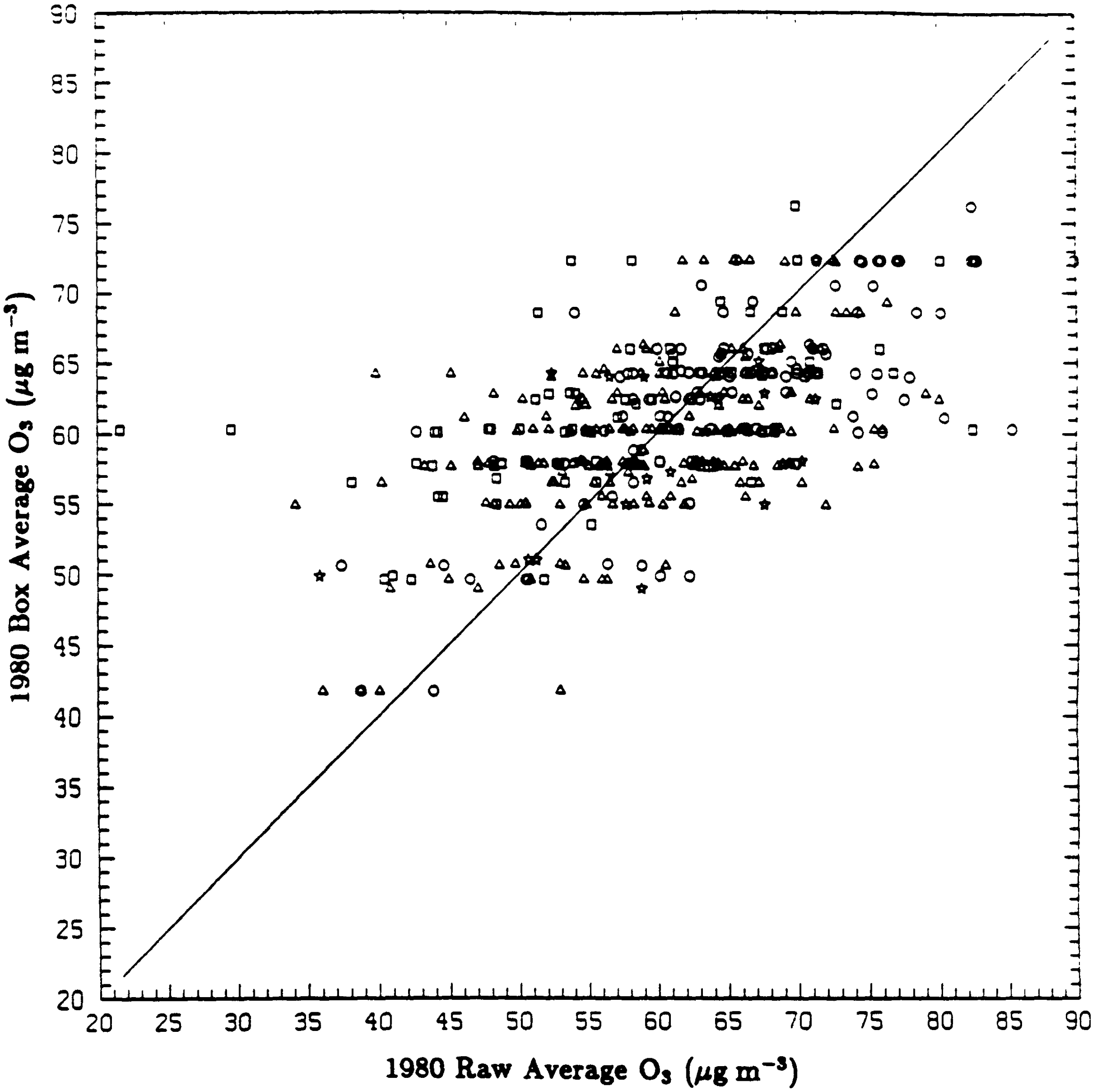

Fig. 2.31 **1985 Seasonal Box Average Ozone vs. Raw Average Ozone (μg m^{-3}). Square, triangle, circle and star symbols denote urban, suburban, rural, and unclassified monitors. Correlation coefficient r=0.59.**

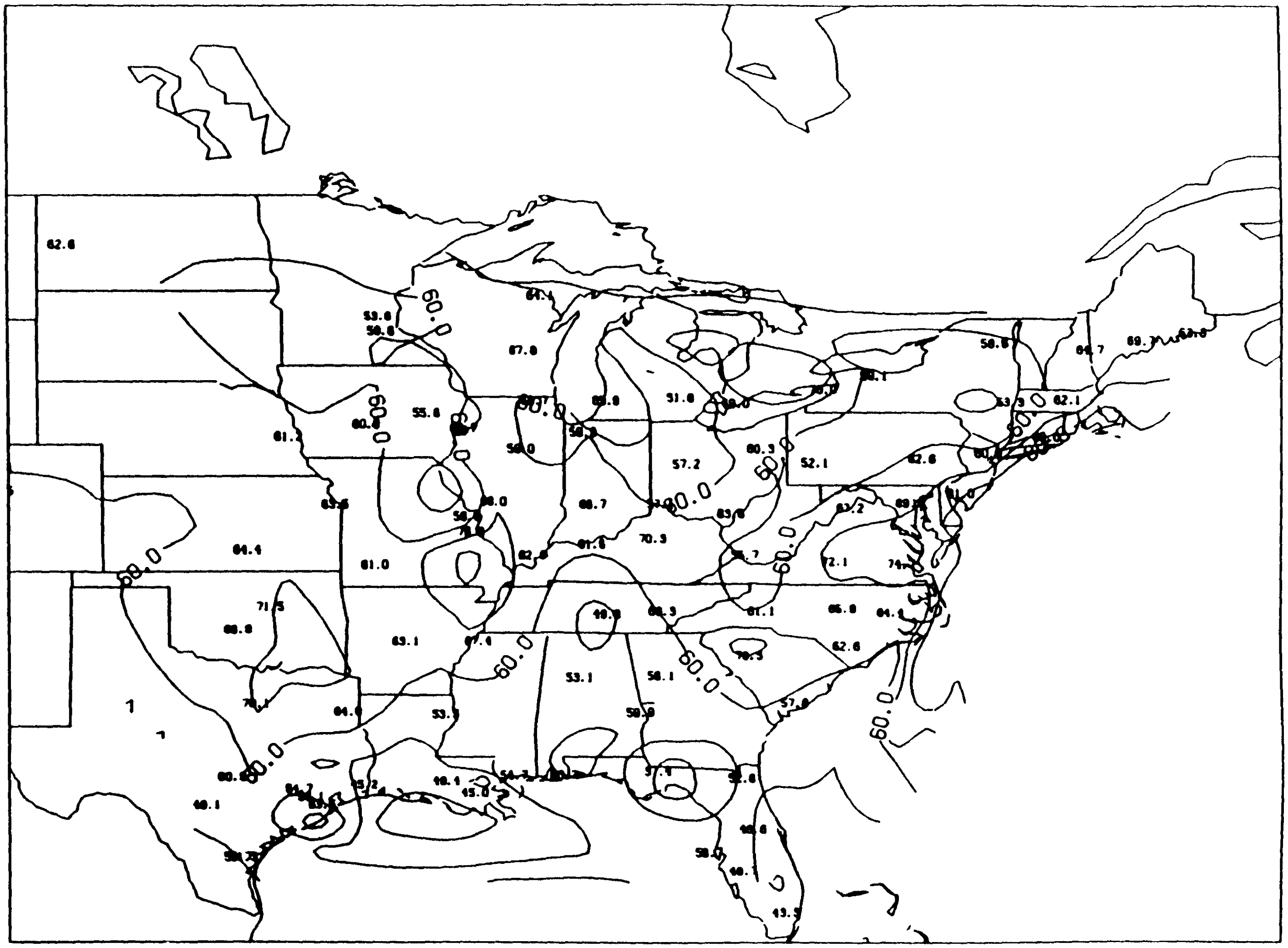

Fig. 2.32 1985 Seasonal Box Average Ozone Concentrations ($\mu g\, m^{-3}$). Box size $2\frac{1}{2}^{\circ}$ longitude by $1\frac{2}{3}^{\circ}$ latitude. Contours from 40 to 80 $\mu g\, m^{-3}$ by 10 $\mu g\, m^{-3}$.

Fig. 2.33 1985 Seasonal Average Ozone Concentrations at Remote Monitoring Sites as Idenitified by Meyer [28] ($\mu g\ m^{-3}$).

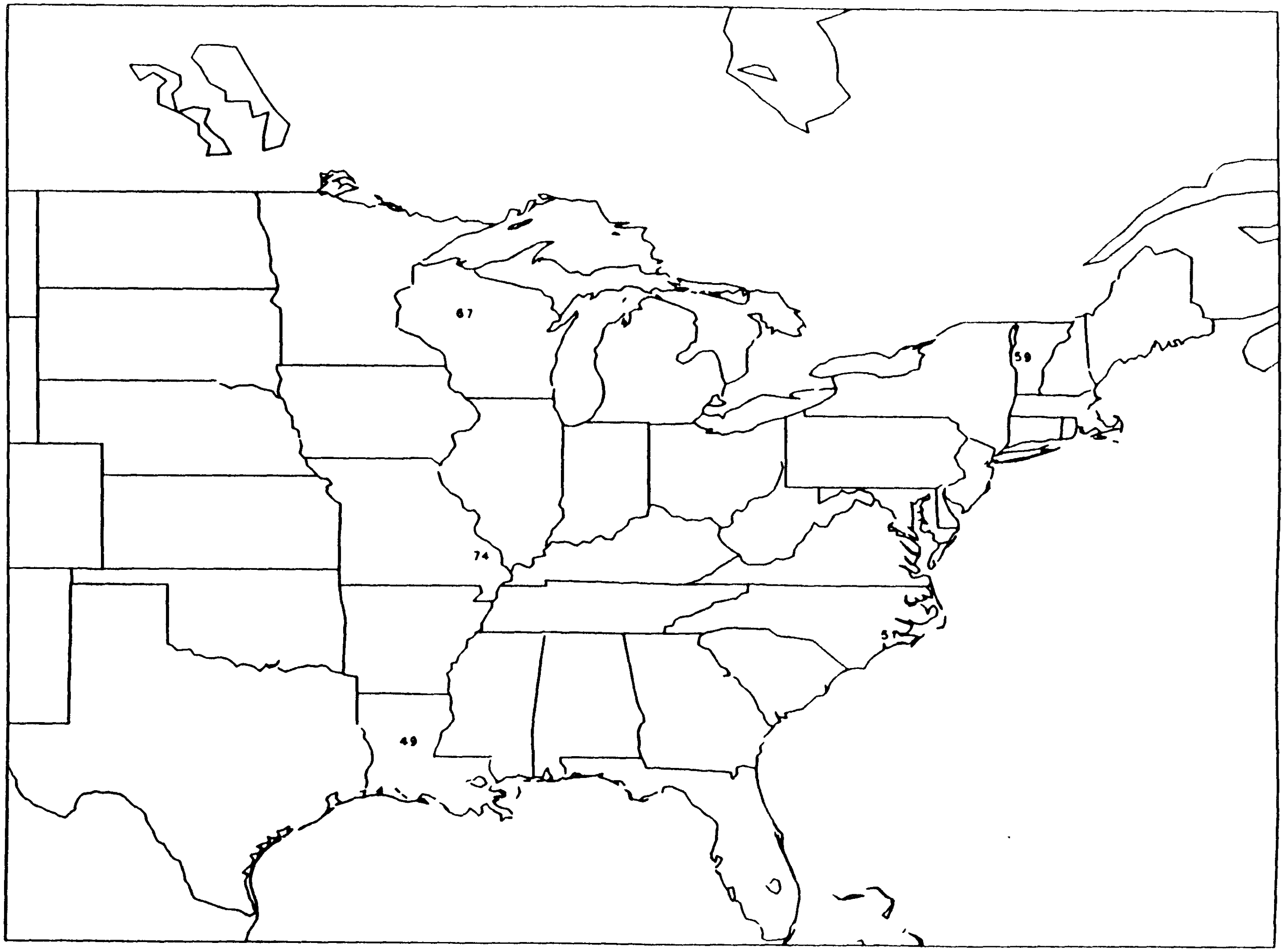

Fig. 2.34 1979 Annual Average Ozone Concentrations at Remote National Park Sites [30] ($\mu g\ m^{-3}$).

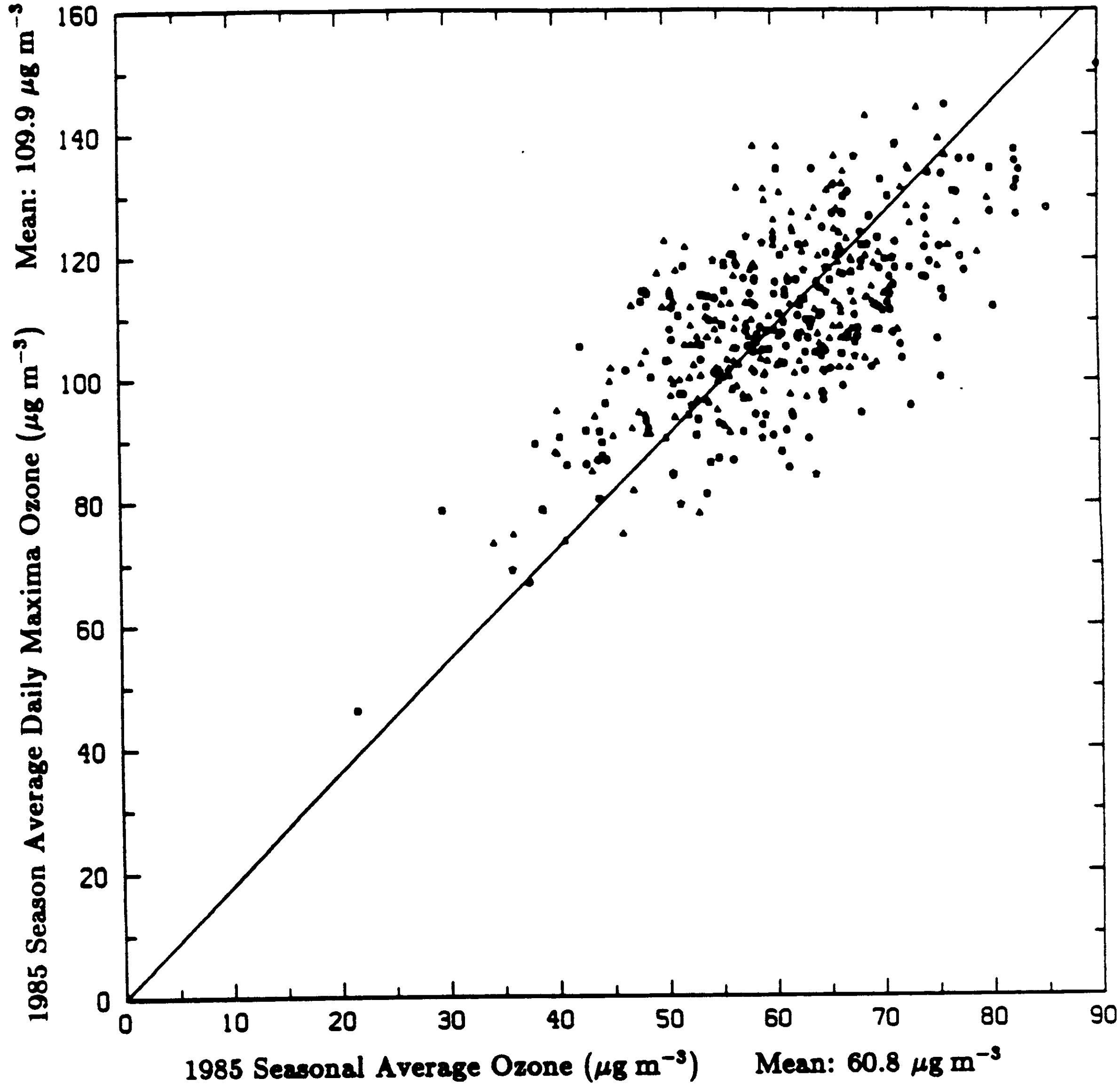

Fig. 2.35 1985 Seasonal Average Daily Maxima Ozone Concentrations vs. 1985 Seasonal Average Ozone Concentrations (μg m^{-3}). Square, triangle, circle and star symbols designate urban, suburban, rural, and unknown site classifications. Correlation coefficient r=0.69.

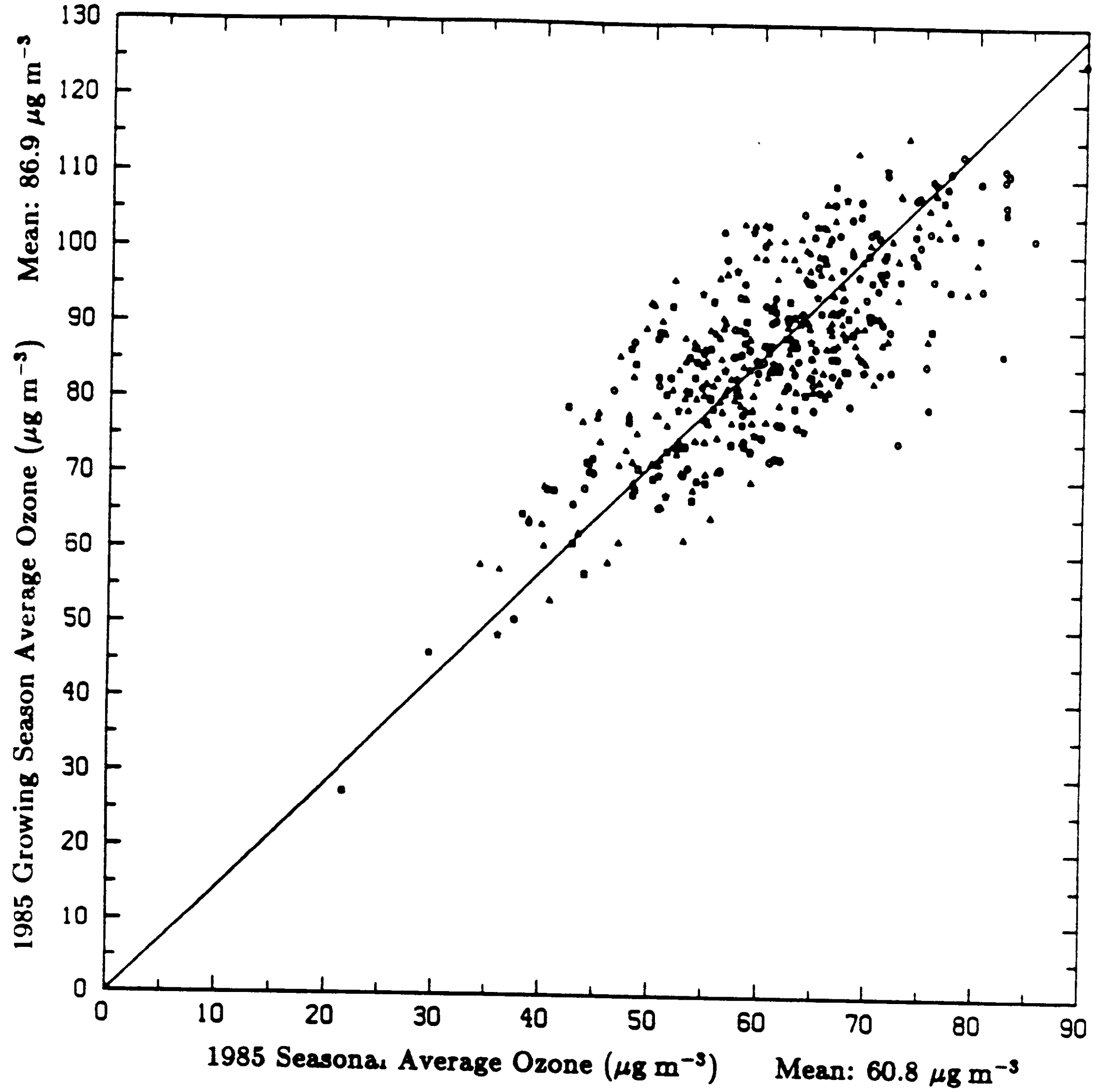

Fig. 2.36 1985 Seasonal 7-Hour Growing Season Average Concentrations vs. 1985 Seasonal Average Ozone Concentrations ($\mu g\ m^{-3}$). Growing season hours 9:00 AM to 4:00 PM. Square, triangle, circle and star symbols designate urban, suburban, rural, and unknown site classifications. Correlation coefficient r=0.76.

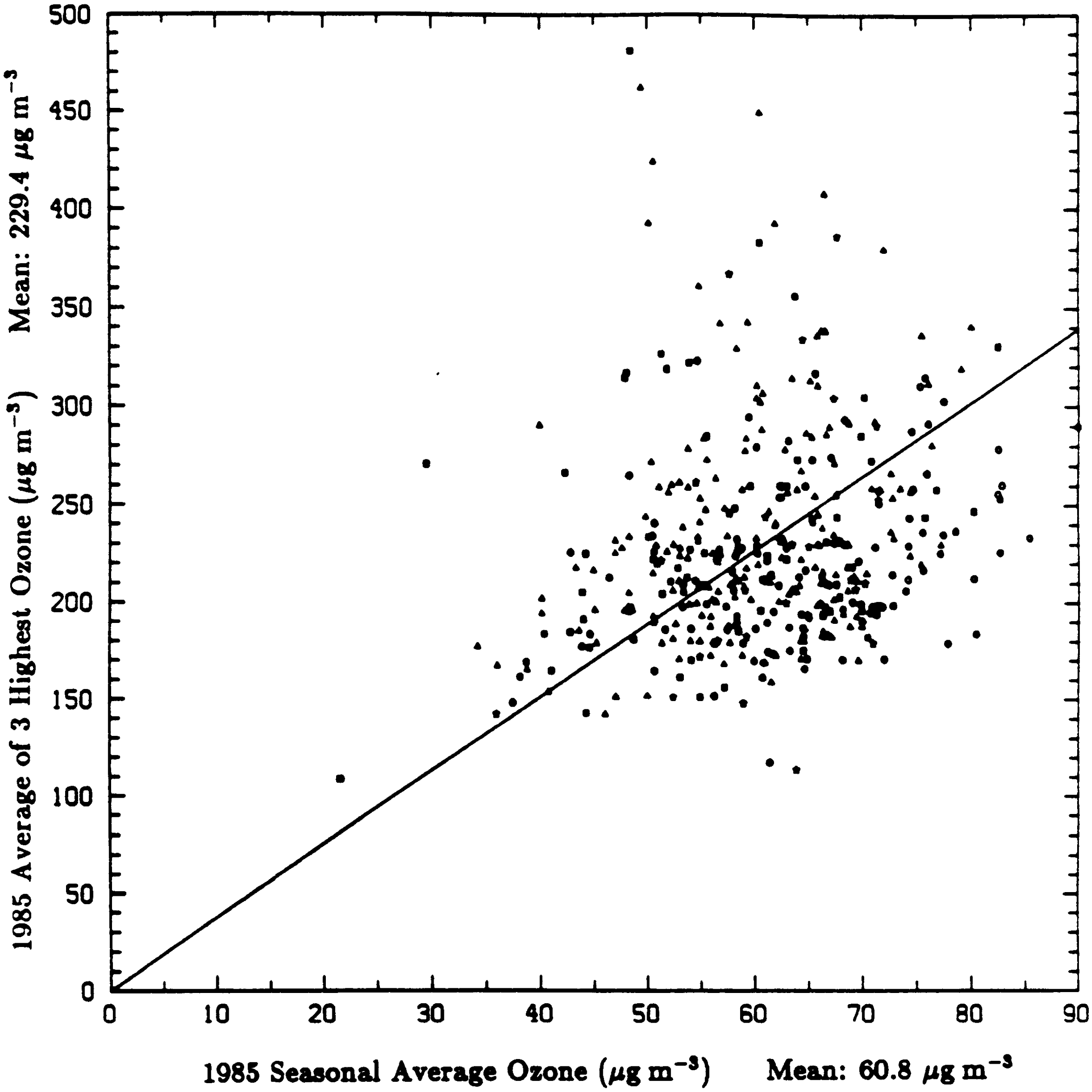

Fig. 2.37 1985 Average of 3 Highest Ozone Concentrations vs. 1985 Seasonal Average Ozone Concentrations ($\mu g\, m^{-3}$). Square, triangle, circle and star symbols designate urban, suburban, rural, and unknown site classifications. Correlation coefficient r=0.21. April- September data.

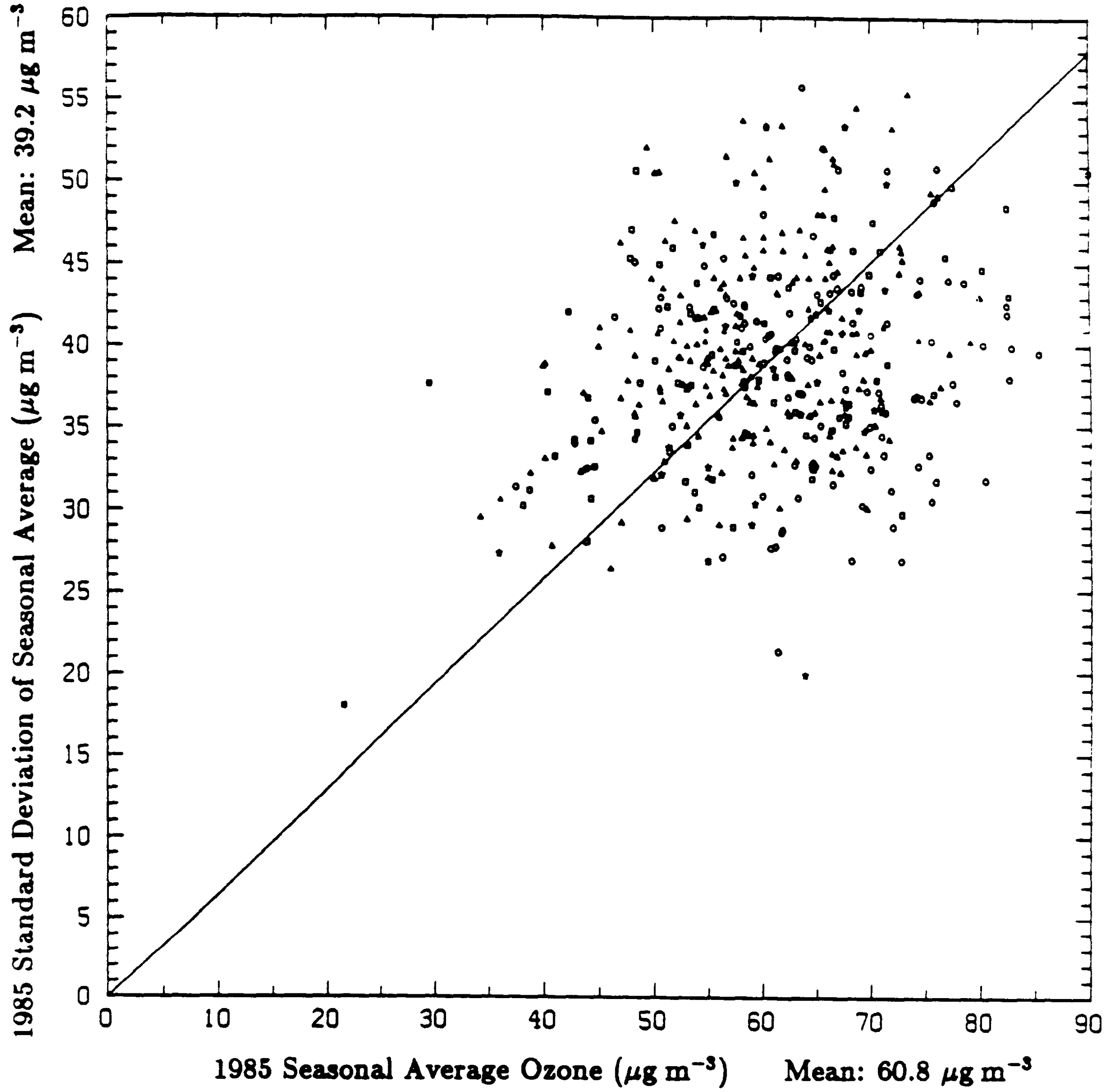

Fig. 2.38 1985 Standard Deviation of Seasonal Average Ozone vs. 1985 Seasonal Average Ozone Concentrations (μg m^{-3}). Square, triangle, circle and star symbols designate urban, suburban, rural, and unknown site classifications. Same data as Fig. 2.38. Correlation coefficient r=0.23.

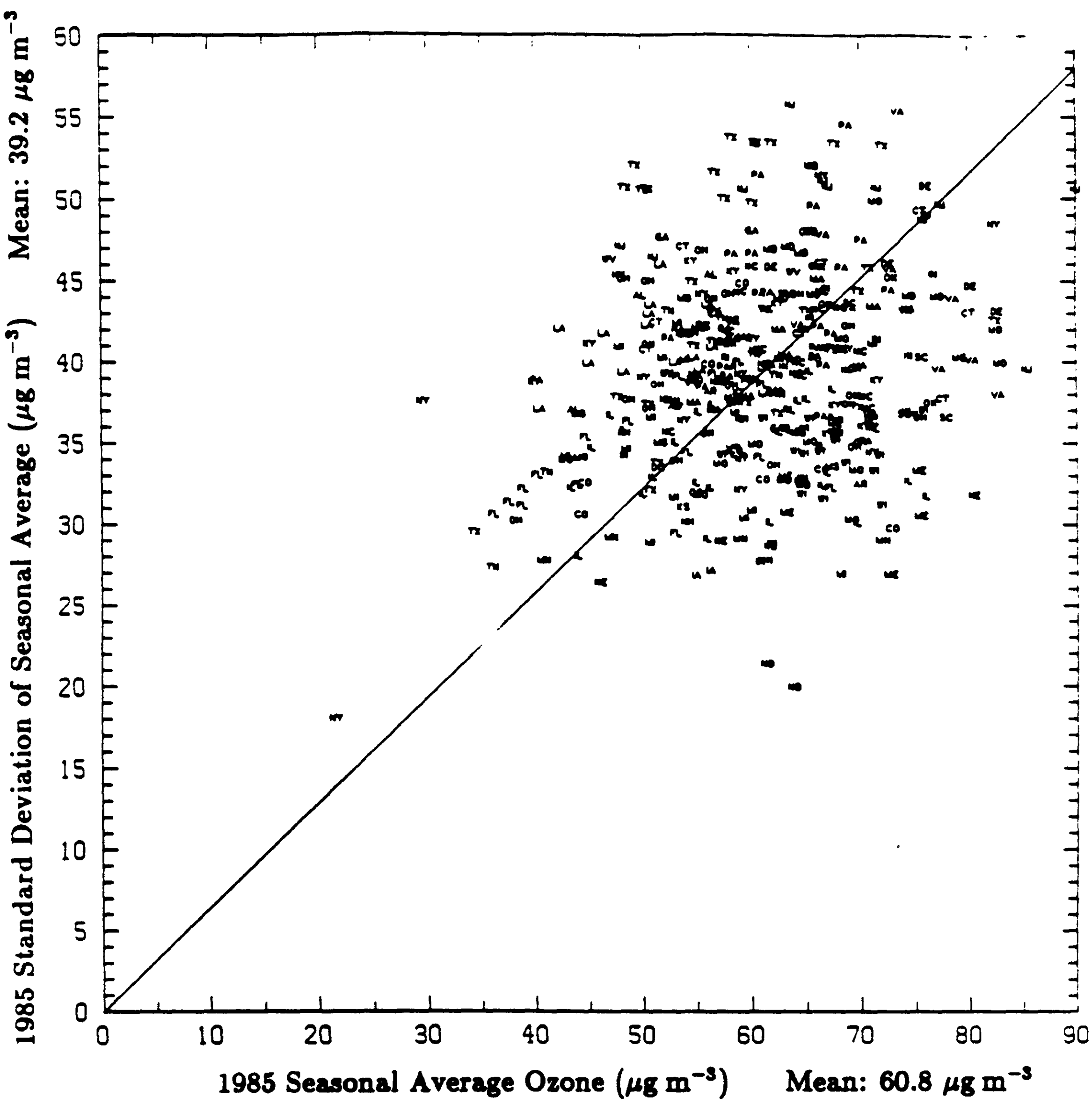

Fig. 2.39 1985 Standard Deviation of Seasonal Average Ozone vs. 1985 Seasonal Average Ozone Concentrations (μg m^{-3}). Two letter abbreviations denote the state in which the monitor is located. Same data as Fig. 2.38. Correlation coefficient r=0.23.

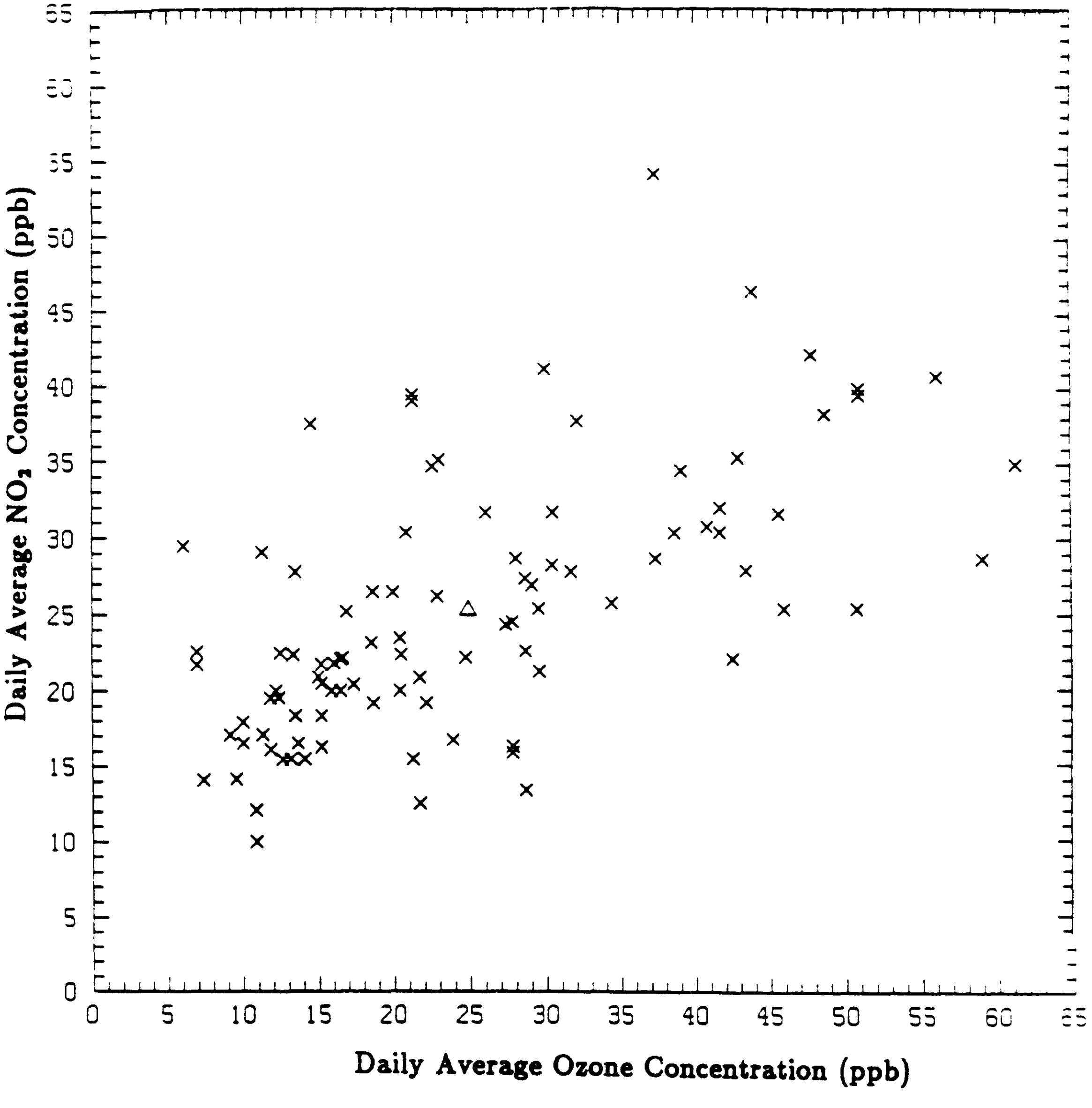

Fig. 2.40 Daily Average NO_2 Concentration vs. Daily Average Ozone Concentration (ppb) at an urban site in Houston, TX. Triangle denotes the mean concentrations. 1985 April-September data. Correlation coefficient r=0.62.

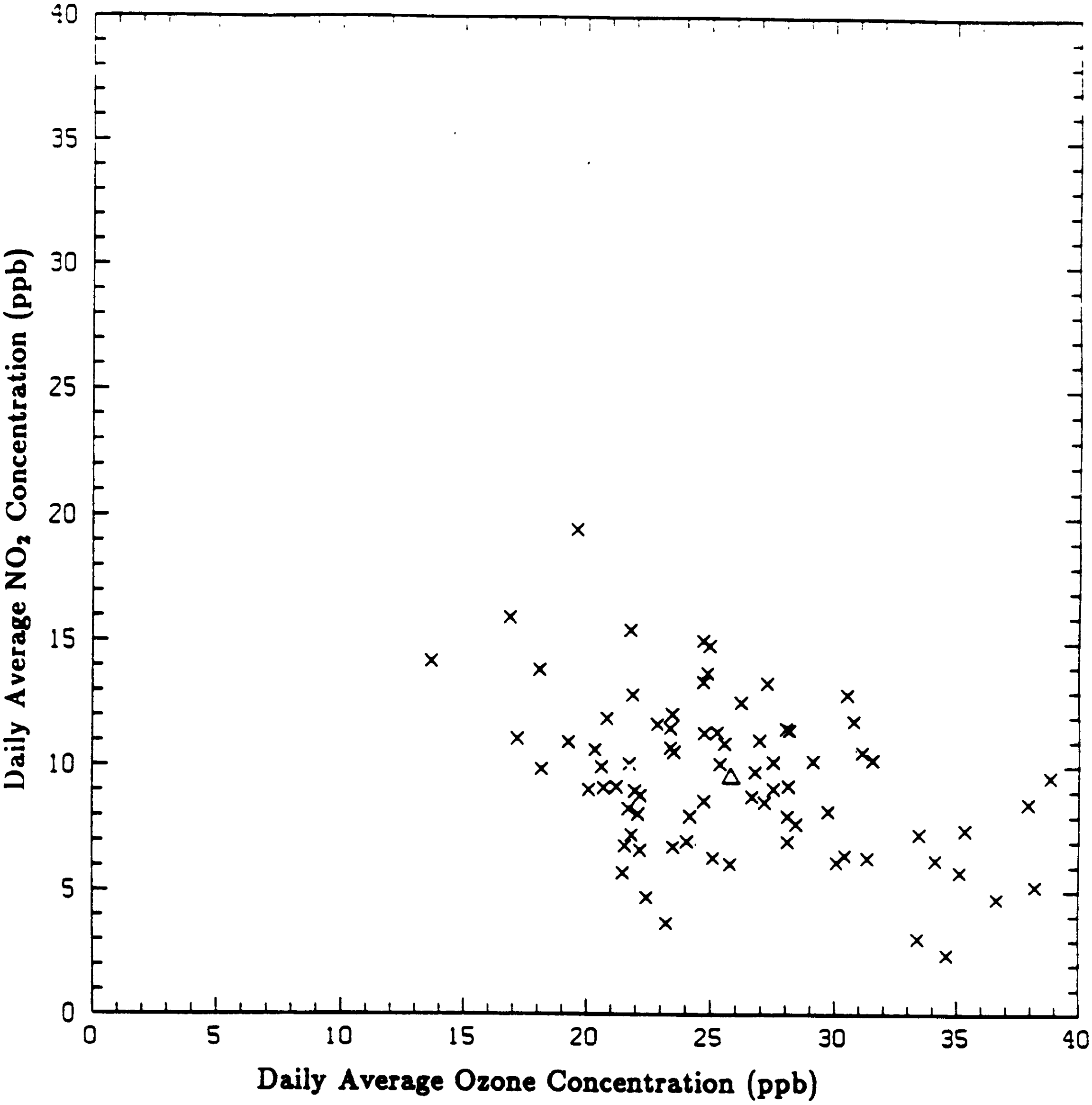

Fig. 2.41 Daily Average NO_2 Concentration vs. Daily Average Ozone Concentration (ppb) at an urban site in Colorado Springs, CO. Triangle denotes the mean concentrations. 1985 April-September data. Correlation coefficient r=-0.44.

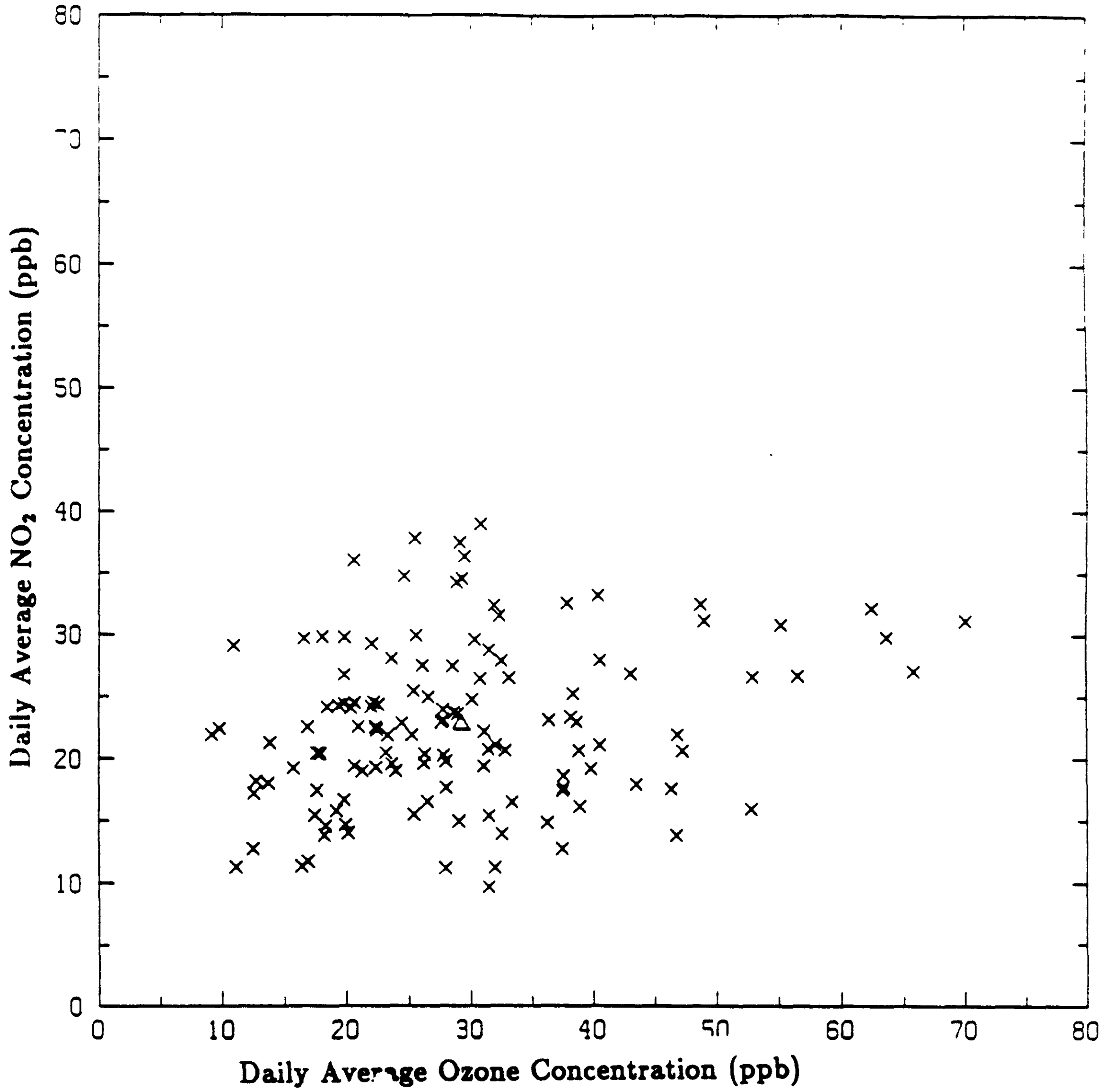

Fig. 2.42 Daily Average NO_2 Concentration vs. Daily Average Ozone Concentration (ppb) at an suburban site in Chelsea, MA. Triangle denotes the mean concentrations. 1985 April-September data. Correlation coefficient r=0.23.

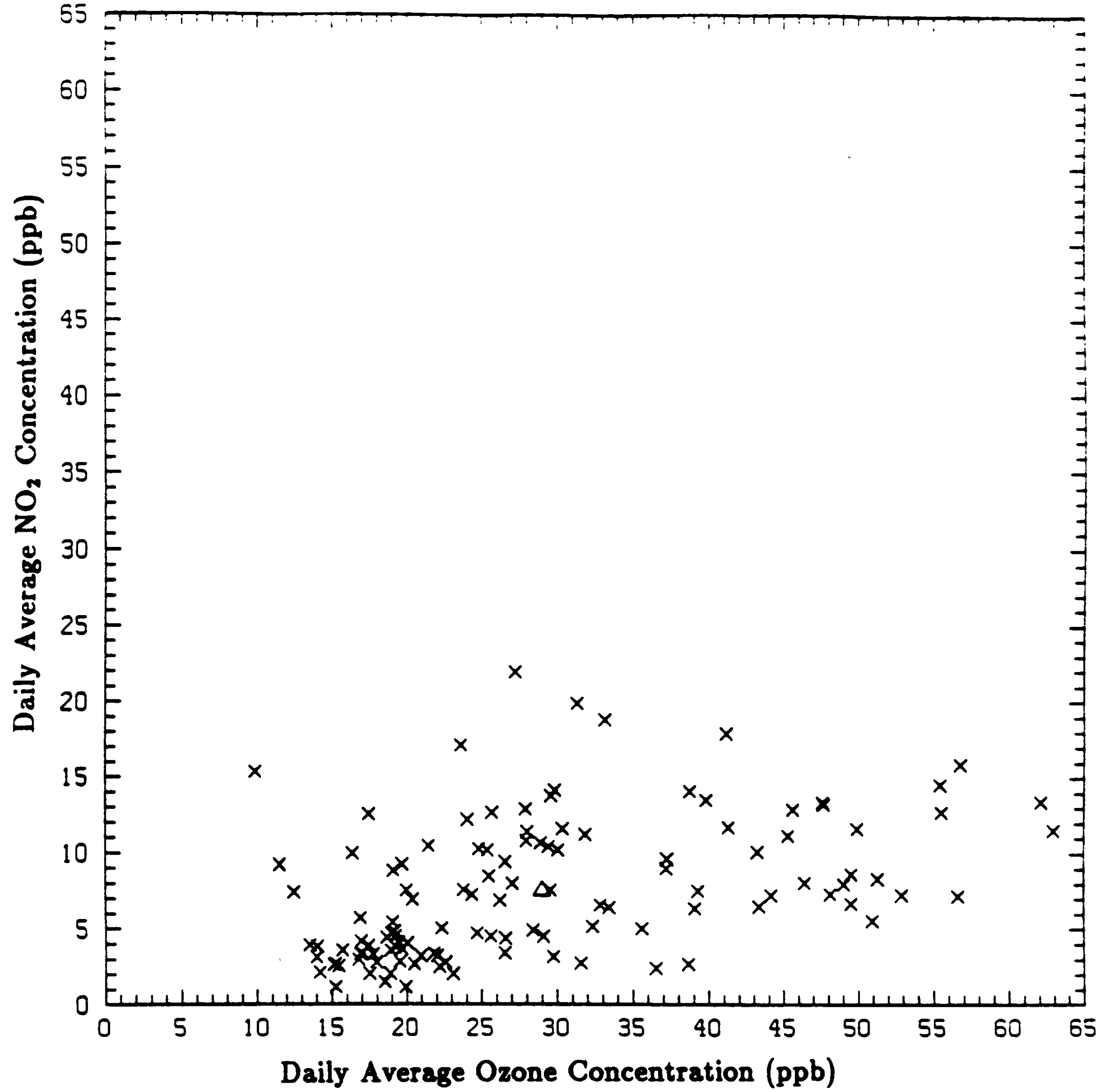

Fig. 2.43 Daily Average NO_2 Concentration vs. Daily Average Ozone Concentration (ppb) at an suburban site in Florida. Triangle denotes the mean concentrations. 1985 April-September data. Correlation coefficient r=0.45.

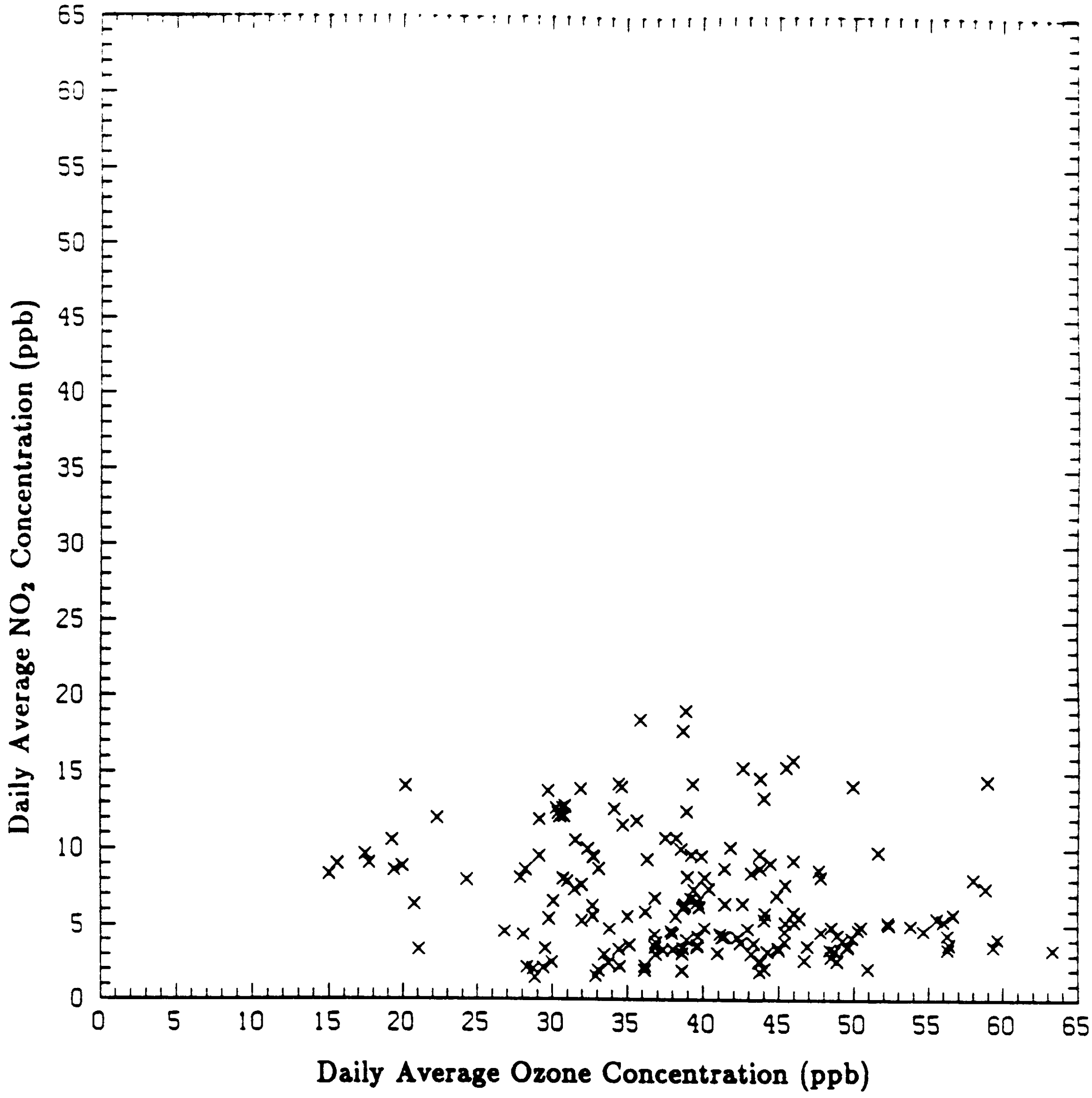

Fig. 2.44 Daily Average NO_2 Concentration vs. Daily Average Ozone Concentration (ppb) at an rural site in Oklahoma. Triangle denotes the mean concentrations. 1985 April-September data. Correlation coefficient r=-0.22.

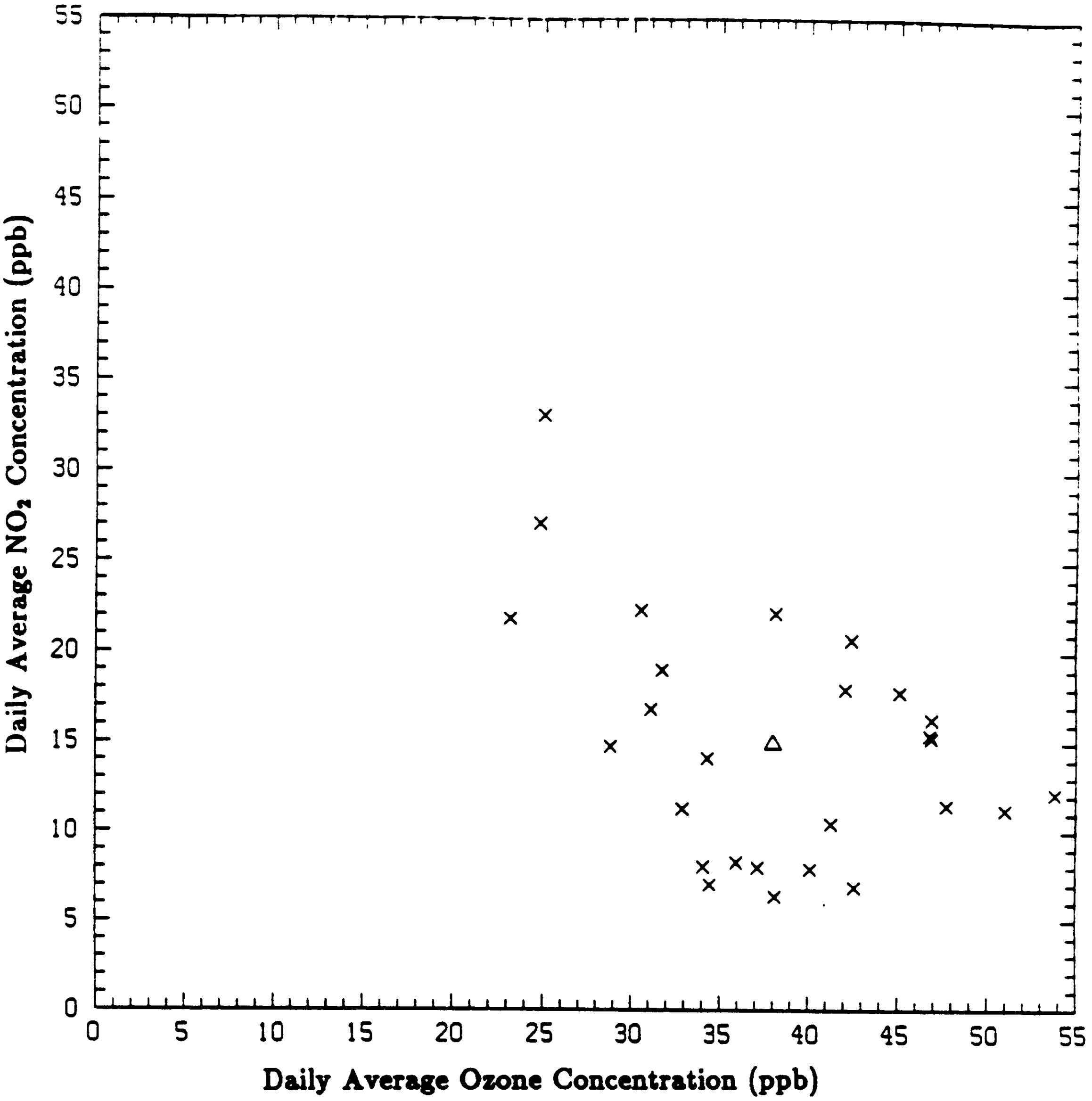

Fig. 2.45 Daily Average NO_2 Concentration vs. Daily Average Ozone Concentration (ppb) at an rural site in Maryland. Triangle denotes the mean concentrations. 1985 April-September data. Correlation coefficient r=-0.43.

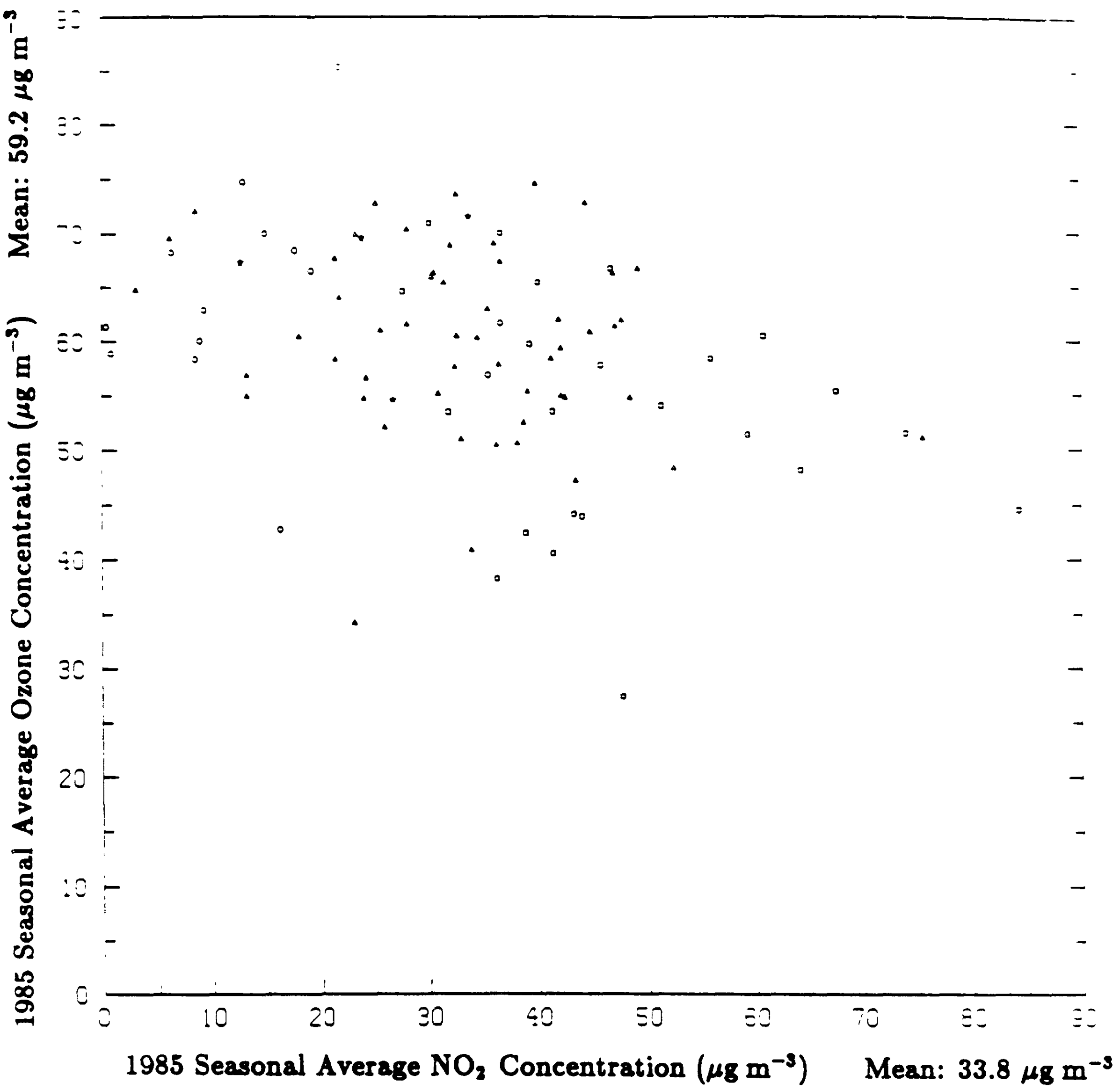

Fig. 2.46 Seasonal Average Ozone Concentration vs. Seasonal Average NO_2 Concentration ($\mu g\,m^{-3}$) at Common Measuring Sites. 1985 April-September data. Square, triangle, circle and star symbols denote urban, suburban, rural and unknown site classifications. Same data as Fig. 2.47. Correlation coefficient r=-0.35.

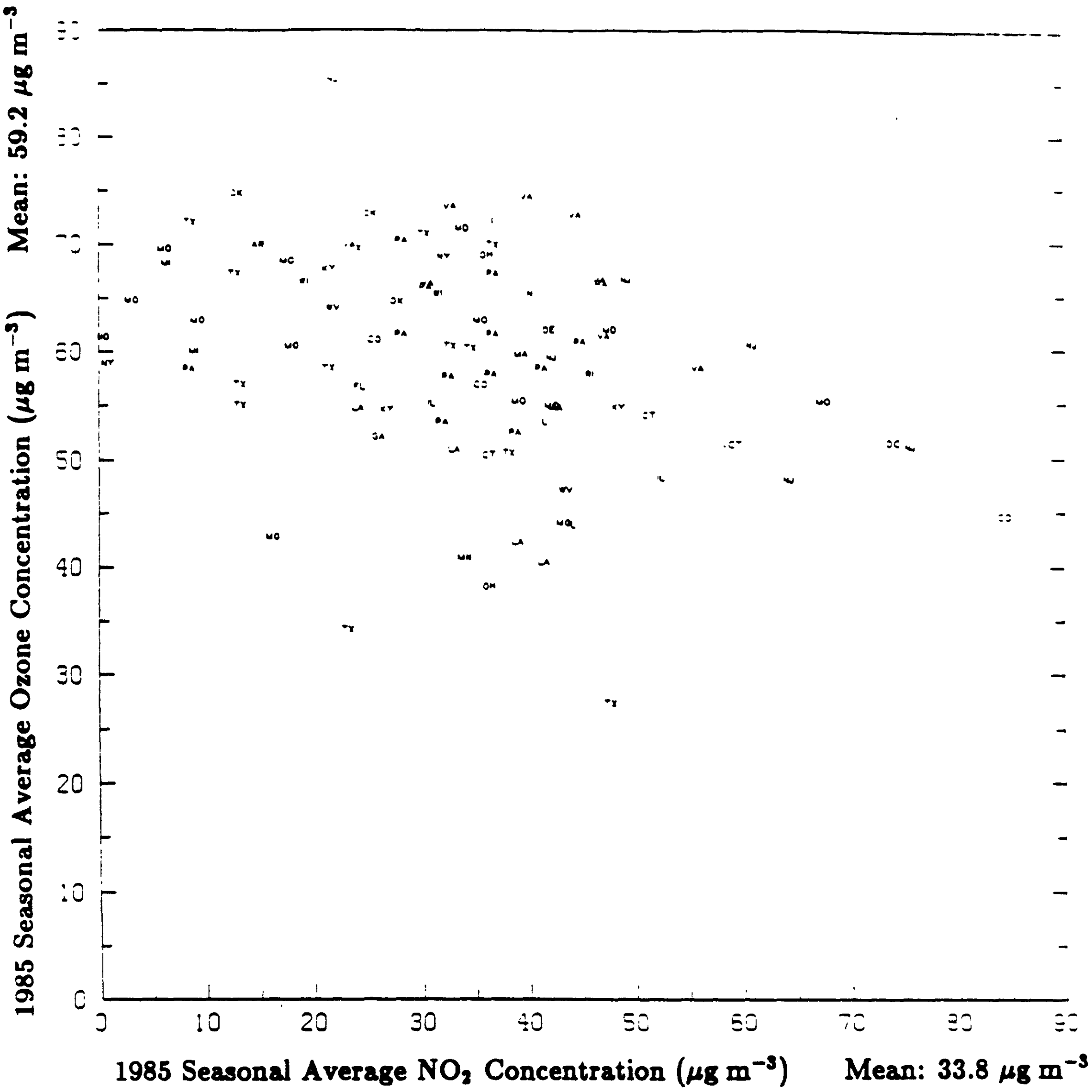

Fig. 2.47 Seasonal Average Ozone Concentration vs. Seasonal Average NO$_2$ Concentration (μg m^{-3}) at Common Measuring Sites. 1985 April-September data. Two letter abbreviations indicate the state in which the site is located. Same data as Fig. 2.46. Correlation coefficient r=-0.35.

Chapter 3

Numerical Dispersion Modeling

3.1 Model Equations

The long range modeling approach employed, adapted from Fay et al. [18,19], is similar for NO_x, VOCs and ozone. The goal is to incorporate the essential physical and chemical processes affecting pollutant dispersion in a simple yet representative manner. Time averaged, steady state conditions are assumed for a single vertically mixed layer. Meteorological transport is modeled by a combination of advection and diffusion terms. Advection is modeled by a resultant wind speed and direction. An isotropic two-dimensional diffusivity coefficient is used to account for both horizontal mixing of pollutants and the variance of winds from the resultant vector throughout the averaging season. A final term, S, denotes the sum of all sources and sinks of the modeled species. In constant radius spherical coordinates, the general transport equation is written as

$$\frac{v_\phi}{r_0}\frac{\partial c}{\partial \phi} + \frac{v_\theta}{r_0 \cos\phi}\frac{\partial c}{\partial \theta} = \frac{1}{r_0^2 \cos\phi}\frac{\partial}{\partial \phi}\left(D\cos\phi\frac{\partial c}{\partial \phi}\right) + \frac{1}{r_0^2\cos^2\phi}\frac{\partial}{\partial\theta}\left(D\frac{\partial c}{\partial\theta}\right) + \mathrm{S} \tag{3.1}$$

where

c is the species concentration,
v is the wind speed,
θ is the longitudinal direction,
ϕ is the latitudinal direction,
r_0 is the radius of the earth,
D is the horizontal dispersion coefficient,
and S is the source/sink term.

Following Fay et al., essentially uniform parameters are maintained throughout the modeling domain. A nonvariant velocity vector in a constant density layer of fixed height violates continuity in the spherical "plane" because of latitudinal effects. Given the two dimensional continuity equation

$$\frac{\partial}{\partial\phi}(v_\phi\cos\phi) + \frac{\partial}{\partial\theta}(v_\theta) = 0 \tag{3.2}$$

a simple adjustment is made such that each component is constant.

$$v_\phi \cos\phi = \text{constant} \tag{3.3}$$

$$v_\phi = \text{constant} \tag{3.4}$$

Thus, with uniform longitudinal but increasing latitudinal components, the velocity magnitude increases and direction turns slightly as latitude increases. The change in velocity is small, however, as the range of latitude covered is not large and v_ϕ is the smaller velocity component in the modeling studies to be presented in chapters four and five.

Generally, the source-sink term is composed of four parts: direct emission into the atmosphere (e), chemical production (p) or destruction (d), and physical removal from the mixed layer (r).

$$\mathrm{S} = \mathrm{e} + \mathrm{p} - \mathrm{d} - \mathrm{r} \tag{3.5}$$

Emissions are specified by a rate density E (emission rate per unit area) which is spatially variant. The source term e is converted to a volumetric flux by dividing by the mixing height h, the vertical extent of the modeled layer.

$$\mathrm{e} = \frac{\mathrm{E}}{\mathrm{h}} \tag{3.6}$$

e is used for NO_x and VOCs modeling but not ozone which has no direct sources. Atmospheric production p is the source of ozone and its functional form, to be treated in detail in chapter five, is assumed dependent upon ambient NO_x and VOCs concentrations.

Chemical destruction is important for all the precursor species. NO_x is consumed when NO_2 is converted to nitric acid. VOCs are oxidized to various products as part of their combustion process. They are modeled in a simple linear fashion; the rate of conversion is assumed proportional to the local concentration divided by a model specific time constant.

$$\mathrm{d} = \frac{c}{\tau_c} \tag{3.7}$$

The rate of physical removal is similarly modeled as linearly proportional to the local concentration normalized by a removal time constant.

$$\mathrm{r} = \frac{c}{\tau_r} \tag{3.8}$$

Removal includes deposition to the ground, exchange with the atmosphere above the mixed layer, and removal by precipitation. As NO_x, VOCs and ozone have low solubilities in water, the latter effect is small.

The similarity of the NO_x, VOCs and ozone models is in part a reflection that the same forces acting on all constituents of the atmosphere. Winds transport all airborne species. The meteorological parameters v_ϕ, v_θ and D are assumed to be the same in all models except for a pair of reoptimized ozone models where they are allowed to differ. The parameters are somewhat uncertain and the discrepancy in values is within the bounds of physical reasonability.

Model differentiation primarily results from the individual chemical nature of each species. Although the generic processes of creation and destruction are common, the rates and mechanisms by which they are accomplished vary significantly for NO_x, VOCs and ozone. Thus, the model parameters differ to capture species dependent properties, and the set of model parameters is unique for each species.

3.2 Numerical Techniques

Given the model equation for species concentration, the practical matter of solving it must be addressed. The NO_x and VOCs models are linear and amenable to the analytical solution of Fay et al. [18,19]. However, a numerical algorithm is adopted here for two reasons. First, the emission inventories for NO_x and VOCs contain thousands of individual point and area sources. Practical constraints on the analytical solution would necessitate source aggregation to limit the total number of sources. A gridded numerical model accomplishes this task more easily by assigning each source to the grid cell into which it is located. The second motivation for a numerical approach is the anticipation of an ozone model whose variable source does not conform to the equation of the analytical solution. The adoption of a numerical solution for all three species is a consistent approach which facilitates comparison and intra-model interaction. This is especially important for ozone modeling which assimilates prior solutions of NO_x and VOCs.

The choice of a specific numerical method involves consideration of several factors. Although finite elements easily adapt to irregular geometries such as eastern North America and could even conform to political boundaries, finite difference methodology is chosen to solve the model equation. The advantages of the latter technique are that the discretized nodal equations correspond directly with the model equation and that VOCs and NO_x emission inventories are geared to a regularly spaced grid. Using second order accurate difference formulae, the general form of the discretized model equation at a single node is given as

$$
\begin{aligned}
(v_\phi)_{i,j}\frac{c_{i,j+1}-c_{i,j-1}}{2r_0\,\Delta\phi} + (v_\theta)_{i,j}\frac{c_{i+1,j}-c_{i-1,j}}{2r_0\,\Delta\theta\,\cos\phi_j} &= \\
\frac{(D\cos\phi)_{i,j+\frac{1}{2}}(c_{i,j+1}-c_{i,j}) - (D\cos\phi)_{i,j-\frac{1}{2}}(c_{i,j}-c_{i,j-1})}{(r_0\,\Delta\phi)^2\cos\phi_j} &+ \\
\frac{D_{i+\frac{1}{2},j}(c_{i+1,j}-c_{i,j}) - D_{i-\frac{1}{2},j}(c_{i,j}-c_{i-1,j})}{(r_0\,\Delta\phi\,\cos\phi_j)^2} &+ \mathrm{S}_{i,j} \qquad (3.9)
\end{aligned}
$$

where i and j refer to local node coordinates as shown in Fig. 3.1. It is possible to vary the parameters v_ϕ, v_θ, D, and the various components of S spatially. The analyses in this thesis, however, treat them constant with the exception of the latitudinal velocity component (eqn. (3.3)).

Each nodal equation incorporates the concentration at the node itself plus those of its four nearest neighbors. Assemblage of eqn. (3.9) over all nodes in the modeling domain constitutes a set of equations which, given boundary conditions, can be solved. The system of node numbering adopted (Fig. 3.1) assigns global coordinates of the two dimensional grid by incremental rows of constant latitude which proceed across the longitudinal domain. If the source term $\mathrm{S}_{i,j}$ has no nonlinear terms in concentration, it can be written in matrix form as

$$[\mathbf{A}]\bar{c} = \bar{f} \tag{3.10}$$

where $\bar{c}$ is the vector of desired concentrations, $\bar{f}$ the forcing vector due to source terms and boundary conditions, and [A] is a somewhat sparse matrix whose bandwidth equals the number of longitudinal grid elements. The matrix equation can be solved directly by inverting the square matrix [A] and multiplying by the forcing function. The computational time required to do the inversion, however, increases roughly as n^p as n, the number of grid elements, is increased. The exponent p depends on the intelligence of the inversion technique. For full Gaussian elimination, p=6; other methods such as L-U techniques can exploit the banded, sparse matrix and reduce p to 4 or lower [32]. Even with sophisticated algorithms, though, inversion of [A] can be difficult as ill conditioning problems often occur when n gets large.

An alternate approach to solving the set of nodal equations is to introduce an artificial time dependence and iterate the solution until a steady state is attained. No matrix needs to be inverted; instead, time is spent iterating the solution. An advantage of iteration, though not of consequence to this work, is that nonlinear terms pose no problem to the solution.

Early comparison with the direct solve (inversion) method indicated that the iterative method obtains the solution faster; it is thus adopted as the "standard" solution technique for all model executions. Time dependence is added to the nodal equation through a $\partial c/\partial t$ term. Using a superscript k to represent concentrations at the present time t and $k+1$ to refer to the new time $t + \Delta t$, the discretized iterative equation becomes

$$\frac{c_{i,j}^{k+1} - c_{i,j}^{k}}{\Delta t} + (v_\phi)_{i,j} \frac{c_{i,j+1}^{k} - c_{i,j-1}^{k+1}}{2r_0\,\Delta\phi} + (v_\theta)_{i,j} \frac{c_{i+1,j}^{k} - c_{i-1,j}^{k+1}}{2r_0\,\Delta\theta\,\cos\phi_j} =$$
$$\frac{(D\,\cos\phi)_{i,j+\frac{1}{2}}(c_{i,j+1}^{k} - c_{i,j}^{k}) - (D\,\cos\phi)_{i,j-\frac{1}{2}}(c_{i,j}^{k} - c_{i,j-1}^{k+1})}{(r_0\,\Delta\phi)^2 \cos\phi_j} +$$
$$\frac{D_{i+\frac{1}{2},j}(c_{i+1,j}^{k} - c_{i,j}^{k}) - D_{i-\frac{1}{2},j}(c_{i,j}^{k} - c_{i-1,j}^{k+1})}{(r_0\,\Delta\phi\,\cos\phi_j)^2} + \mathbf{S}_{i,j} \tag{3.11}$$

Gauss-Seidel iteration is used to take advantage of the newly computed concentrations as they become available to subsequent nodal equations during the marching process [32]. The equation for the updated concentration $c_{i,j}^{k+1}$ is easily obtained by transferring the appropriate terms to the right hand side of eqn. (3.11).

A timestep $\Delta t = 1$ was arbitrarily assumed for iteration. No stability problems were encountered by this choice. Trials with larger Δt would probably produce faster convergence. However, an adequate turnaround time negated the necessity of finding the optimal timestep.

A final enhancement used to speed the iterative process is the method of overrelaxation. The concentration predicted at time $t + \Delta t$ is extrapolated further from the old value; assuming the true solution is being approached asymptotically, this overshooting technique can produce quicker convergence. The equation for the accelerated concentration c^* is given by

$$c_{i,j}^{*} = \frac{c_{i,j}^{k+1} - \alpha\, c_{i,j}^{k}}{1 - \alpha} \tag{3.12}$$

where α is the over-relaxation factor. An optimal and stable value of $\alpha = 1.4$ was obtained empirically from early model testing and is used as part of the standard solution algorithm.

The nodal equations are iterated until the change at each nodal point is very small in comparison to its average magnitude. This is assumed to correspond to the steady-state solution. Specifically, the solution is obtained when

$$\frac{c^{*}_{i,j} - c^{k}_{i,j}}{c^{*}_{i,j} + c^{k}_{i,j}} < \beta, \qquad \text{for all } i,j. \tag{3.13}$$

In practice β, the convergence criteria, is set to 5.0E-09 in the double precision iteration. A further check is made to ensure that the actual residual between the left and right hand sides of eqn. (3.9) is also relatively small. This confirms that the nodal solution is near completion and protects against the possibility of a slow time evolution of an iterating solution which is nowhere close to steady state.

3.3 Model Application and Testing

As mentioned previously, boundary conditions are necessary to solve the numerical model. Although other possibilities exist, the solutions presented in this dissertation specify the concentration at the boundary nodes. This requires careful consideration as the choice of boundary values also affects the values at nodes in the interior solution. One approach is to iterate and update boundary conditions by running the model several times until the boundary conditions have no physically unrealistic effect on the interior solution. The computational time consumption of multiple model executions makes this option undesirable. A second approach is to use a computational grid which is much larger than the domain where sources are located and to set the boundary conditions to zero. This is acceptable because pollutants concentrations generally are negligible at distances sufficiently far from their source. A disadvantage is the large grid which necessitates sacrificing either grid resolution or speed of solution. A third alternative adopted in this work is a dual grid solution (Fig. 3.2) in which a large and coarsely discretized outer grid is solved assuming zero boundary conditions to provide an initial estimate of the concentration field. Boundary conditions for the inner solution are interpolated from the outer solution. Fig. 3.2 specifies the grid parameters used in the modeling studies throughout this work. Note that the outer grid has approximately four times the area of the inner grid. Outer grid cells are about 160 km on a side while the inner grid scale is 40 km. The number of nodes in the domain is the same for both the inner and outer discretizations.

NO_x and VOCs models require emission densities in units of kg $km^{-3}s^{-1}$ specified at nodal points of the grid. Raw inventories are specified in either metric or English tons per year. Point sources have associated coordinates; area sources have specified emission centroids. The program treats both point and area sources similarly. The source coordinates are used to locate the numerical grid cell into which it falls, and then the source is corrected (if necessary) to consistent metric units and bilinearly interpolated to the four nodal points of the cell. (Sources which fall in boundary cells are allocated to the interior nodes). After all sources are gridded, the sums at the nodal points are divided by the volume of the grid cell to yield an emissions density. An example of the bilinear interpolation scheme is shown in Fig. 3.3.

Area sources for the NAPAP emission inventories are pre-gridded to a scale finer than the grid discretization used in this modeling study [21]. Thus, they are in effect aggregated to a coarser grid by the bilinear interpolation scheme. The biogenic VOCs emissions, however, are specified on a countywide basis. A potential pitfall of gridding irregularly spaced sources is that the area that they actually represent is likely to be different than the area covered by a grid cell. This distorts the emission field in the vicinity of the area source. Far away, only the integrated strength of the source is important, so the effect is minimal on long range transport. The effect is probably not very significant in the near field either, as grid cell areas are of the same order of magnitude as county areas.

The computer program which performs the finite difference solutions has evolved over time to become a multipurpose and flexible modeling tool. A listing of the fortran source code is included in Appendix IV. The program is modular and an effort has been made to develop a computationally efficient algorithm. The two dimensional computational field is compressed into single dimension arrays to conserve memory usage; real variables are declared double precision to provide accurate, well converged solutions. The program is designed to run on the VAX/VMS operating system; adaptation to other environments will require modification of the file identification and accessing conventions.

The finite difference program may be utilized to model airborne concentrations of sulfur oxides (SO_2 and $SO_4^=$), nitrogen oxides (NO_2 and NO_3^-), VOCs (both anthropogenic and biogenic), and ozone. Additionally, grid geometry, discretization, and solution convergence criteria can be varied as input to the program. The user specifies which species is to be modeled; the program reads the appropriate parameters, source data, boundary conditions, and grid geometry from conventionally named interdependent files.

Given the complexity of the numerical code, several checks were performed to ensure that it executes properly. Considering diffusion and linear destruction only, model runs with a single source at the center of the grid and zero boundary conditions produced anticipated symmetrical decreasing concentration gradients with respect to the source. Adding a convective wind, concentrations were skewed in the downwind direction.

Program executions to compare concentrations given by the numerical code and the analytical solution were made for similar modeling problems. Differences were apparent. Further investigation revealed two interacting contributions. The first was attributable to differing coordinate systems. While the numerical model uses constant radius spherical coordinates to represent the earth's surface, the applied analytical solution melds cylindrical coordinates with great circle distances to approximate source-receptor configurations. This effect was identified by scaling the solution to simulate a large radius, essentially flat, planar surface. Results of the scaled solutions matched much more closely. The second contribution was discretization error; the numerical solution cannot precisely resolve the gradients from a point source (the analytical solution is actually singular at the source!). Finer grid spacing was able to reduce the discretization error. Regional scale multi-source executions matched to within a few percent at all locations.

As an example of the capabilities of the numerical code, model executions of airborne sulfur oxides are presented in Appendix V. Plots of primary SO_2 and secondary $SO_4^=$ concentrations are produced which agree well with the analytical modeling previously done by S. Kumar in his Ph.D. dissertation [33]. The numerical model can easily be expanded to calculate wet and dry depositions. Boundary flux calculations are also a simple extension of the numerical code. The flexibility of the code enables future investigation of spatial parameter variation and nonlinear effects.

Program execution time for a combined inner and outer solution using the grid discretizations described in Fig. 3.3 is about fifteen minutes CPU time on a VAX 11/750 computer. Performance can probably be improved by increasing the iterative timestep. This enhancement and/or application on a faster machine should make it possible to refine the numerical meshes even further. Matching the inner grid with the 20 km spacing of the NAPAP inventory may provide slightly more accurate solutions, though increased refinement beyond that point will serve no purpose as the grid will become over-resolved compared with the emission inventory.

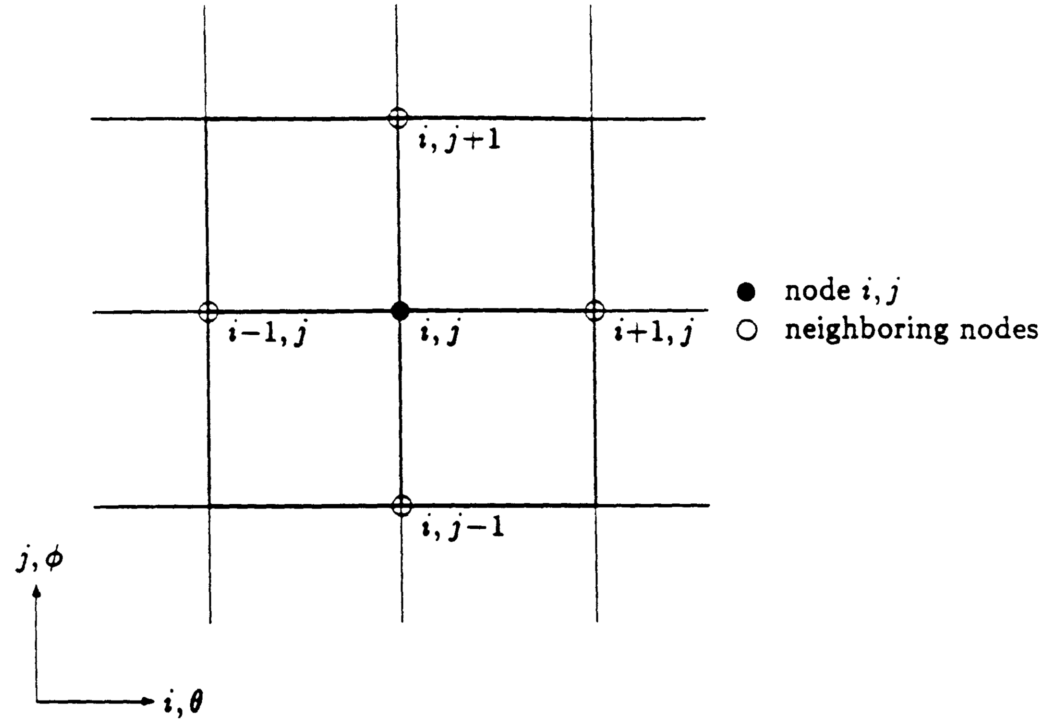

Global Node Number = nlon(j-1) + i

where nlon is the number of longitudinal nodes

Fig. 3.1 Finite difference node discretization and local-global node numbering conventions.

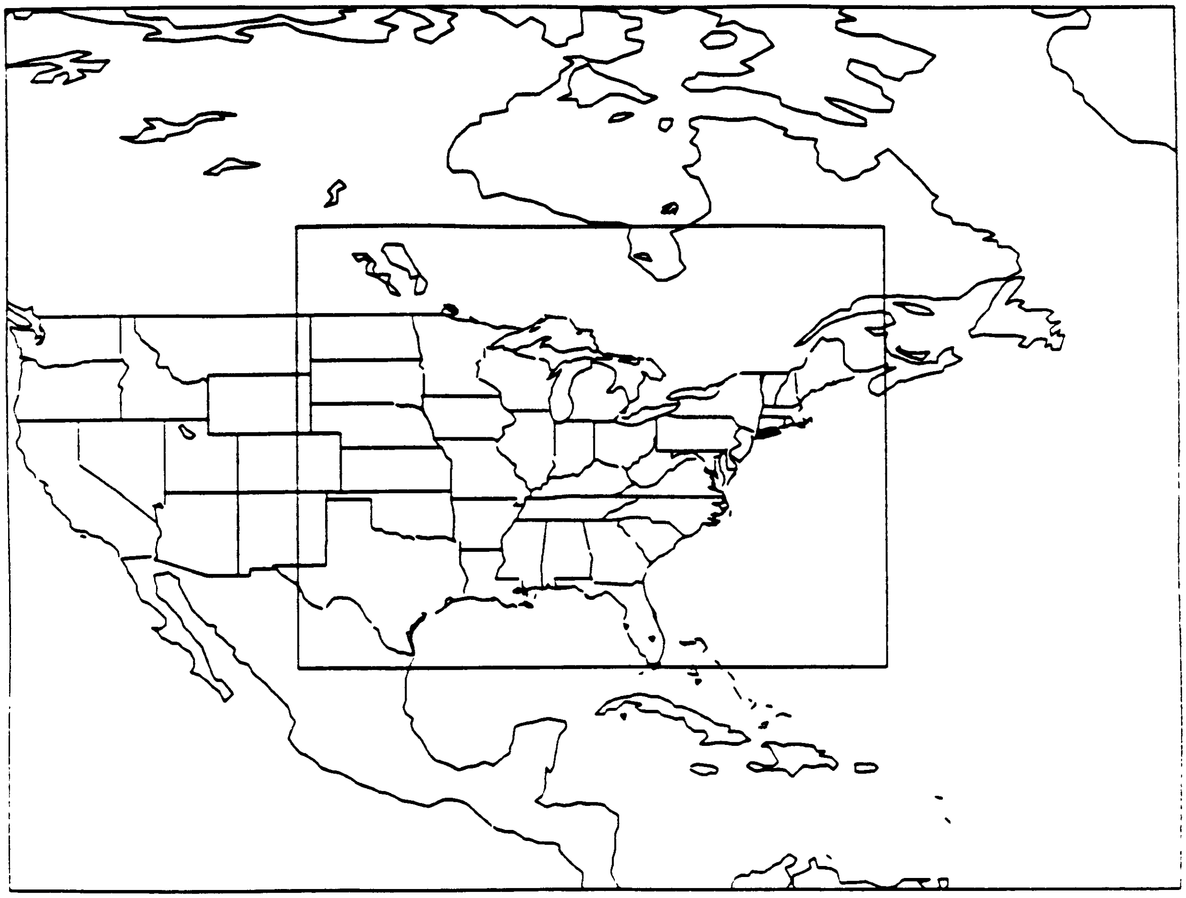

	Inner Grid	Outer Grid
Western Boundary (° W)	105	125
Eastern Boundary (° W)	65	45
Northern Boundary (° N)	55	70
Southern Boundary (° N)	25	10

Fig. 3.2 Projections used in numerical modeling studies of eastern North America. Table lists boundaries of outer and inner grids.

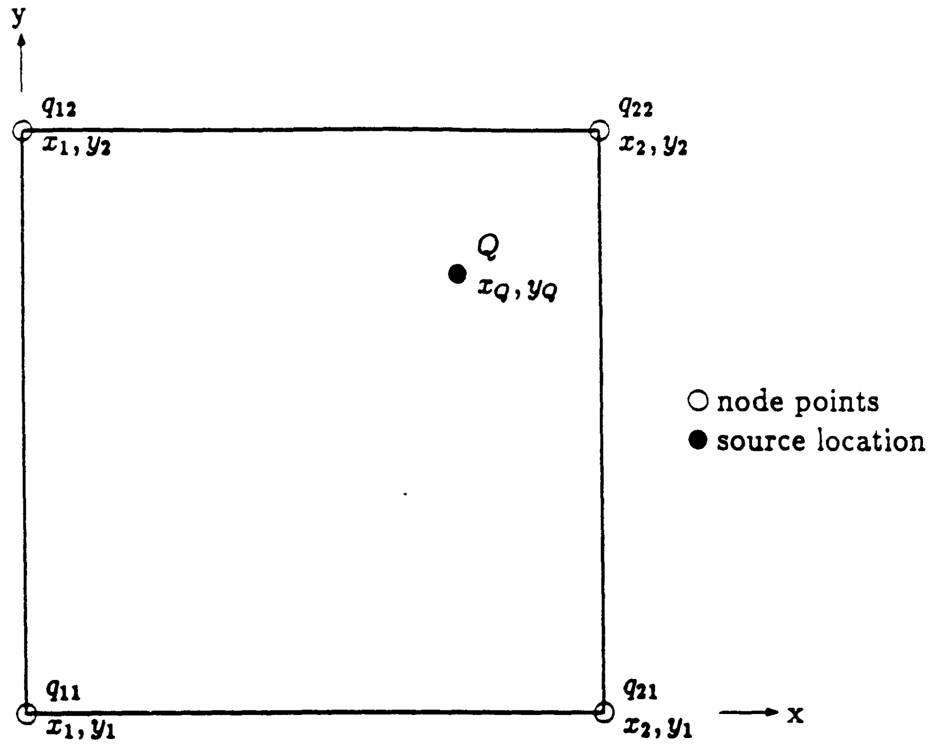

$$
\begin{aligned}
f_x &= \frac{x_Q - x_1}{x_2 - x_1} \\
f_y &= \frac{y_Q - y_1}{y_2 - y_1} \\
q_{11} &= (1 - f_x)(1 - f_y)Q \\
q_{12} &= (1 - f_x)f_yQ \\
q_{21} &= f_x(1 - f_y)Q \\
q_{22} &= f_xf_yQ
\end{aligned}
$$

Fig. 3.3 Bilinear allocation method used to aggregate sources to grid nodal points.

Chapter 4

Precursor Models: NO_X and VOCs

This chapter describes the development of regional models of ozone precursors NO_x ($NO + NO_2$) and VOCs (volatile organic compounds) for eastern North America (ENA). Each model is constructed with the numerical methodology discussed in chapter three. The NO_x is more developed than that of VOCs for two reasons. First, a similar model has already been published by Fay et al. (hereafter referred to as the FGK model) [19] in their effort to model wet nitrate deposition in eastern North America. Second, monitored NO_2 data (presented in chapter one) is readily available whereas measurements of VOCs are rare. In fact, there are presently no seasonal measurements of VOCs available for comparison with model results. The lack of data prohibits a consistency check of model predictions. The models can be updated as pertinent information becomes available in the future.

The NO_x and VOCS models constructed in this chapter make it possible to predict concentrations of these species throughout ENA. Important for their own sake, the value of the models is magnified because of their role as ozone precursors.

The fifth chapter uses the NO_x and VOCs model results to build a regional model of seasonally averaged ozone for ENA.

4.1 Regional NO_x Model

NO_x is actually the sum of two nitrogen oxide species, NO and NO_2. The FGK applied model of wet nitrate deposition does not distinguish between the NO and NO_2 components of NO_x transported in the atmosphere [19]. In actuality, the majority of NO_x is released as NO and rapidly oxidized to NO_2. Additionally, photochemistry causes a diurnal variation in both NO and NO_2. The FGK model successfully predicts wet deposition even though it does not speciate NO_x. This suggests that, at least in modeling deposition, the form of NO_x is not critical and all emitted molecules can ultimately be converted to nitric acid. Thus, the treatment of NO_x as a single species is appropriate when modeling the long range transport and acid formation essential to wet deposition.

Airborne concentrations of NO and NO_2 are both spatially and temporally variable. It is possible to construct a two species time averaged model of NO and NO_2, but such an approach is assumed unnecessary. Similar to the FGK approach, NO_2 is modeled as a surrogate for NO_x concentrations. The justification proceeds as follows.

A portion of NO_x exists as NO during photolytic daytime hours. On average, higher levels of NO_x correspond to higher levels of both NO and NO_2. If the ratio of NO to NO_x is spatially constant NO_2 is a proportional surrogate for NO_x. But such uniformity does not exist in the real world. Limited simultaneous measurements of the two species show the ratio to be variable. However, NO_2 concentrations are in general significantly higher than those of NO [34]. The predominance of NO_2 makes it an acceptable though imperfect NO_x substitute. Thus, this section develops a single species NO_2 model as a surrogate for the precursor NO_x concentrations ultimately used in ozone source modeling.

NO_2 is extensively monitored as it is the subject of a federal air quality standard. The 1980 and 1985 data presented in the geographic distributions of chapter two are compared with model results and are used to help determine model parameters. The fact that a large number of the monitoring stations are located in highly polluted urban areas presents some difficulty. The presence of proximate sources of NO weakens the NO_2-NO_x surrogate argument. Thus, a portion of the stations in the network probably violate the assumption, and the correlation of model results with observations will likely be degraded. Successful ability of model to predict measured values will support the validity of treating NO_x and NO_2 interchangeably.

4.1.1 NO_x Long Range Transport Model

The time averaged transport equation used to model all pollutants in this study is detailed in chapter three. The model is defined by the formulation of the source-sink term S (eqn. 3.5) and the specification of the model parameters. The source of NO_x is direct emission from anthropogenic activities. The causes of its elimination are primarily chemical conversion to nitric acid and physical removal by dry and wet deposition or transport out of the mixed layer. Modeling the loss terms as linearly proportional to concentration, the source term for the NO_x equation is written

$$S_{NO_x} = e - \frac{c}{\tau_c} - \frac{c}{\tau_r} \tag{4.1}$$

where e is the emission density and τ_c and τ_r are time constants inversely proportional to the average rates of conversion and physical removal, respectively. The emission density is further defined as the two-dimensional emissive flux E normalized by the height h of the mixed layer.

$$e = \frac{E}{h} \tag{4.2}$$

The gridded distribution of E is shown in Fig. 2.1 of chapter two and is used as input by the subsequently described models.

The NO_x model requires the specification of the model parameters v_ϕ, v_θ, D, τ_c, τ_r and h. Estimates of their values are available from the analytically based FGK summer nitrate model and are listed in Table 4.1. Listed is the complete set of parameters as determined for the FGK nitrate model and their appropriate form for the present numerical model. Several representational differences exist between the numerical and FGK models. Velocity components v_ϕ and v_θ correspond to windspeed w and direction γ. The FGK model considers two removal processes of the primary species, and thus the parameter τ_r is represented by separate wet and dry deposition time constants τ_{wp} and τ_{dp}. The parameters τ_{ws} and τ_{ds} are used in the determination of secondary NO_3^- concentrations and depositions and are thus absent from the numerical NO_x model. See Kumar [33] for a more detailed treatment of the FGK wet deposition model. The relationships between appropriate FGK and numerical model parameters are given by the following equations.

$$v_\phi = w \sin(\gamma - \pi) \tag{4.3}$$

$$v_\theta = w \cos(\gamma - \pi) \tag{4.4}$$

$$\frac{1}{\tau_r} = \frac{1}{\tau_{wp}} + \frac{1}{\tau_{dp}} \tag{4.5}$$

Adopting the parameters in Table 4.1, an initial model of airborne NO_x concentrations is constructed with the standard outer-inner grid technique outlined in the third chapter. Contoured results of the numerical solution are presented in Figs. 4.1 and 4.2. Concentrations are expressed in units of $\mu g\, m^{-3}$ NO_2. The magnitudes and spatial patterns are similar to those found in the development of the analytical version [33]. The agreement is not surprising as the two models are essentially the same. Some minor discrepancies between the solutions are apparent, resulting primarily from differing emission inventories and secondarily from incongruities in solution algorithms.

Several localized peaks of NO_x concentrations occur in proximity to areas of dense emissions. The contour roughness emphasizes the fact that NO_x is a primary pollutant; the linear destruction terms govern an exponential-type decay near sources. A broad elevated region across the midwestern and eastern United States reflects widespread emissions in ENA. Relatively high values in Texas are a consequence of concentrated emissions and are further accentuated by the low background concentrations of the surrounding region. Long range transport effects are evidenced by the stretching of the outer contours in the direction of the resultant wind vector.

Comparison of the model results with measured NO_2 data is less than satisfactory, however. A scatter plot highlighting the problem is shown in Fig. 4.3. Observations are 1980 April-September average concentrations at rural sites only. Two letter abbreviations correspond to the state in which each monitor is located. The rural category is selected because of its apparent distinction of having reduced near source influence (see chapter two), making it the group of monitors most representative of regional concentrations. As is evident from the comparison, the model results significantly underpredict observations at the monitoring sites. A slightly positive correlation is suggested, and it appears as though the model seriously underpredicts the magnitude of ambient ground level concentrations.

This shortcoming went undiscovered during the development of the analytical FGK model because the results were compared solely with wet nitrate deposition data. The calculation of wet deposition considers two species: NO_x and its oxidized product, airborne nitrate. The insolubility of NO_x in rainwater means that wet deposition is predominantly attributable to the contribution of the secondary NO_3^- species. Thus, ambient NO_x levels are not constrained by wet deposition and it may be possible to choose a different set of parameters to predict higher levels of NO_x without significantly altering the distribution of wet deposition.

The determination of an optimal set of parameters is a difficult task using a numerical model. Each potential combination must be individually solved and the results used to update the parameter set. Given six variable parameters in the full FGK wet deposition model, a fair amount of trial and error iteration can be anticipated, and the task becomes prohibitively time consuming.

Fortunately an alternative exists. The analytical solution can be applied in a program designed to automatically find a set of parameters which minimizes the error between observations and model predictions. Such an approach was employed in the original determination of parameters for the analytical FGK wet deposition model [33]. Parameters were permitted to vary simultaneously in an effort to minimize the sum of residuals between predicted and measured depositions.

The approach is easily modified to additionally include airborne NO_x concentrations in the residual sum. Thus, the objective function to be minimized is the total of both wet nitrate deposition and airborne NO_x concentration residuals. The gridded NO_x inventory (Fig. 2.1) is aggregated to 107 discrete point sources across North America, with a disproportionately larger number of them concentrated in the eastern half of the continent. Summer wet deposition data for the year 1980 is extracted from the Acid Deposition System database [35]. Eighty sites are selected throughout ENA which have a minimum of 75% precipitation coverage length. They are combined with all but one of the 1980 summer NO_2 measurements shown in Fig. 4.3 (the Illinois site is not considered as its overly high concentration implies local source contamination).

A previously written computer program systematically iterates to find a set of parameters corresponding to a functional minimum in multi-dimensional space. The optimizing algorithm updates parameter estimates simultaneously using a modified method of steepest descent to approach a minimum extremum in the objective error function. It accepts a range over which each parameter is allowed to vary. The limits of each range are user specified to prevent the optimizer from considering physically unrealistic parameter values. For example, w is permitted to vary between 5-10 $\mathrm{m\,s^{-1}}$, a range representative of average wind speeds. Three parameters are fixed on physical bases. The NO_x conversion time constant τ_c is set to $1.0\text{x}10^5$ s. This corresponds to a 3.5% per hour nitric acid formation rate, consistent with physical estimates. The NO_x wet scavenging coefficient τ_{wp} is fixed at $1.0\text{x}10^7$ s to permit minimal NO_x incorporation into rain and thus mimic its low solubility. The model layer thickness h is kept at 550 m to correspond to a reasonable averaged diurnal mixing height and to be consistent with the value determined by Kumar in the course of developing a model of wet sulfate deposition [33].

Optimized parameter values of the dual NO_x/nitrate deposition are summarized in Table 4.2. Similar to Table 4.1, the entries listed in the lefthand portion correspond to the full analytical FGK model and are in the form used by the optimizing program. The wind speed w is the only variable parameter constrained at the edge of its permitted range. Scatter plots of predictions and observations for the analytical model optimization are shown in Figs. 4.4 and 4.5. Symbols distinguish monitors from northeastern, northwestern, and southern sectors of ENA. Using subscripts p and m to designate predictions and measurements, an average error $\mathcal{E}$ defined as

$$\mathcal{E} = 100\% \times \sqrt{\frac{\sum(c_p - c_m)^2}{\sum(c_m)^2}}. \tag{4.6}$$

$\mathcal{E}$ is 23.9% for wet nitrate deposition (Fig. 4.4) and 48.9% for airborne concentrations (Fig. 4.5). $\mathcal{E}$ for the original FGK wet depostion model is 19.8%. Thus, the ability to predict wet deposition is compromised somewhat by the reoptimized model. Comparison of the set of reoptimized parameters (Table 4.2) with the original FGK values (Table 4.1) shows that several have changed significantly, though generally within an order of magnitude. Both sets are physically justifiable given the uncertainties in our understanding of atmospheric processes. The differences between the two models emphasize the fact that several of the parameter values are ill-determined; a variety of combinations can be found which predict similar patterns of wet nitrate deposition. The inclusion of airborne concentrations in the optimization adds further information which hopefully produces a more realistic model.

The chief advantage of the new model is its prediction of higher levels of airborne NO_x which are consistent with the values observed at the network of rural monitors. This is accomplished principally by a lower value of τ_{dp} which allows the primary species a longer lifetime. The high level of scatter present in the comparison of airborne concentrations in Fig. 4.5 reflects the unpredictable nature of a primary pollutant sensitive to local sources which cannot be properly treated by the long range transport equation.

The complete set of parameters which comprise the numerical NO_x model are tabulated in the righthand section of Table 4.2. The velocity component v_ϕ corresponds to a latitude of 40° N; its dependence at other latitudes is given by eqn. 3.3. τ_{wp}, the wet scavenging time constant, is very large compared to τ_{dp}, the dry deposition parameter; τ_r thus closely corresponds to τ_{d_p} of the analytical FGK model.

The regional effect of the reoptimized parameter values can be seen in Figs. 4.6 and 4.7 which map the numerically modeled NO_x solution. The qualitative patterns are similar to those of Figs. 4.1 and 4.2, but the levels of the new NO_x values are about twice as high as those given by the solution using analytical FGK model parameters. Peak values greater than 30 $\mu g\,m^{-3}$ are present near large emission sources in the Ohio River Valley and over northern New Jersey. The local effects of several metropolitan sources are apparent, especially in a large secondary peak region over eastern Texas.

Comparison of the numerical NO_x model with the full network of urban, suburban, rural and unclassified measurements is presented in Figs. 4.8-4.11. Two letter state abbreviations denote the location of each monitor. Fig. 4.10, the rural classification, is quite similar to the analytical result from the optimizing program (Fig. 4.5). Differences are attributable to the uniqueness of each solution algorithm. Though considerably scattered, the overall range and average of modeled rural concentrations agrees well with observations. In general, the range of measurements within a single state is larger than that predicted by the long range transport model. This suggests variance in ground level concentrations occurs over distances shorter than can be modeled by the long range transport assumptions.

Figs. 4.8 and 4.9 show another limitation of the transport model. Non-rural measurements are generally much greater than model predictions; the latter have a significantly smaller overall range. In fact, model predictions reach a plateau just above 30 $\mu g\, m^{-3}$. Better agreement with the class of rural monitors is largely the result of a lower level of observations. This indicates that the urban and suburban classifications differ in some fashion. In general, non-rural monitors are likely to be situated in areas of dense source emission. The long range transport model improperly handles proximate sources. The analytical expression for pollutant concentration varies as $\frac{1}{\ln(r)}$ at small r. The true dependence of a well mixed source near its origin is $\frac{1}{r}$. Thus, as $r \rightarrow 0$, the analytical solution is not singular enough and concentrations are underpredicted by the model. If monitors are sufficiently far away from the source the singularity effect disappears and the long range model is adequate. Monitors must be individually considered to assess the effects of local sources [36].

4.1.2 Local NO_x Model

The NAPAP inventory can be used to identify individual point and area sources. The area of influence around a site is defined as a rectangular region which extends about 50 km away from the monitor in each of the principal directions. Considering the 5 $m\, s^{-1}$ convection speed of the model, the travel time from the monitor to the edge of the local domain is about a half day. The local source region corresponds to a grid section $1\frac{1}{4}^\circ$ longitude by $\frac{5}{6}^\circ$ latitude centered about the $\frac{1}{4}^\circ$ by $\frac{1}{6}^\circ$ grid cell in which the monitoring site is located. Fig. 4.12 illustrates the extent of the local source region which is comprised of 25 emission grid elements, each of which is approximately 20 km on a side.

A pollutant is generally mixed and dispersed within the turbulent boundary layer as it is convected away from its origin. Thus, the distance from each source to the measuring site is important. A variable chosen to investigate near field effects is the sum of all local sources normalized by their distance to the monitor.

$$q_{local} = \sum \frac{Q}{r} \tag{4.7}$$

Q is an individual source within the local region and r the source-receptor distance. Point sources are readily amenable to the summation process. Area sources also conform assuming each is concentrated at the centroid of its cell. An exception is made at the center cell whose area source is taken to be 10 km away from the monitor irrespective of where the latter falls within the cell. This eliminates artificial scatter which would result from unknown random orientation within the cell. Compiled values of q_{local} vs. measured NO_x are plotted in Fig. 4.13. Symbols differentiate the four site classifications. Values of q_{local}, in units of $\mu g\, m^{-1} s^{-1}$, range over three orders of magnitude on the semi-log scale. Although scatter is pervasive, a very rough proportionality is evident. This supports the hypothesis that local sources are affecting monitored concentrations. Site classifications extensively overlap, though q_{local} values for rural sites appear lower on average than those of the other groups.

The effects of nearby sources can be estimated in a simple manner with a local model whose principal assumption is that emissions proximate to a monitoring site are not mixed throughout the boundary layer. Rather, they are assumed to be concentrated in a subregion near the ground. Nightime inversions are physical evidence that such a situation can and does occur naturally in the real world. Given the suppressed mixing assumption there are a variety of ways to model the source region flow, two of which are investigated. The first is a simplistic approach in which each source is assumed to stream symmetrically from its origin within the shallow layer. Concentrations from a source emitting at rate Q as a function of distance r from its origin are given by

$$c_{local} = \sum \frac{Q}{2\pi r \overline{vh}} \tag{4.8}$$

The quantity $\overline{vh}$ is assumed to be an empirical constant which combines the rate of convection away from the source with the reduced height of the flow region. Effects of chemical conversion and deposition are ignored by this simple model; its sole requirement is that the rate of pollutant emission be conserved through a cylindrical surface encompassing the source. (As a practical constraint, r is limited to minimum distance of 1 km to truncate its singular behaviour at small value). Note the similarity of eqns. (4.7) and (4.8); they are simply related by

$$c_{local} = \frac{q_{local}}{2\pi \overline{vh}}. \tag{4.9}$$

The second local model is more elaborate than the first but it is also more consistent with the long range modeling approach. It is an extension of the analytical FGK solution which embodies a reduced mixing height for nearby sources. Thus, the effects of source-receptor orientation, dispersion, convection, and destruction are still included. The modified FGK analytical equation describing the concentration field from a point emission is given by

$$c_{local} = \sum \frac{Q}{2\pi D h_{local}} \exp\left(-\frac{wr\cos\delta}{2D}\right) \mathrm{K}_0(\eta r) \tag{4.10}$$

where

$$\eta = \sqrt{\frac{1}{D}\left(\frac{1}{\tau_c} + \frac{1}{\tau_{wp}} + \frac{1}{\tau_{dp}}\right) + \frac{w^2}{4D^2}} \quad . \tag{4.11}$$

Q and r are defined as in eq. (4.7). D, w, τ_c, τ_{wp}, and τ_{dp} are FGK model parameters whose values are listed in Table 4.2, δ is the angle between the resultant wind direction γ and the source-receptor orientation, and K_0 is modified Bessel function. Note that the lead factor of the local FGK model (eqn. (4.10)) is similar to the local streaming model (eqn. (4.8)). The additional terms of the local FGK model make it a more sophisticated approach. The parameter h_{local} is assumed to depend on the source-receptor distance; it is modeled as a simple power law.

$$h_{local} = \sigma r^{\lambda} \tag{4.12}$$

A consistency constraint is enforced that ensures h_{local} does not exceed 550 m, the mixing height of the long range transport model. The r dependence of the local mixing height strengthens the near source singularity as eqn. (4.10) varies inversely with the product $\mathrm{r}^{\lambda}\ln(\mathrm{r})$ close to the source.

As all sources in the modeling domain are used in the generation of the long range concentration, care must be taken not to doubly count local sources when total NO_x (long range + local) is estimated. The contribution of local sources to the numerical solution shown in Fig. 4.7 must be subtracted to provide the long range component from distant sources. The strictly proper way to find the adjusted long range value is to redo the numerical solution with the local sources omitted. However, such an approach is impractical to perform for each of the several hundred NO_x monitors shown in Figs. 2.14-2.17. Fortunately, the analytical FGK solution can be used to make the necessary correction. The formula for calculating FGK long range concentrations is the same as eqn. (4.10) except that the mixing height is simply equal to h, the value of the full mixed layer. Total NO_x is calculated as the numerical component interpolated from Fig. 4.7 plus the sum of local concentrations given by eqn. (4.8) or '4.10) less the sum of local FGK concentrations given by eqn. (4.10) with h_{local} replaced by h.

$$\begin{aligned}\text{Total } NO_x = &\text{ Numerical long range } NO_x \text{ (from Fig. 4.7)} \\ &+ \sum(\text{local } NO_x - \text{FGK } NO_x)\end{aligned} \tag{4.13}$$

The local models contain empirical parameters whose values are estimated by calculating total NO_x and comparing with observations. Application of the local models requires the individual consideration of all sources in the proximate area of each monitoring station. This is accomplished by searching the NAPAP inventory and summing the contributions of each point and area source situated within the monitor's local area. A computer algorithm automates the process over the NO_x measurement network and tests ranges of parameters in an effort to minimize the overall error between observations and predictions (eqn. (4.6)). The "optimal" value of $\overline{vh}$ for the overall network is 0.0021 km^2s^{-1}. The best values of λ and σ are found to be 0.3 and 16.0 $km^{0.7}$.. Average errors and correlation coefficients are compiled in Table 4.3. Scatter plots of total NO_x vs. observations are shown in Figs. 4.14 and 4.15 for the local streaming model; comparable plots for the local FGK model are presented in Figs. 4.16 and 4.17. The scatter is significant in all cases. Each model is biased by a group of Texas monitors whose large local sources constrain the local parameter optimization. Figs. 4.18-4.21 present scatter plots with all Texas monitors removed. Average errors are reduced (Table 4.3) and the correlations improve slightly. Elimination of the Texas sites serves to eliminate the visual bias, suggesting that the local model formulation may not be appropriate to these monitors which are located in a region of high emission density.

The local FGK model performs slightly better than the streaming model for the 1980 dataset. Apparently the additional sophistication embodied in the local FGK model is able to differentiate some of the scatter in the network. The most successful solution - the local FGK model with Texas sites removed - is able to achieve an average error of 38.9% and a correlation coefficient of 0.61. The high degree of scatter in Figs. 4.14-4.21 is a manifestation of the near field variability exhibited in the local source sums of Fig. 4.13. This emphasizes the uniqueness of each site. The network of monitoring stations observes variations on a short scale length which are impossible to resolve with the long range model. Simplistic models such as eqns. 4.8 and 4.10 cannot be expected to explain the peculiarities of individual monitors. A local source model more sophisticated than those described in this chapter is necessary for detailed, accurate urban airshed analyses. Such a model might even require emission estimates on a finer scale than the 1980 NAPAP inventory. This does not mean that these simplistic models are worthless. They are extremely useful in identifying the gross spatial trends present within a network. However, care must be taken not to avoid overextending the model to problems it is not able to address.

The general agreement obtained by the local models implies that a significant portion of NO_x monitors are influenced by sources only partially mixed through the boundary layer. It is logical that such monitors should occur near urban areas, i.e., near NO_x emissions. This hypothesis is supported by he metropolitan siting bias present within the monitoring network. Underdispersed sources, which inflate ground level concentrations above average mixed level layers, could be the result of proximate sources or inversion conditions (typical of nightime hours).

As discussed previously, a readily observable difference exists between measurements from the rural site category and the other monitoring groupings. The overall level of concentrations is lower and few sites exhibit excessive levels indicative of local source influence. The uncertainty in site classification prevents a blanket generalization, but it does appear that the long range transport model is more appropriate for the rural monitors. Concentrations in truly rural areas are likely to be caused by well mixed distant sources.

A regional contour map of total NO_x computed with the local FGK model is illustrated in Fig. 4.22. The contours are generated from a 76x84 rectangular array of values. The effects of the local model are most prevalent near metropolitan areas which are the concentrated areas of NO_x emissions. These regions appear as islands of intensified contour density where concentrations can be several times larger than the long range component. However, total NO_x levels in non-urban areas are not significantly larger than those calculated by the long range numerical model alone. These features are reinforced by Fig. 4.23 which maps the ratio of NO_x due to local sources to total NO_x. Local sources generally contribute less than 20% of the total except in the urban islands where more than half of the total NO_x is attributable to nearby emissions. The urban "hot spots", though numerous, comprise only a small portion of land surface area. Regional NO_x is not well represented by the monitoring network which concentrates sites in metropolitan areas.

Thus, it appears that a large part of ENA is rural in character (though not well monitored), and the numerical long range transport solution (Fig. 4.7) is likely to be representative of regional NO_x concentrations, especially in terms of its ozone production capacity which is integrated through the entire mixed layer. Monitoring of nonurban areas seems to be too sparse to confirm this phenomena, although the general trend of the rural subclass of measurements supports the hypothesis. Therefore, the numerically modeled long range NO_x, and not total NO_x, is used as the appropriate precursor concentration for ozone modeling in the subsequent chapter.

A final set of NO_x plots compares 1985 NO_2 measurements (Figs. 2.20-2.23) with model predictions. Figs. 4.24 and 4.25 present the local streaming model while

Figs. 4.26 and 4.27 portray the results of the local FGK model. Model estimates of total NO_x generally exceed observations. A subgroup of Texas monitors is once again an obvious anomaly, but the general level of agreement as degraded as well. Discounting Texas sites, the average error of the streaming model is 41.5% (r=0.48) and that of the local FGK model 42.9% (r=0.46). The consistency of the model overprediction may be caused by several factors. Perhaps 1985 meteorology varied significantly from that of 1980, thus implying a year-to-year model dependence. Additional bias may be the result of the smaller number of 1985 monitors or of uncertainty in the model parameters.

The essence of the long range transport model is embodied by the complete set of parameters as their values affect the interactions and relative importance of the convective, diffusive, chemical and depositive processes governing pollutant dispersion. The determination of these parameters is much more of an art than a science. Processes can be interchanged with one another to produce the same net effect; for example, an increase in the rate of deposition can be compensated by a faster windspeed which convects the species downstream before it is removed from the atmosphere. The NO_x model parameters are not well determined; a number of other sets could be selected to produce approximately the same agreement that the optimizing program achieves in predicting wet depositions and airborne concentrations (Figs. 4.6 and 4.7). A second factor in choosing parameters is physical intuition. The values need to be consistent with empirical knowledge and scientific reasonability. The latter criterion plays a crucial role as the understanding of long range transport is currently incomplete. New information, as it becomes available, will help to establish parameter values with more certainty.

The long range transport model for NO_x embodies six adjustable parameters: v_ϕ, v_θ, D, τ_c, τ_r, and h. Each uniquely affects the solution of the governing advection-diffusion equation. The multi-term partial differential equation (eqn. 3.1) generally obscures the effects of each parameter making it difficult to ascertain their individual importance to the solution. One exception is the mixing height h with which the model solution inversely varies. Doubling h halves the solution, and vice-versa. The variance is purely a dilution effect.

The results of a partial sensitivity study appear in Appendix VI. Model executions are presented which vary the remaining five parameters. Each solution is normalized by the long range transport solution of Fig. 4.7 to facilitate comparison. In general, the effects of parameter variance are greatest near the edges of the modeling domain, far away from the source region. Concentrations are lowest in those regions as pollutants require a long travel time, thereby providing the greatest opportunity for the integrated effects of parameter variance to manifest themselves. The solution is relatively insensitive to changes in D within the source region. Changes in the magnitude of the velocity components v_ϕ and v_θ affect concentration at the edges of the source region; a change in direction further magnifies this effect. Varying τ_c produces an almost linear change in concentrations within the modeling domain. Changing τ_r has a much smaller effect as it is overshadowed by the more dominant chemical conversion process.

4.2 Regional VOCs Model

The methodology to develop the regional model of Volatile Organic Compounds (VOCs) is the same as that used in regional NO_x modeling with a single but fundamental difference: there exist no seasonal measurements of VOCs to guide model parameter selection. As a consequence the reliability of model predictions cannot be ascertained at this time. Fortunately, the technical knowledge is sufficient to construct a reasonable model. Transport is likely to be similar for all species as they are convected commonly by winds and weather systems. The meteorological parameters v_ϕ, v_θ, D and h are assumed to be the same as found in the NO_x model. The VOCs model is distinguished by the choice of the species dependent destruction and transformation parameters τ_r and τ_c. Estimates of each are obtained from the literature. Thus the resulting VOCs model is conservatively constructed and reflects the current understanding of VOC activity in the atmosphere.

State-of-the-art knowledge indicates that there are two major sources of VOCs which are important to ozone production. Anthropogenic emissions result from both direct emission and incomplete combustion of fossil fuels. Biogenic VOCs are emitted from trees and other vegetation. As seen in the second chapter, the aggregate mass of biogenic emissions is estimated to be larger and the spatial patterns of the two sources are quite different. The approach adopted in this section is to model the two sources separately and then superspose the results to provide an estimate of total regional VOCs concentrations. Because the set of parameters used is the same for each solution it would be equally valid to sum the emission inventories and produce a single modeling effort. The distinction of each source, however, provides additional information as to their relative contribution to the total. Such knowledge is currently a subject of debate and it has important ramifications which will impact future NO_x and VOCs control strategies aimed at reducing ozone levels [37].

VOCs is a rather ambiguous term which blankets a variety of species and lumps them together in a single category. The gridded 1980 NAPAP inventory [21] specifies mass totals of VOCs, making it impossible to distinguish the spatial patterns of each individual species. Differing species reactivities and other variable properties preclude categorization of VOCs as a single compound. Fortunately, they can be grouped into a limited number of classes whose constituents behave in a reasonably similar fashion. NAPAP breaks the anthropogenic VOCs inventory into six categories of hydrocarbons: reactive and unreactive alkanes, alkenes, aromatics, aldehydes and organic acids. The alkenes, aromatics and reactive alkanes have high reactivities and are thought to contribute the most to ozone production. Together these groups account for about 60% of manmade VOC emissions in the United States. Biogenic emissions are also a nonhomogeneous group. The principal constituents are isoprene and α- pinene [24].

It is feasible to construct models for each of the classes of VOCs. However, as stated in the previous paragraph, the fast reacting species are the principal VOCs involved in boundary layer ozone production. As a simplification, this study assumes that a fast reacting model alone is sufficient to represent the VOCs precursor, and a single set of long range model parameters is developed. The parameters which constitute the VOCs model are listed in Table 4.4. As discussed previously, the values of the transport parameters are assumed to be the same as those of the long range NO_x model. The source function is also of the same form as in the NO_x model

$$S_{VOCs} = e - \frac{c}{\tau_c} - \frac{c}{\tau_r} \tag{4.14}$$

except that the values of τ_c and τ_r differ. Reactive VOCs are consumed rapidly in the environment. The value of 2.0×10^4 s for τ_c (which corresponds to a 16% per hour conversion rate) is typical of those reported in the literature and results in a relatively fast rate of chemical destruction. The value of $\tau_r = 6.0 \times 10^4$ is adapted from Bidleman's estimation of VOCs dry and wet depostion rates. The former removal mechanism is thought to be dominant as hydrocarbons have limited solubilities in water [38].

Similar to the NO_x long range model, the numerical methodology described in chapter three is used to solve the model equation (3.1) using the VOCs parameters. The anthropogenic model uses the gridded NAPAP inventory presented in Fig. 2.2. Contour maps of the outer and inner numerical solutions are shown Figs. 4.28 and 4.29. Contour levels exceed 18 $\mu g\, m^{-3}$. Local peaks are abundant and are located near major areas of emissions. The sharp gradient around each peak reflect the fast reacting characteristic which consumes VOCs close their point of emission.

A second numerical solution using the biogenic VOCs emission inventory of Fig. 2.3 as input is illustrated in Figs. 4.30 and 4.31. The maximum contour level of 13.8 $\mu g\, m^{-3}$ is somewhat lower than its anthropogenic counterpart. The general concentration level, though, is higher in the biogenic distributions. Local peaks are again present near dense emission areas, but their number and severity are not as great as for the anthropogenic case. This reflects a smoother spatial distribution of emissions. The highest region of biogenic VOCs is in the southern U.S. and is not coincident with peak manmade concentrations.

Both anthropogenic and biogenic VOCs participate in atmospheric chemistry. Additionally, both contain fast reacting species and are thought to contribute to the production of ozone. Thus, each VOCs source must be considered as an ozone precursor. The linear VOCs model permits superposition of solutions. A total VOCs model is generated simply by summing the anthropogenic and biogenic executions. This calculation is shown in Fig. 4.32 which is a linear combination of the inner model solutions of Figs. 4.29 and 4.31. Total VOCs is assumed to be all of the biogenic solution plus 60% of the manmade distribution, the latter being the reactive component important to ozone production [1]. The superposed total VOCs levels typically range from 4 to $8 \mu g\,m^{-3}$, with a maximum contour level of $14.6\ \mu g\,m^{-3}$. The combined solution reduces the relative height of local urban peaks by providing a higher biogenic background for contrast. The ratio of manmade to total modeled VOCs is mapped in Fig. 4.33. Generally, anthropogenic VOCs account for 20% of the superposed solution, a relatively small fraction of total VOCs. In some urban areas, however, the anthropogenic component well exceeds 50%. This implies that control strategies aimed at reducing VOCs concentrations can be effective only in proximity to urban areas. Even there, some areas may be largely influenced by biogenic emissions. It should be emphasized that these results are preliminary and based upon a number of modeling assumptions and highly uncertain emission inventories. Nevertheless, they do suggest that more research be undertaken to assess the relative contributions of anthropogenic and biogenic VOCs before costly and potentially erroneous control strategies are pursued.

A sensitivity analysis of the total VOCs model to parameter selection is included in Appendix VI. The results are potentially of even more importance than the parallel NO_x study discussed previously as the VOCs model is not supported by comparisons with observations. Thus it is useful to examine potential changes in the event that future information necessitates refinement of the model parameters.

The total VOCs model is an interesting candidate for sensitivity analysis because of its fast reacting rate capable of producing sharp gradients near major sources. Changes in the meteorlogical parameters produce only slight concentration variances in the source region. Concentrations over the Gulf of Mexico and Atlantic Ocean are highly sensitive, however. Changes to the conversion time constant τ_c produces strong, almost linear effects on concentration levels. The general pattern is similar to that of NO_x. The removal constant τ_r is somewhat sensitive to reduction as it then becomes comparable in importance to τ_c. The solution is much less sensitive to increases in τ_r, however, as the rapid chemical conversion masks the effect in the source region.

FGK Analytical Model		Numerical Model	
Parameter	Value	Parameter	Value
w	10 $\mathrm{m\,s^{-1}}$	v_θ	5.4 $\mathrm{m\,s^{-1}}$
γ	213 °	v_ϕ	8.4 $\mathrm{m\,s^{-1}}$
D	$2.0\mathrm{x}10^6$ $\mathrm{m^2\,s^{-1}}$	D	$2.0\mathrm{x}10^6$ $\mathrm{m^2\,s^{-1}}$
h	550 m	h	550 m
τ_c	$1.0\mathrm{x}10^5$ s	τ_c	$1.0\mathrm{x}10^5$ s
τ_{wp}	$1.0\mathrm{x}10^7$ s	τ_r	$8.1\mathrm{x}10^4$ s
τ_{dp}	$8.2\mathrm{x}10^4$ s		
τ_{ws}	$4.6\mathrm{x}10^4$ s		
τ_{ds}	$1.0\mathrm{x}10^7$ s		

Table 4.1: FGK Nitrate Deposition Parameters

FGK Analytical Model		Numerical Model	
Parameter	Value	Parameter	Value
w	5 $\mathrm{m\,s^{-1}}$	v_θ	4.4 $\mathrm{m\,s^{-1}}$
γ	242 °	v_ϕ	2.3 $\mathrm{m\,s^{-1}}$
D	$9.3\mathrm{x}10^5$ $\mathrm{m^2\,s^{-1}}$	D	$9.3\mathrm{x}10^5$ $\mathrm{m^2\,s^{-1}}$
h	550 m	h	550 m
τ_c	$1.0\mathrm{x}10^5$ s	τ_c	$1.0\mathrm{x}10^5$ s
τ_{wp}	$1.0\mathrm{x}10^7$ s	τ_r	$7.8\mathrm{x}10^5$ s
τ_{dp}	$8.5\mathrm{x}10^5$ s		
τ_{ws}	$1.5\mathrm{x}10^5$ s		
τ_{ds}	$1.4\mathrm{x}10^5$ s		

Table 4.2: NO_x Model Parameters

Local Model	Parameters	All Data		∉ Texas	
		Error (%)	r	Error (%)	r
Streaming	$\overline{vh} = 2.1x10^3\ m^2s^{-1}$	46.8	0.52		
	$\overline{vh} = 1.5x10^3\ m^2s^{-1}$			41.2	0.53
FGK	$\lambda = 0.3; \sigma = 16\ km^{0.7}$	43.4	0.58		
	$\lambda = 0.3; \sigma = 20\ km^{0.7}$			37.9	0.61

Table 4.3: Local NO_x Model Summary

Numerical Model	
Parameter	Value
v_θ	$4.4\ m\,s^{-1}$
v_ϕ	$2.3\ m\,s^{-1}$
D	$9.3x10^5\ m^2\,s^{-1}$
h	550 m
τ_c	$2.0x10^4$ s
τ_r	$5.7x10^4$ s

Table 4.4: VOCs Model Parameters

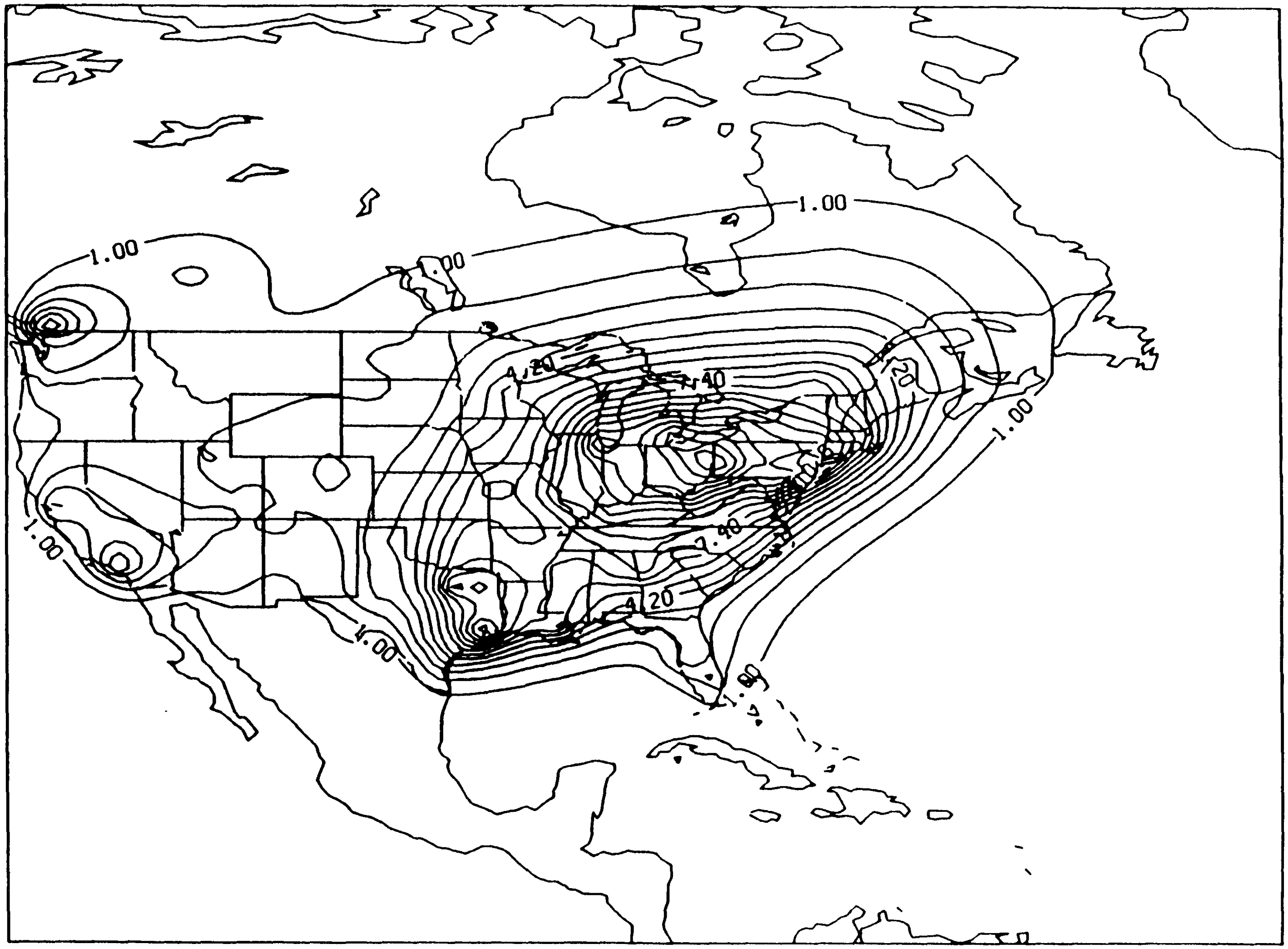

Fig. 4.1 Airborne NO_x ($\mu g\ m^{-3}\ NO_2$) using FGK wet deposition model parameters. Outer solution contours from 1.0 to 14.6 $\mu g\ m^{-3}$ by 0.8 $\mu g\ m^{-3}$.

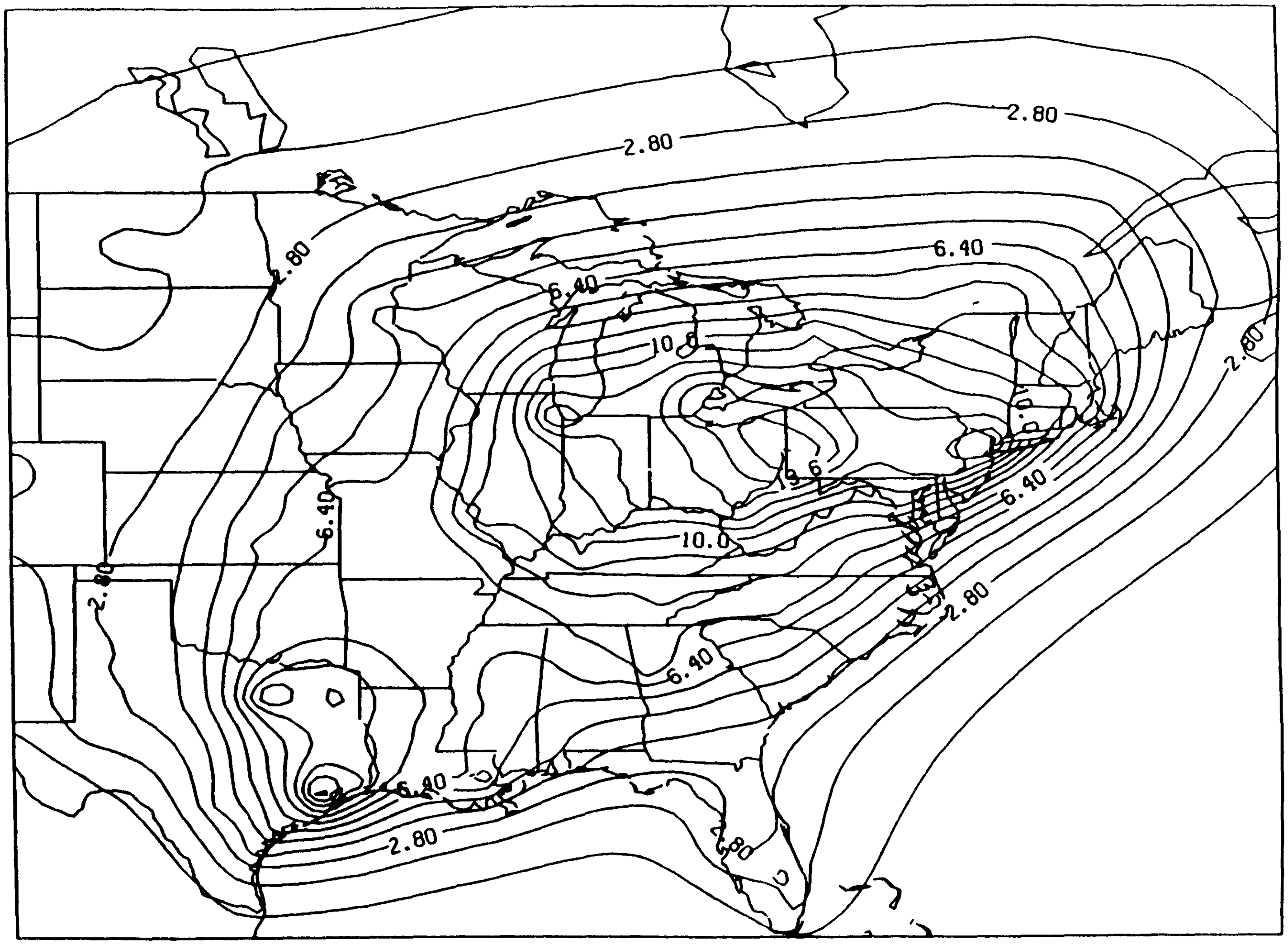

Fig. 4.2 Airborne NO_x ($\mu g\, m^{-3}\ NO_2$) using FGK wet deposition model parameters. Inner solution contours from 1.0 to 15.4 $\mu g\, m^{-3}$ by 0.9 $\mu g\, m^{-3}$.

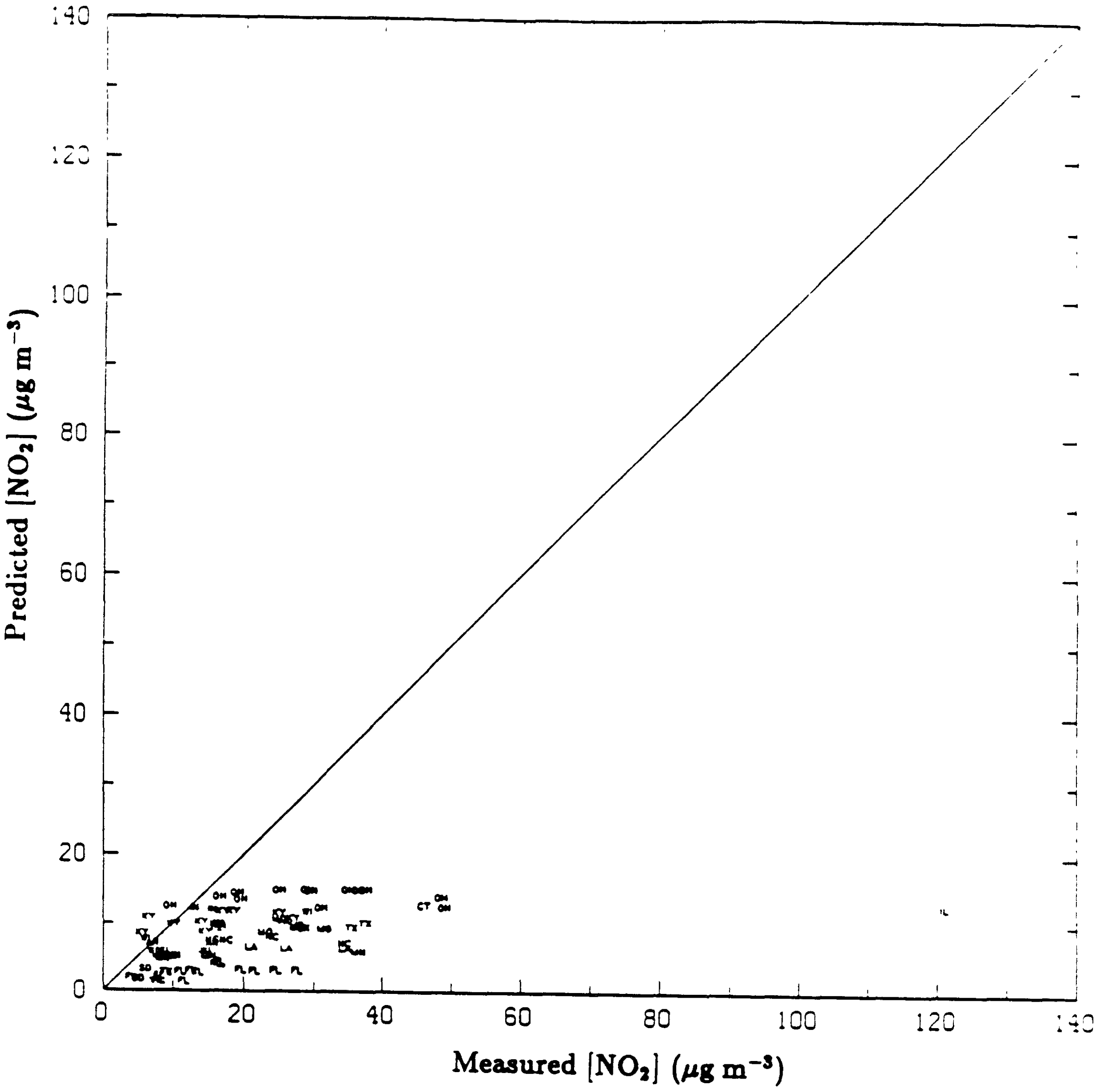

Fig. 4.3 Predicted vs. measured airborne NO_2 ($\mu g\ m^{-3}$) at rural monitors using FGK wet deposition model parameters. Two letter state abbreviations indicate monitor location. 1980 data, correlation coefficient r=0.48.

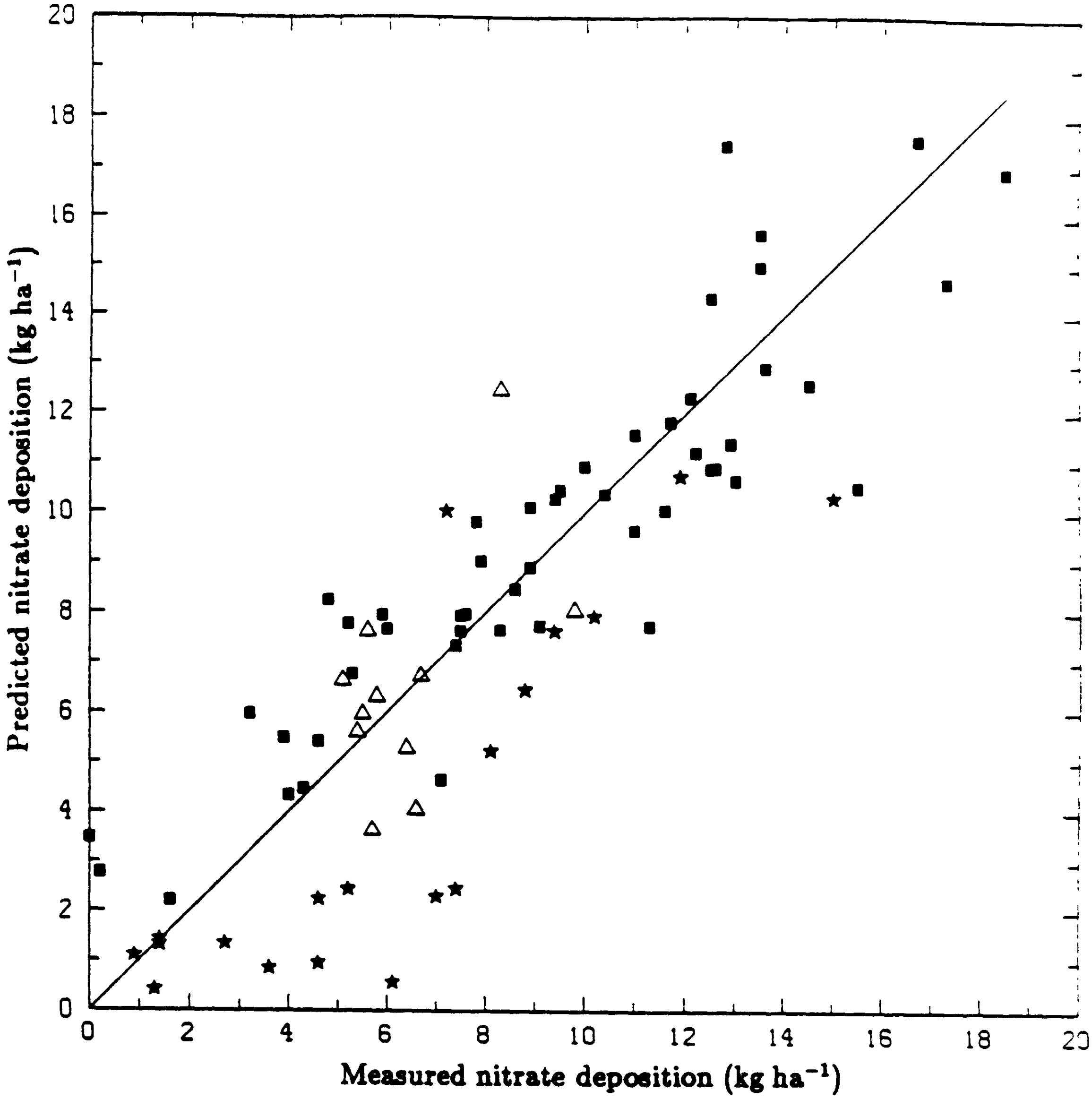

Fig. 4.4 Predicted vs. measured wet nitrate depositions. (kg ha^{-1}). Optimized NO_x model parameters. Squares, triangles and stars indicate NE, NW, and S sections of eastern North America. 1980 data from ADS database [35]. Average error is 23.9%.

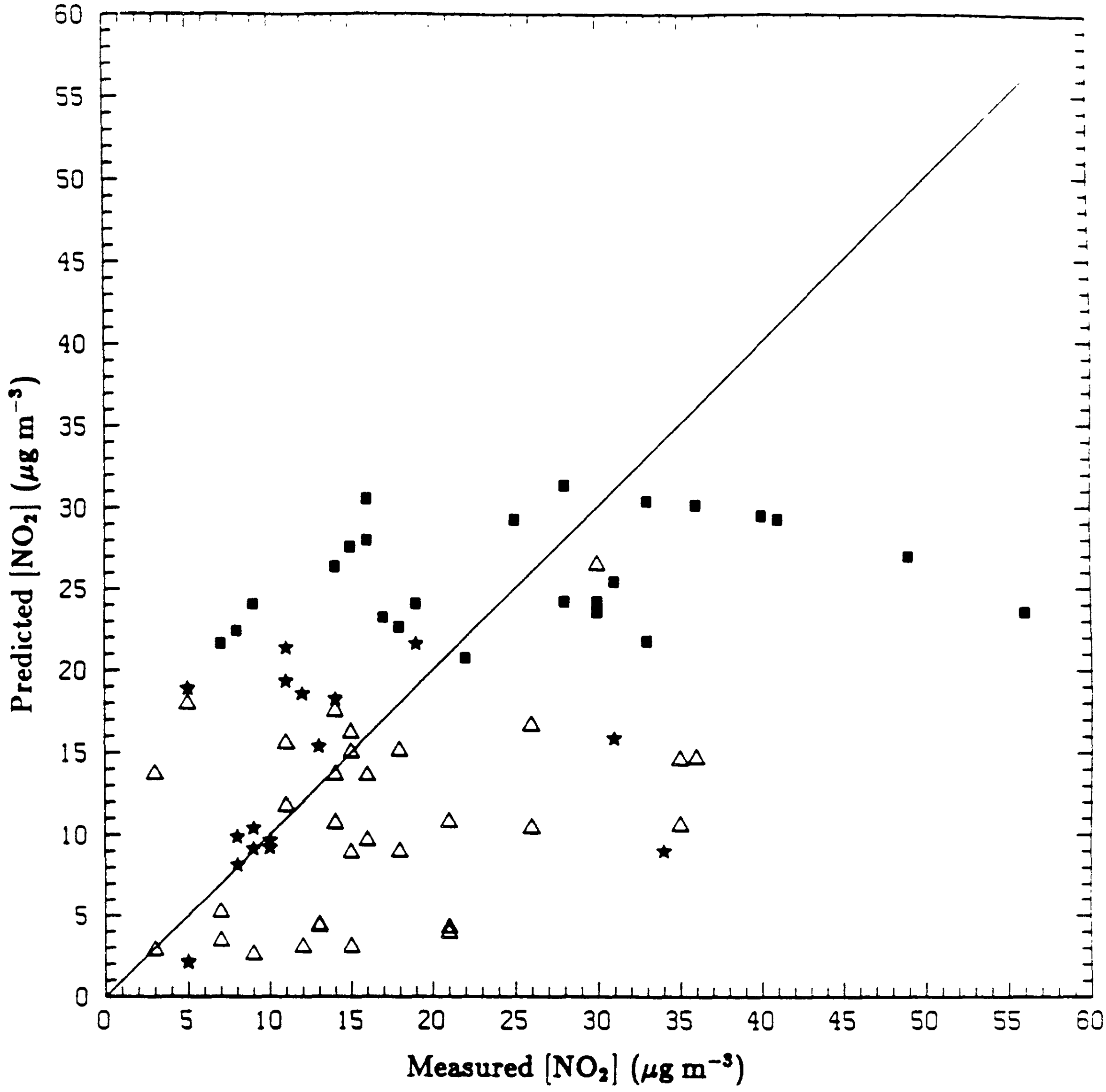

Fig. 4.5 Predicted vs. measured airborne NO_2 concentrations. (μg m^{-3}). Optimized NO_x model parameters. Squares, triangles and stars indicate NE, NW, and S sections of eastern North America. 1980 data at rural monitors. Average error is 48.9%.

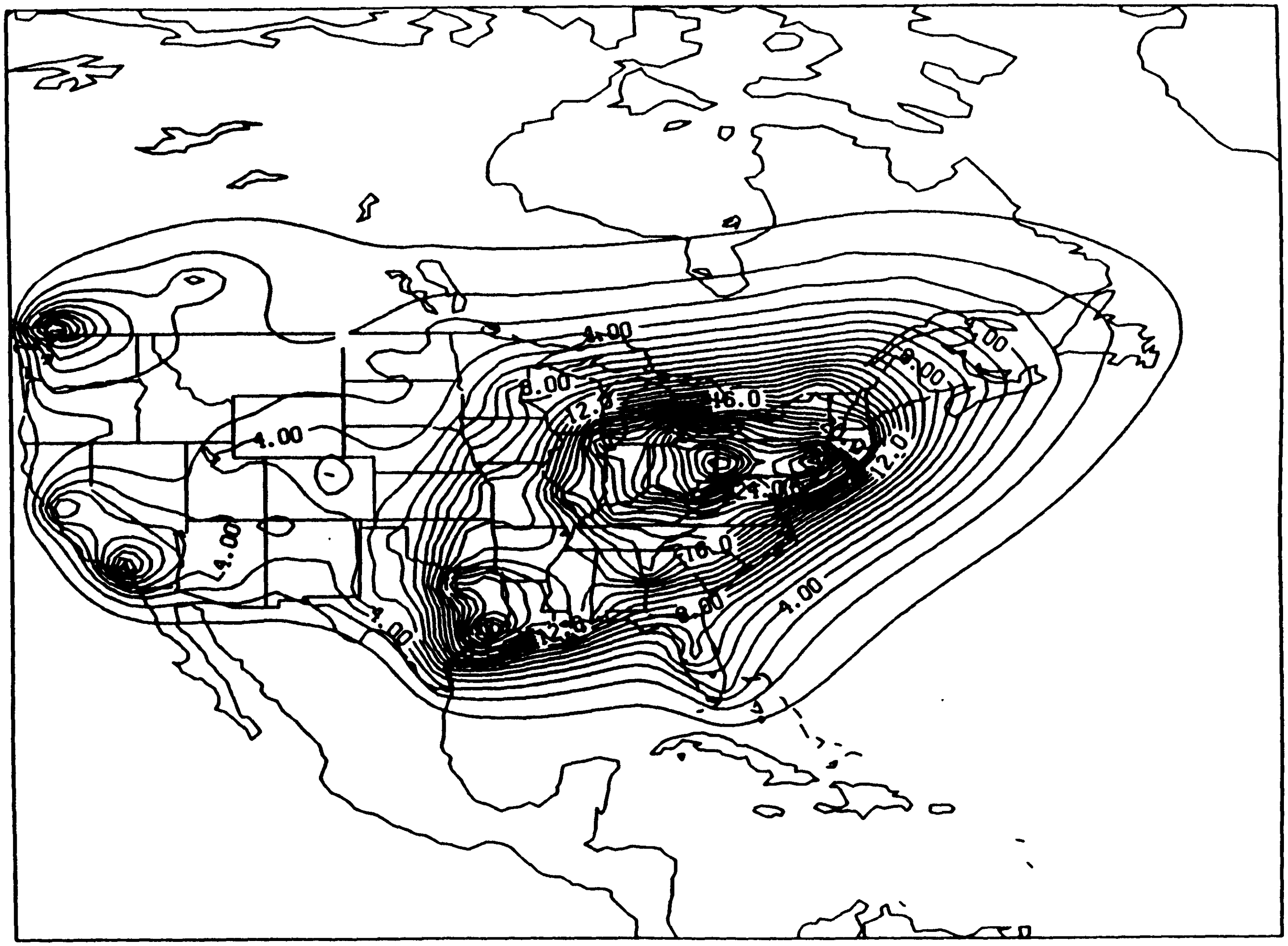

Fig. 4.6 Airborne NO_x ($\mu g\ m^{-3}\ NO_2$) using optimized NO_x model parameters. Outer solution contours from 1.0 to 31.0 $\mu g\ m^{-3}$ by 1.0 $\mu g\ m^{-3}$.

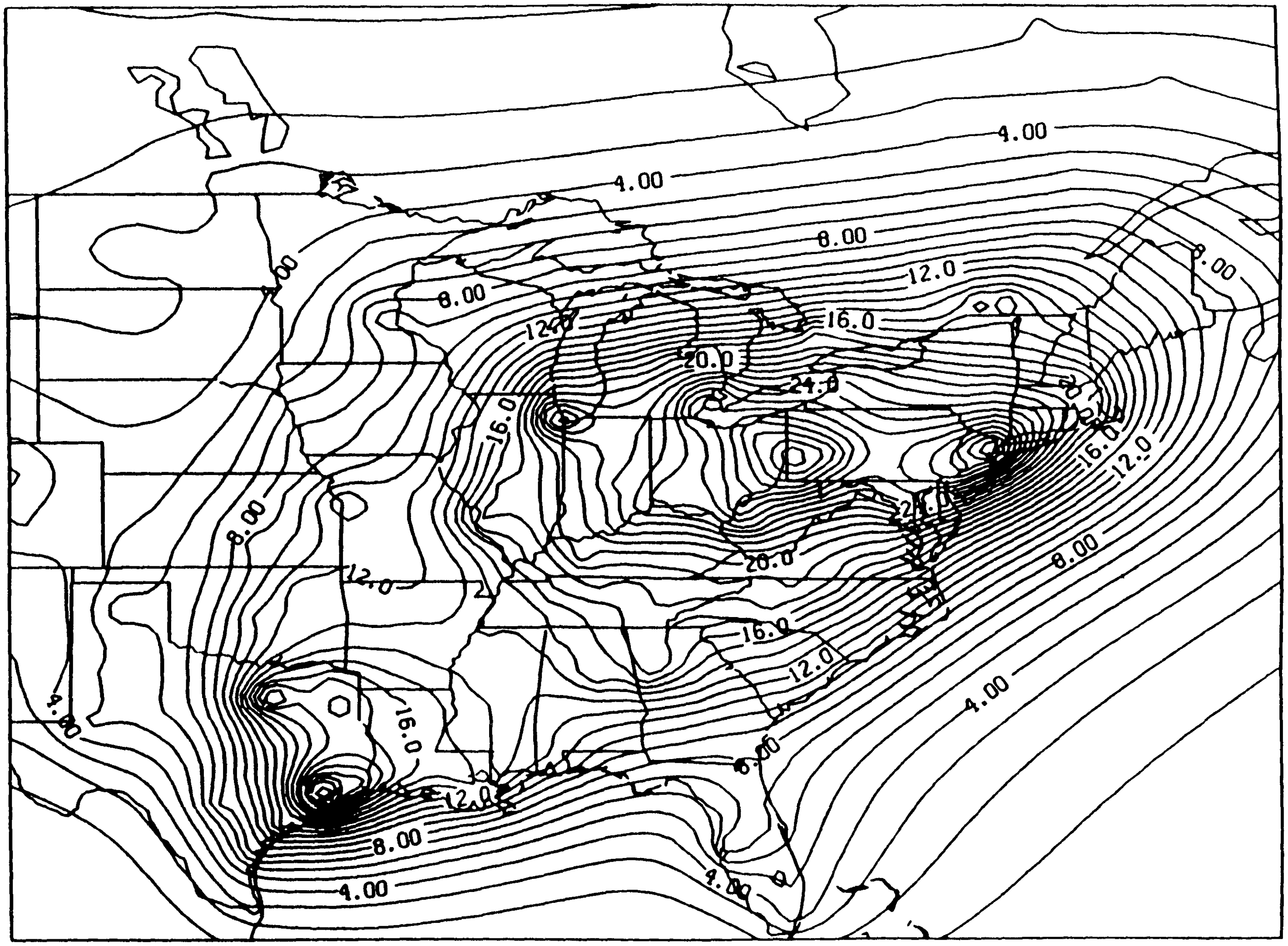

Fig. 4.7 Airborne NO_x ($\mu g\, m^{-3}$ NO_2) using optimized NO_x model parameters. Inner solution contours from 1.0 to 32.0 $\mu g\, m^{-3}$ by 1.0 $\mu g\, m^{-3}$.

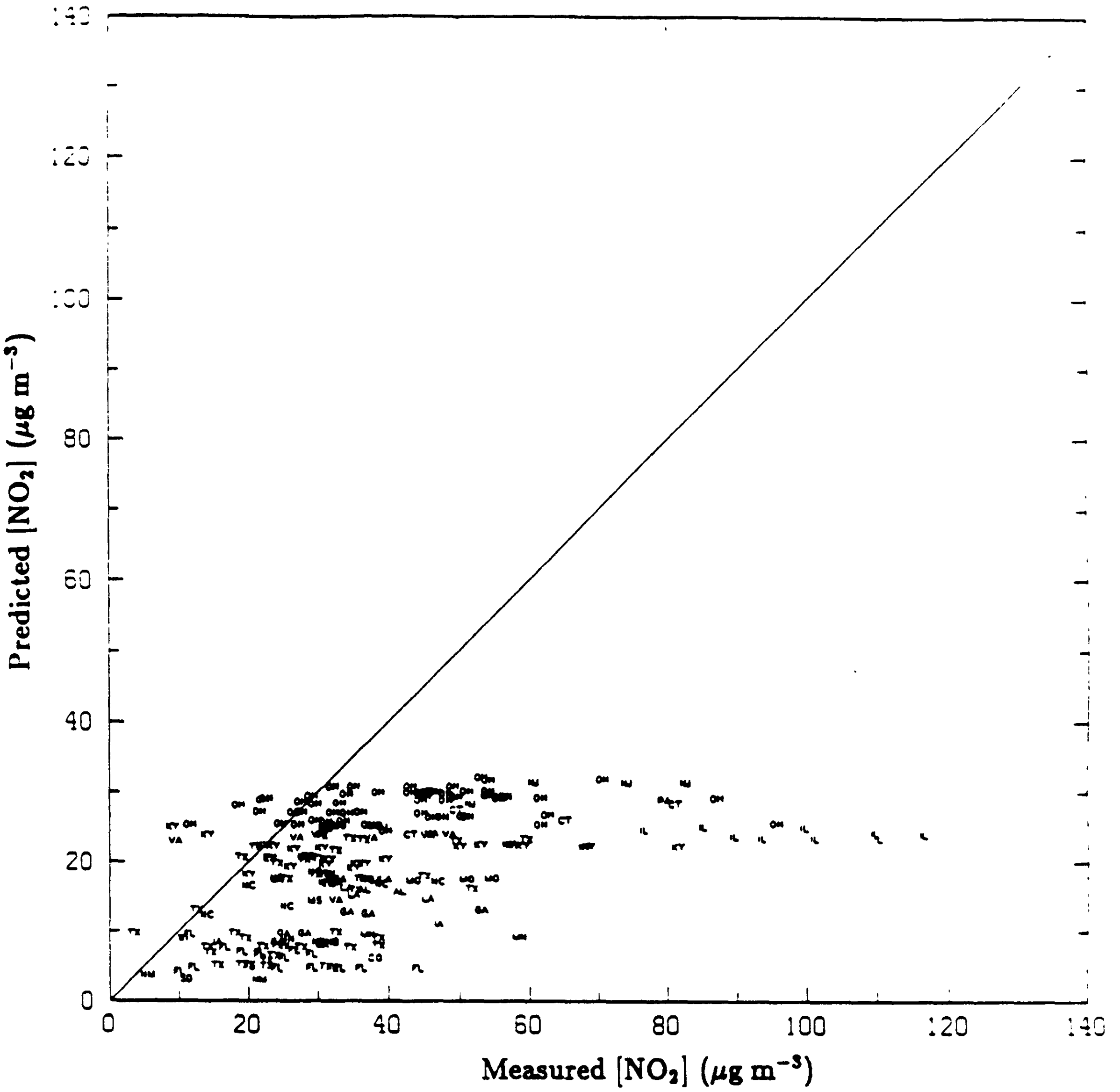

Fig. 4.8 Predicted vs. measured airborne NO$_2$ (μg m^{-3}) at urban monitors using optimized NO$_x$ long range transport model parameters. Two letter state abbreviations indicate monitor location. 1980 data, correlation coefficient r=0.46.

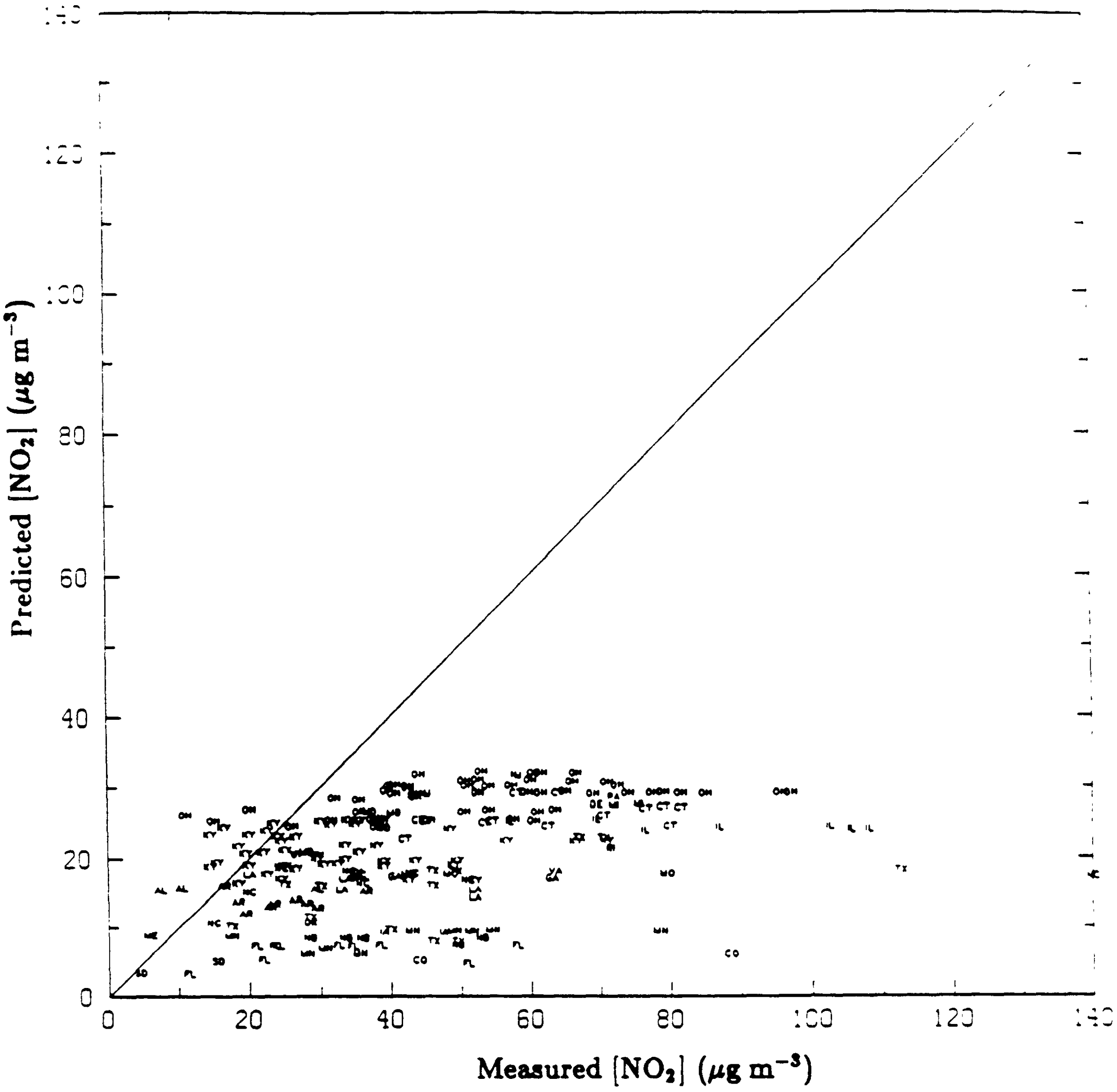

Fig. 4.9 Predicted vs. measured airborne NO_2 ($\mu g\ m^{-3}$) at suburban monitors using optimized NO_x long range transport model parameters. Two letter state abbreviations indicate monitor location. 1980 data, correlation coefficient r=0.38.

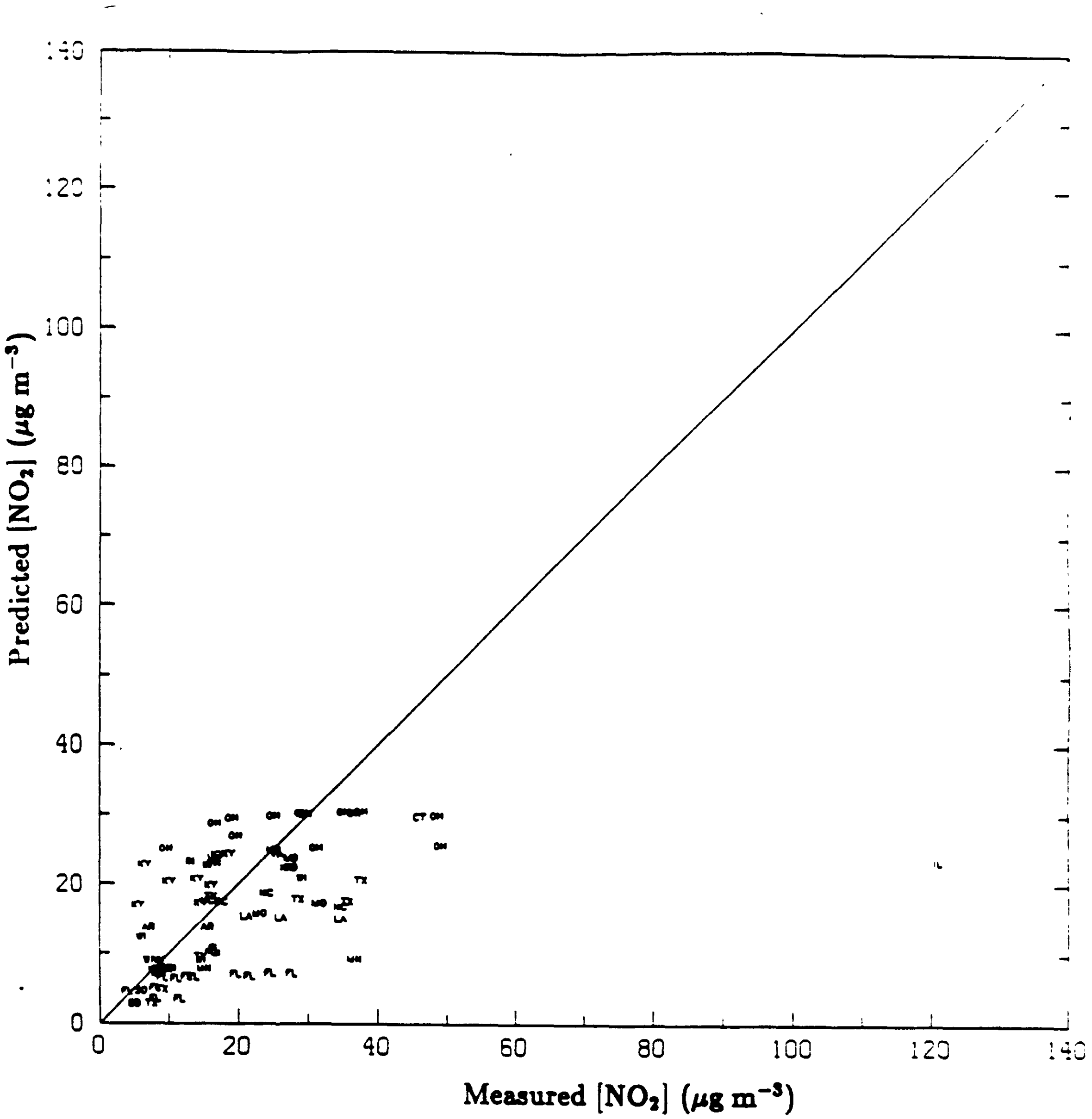

Fig. 4.10 Predicted vs. measured airborne NO_2 (μg m^{-3}) at rural monitors using optimized NO_x long range transport model parameters. Two letter state abbreviations indicate monitor location. 1980 data, correlation coefficient r=0.48.

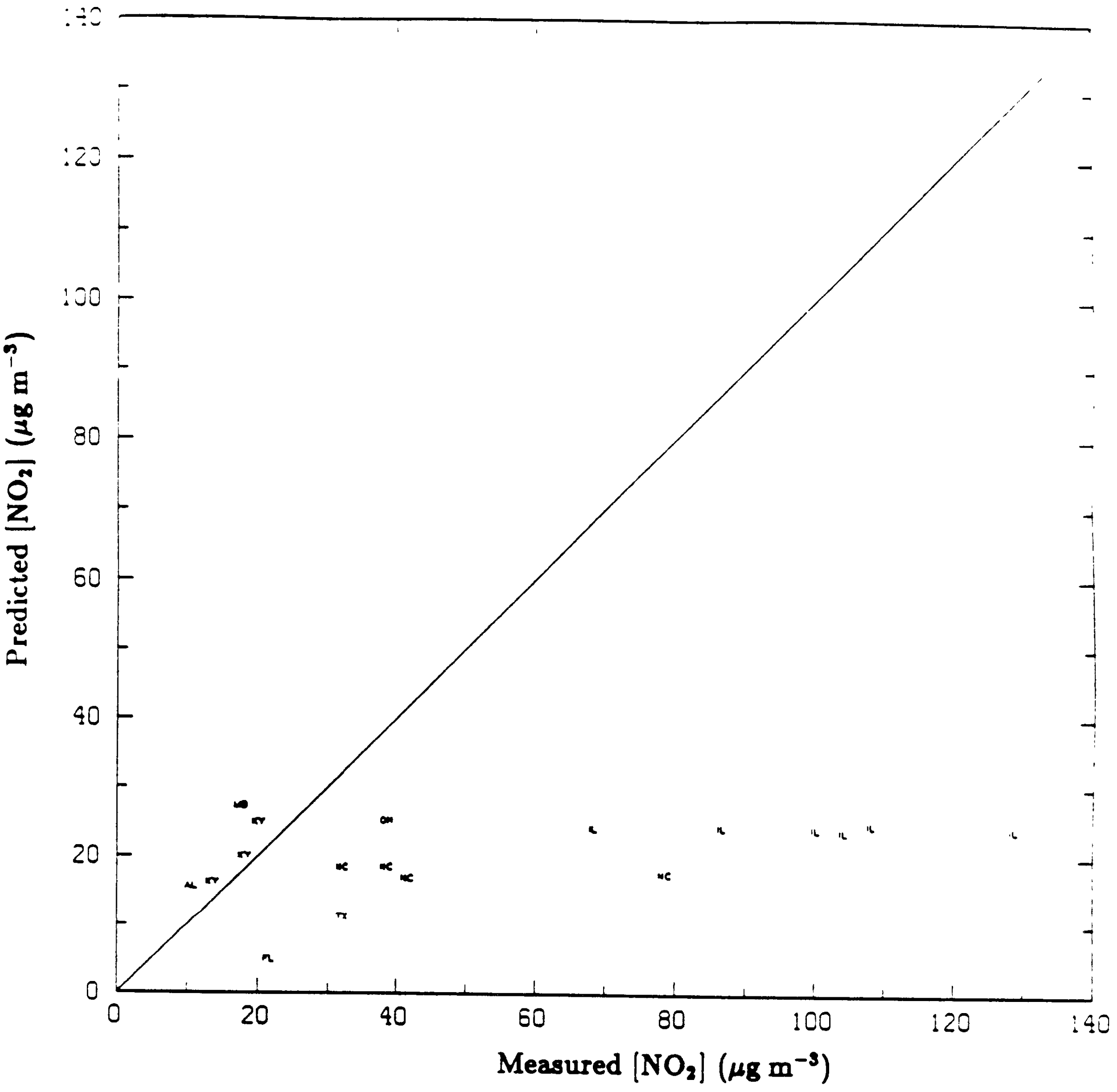

Fig. 4.11 Predicted vs. measured airborne NO$_2$ (μg m^{-3}) at unclassified monitors using optimized NO$_x$ long range transport model parameters. Two letter state abbreviations indicate monitor location. 1980 data, correlation coefficient r=0.45.

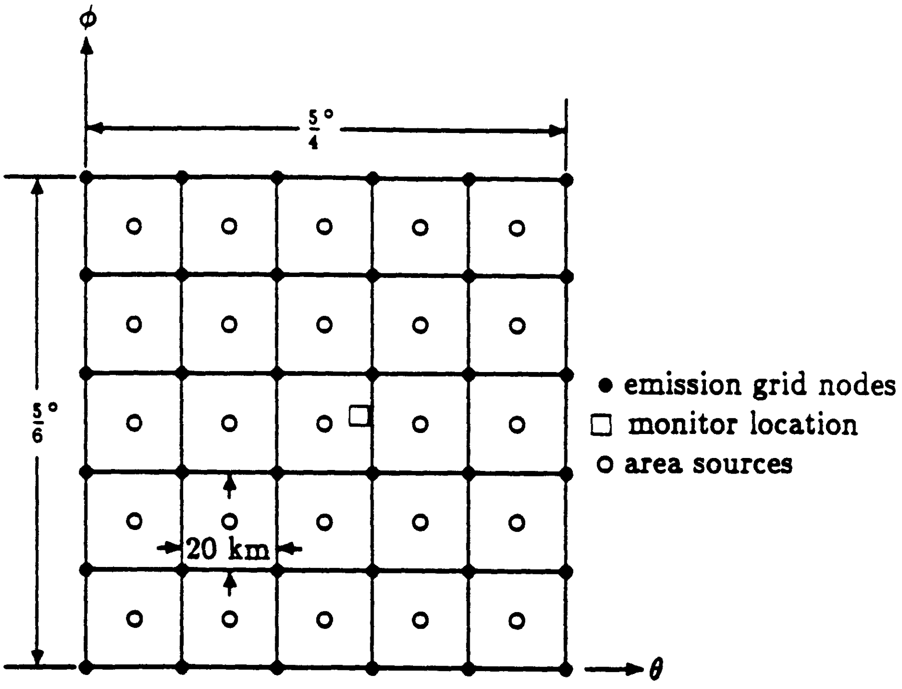

Local Source Region

Fig. 4.12 Local source region around an arbitrary monitoring region. Area sources are located at the centroid of each cell. Point sources (not shown) may be situated anywhere within the region.

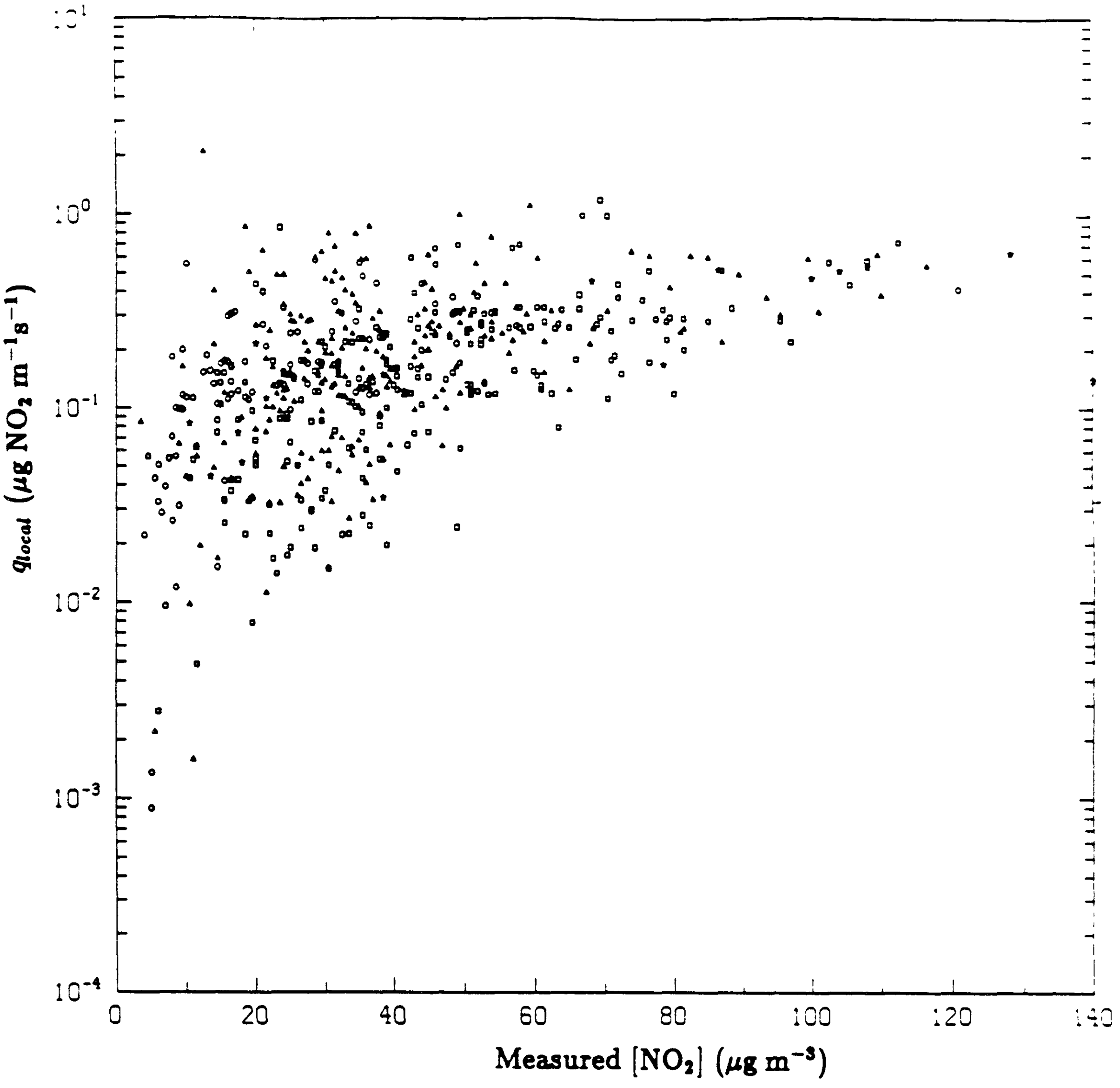

Fig. 4.13 q_{local} (the sum of local sources normalized by their proximity to the measuring site) (μg NO$_2$ m^{-1}s^{-1}) vs. measured NO$_2$ (μg m^{-3}). Square, triangle, circle and star symbols indicate urban, suburban, rural and unclassified monitoring sites. 1980 data.

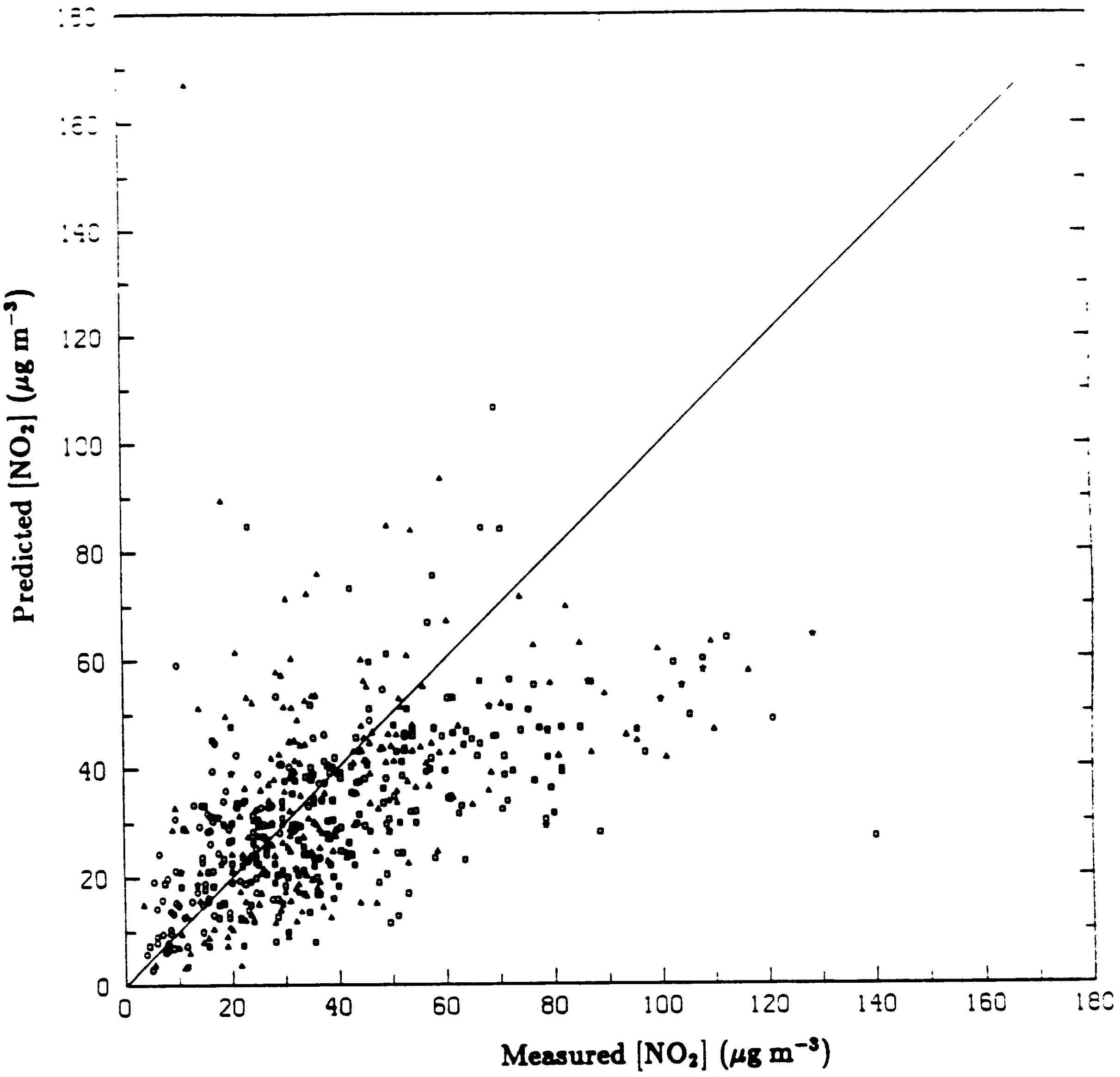

Fig. 4.14 Total predicted vs. measured NO$_2$ concentrations. (μg m^{-3}). Local streaming model. Square, triangle, circle and star symbols indicate urban, suburban, rural and unclassified monitoring sites. Average error is 46.8% and the correlation coefficient r=0.52. Companion plot to Fig. 4.15. 1980 data, $\overline{vh}$=2100 m^{2}s^{-1}.

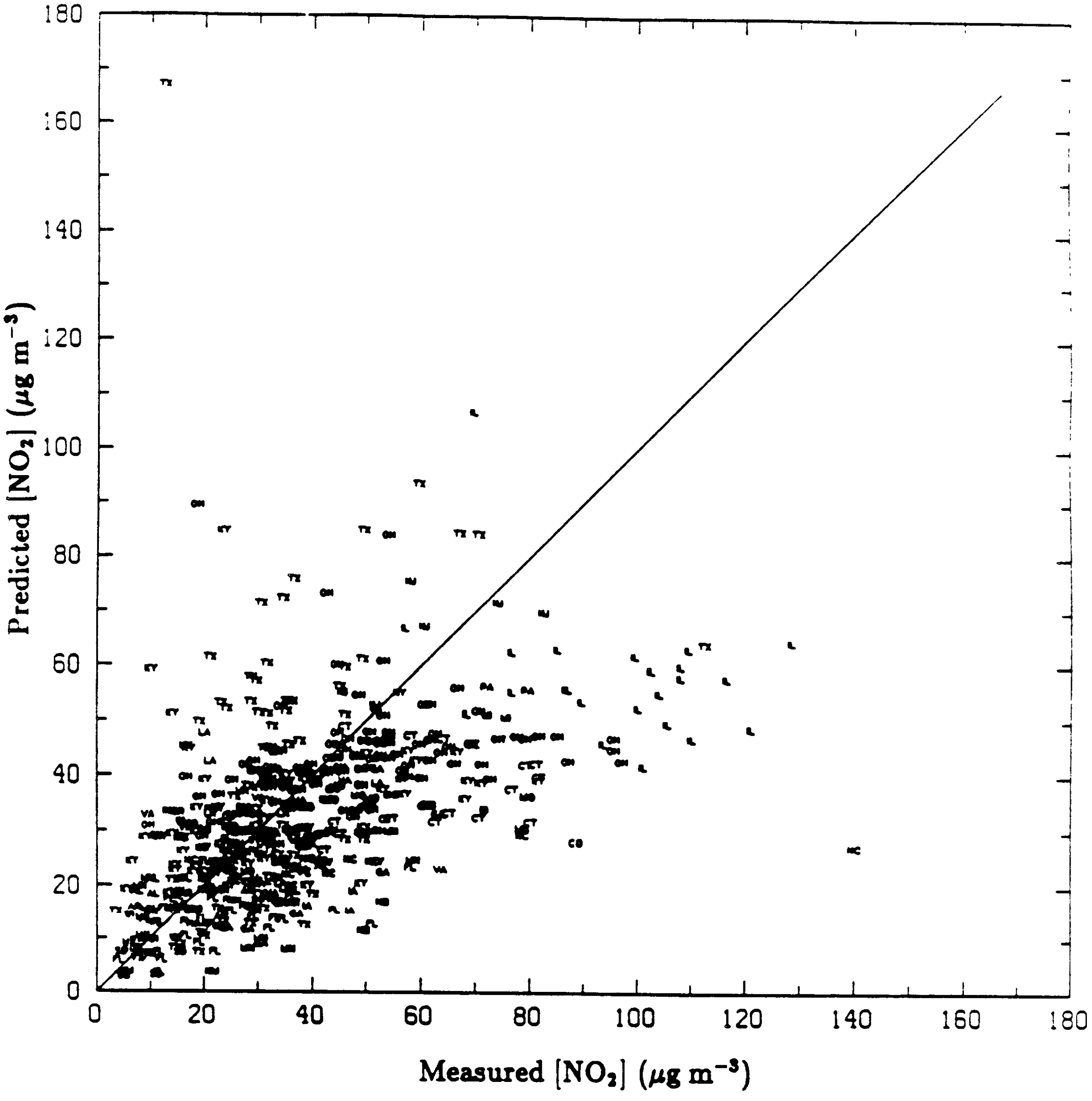

Fig. 4.15 Total predicted vs. measured NO_2 concentrations ($\mu g\ m^{-3}$). Local streaming model. Two letter state abbreviations identify the location of each monitoring site. Average error is 46.8% and the correlation coefficient r=0.52. Companion plot to Fig. 4.14. 1980 data, $\overline{vh}$=2100 m^2s^{-1}.

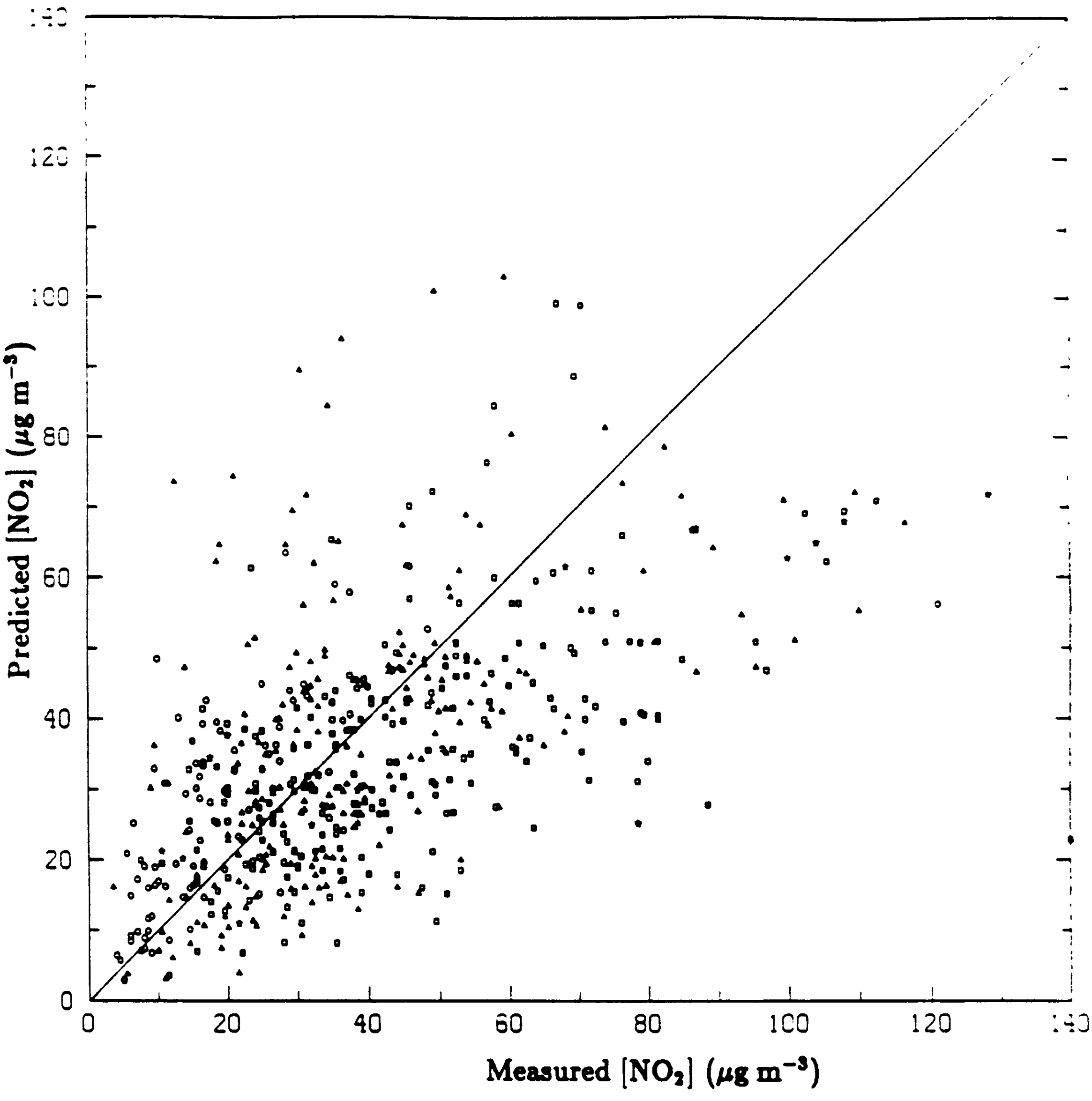

Fig. 4.16 Total predicted vs. measured NO_2 concentrations. ($\mu g\ m^{-3}$). Modified FGK local model. Square, triangle, circle and star symbols indicate urban, suburban, rural and unclassified monitoring sites. Average error is 43.4% and the correlation coefficient r=0.58. Companion plot to Fig. 4.17. 1980 data, $\lambda=0.3$, $\sigma=16\ km^{0.7}$.

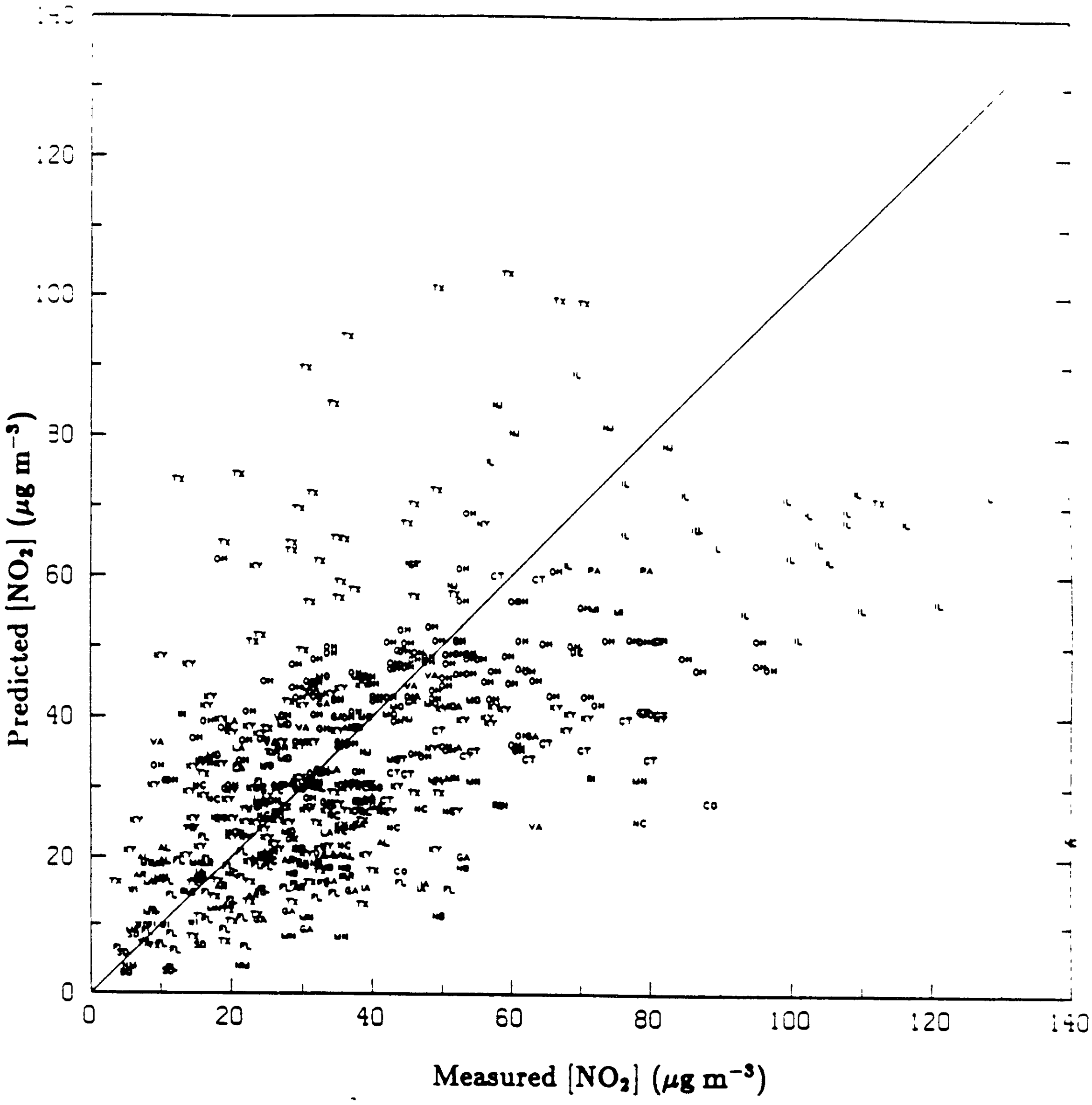

Fig. 4.17 Total predicted vs. measured NO$_2$ concentrations. (μg m^{-3}). Modifed FGK local model. Two letter state abbreviations identify the location of each monitoring site. Average error is 43.4% and the correlation coefficient r=0.58. Companion plot to Fig. 4.16. 1980 data, λ=0.3, σ=16 km$^{0.7}$.

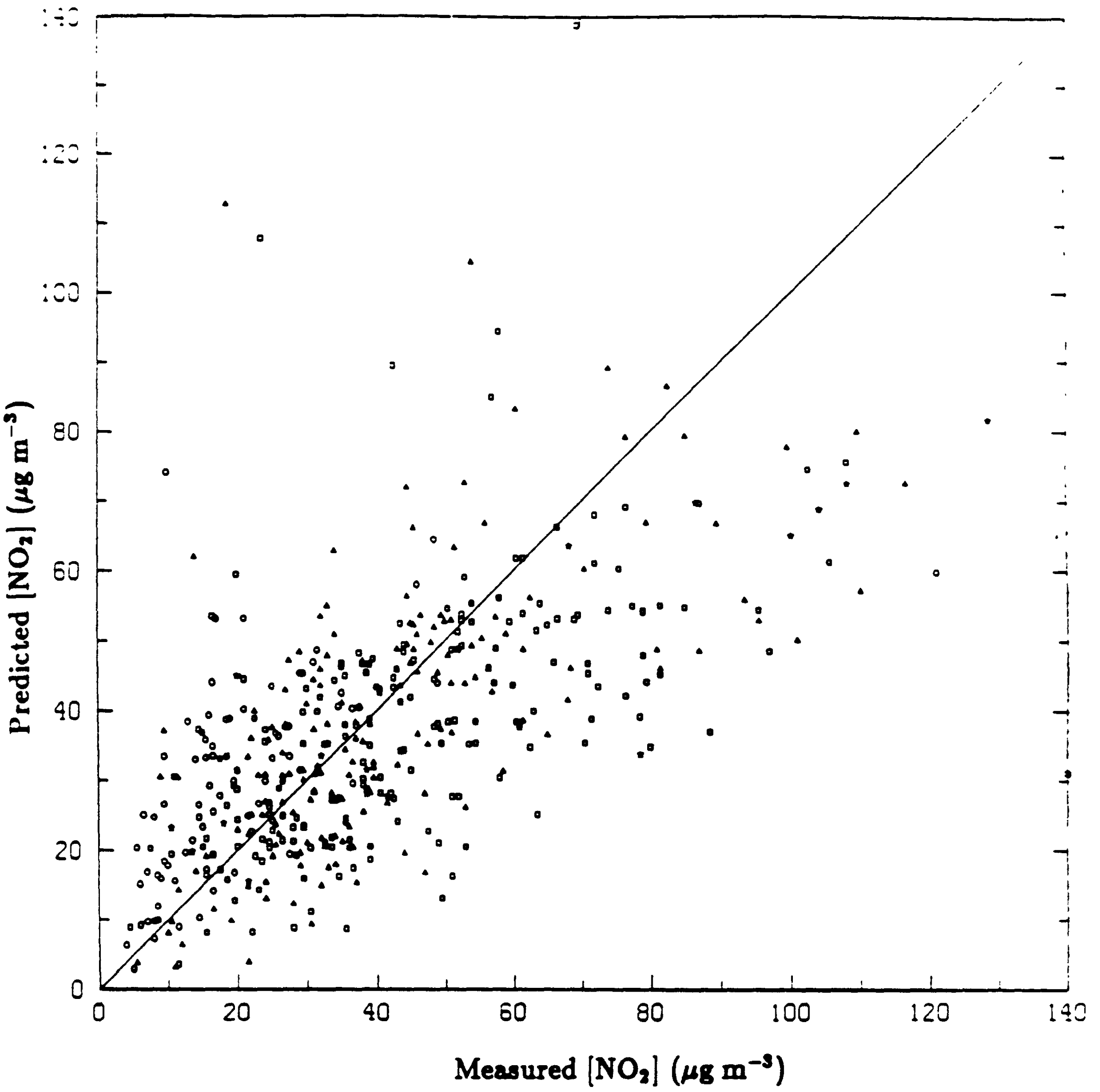

Fig. 4.18 Total predicted vs. measured NO_2 concentrations. (μg m^{-3}). Local streaming model with Texas sites omitted. Square, triangle, circle and star symbols indicate urban, suburban, rural and unclassified monitoring sites. Average error is 41.2% and the correlation coefficient r=0.53. Companion plot to Fig. 4.19. 1980 data, $\overline{vh}$=1500 m^{2}s^{-1}.

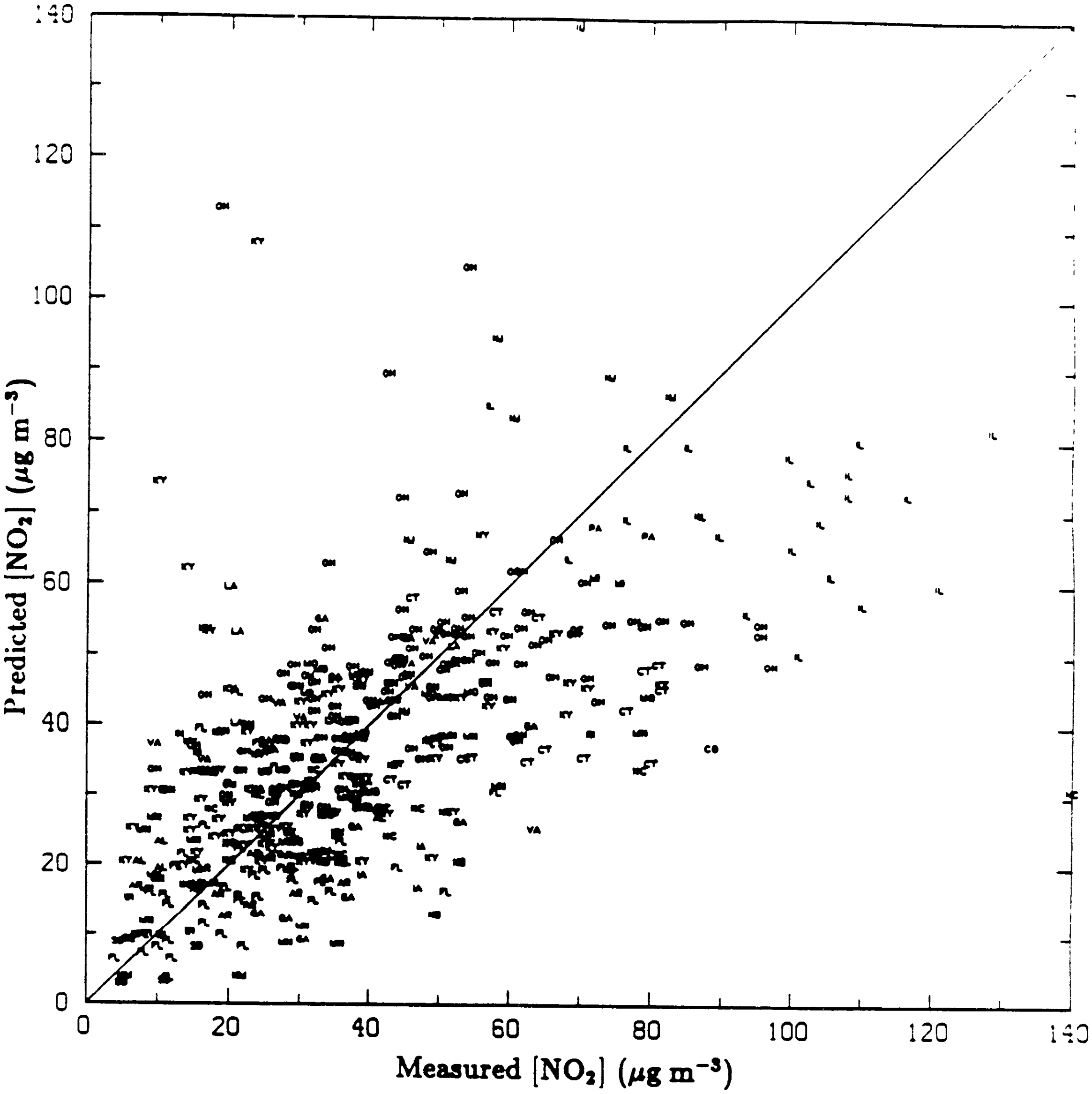

Fig. 4.19 Total predicted vs. measured NO$_2$ concentrations. (μg m^{-3}). Local streaming model with Texas sites omitted. Two letter state abbreviations identify the location of each monitoring site. Average error is 41.2% and the correlation coefficient r=0.53. Companion plot to Fig. 4.18. 1980 data, $\overline{vh}$=1500 m^{2}s^{-1}.

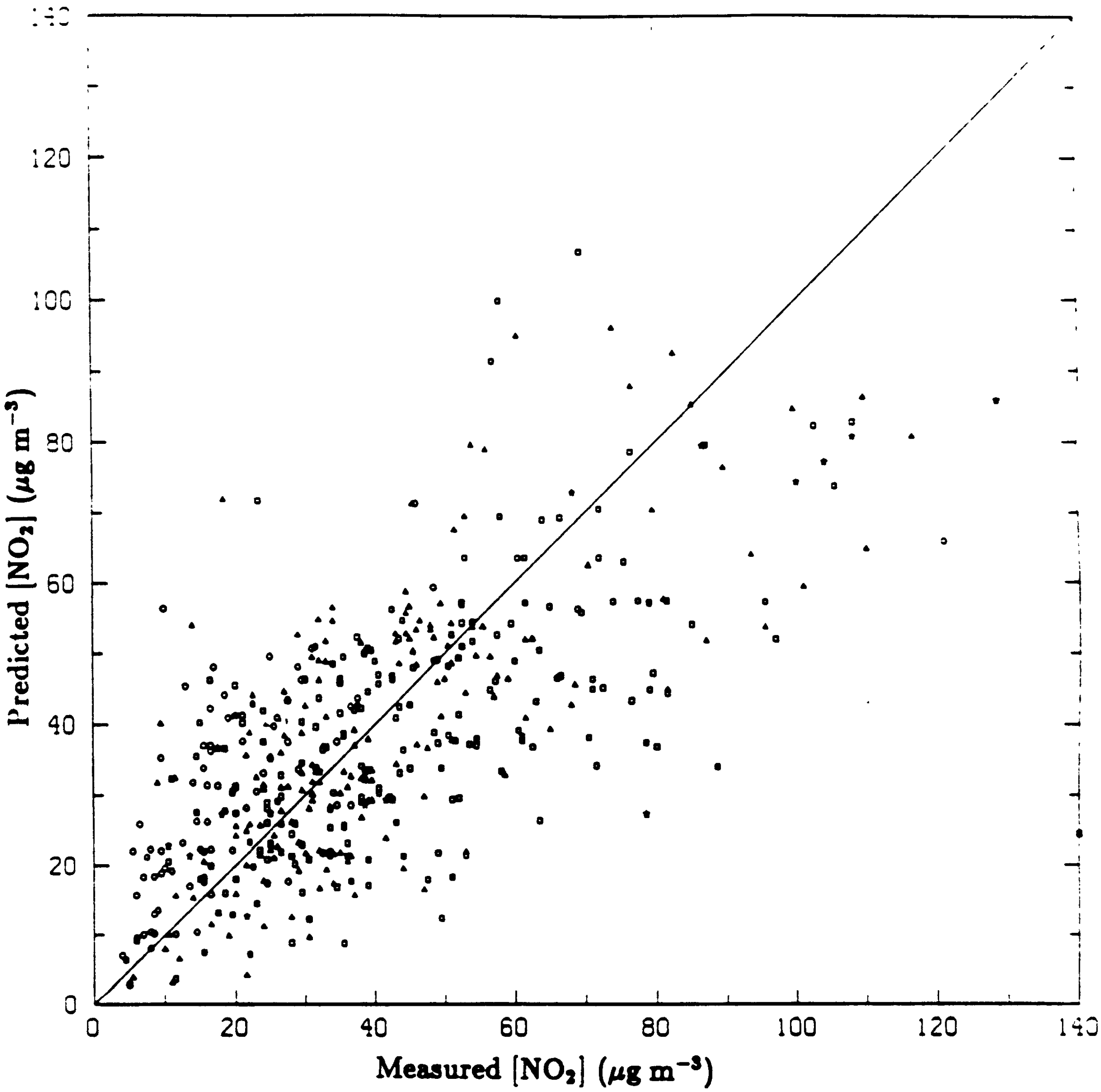

Fig. 4.20 Total predicted vs. measured NO$_2$ concentrations. (μg m^{-3}). Modified FGK local model with Texas sites omitted. Square, triangle, circle and star symbols indicate urban, suburban, rural and unclassified monitoring sites. Average error is 37.9% and the correlation coefficient r=0.61. Companion plot to Fig. 4.21. 1980 data, λ=0.3, σ=20 km$^{0.7}$.

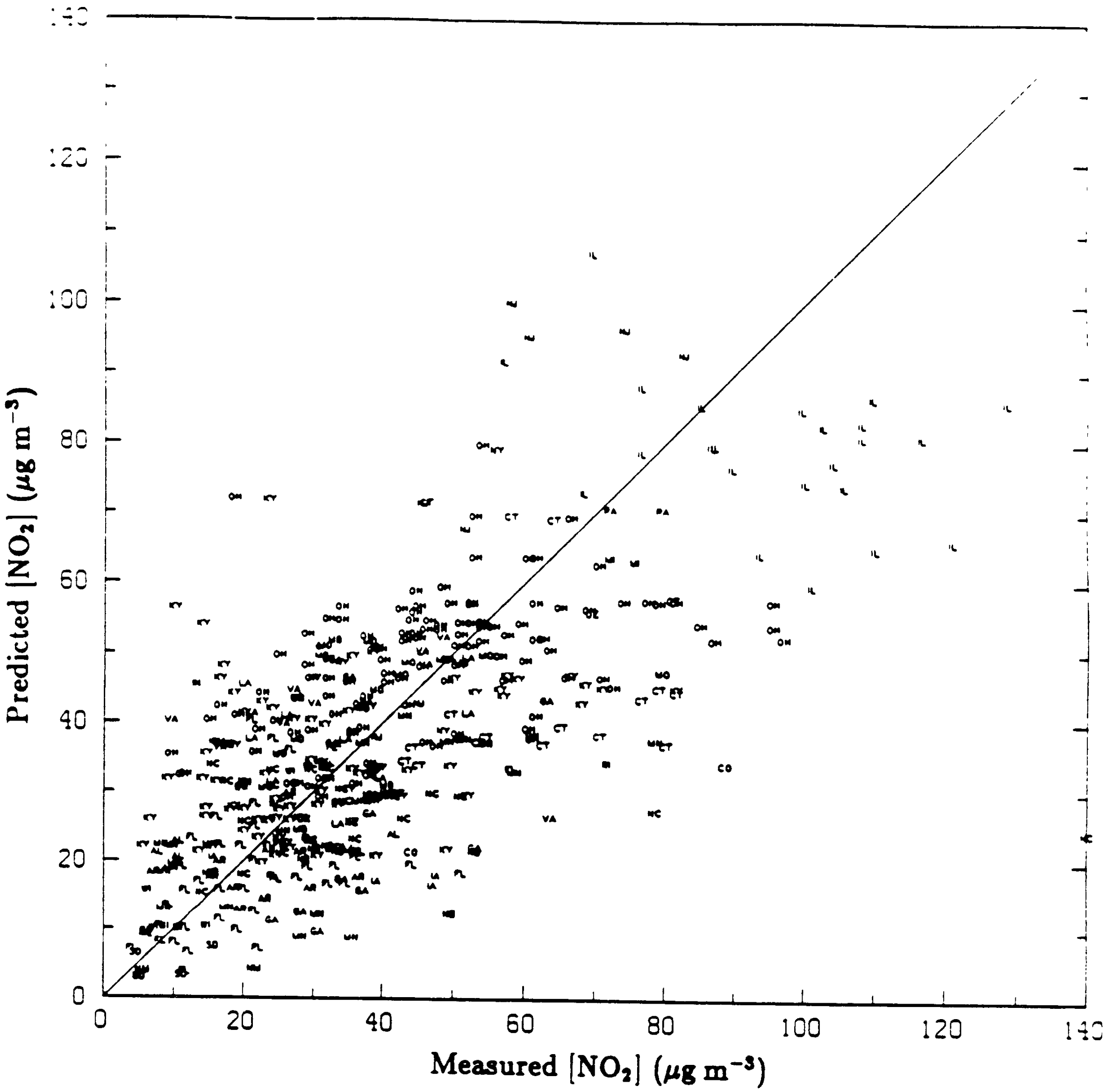

Fig. 4.21 Total predicted vs. measured NO_2 concentrations. ($\mu g\, m^{-3}$). Modifed FGK local model with Texas sites omitted. Two letter state abbreviations identify the location of each monitoring site. Average error is 37.9% and the correlation coefficient r=0.61. Companion plot to Fig. 4.20. 1980 data, λ=0.3, σ=20 $km^{0.7}$.

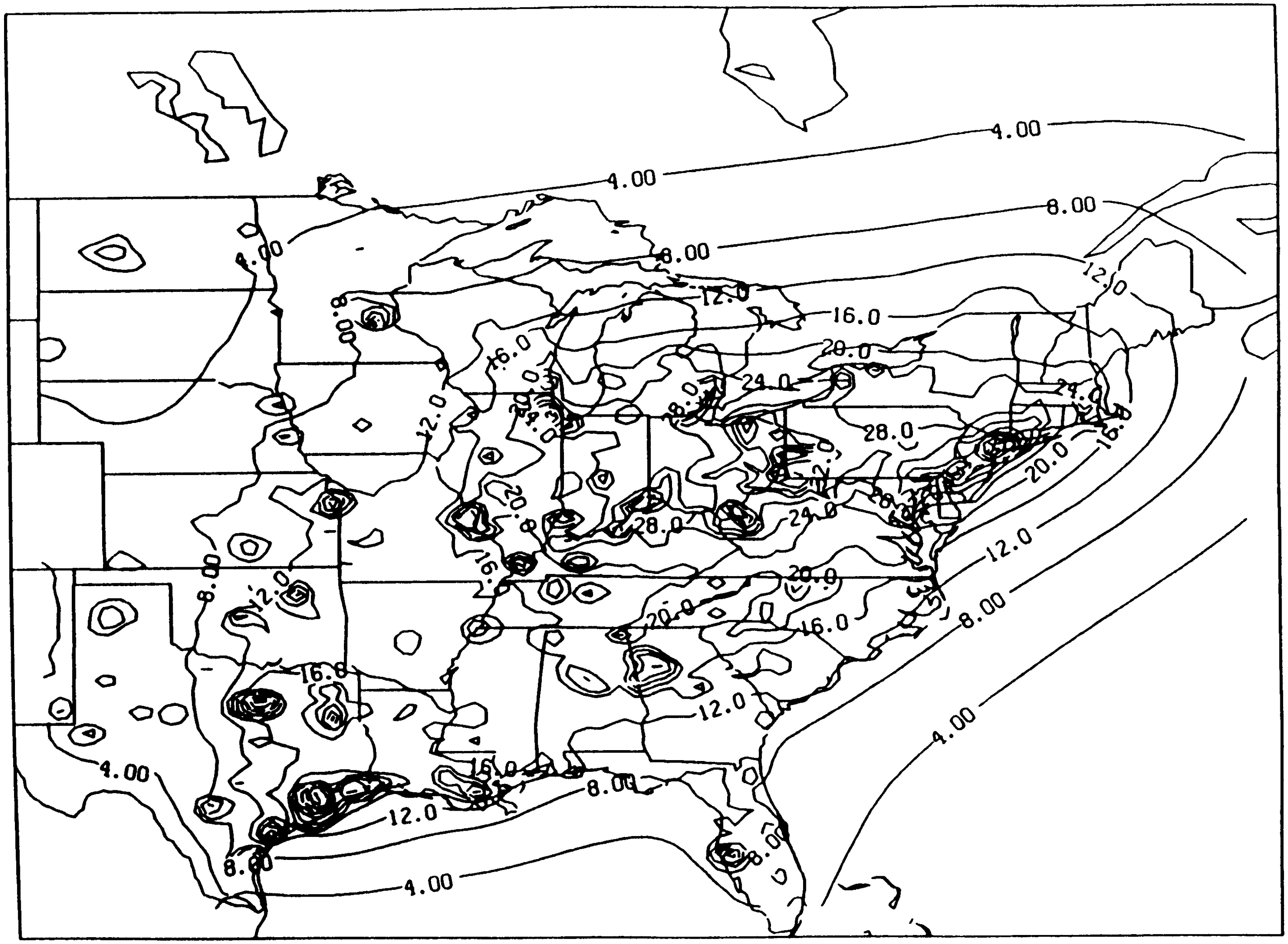

Fig. 4.22 Total modeled NO_x ($\mu g\, m^{-3}$ NO_2) computed with the modified FGK local model. Contours from 4 to 88 $\mu g\, m^{-3}$ by 4 $\mu g\, m^{-3}$.

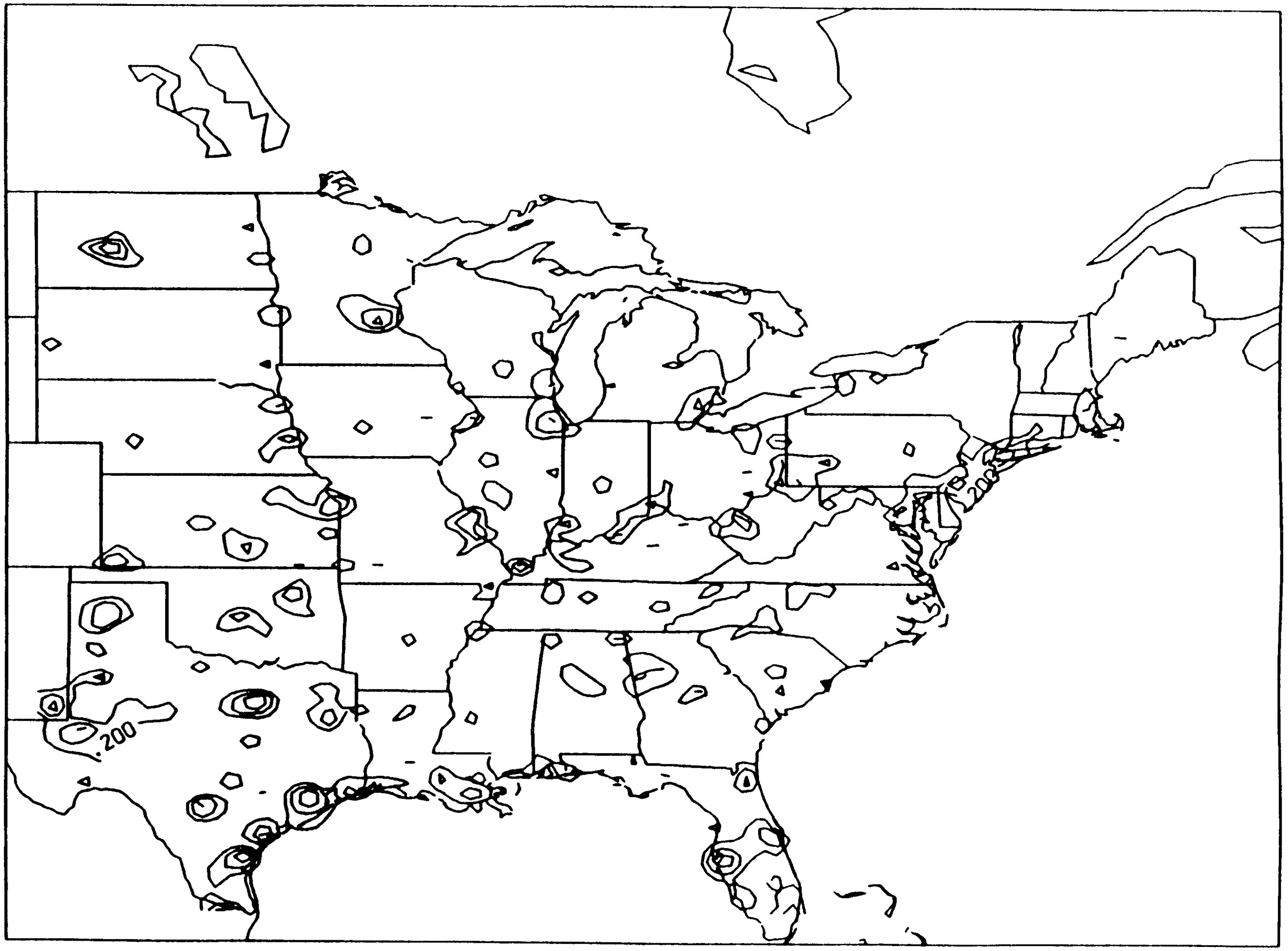

Fig. 4.23 Ratio of long range modeled NO_x (Fig. 4.7) to total modeled NO_x (Fig. 4.22). Contours from 0.2 to 0.8 by 0.2.

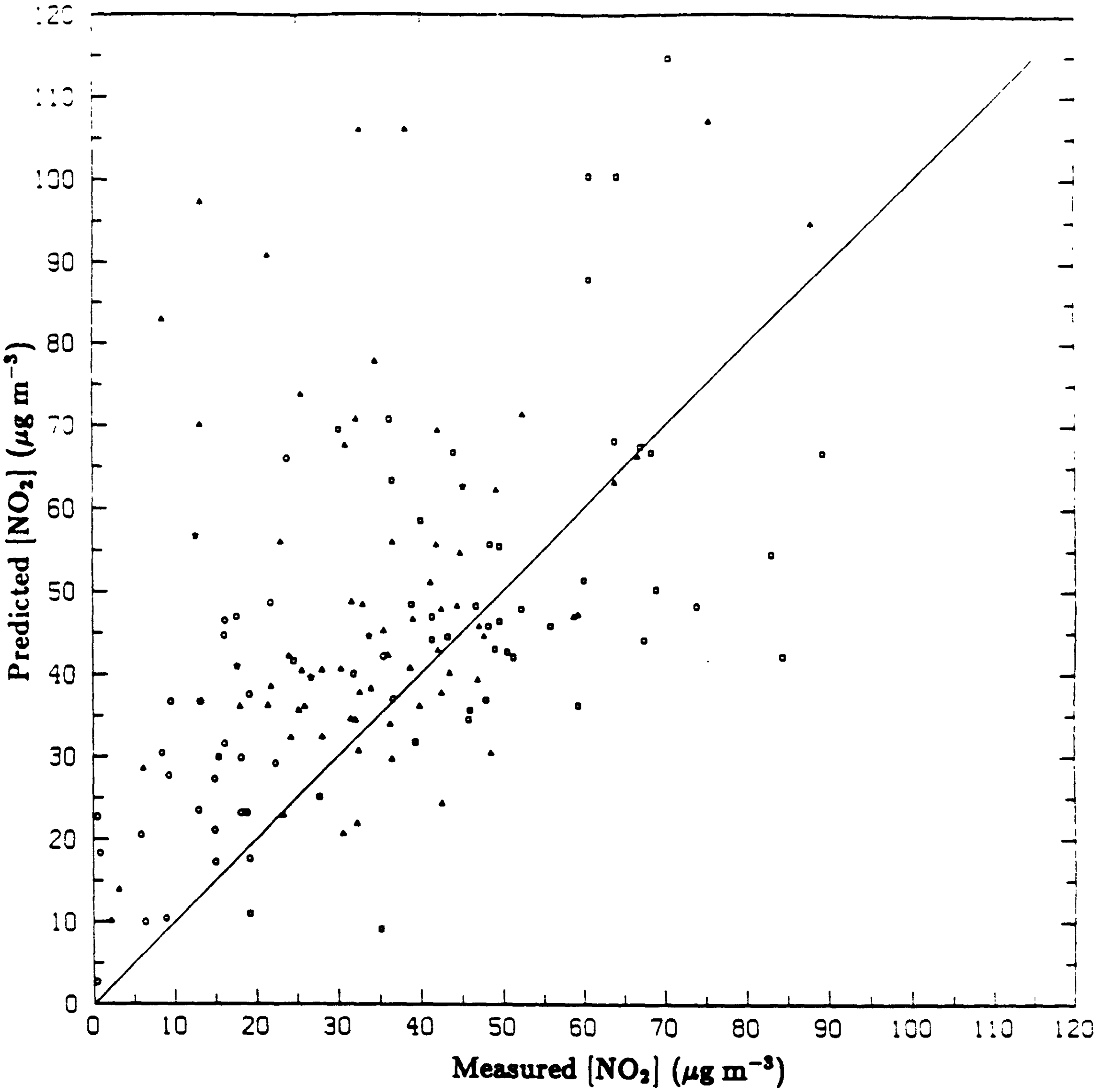

Fig. 4.24 Total predicted vs. measured NO$_2$ concentrations. (μg m^{-3}). Local streaming model. Square, triangle, circle and star symbols indicate urban, suburban, rural and unclassified monitoring sites. Average error is 41.5% and the correlation coefficient r=0.48 (Texas sites excluded from statistics). Companion plot to Fig. 4.25. 1985 data, $\overline{vh}$=1500 m^{2}s^{-1}.

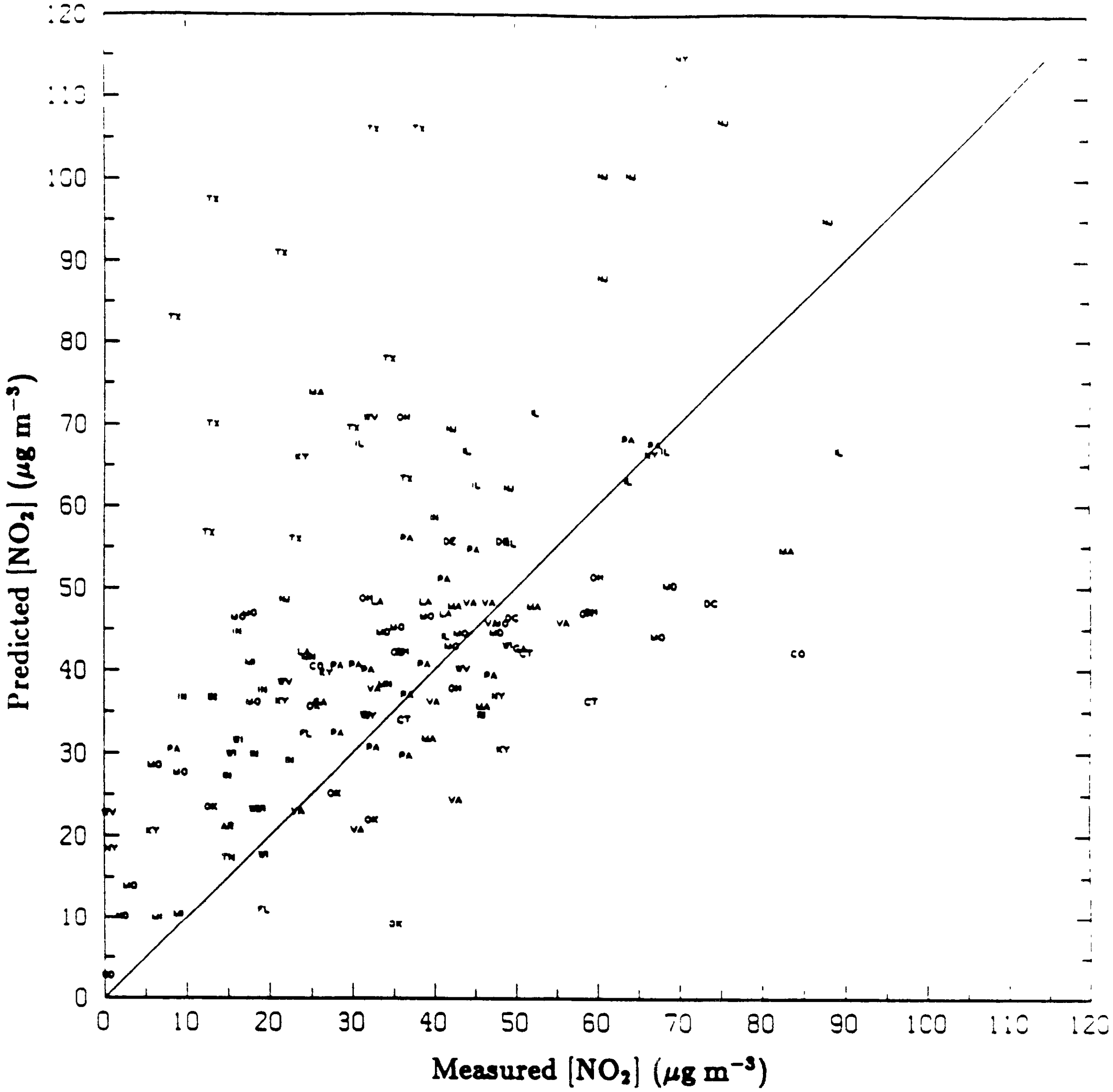

Fig. 4.25 Total predicted vs. measured NO$_2$ concentrations. (μg m^{-3}). Local streaming model. Two letter state abbreviations identify the location of each monitoring site. Average error is 41.5% and the correlation coefficient r=0.48 (Texas sites excluded from statistics). Companion plot to Fig. 4.24. 1985 data, $\overline{vh}$=1500 m^{2}s^{-1}.

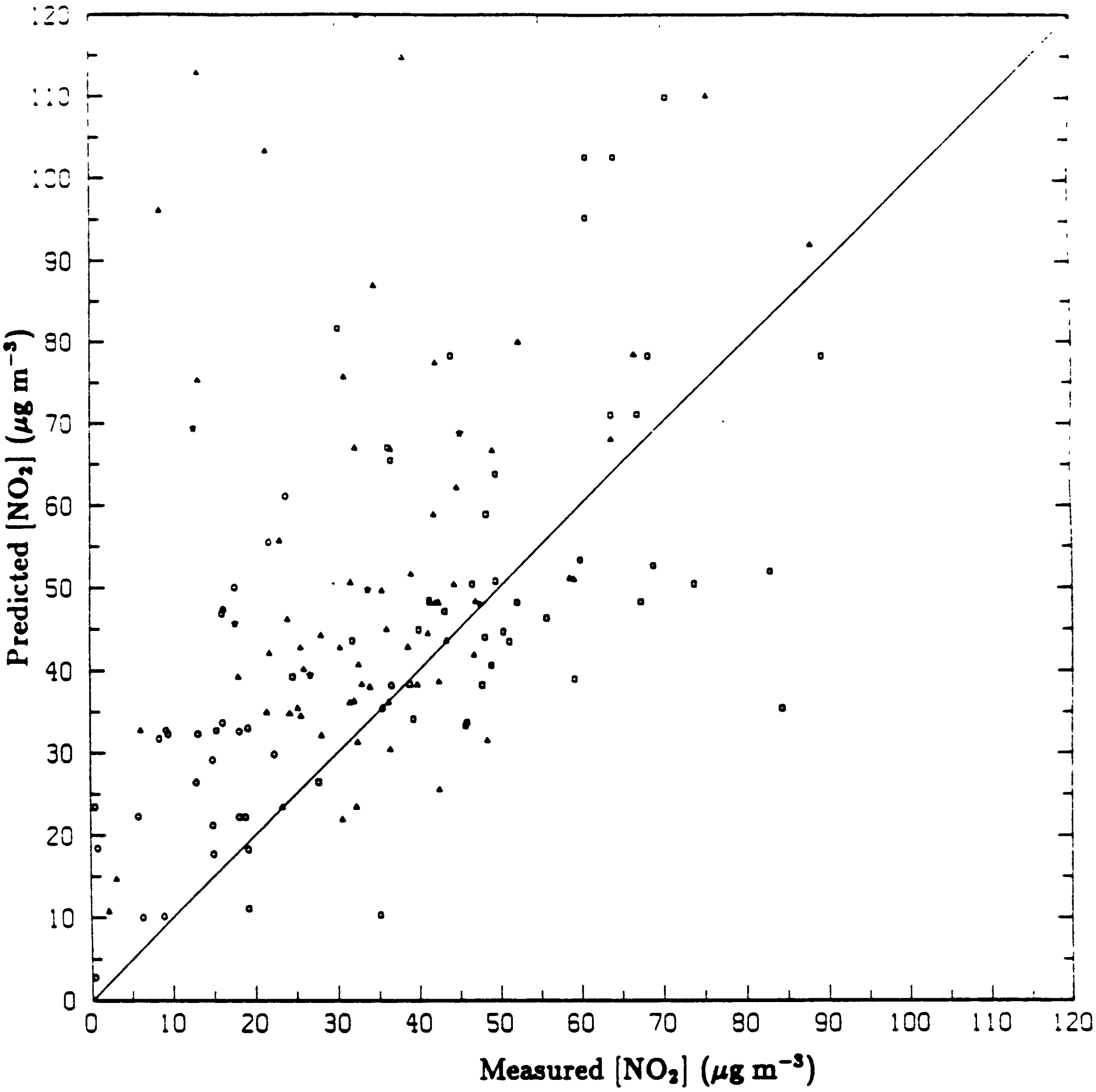

Fig. 4.26 Total predicted vs. measured NO_2 concentrations. (μg m^{-3}). Modified FGK local model. Square, triangle, circle and star symbols indicate urban, suburban, rural and unclassified monitoring sites. Average error is 42.9% and the correlation coefficient r=0.46 (Texas sites excluded from statistics). Companion plot to Fig. 4.27. 1985 data, λ=0.3, σ=20 km$^{0.7}$.

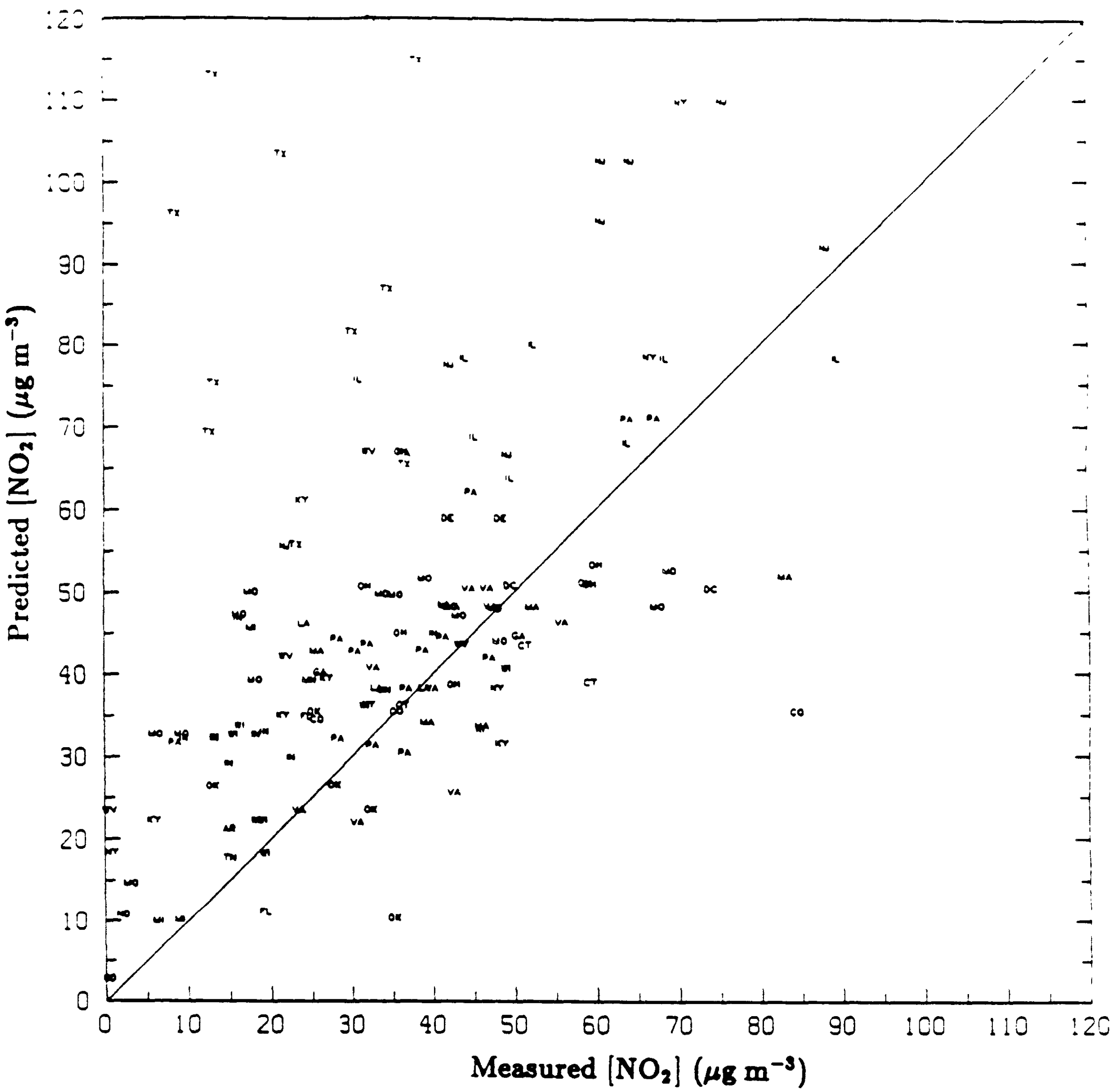

Fig. 4.27 Total predicted vs. measured NO$_2$ concentrations. (μg m^{-3}). Modifed FGK local model. Two letter state abbreviations identify the location of each monitoring site. Average error is 42.9% and the correlation coefficient r=0.46 (Texas sites excluded from statistics). Companion plot to Fig. 4.26. 1985 data, λ=0.3, σ=20 km$^{0.7}$.

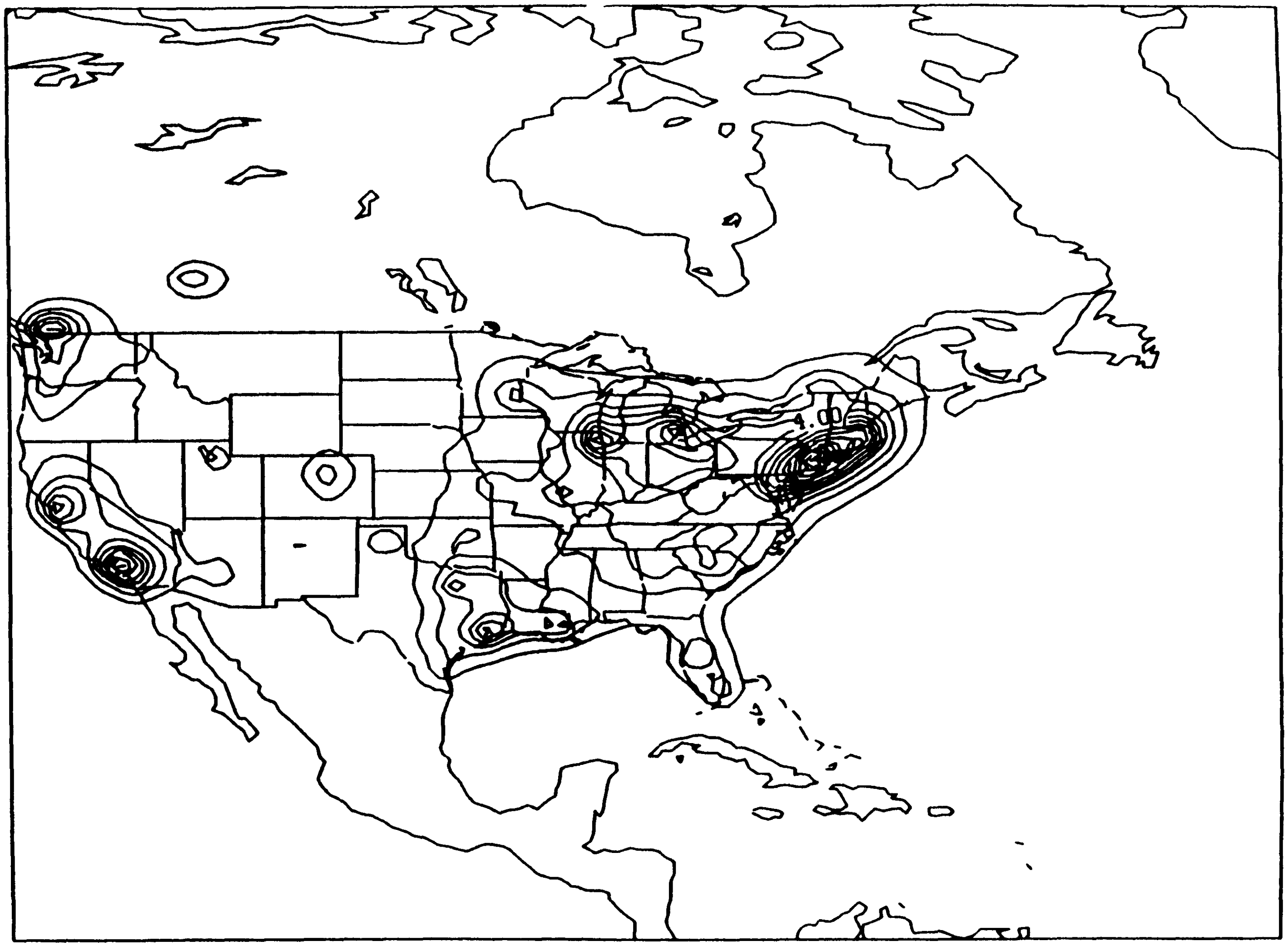

Fig. 4.28 Modeled anthropogenic VOCs concentrations ($\mu g\ m^{-3}$). Outer solution contours from 1 to 17 $\mu g\ m^{-3}$ by 1 $\mu g\ m^{-3}$.

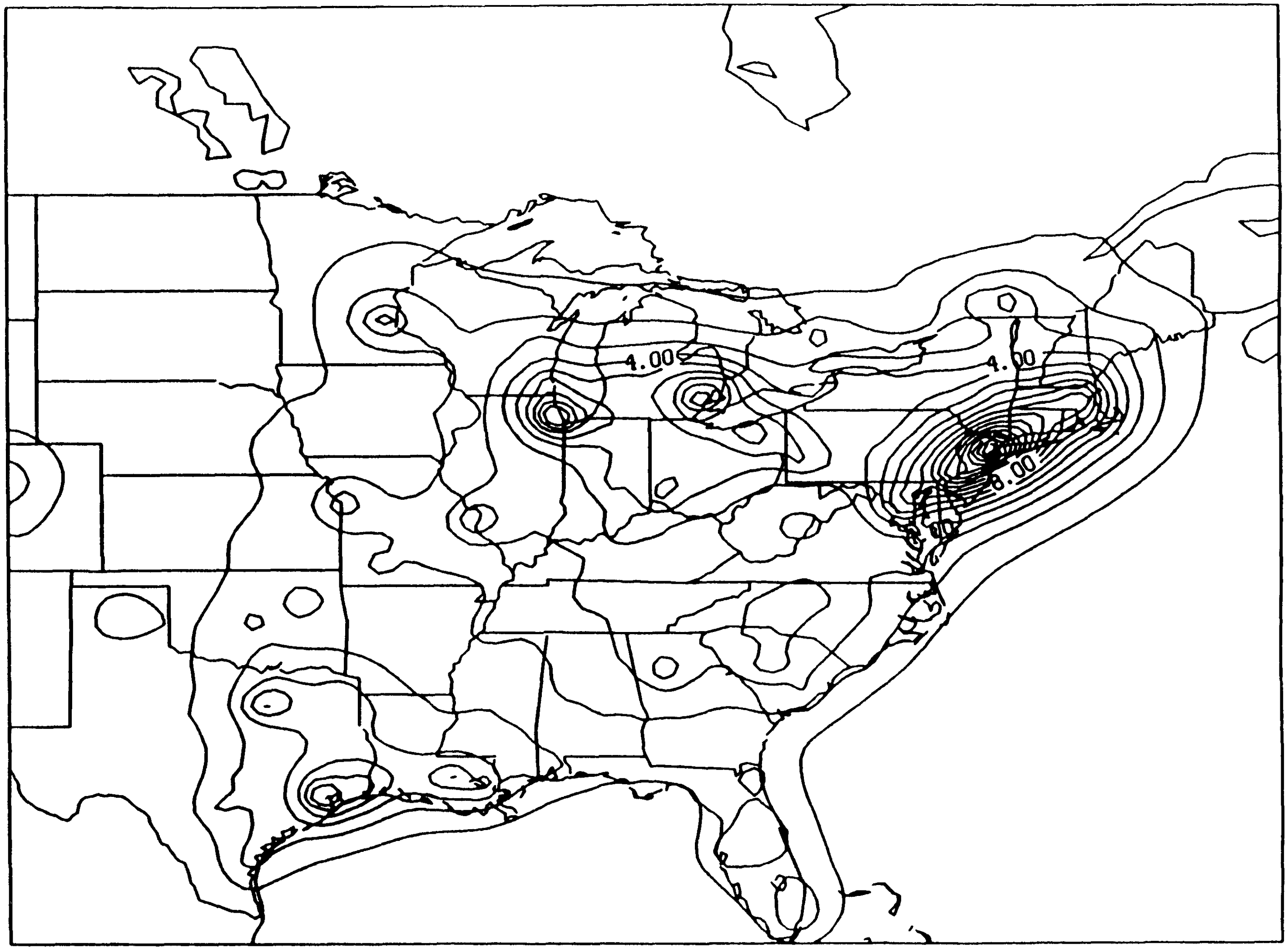

Fig. 4.29 Modeled anthropogenic VOCs concentrations ($\mu g\,m^{-3}$). Inner solution contours from 1 to 18 $\mu g\,m^{-3}$ by 1 $\mu g\,m^{-3}$.

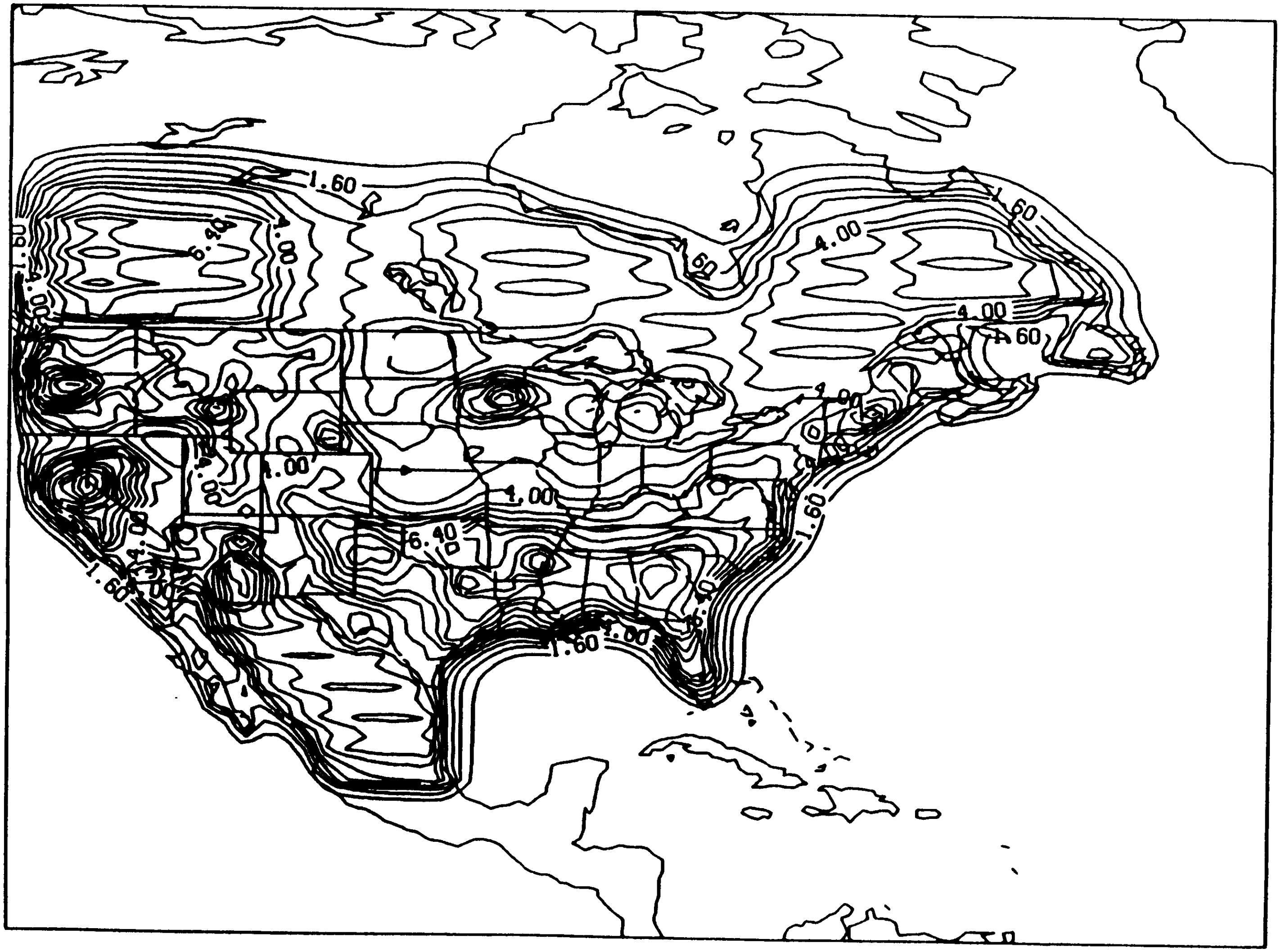

Fig. 4.30 Modeled biogenic VOCs concentrations ($\mu g\ m^{-3}$). Outer solution contours from 1.0 to 10.6 $\mu g\ m^{-3}$ by 0.6 $\mu g\ m^{-3}$.

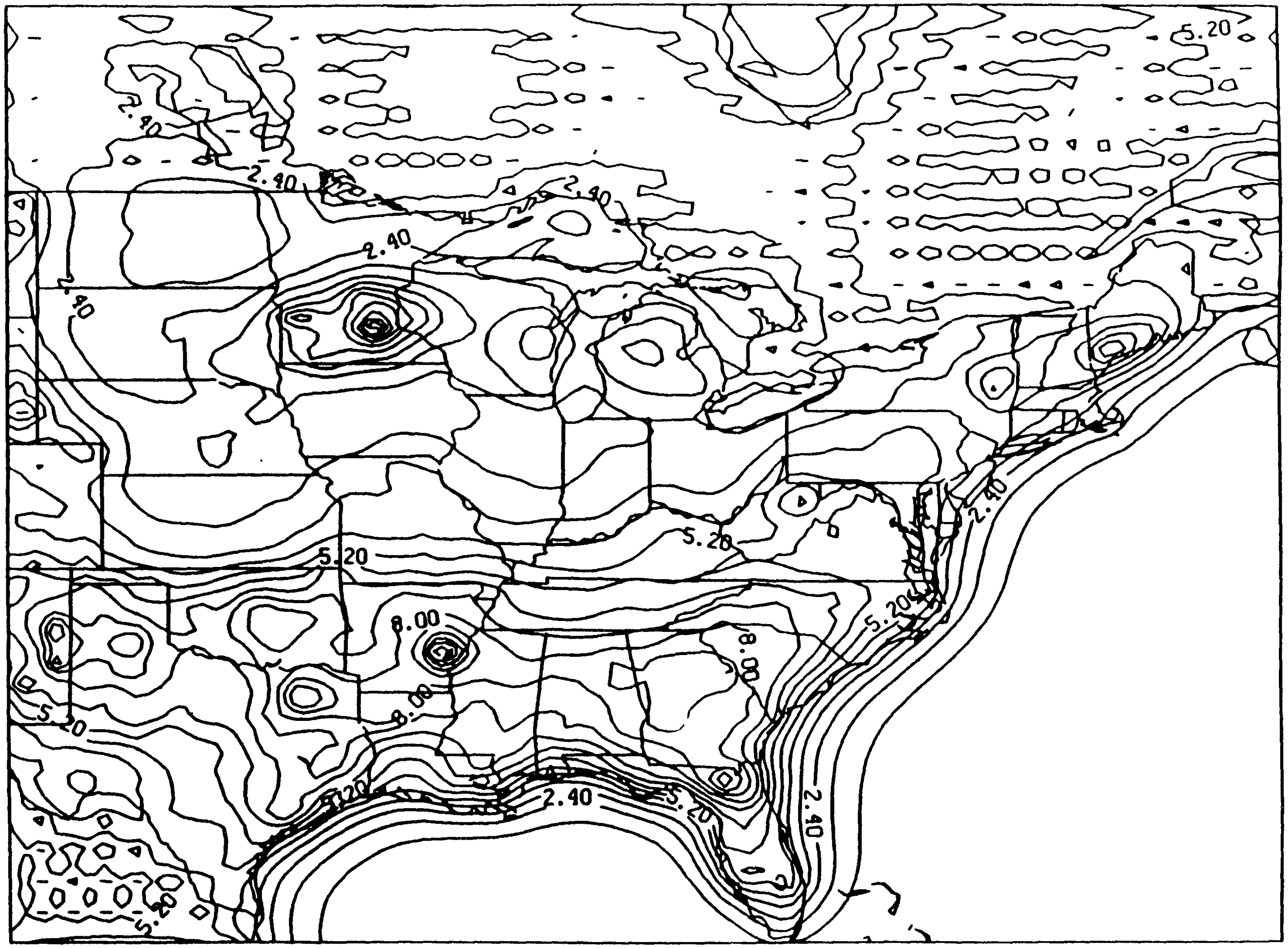

Fig. 4.31 Modeled biogenic VOCs concentrations ($\mu g\ m^{-3}$). Inner solution contours from 1.0 to 13.6 $\mu g\ m^{-3}$ by 0.7 $\mu g\ m^{-3}$.

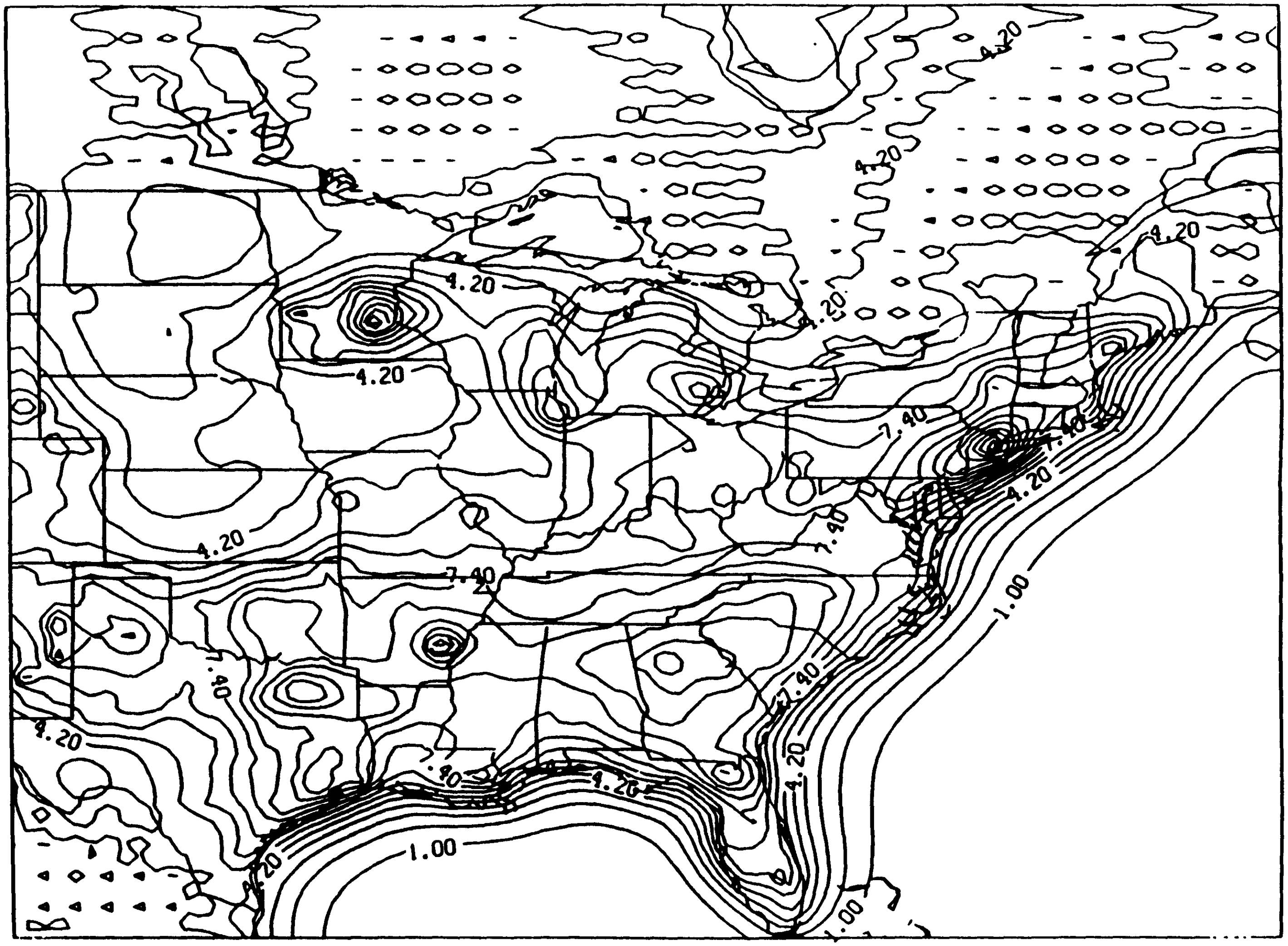

Fig. 4.32 Total modeled VOCs concentrations ($\mu g\ m^{-3}$) important in ozone production. Superposition of biogenic VOCs (Fig. 4.31) and 60% of anthropogenic VOCs (Fig. 4.29). Inner solution contours from 1.0 to 14.6 $\mu g\ m^{-3}$ by 0.8 $\mu g\ m^{-3}$.

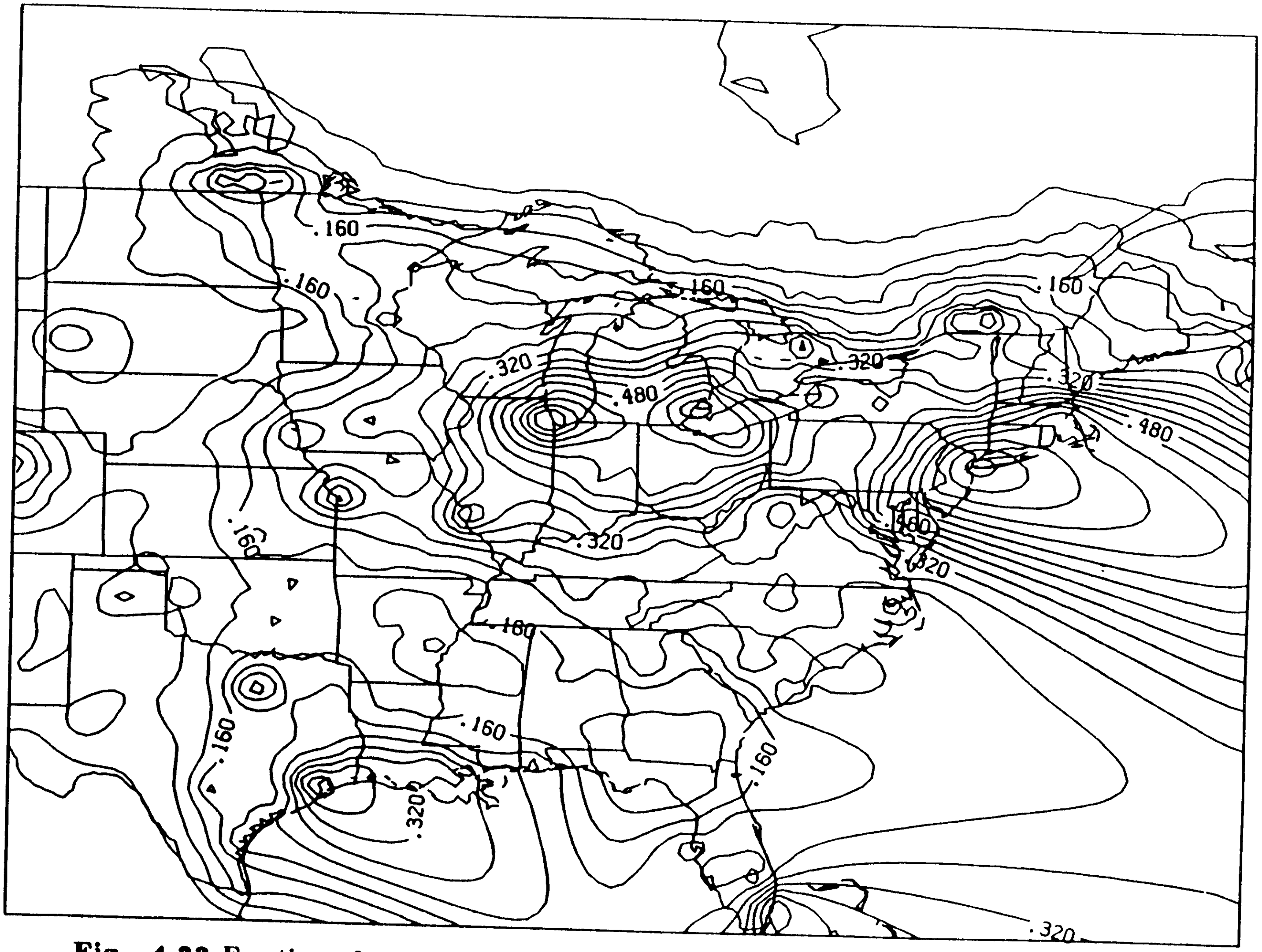

Fig. 4.33 Fraction of total VOCs due to anthropogenic sources. Inner solution contours from 0.04 to 0.72 by 0.04.

Chapter 5

Ozone Modeling

The primary goal of this chapter is to develop a long range transport model of seasonally averaged ozone in the planetary boundary layer. Many of the same techniques used to construct the NO_x and VOCs models in the preceding chapter are also applicable to ozone. The key factor which differentiates the ozone species is its source term. NO_x and VOCs are introduced to the atmosphere via anthroprogenic and biogenic emissions. Ozone, though, has no direct source of emissions; rather, it is a photochemical product of atmospheric chemistry.

The fundamental assertion of this thesis is that the average ozone production rate is principally related to the average precursor concentrations of NO_x and VOCs. Ozone generation is influenced by other factors as well. Insolation, temperature, meteorological conditions, and local emission patterns also affect ozone formation. These effects are considered, on average, to be smaller than those due to precursor concentrations.

The validity of the precursor-source assumption is tested by the ability of the model to predict observed concentrations throughout eastern North America. Generally, the ozone models discussed have difficulty in matching empirical patterns of ozone. A portion of the problem can probably be attributed to the selection of monitoring sites as previously seen in the NO_x model. The network of ozone measurements (see chapter two) is urban biased and irregularly situated, and there is some question as to whether it portrays an accurate distribution of typical ozone levels across the United States. An extensive network of measurements which reflects average mixed layer concentrations does not exist.

Inconsistent model results can reflect weaknesses in either the model assumptions or measurement representativeness (or both!). Thus, the issue addressed in this chapter is not limited to the development of ozone models but extends to an estimation of the quality of the models. The efforts described in this chapter represent the best attempt to construct simple models of boundary layer ozone. Because their reliability cannot be ascertained at this time, the model results pose many more interesting questions about regional ozone than they resolve; they emphasize the need for further research.

5.1 Empirical Ozone vs. Modeled Precursors

Ozone production is assumed to be dependent on the levels of its precursors, NO_x and VOCs. Though confounded by the effects of transport and background levels, peak levels of ambient ozone can be expected to be proximate to the areas of highest production. Thus, areas of high precursor concentrations generally should be associated with regions of augmented ozone. However, the concurrent NO_2-O_3 measurements described in section 2.2.5 fail to exhibit such a relationship.

The ability of a precursor based model to predict ozone concentrations consistent with observations is dependent on a general correspondence between ozone, VOCs, and NO_x levels. A rough estimation of the quality of this relationship can be garnished from a comparison of measured ozone with model estimates of NO_x and VOCs. Figs. 5.1-5.8 compare the 1985 average seasonal ozone concentrations shown in Figs. 2.26-2.29 with estimated precursor levels determined by the long range transport models (Fig. 4.7 for NO_x and Fig. 4.32 for VOCs). The plots alternate between precursors and are segregated on the basis of site category. Two letter state abbreviations identify sites. Measured O_3 varies significantly more within a given state than do modeled NO_x and VOCs concentrations. Scatter is prevalent in all plots reflecting the individuality of each monitor. Still, some general tendencies are revealed. Ozone levels show a slight but discernable increase with modeled NO_x for all categories (Figs. 5.3, 5.5 and 5.7) except urban sites (Fig. 5.1) where the opposite is true. The inverse relationship may be the result of ozone scavenging by NO in dense emission areas. Ozone vs. VOCs plots show even less correlation. Least squares regressions indicate a positive slope for the suburban and rural categories (Figs. 5.4 and 5.6) but negative relationships for the less numerous urban and unknown classes (Figs. 5.2 and 5.8).

The high level of short length scale variation in ozone concentrations obscures its relation to NO_x and VOCs. Some of this scatter can be eliminated by using the box average ozone concentrations of Fig. 2.32 for comparison. Plots of box average ozone versus modeled NO_x and VOCs are presented in Figs. 5.9 and 5.10. Two letter abbreviations correspond to quadrants of eastern North America with the lines of delineation defined as 40° N latitude and 85° W longitude. As the box averages include the monitors from all site classes, the plots represent a composite of the overall ozone network. A positive but scattered relationship between NO_x and ozone is apparent in Fig. 5.9. However Fig. 5.10, the overall ozone-VOCs plot, is essentially uncorrelated. Some regional clustering is apparent in the two plots although the concentration ranges of the four quadrants overlap extensively.

The poorly correlated relationships of measured ozone and modeled precursors indicate that an empirically consistent ozone model may be difficult to construct. Important effects are ignored by this simple analysis, however. The relative consequence of local ozone production on ambient concentration differs because of geographically variant transport and dispersion effects. The true nature of the relationship (or lack thereof) between ozone and its precursors is better determined by a regional modeling technique.

5.2 Ozone Chemistry and Production

The cursory treatment of ozone formation presented in the first chapter is elaborated herein to emphasize the important role of the NOx and VOCs precursors. NO_x is defined as the sum of nitrogen oxide and nitrogen dioxide.

$$[NO_x] \equiv [NO] + [NO_2] \tag{5.1}$$

Ozone is created when an photoenergized NO_2 molecule dissociates into NO and an oxygen atom. The latter usually combines with an oxygen molecule to form ozone. The net reaction is given by

$$[NO_2] \xrightarrow{h\nu, O_2} [NO] + [O_3] \qquad (k_1). \tag{5.2}$$

The rate of this reaction, k_1, is zero at night when photolysis is absent. During daylight hours it varies as a function of the solar zenith angle and meteorological conditions such as cloud cover, temperarture and humidity. Assuming a random influence of the meteorological effects, the average photolysis rate is approximated as

$$k_1 = k_1^* \sin(\omega t), \qquad \omega = \frac{\pi}{\tau_d} \tag{5.3}$$

where k_1^* is the peak average photolytic rate and τ_d is the length of daytime. Thus, the rate of photolysis is zero at sunrise, rises to a maximum at midday, then declines to zero again at sunset.

Once created, the dissociated products may simply recombine in the reverse reaction.

$$[NO] + [O_3] \rightarrow [NO_2] + [O_2] \qquad (k_2) \tag{5.4}$$

Alternatively, the NO molecule can be reoxidized to NO_2 by a peroxyl radical.

$$[RO_2] + [NO] \rightarrow [RO] + [NO_2] \qquad (k_3) \tag{5.5}$$

The NO molecule thus has two available oxidation routes. Recombination (eqn. (5.4)) eliminates the newly generated ozone. However, a net ozone molecule is formed each time the peroxyl pathway (eqn. (5.5)) is traversed.

VOCs are an important source of peroxyl radicals in the atmosphere. Generation of a peroxyl radical can occur through multiple pathways. The basic oxidation of a hydrocarbon (RH) to form a peroxyl radical is a two step process [1].

$$[RH] + [OH] \rightarrow [R] + [H_2O] \tag{5.6}$$

$$[R] + [O_2] \rightarrow [RO_2] \tag{5.7}$$

Short lived radicals such as [OH] are of paramount importance in atmospheric chemistry and are the subject of current research. All VOC oxidations do not necessarily result in peroxyl formation. However, a working hypothesis of this thesis is that RO_2 concentrations are proportional to ambient VOCs levels.

$$[RO_2] \propto [VOCs] \tag{5.8}$$

Local deviations from this proportionality can be expected. This study assumes that the relationship holds on average and that it is not affected by NO_x variations.

Atmospheric chemistry is complex and not completely understood. However, eqns. (5.2)-(5.5) are accepted as the basic ozone production mechanism. A net amount of ozone is created as NO_2 is photolyzed and recycled through the dual channel processes. However, ozone exhibits diurnal variation even in the absence of the peroxyl reaction. Any excess ozone present at sunset necessarily recombines during the night to form NO_2, thus resulting in no net generation.

The rates of formation of NO_2, NO and O_3 from the sequence of reactions in eqns. (5.2)-(5.5) are written as follows.

$$\begin{aligned}
[\dot{N}O_2] &= -k_1[NO_2] + k_2[NO][O_3] + k_3[NO][RO_2] && (5.9)\\
[\dot{N}O] &= k_1[NO_2] - k_2[NO][O_3] - k_3[NO][RO_2] && (5.10)\\
[\dot{O}_3] &= k_1[NO_2] - k_2[NO][O_3] && (5.11)
\end{aligned}$$

Note that $[\dot{N}O_2] = -[\dot{N}O] = -[\dot{O}_3] + k_3[NO][RO_2]$. Thus, the instantaneous rate of ozone production equals the net rate of NO formation plus the NO converted to NO_2 via the peroxyl reaction (eqn. (5.5)). The amount of ozone created by the reaction cycle depends on the relative concentrations of each species and the rate constants. The lower limit, in which each ozone molecule generated by eqn. (5.2) is reconverted by eqn. (5.4), is zero net ozone. The upper limit corresponds to the situation where each NO_2 dissociated by reaction (5.2) is recycled via eqn. (5.5) thereby producing a net ozone molecule. In this case, the maximum amount of ozone generated from photolysis, $(\Delta O_3)_{max}$, is given simply as the integral of the dissociation reaction.

$$(\Delta O_3)_{max} = \int_0^{\tau_d} k_1^*[NO_2]\sin(\omega t)dt = \frac{2k_1^*[NO_2]}{\omega} \qquad (5.12)$$

Both NO recycling pathways are active in typical atmospheric conditions. The rate of production equations (5.9-5.11) illustrate two important points. First, ozone generation increases as the level of NO_2 (and hence NO_x) is raised. Second, increases in RO_2 (and by assumption, VOCs) also augment ozone levels by reducing the self-scavenging of the dissociated NO_2 products. Thus, the simplified reaction scheme predicts higher levels of ozone as either or both of the precursors, NO_x or VOCs, is increased.

The sensitivity of ozone production to its precursor concentrations can be used to investigate the nature of the source function. The goal is to try to estimate ozone behaviour for varying levels of NO_x and VOCs through integration of eqns. (5.9)-(5.11). Values of 5, 15, and 25 $\mu g\,m^{-3}$ are selected from the modeled NO_x solution (Fig. 4.7) as representative concentrations. These correspond to roughly to concentrations of 2.6, 7.9, and 13.2 parts per billion (ppb) at standard conditions. Similarly, Fig. 4.32 is used to select typical VOCs concentrations of 4, 6, and 8 $\mu g\,m^{-3}$. The rate equations, however, require RO_2 values. Derwent estimates a typical ambient RO_2 concentration to be 0.04 ppb [39]. Associating this value with the midrange of typical VOCs, the proportionality assumption (eqn. (5.8)) sets test levels of RO_2 at 0.027, 0.040, and 0.050 ppb. Typical values of the rate constants are obtained from the literature and are tabulated in Table 5.1 [39-41].

Eqns. (5.9)-(5.11) are integrated using a 4th order Runge-Kutta method. The length of the daylight period τ_d is set to 14 hours to mimic a summer day. Initial conditions, assuming all NO_x is initially in the form of NO_2 at sunrise and ozone is at its background level, are set at $[NO_2]_0=[NO_x]$, $[NO]_0=0$, and $[O_3]_0=20$ ppb.

The integration proceeds until the end of the day when photolysis is switched off. Recombination of NO and ozone through the 10 hour nighttime period essentially eliminates the remaining NO produced during the day.

Values of ΔO_3, the incremental ozone (final value less background) photochemically produced over the course of a 24 hour period, are graphed against NO_x and RO_2 in Figs. 5.11 and 5.12. Each plot contains three curves which correspond to fixed levels of the other precursor. Thus, the two figures complement each other and contain the same nine points. Levels of ΔO_3 are consistent with observed ambient ozone production although the values may be somewhat high for average production rates. The slopes of the curves in Figs. 5.11 and 5.12 are fairly linear and a power law representation of the form

$$\Delta O_3 = \kappa [NO_x]^{P_N} [RO_2]^{P_R} \tag{5.13}$$

with coefficients κ=173 ppb$^{-0.23}$s^{-1}, P_N=0.72, and P_R=0.51, fits the data well.

The higher dependence on NO_x results from a combination of parameter values and the ranges of precursors. The maximum values of ΔO_3 possible, as predicted by eqn. (5.12), are 83, 253, and 424 ppb for the NO_x levels of 2.6, 7.9, and 13.2 ppb, respectively. Thus, in the presence of infinite VOCs, each NO_x molecule is able to produce 31 ozone molecules per day. The ΔO_3 values in Figs. 5.11 and 5.12 are considerably lower than the maximum given by eqn. (5.12). The recycling efficiency of VOCs at fixed NO_x decreases at higher RO_2 concentrations. Similarly, ozone production from NO_x at constant and finite RO_2 becomes less efficient at high concentrations. Both effects are a consequence of the self-limiting sink term in the ozone rate equation (eqn. (5.11)).

The precursor dependence of the source function is not precise for several reasons. First, the range of RO_2 concentrations tested as a surrogate for VOCs is highly uncertain. There is also some uncertainty in the choice of reaction rate constants. Lastly, the reaction cycle of eqns. (5.2)-(5.5) is only an approximation of intricate and complex atmospheric chemistry. Nevertheless, the results support the basic modeling premise; ozone production increases less than linearly with each of its NO_x and VOCs precursors. Appendix VII extends this integration technique to develop a simple time dependent box model of ozone. The model illustrates the basic mechanism responsible for the diurnal variation of ozone but its embodied assumptions severely limit its application to the actual atmosphere.

5.3 Regional Ozone Modeling

Ozone is modeled with the same basic transport equation (see chapter three) used to model NO_x and VOCs in chapter four. Flow conditions are time averaged over a six month summer season extending from April through September. Convective and diffusive processes serve to transport and disperse the pollutant in a single, fixed height mixed layer. Ozone is distinguished by its source term which is the essence of the model. Photochemical production, discussed in the preceding section, is assumed proportional to a power function of NO_x and VOCs precursor concentrations. Loss terms from chemical consumption outside the production cycle and from physical removal from the air column are modeled as linearly proportional to ozone concentration. The complete source function is written

$$S = \kappa[\mathrm{NO_x}]^{\mathrm{P_N}}[\mathrm{VOCs}]^{\mathrm{P_V}} - \frac{c}{\tau_r} \tag{5.14}$$

$$\frac{1}{\tau_r} = \frac{1}{\tau_c} + \frac{1}{\tau_w} + \frac{1}{\tau_d} \tag{5.15}$$

where c is ozone concentration and τ_r is an overall removal constant which incorporates the effects of photochemical loss (τ_c), wet scavenging (τ_w) and dry deposition (τ_d). κ, $\mathrm{P_N}$ and $\mathrm{P_V}$ are source function parameters. Adding the meteorological variables, a total of 10 parameters (v_ϕ, v_θ, D, h, τ_c, τ_w, τ_d, κ, $\mathrm{P_N}$ and $\mathrm{P_V}$) constitute the ozone long range transport model.

Ambient ozone concentrations are composed of two sources. The long range model predicts ozone generated photochemically within the atmospheric boundary layer. A second component, termed background ozone, arises from the mixing of tropospheric ozone into the boundary layer. Total ozone is modeled simply as the sum of the two components.

$$[\mathrm{O_3}]_{\mathrm{model}} = [\mathrm{O_3}]_{\mathrm{background}} + [\mathrm{O_3}]_{\mathrm{photo}} \tag{5.16}$$

The background level generally is a function of both space and time. However, the seasonally averaged model assumes a uniform regional value. A local balance of tropospheric input and loss to the ground is required to maintain the constant background level. The magnitude of background ozone is uncertain. Typical estimates range from 20-40 $\mu g\,m^{-3}$ [42], though levels as high as 60-100 $\mu g\,m^{-3}$ have been observed [43]. The latter are thought to result from the injection of stratospheric ozone into the troposphere.

The ozone measurements presented in the second chapter are used to compare with model results and to aid in determining the values of model parameters. The bulk of the comparisons are made with the network of measurements compiled by the EPA. Significant local scale variation (see section 5.1) obscures relationships between observed and modeled concentrations. As a consequence, sets of selected monitors are analyzed in some cases to procure additional information.

The following two subsections describe models developed with somewhat different approaches. The sequence reflects the attempt to refine the model to obtain the most satisfactory agreement with observations. The first model selects ozone parameters consistent with the precursor models and with the physical and chemical processes affecting ozone as discussed in the literature. Empirical ozone concentrations are used to establish the proper level of ozone production. The second family of models expands the optimization algorithm to examine all parameters. The goal is to minimize the absolute residuals between modeled and empirical concentrations. Constraints are imposed to assure the parameters are physically reasonable. The two approaches suggest somewhat different precursor dependencies, and a discussion of their relative merits concludes the section.

The outer-inner solution algorithm described in the third chapter is used to obtain all finite difference solutions. In order to reduce clutter a convention is adopted to display only the inner solutions. The outer solutions are collectively amassed in Appendix VIII. Appropriate cross references are contained in individual figure captions.

5.3.1 A Consistent Physical Model

The parameters chosen for a physically based model must be consistent with the collective knowledge of atmospheric dynamics and chemistry. Although there are serious gaps and uncertainties in the understanding of ozone formation, reasonable estimates of parameter values are possible. The ozone models constructed in this section adopt the same meteorological parameters that are used in the NO_x and VOCs models in the preceding chapter. This is not a mandatory requirement, but it does provide for a consistent approach between models.

The uniqueness of the ozone model is established by the six parameters embodied in the source function. Ozone is produced and consumed rapidly in the NO_x photodissociation-recombination cycle. Net ozone, generated as VOCs recycle NO to NO_2, has a significantly long residence time in the atmosphere. Liu et al. [13] claim ozone lifetimes are several days in the summer and upwards of several months in the winter. A typical value of $\tau_c = 10^5$ s is assumed to model chemical destruction which results principally from photolysis. A fair amount of research has been devoted to dry ozone deposition. The principal mechanism of interest is ozone absorption by forests and crops. Two studies, one empirical [44] and the other theoretical [45], support an average deposition velocity of 0.5 cm s^{-1}. Given the model mixed layer height of 550 m, this corresponds to a dry deposition time constant of $\tau_d = 10^5$ s. Ozone is soluble in water and is believed to be an oxidant in aqueous phase reactions [1]. A value of $\tau_w=10^5$ s, typical of previous long range models [33], is taken as an appropriate estimate of wet scavenging.

Specification of the production parameters κ, P_N, P_V, and $[O_3]_{\text{background}}$ completes the model. P_N and P_V are fixed at 0.75 and 0.50, respectively, in lieu of the integration results of section 5.2. The numerical model estimates the amount of ozone photochemically produced in the troposphere. Total ozone (eqn. (5.16)) simply sums the background and long range components.

Two principal statistical measures are used to evaluate model results throughout this chapter. The average error $\mathcal{E}$ and correlation coefficient r are defined by the following series of equations

$$[O_3]_{\text{residual}} = [O_3]_{\text{measured}} - [O_3]_{\text{model}} \tag{5.17}$$

$$\mathcal{E} = \sqrt{\frac{\sum([O_3]_{\text{residual}})^2}{\sum([O_3]_{\text{measured}})^2}} \tag{5.18}$$

$$\Upsilon_{\text{model}} = [O_3]_{\text{model}} - \overline{[O_3]}_{\text{model}} \tag{5.19}$$

$$\Upsilon_{\text{measured}} = [O_3]_{\text{measured}} - \overline{[O_3]}_{\text{measured}} \tag{5.20}$$

$$r = \frac{\sum(\Upsilon_{\text{model}}\Upsilon_{\text{measured}})}{\sqrt{\sum \Upsilon^2_{\text{model}} \sum \Upsilon^2_{\text{measured}}}} \tag{5.21}$$

where the $\overline{[O_3]}$ concentrations are arithmetic averages computed over the measuring network. The correlation coefficient can be a misleading measure. It signifies the strength of a linear relationship without regard to its slope. As an extreme example, if $[O_3]_{\text{model}}$ is constant, then r=1, implying perfect correlation. Thus it is necessary to consider the trend of the data simultaneously with r.

A plot of $\mathcal{E}$ versus background ozone level is shown in Fig. 5.13. Each point corresponds to a value of κ which minimizes $\mathcal{E}$ over the full network of EPA monitors (Figs. 2.26-2.29). The lowest error is achieved at values of $[O_3]_{\mathrm{background}} = 40\mu\mathrm{g\,m^{-3}}$ and $\kappa = 3.0\mathrm{x}10^{-5}\,[\mu\mathrm{g\,m^{-3}}]^{-\frac{1}{4}}\mathrm{s}^{-1}$. The resulting error and correlation coefficient are 17.9% and 0.17 for the combined measurement network. A complete set of parameters is listed in the first column of Table 5.2.

Fig. 5.14 presents contours of total ozone concentration in units of $\mu\mathrm{g\,m^{-3}}$. The contour pattern reflects the general distributions of its precursor sources though the continental gradients ozone are shallower. This is a consequence of ozone being a secondary pollutant; dispersion acts to smooth the emitted precursors which are subsequently smoothed again in the calculation of ozone. The peak level of 68 $\mu\mathrm{g\,m^{-3}}$ roughly encompasses Pennsylvania and is about 25 $\mu\mathrm{g\,m^{-3}}$ greater than values in southern Florida. On land, photochemical contributions represent only a 30-70% increment over the optimized background concentration of 40 $\mu\mathrm{g\,m^{-3}}$. The high background, about $\frac{2}{3}$ of the regional average, severely limits the amount of ozone reduction that could be achieved by reducing precursor emissions. Significant ozone concentrations are found over the Atlantic Ocean and the Gulf of Mexico where there are no precursor sources. Remote concentrations in excess of the background level are due to both transported ozone and local production from transported precursors.

Comparisons of modeled and measured values are shown in Figs. 5.15-5.21. The first four plots (Figs. 5.15-5.18) separate the data by site category. Two letter state abbreviations identify monitors. Each category shows significant scatter. Sites from the same state can generally be found on both sides of the 45° line, suggestive of local influences. The range of observations in a given state is typically much larger than the modeled range. Similar to the NO_x model, the variation occurs on scale lengths smaller than the long range transport approach can model.

The urban monitors (Fig. 5.15) show the least intragroup correlation between predictions and observations, being influenced by several outlying points. The urban category also possesses the highest average error (24.3%). Suburban (Fig. 5.16) and rural (Fig. 5.17) sites correlate better and have lower average errors (16.1% and 17.1% respectively). Unclassified sites (Fig. 5.18) are too sparse to suggest generalizations. A categorical bias is evident which differentiates the rural monitor class. On average, the model underpredicts rural concentrations by about 8%. This is compensated by modest overestimations at urban and suburban sites. The difference supports the hypothesis that urban and suburban ozone is suppressed by NO emission scavenging. General model underprediction is also evident at remote sites. Fig. 5.19, which isolates the subset of remote sites identified by Meyer (Fig. 2.33), shows modeled ozone about 10% lower on average than the measured concentrations. The data at five national park sites (Fig. 2.34), plotted in Fig. 5.20, are also modeled lower on average, although underpredictions occur at only two of the five sites. The measured values, which are annual averages, probably underestimate their higher seasonal concentrations; the actual level of model underprediction is probably greater than shown.

Some of the scatter can be eliminated by examining the averaged concentrations of proximate monitors. Fig. 5.21 is a scatter plot of the box averaged data of Fig. 2.32. Monitors are identified by their quadrant of origin, with eastern North America divided at 40° N and 85° W. The error is reduced to 14.5% and the correlation coefficient rises to 0.37. However, the slope of the best-fit line is rather shallow, emphasizing the smaller range of model predictions compared with that of the box averaged values. No strong geographic bias is evident. The scatter remains significant, however. The uneven data distribution used to construct the box averages is partly responsible for the randomness. Deriving a representative concentration field for eastern North America from the data in Figs. 2.26-2.29 is a difficult if not impossible task.

5.3.2 Optimized Models

Is it possible to achieve even better results? This subsection attempts to improve the physical model by examining alternate combinations of parameters which lower the average error $\mathcal{E}$ while simultaneously raising the correlation coefficient r.

The source function is the most crucial and uncertain element of the ozone model. The production mechanism is unique to this model; in fact, the purpose of this study is to establish its dependence on NO_x and VOCs. To this end, the three production parameters - κ, P_N and P_V - are varied to determine the combination which yields the best agreement with observations. Disregarding the possibility of unusual (and nonintuitive) nonlinearities, an upper limit of unity is assumed for P_N and P_V. Zero is established as the lower limit which corresponds to no precursor dependence in the ozone source. (Inverse dependence is assumed to be physically unrealistic in view of the discussion in section 5.2). Both P_N and P_V are tested over the range $\{0,\frac{1}{4}, \frac{1}{2},\frac{3}{4},1\}$. All other parameters, including the background ozone level, are maintained at the values listed in the first column of Table 5.2.

Values of κ are determined by requiring the average residual to be zero over the complete network of urban, suburban, rural and unclassified monitors (Figs. 2.26-2.29). Finite difference solutions of $[O_3]_{photo}$ are obtained for the permutated combinations of P_N and P_V. Corresponding error statistics are compiled in Tables 5.3 and 5.4 for the 25 combinations of source parameters P_N and P_V. Four separate groupings of monitoring sites are considered. In Table 5.3 the subscript o refers to the overall network (all urban, suburban, rural and unclassified sites) and b to their box averages as presented in Fig. 2.32. Table 5.4 summarizes two subgroups. The subscript r corresponds to the rural classification and m refers to the limited group of "remote" monitors identified by Meyer (Fig. 2.33) [28].

A specific level of source production is necessary to maintain a local balance between ozone generated and removed from the boundary layer. The case of $P_N = P_V = 0$ corresponds to the special case of uniform production and ambient concentration. The absence of gradients permits a simple balance between production and removal. Since bases raised to the zero power are unity, the level of generation is given by

$$\kappa = \frac{c}{\tau_r}. \tag{5.22}$$

The appropriate value of c to minimize residuals is the arithmetic mean of the observations less the background value, which is 20.8 $\mu g\, m^{-3}$ for the set of EPA monitors. Dividing by the removal constant of $3.33 x 10^4 s$, a production rate of

$6.25\text{x}10^{-4}$ μg m^{-3}s^{-1} is found. This corresponds to 54 μg m^{-3} per day production.

A zero power source dependency is not a realistic model, however. Such a scenario predicts uniform concentrations everywhere, including sites over water. The chances are remote that such a model is physically applicable. In general, a non-zero source power dependence corresponds to a spatially variant source function. Two measures of the source function, Π and Φ, are included in Table 5.3 as a measure of the peak and average variabilities between scenarios. Π is an area averaged value, and Φ is a relative estimate of the peak production rate.

$$\Pi = \overline{\kappa[\mathrm{NO_x}]^{P_N}[\mathrm{VOCs}]^{P_V}} \tag{5.23}$$

$$\Phi = \kappa[\mathrm{NO_x}]^{P_N}_{\mathrm{peak}}[\mathrm{VOCs}]^{P_V}_{\mathrm{peak}} \tag{5.24}$$

Π is averaged over an area which extends from 95-75° W, 30-50° N. Φ is calculated using representative peak NO_x and VOCs values of 30 and 10 μg m^{-3}, respectively.

Values of Π vary only by about 25% over the range of source powers. The model is forced to predict about the same average production in each case so that predictions are in reasonable agreement with measurements. Typical values are $5.0\text{-}6.0\text{x}10^{-4}$ μg m^{-3}s^{-1} which corresponds to an average daily production of about 50 μg m^{-3}. This generation must be compensated by loss and tranport terms to achieve a local balance. Φ values differ by more than a factor of two over the parametric study. The trend of rising peak Φ values accompanied by slowly falling average Π values emphasizes the effects of introducing concentration gradients with higher, more sensitive source dependencies.

The production parameter κ, tabulated along with the error statistics in Table 5.4, ranges two orders of magnitude over the combinations analyzed. The variation is the result of the adjustment necessary to maintain the relatively constant level of regional production. Overall errors (Table 5.3) are typically 16-20%; box average errors, where some of the local scatter has been removed from the data, are lower. Correlation coefficients are low for the overall data but improve for the box average comparison, a further reflection of the local variation in concentrations which the long range model cannot resolve. Errors for the rural subclass of monitors (Table 5.4) differ only slightly from the overall values. Correlation coefficients generally improve, however. Average errors for the Meyer remote monitors are lower than the overall group but there is little correlation between predictions and observations among the limited number of monitors.

The lowest overall errors occur at small values of P_N and P_V, indicating little preference for a source dependence on either NO_x or VOCs. The differing effects of the two precursors are emphasized by Figs. 5.22 and 5.23 which present model solutions of ozone concentration for the cases of single precursor dependence. The source parameter combination is selected to minimize the overall error. Dependence on NO_x alone is portrayed in Fig. 5.22 ($PN = \frac{1}{4}$, $P_V = 0$). Fig. 5.23 displays the complementary VOCs only solution ($P_N = 0$, $P_V = \frac{1}{4}$). Contours are smoother than those of the precursor models, a consequence of a more gently varying source function. Furthermore, the contour pattern is remarkably flat compared to the NO_x and VOCs model solutions (Figs. 4.7 and 4.32). The contour patterns shifts to reflect differences in the distributions of the precursor sources. NO_x generated ozone levels (Fig. 5.22) peak over an ovoid region centered around Pennsylvania and Ohio. The highest levels of VOCs generated ozone (Fig. 5.23) occur over a wider region centered much further to the south. In addition, contours of VOCs generated ozone show a much sharper gradient in Florida and over water.

The parameter combination of $P_N = P_V = \frac{1}{4}$ results in the lowest overall $\mathcal{E}$. It also corresponds to the box average comparison of smallest $\mathcal{E}$ and highest r. The model solution is displayed in Fig. 5.24. The contour pattern appears to combine the features of the two single precursor solutions, though it more closely resembles the VOCs only solution (Fig. 5.23). Highest ozone concentrations are predicted over Pennsylvania, and the range and peak value are each slightly higher than for the cases of single precursor dependence. However, the pattern is significantly different than that of the physical model (Fig. 5.14). Although peak levels are approximately the same, the reduced source function dependence on both NO_x and VOCs flattens the contour pattern. The concentration difference between Pennsylvania and central Florida is decreased from 23 $\mu g\,m^{-3}$ in the physical model to only 12 $\mu g\,m^{-3}$ for the optimized model.

Comparisons with observations are presented in three plots. Figs. 5.25 and 5.26 combine the 1985 seasonal averages presented in Figs. 2.26-2.29. Fig. 5.25 distinguishes monitors by site class, Fig. 5.26 by geographic location. The average error is 15.8% and overall correlation coefficient 0.21, both improvements over the physical model (17.9% and 0.17). The range of predicted concentrations is much smaller overall than the range of measured values. The crowded figures make it impossible to visually identify trends, but they do identify the outlying monitors.

Expanded plots (not shown) reveal that ranges within a single state are broad as well, thus reducing the likelihood of an overall regional bias. The greatest variation occurs among urban monitors which are probably the most susceptible to local near source effects. The mean of measured concentrations is lower than the predicted mean at urban locations, possibly evidence of scavenging by fresh NO emissions. The opposite tendency is true at rural monitors where the predicted concentrations are 6.9% lower than observed values.

Fig. 5.27 compares model results with the box averaged data of Fig. 2.32. Similar to its physical model counterpart (Fig. 5.21), sites are sorted into quadrants of eastern North America. The average error $\mathcal{E}$ is 12.0% and the correlation coefficient 0.42. Both are statistically better than the physical model (14.5% and 0.37). The improvements are achieved by squeezing the range of predictions, thereby moving the average point closer to the 45° line. The flatter distribution emphasizes the outlying points and suggests a fair degree of measurement scatter. Because the box averages are not uniformly representative (some contain only a single monitor), such variation is permissible even though the data are smoothed by the averaging process. Based on average error and overall correlation with measurements, the optimized model is somewhat better than the physical model.

Is it possible for even more improvement?

All parameters affect the model solution in an interactive manner. Finding the set which yields the lowest error is a monumental task considering the vast number of ways the eleven parameters can be combined. One possible approach is to vary one parameter at a time to iteratively converge on an optimal combination. However, the time required to evaluate the large number of numerical solutions is prohibitive. The NO_x model optimization (chapter 4) is facilitated by exploiting the analytical solution and thus permitting rapid examination of multiple concentration fields.

Practical application of the optimization algorithm requires the specification of a limited number of point sources and measurements as input. Although ozone has no direct emissions, point sources can be roughly approximated by the precursor source dependency

$$Q_{point} = k[NO_x]_{avg}^{P_N}[VOCs]_{avg}^{P_V} \tag{5.25}$$

where NO_x and VOCs are area averaged concentrations and k an appropriate production constant. Such an approach is undertaken using 72 area sources averaged over 5°x5° regions from 25°-55° N, 125°-65° W. The error function, defined as $\frac{\varepsilon}{r}$ to encourage low error and high correlation, is minimized with respect to the box average concentrations of Fig. 2.32.

The set of fully optimized parameters is listed in the third column of Table 5.2. There are several important differences and similarities with the other two models. The meteorological parameters v_ϕ, v_θ, and D increase in magnitude, indicative of a faster (though similar in direction) and more diffusive flow. The higher τ_r increases the residence time of ozone, but it is compensated by a lower production rate κ. The background ozone level remains at the 40 $\mu g\, m^{-3}$. The source parameters P_N and P_V are consistent with those of the previous optimized model. Their similar but relatively small magnitudes suggest a comparable but weak effect on ozone production. This supports an observed limited dependence of ozone levels on precursor concentrations [1].

Fig. 5.28 is a contour map of the fully optimized solution. Compared with the previous optimized model (Fig. 5.24) the contours are smoother and extended, especially in the downwind direction. The peak region, though it remains over Pennsylvania, is much smaller. These effects are largely the consequence of the higher transport parameters and longer residence time which produce an even flatter and more dispersed solution.

Measurement comparisons, shown in Figs. 5.29-5.35, further illustrate the reduced range of predictions. The average error over the EPA network is 15.6% with a 0.25 correlation coefficient, compared with 15.8% and 0.21 for the previous optimized model. The box averaged data (Fig. 5.35) achieves a similar small improvement over the source-only optimized model. $\mathcal{E}$ is reduced to 12.0% to 11.6% and r rises from 0.37 to 0.47.

These enhancements are minor and may not reflect real improvement. The use of the correlation coefficient r in the denominator of the error function introduces a potential problem as maximizing r does not necessarily make the model results better. The optimization might suggest a model of constant ozone which corresponds to r=1. A second optimization using the solely the residual sum as the error function yielded similar parameters, thus the potential pitfall is not encountered.

Figs. 5.29-5.32 present scatter diagrams for the four EPA site classifications. Consistent with the other models, the average urban site is overpredicted and rural concentrations are underpredicted. Average error is highest among the urban sites.

Meyer's remote sites (Fig. 5.33) follow the rural trend of underprediction while the national park sites (Fig. 5.34) scatter about the 45° line. The latter datapoints are annually averaged measurements which probably dilutes their summer seasonal averages. Thus, they probably are underpredicted as well.

Systematic model errors are difficult to identify. Figs. 5.36-5.43 are included to demonstrate the randomness of comparisons within the monitoring network. The ordinate of each plot is the ozone residual, defined as

$$[O_3]_{\text{residual}} = [O_3]_{\text{modeled}} - [O_3]_{\text{measured}}. \tag{5.26}$$

Companion plots identify site classifications and locations. Figs. 5.36-5.37 plot residuals as a function of latitude; Figs. 5.38-5.39 segregate monitors by longitude. Consistent class biases are unapparent. Most states have both under and overpredicted concentrations. Exceptions can be found, however. These may reflect inadequacies of the model, but they also may be due to differences in siting practices among states. No overall statistical trends are significant with respect to latitude or longitude. Figs. 5.40-5.43 examine precursor source effects. The sites are ranked by their proximate emission strengths (low to high). Care must be taken in interpreting the plots as they are depicted relatively and do not reflect absolute emissions. Generally, residuals vary randomly with both NO_x (5.40-5.41) and VOCs (5.42-5.43). A slight overall trend may be present though it is not statistically robust. Site classes overlap extensively. Rural monitors tend toward the lower end of NO_x emissions. The state distributions emphasize the spread of emissions within an individual state which seem to be uncorrelated with model predicitions.

A sensitivity study of the fully optimized ozone model is included in Appendix VI. Only a few parameters significantly alter the prediction of total ozone. The dominance of the background term makes $[O_3]_{\mathrm{background}}$ the most sensitive parameter. Increases in the source parameters κ, P_N and P_V yield a higher photolytic component which translates into a modest but meaningful gain when the background is added. The effects of the other parameters are effectively damped by the background level.

5.3.3 Model Comparison and Discussion

Although the full optimization does modify the meteorological parameters the inconsistency between the precursor and ozone models is not a major concern for two reasons. First, the models are relatively insensitive to wind speed and diffusivity. Wind direction is important but the value does not change significantly in the course of optimization. Second, ozone is introduced into the atmosphere differently than the precursors and it is subject to strong diurnal effects. It is not physically unreasonable that its transport parameters may also differ.

The convection, diffusion and species destruction terms can be compared to one another in a simple manner to illustrate relative differences between the physical and fully optimized models. Assuming all three processes are important, the model equation requires a rough equivalence of their corresponding differential terms. Using l as a generic length scale, c as species concentration, v as a convective speed, D for diffusivity, and τ as a destruction time constant, the similarity can be expressed as

$$v\frac{\partial c}{\partial l} \sim D\frac{\partial^2 c}{\partial l^2} \sim \frac{c}{\tau}. \tag{5.27}$$

Assuming that the change in concentration over the length scale L is comparable to the concentration itself eqn. (5.27) can be further approximated by

$$\frac{vc}{\mathrm{L}} \sim \frac{Dc}{\mathrm{L}^2} \sim \frac{c}{\tau}. \tag{5.28}$$

Equating any two of the three terms yields an expression for a length scale over which they are comparable. Three such quantities can be defined; using subscripts v, D, and t to represent convection, diffusion, and destruction, the length scales are given as

$$\mathrm{L}_{v-D} = \frac{D}{v} \tag{5.29}$$

$$\mathrm{L}_{v-t} = v\tau \tag{5.30}$$

$$\mathrm{L}_{t-D} = \sqrt{D\tau} \tag{5.31}$$

Length scale values are computed for the physical and fully optimized models and are compiled in Table 5.5. Two major differences are apparent. The higher value of L_{v-D} for the fully optimized model reflects a relatively greater diffusion away from the source in the near field. The lower value of L_{v-t} for the physical model emphasizes its faster rate of destruction.

The difference in destruction rates parallels a disparity in production rate between the two models. Neglecting concentration gradients and assuming a local balance of ozone generation and destruction, the production rate P is approximated simply as

$$P \sim \frac{c}{\tau}. \tag{5.32}$$

P varies roughly with τ^{-1}. The model constant τ_r is a measure of the time required for ambient concentrations to decay as they are dispersed from a source. Values of τ_r are 9 and 31 hours for the physical and fully optimized models. The slower destruction rate of the fully optimized model requires less local generation than the physical model to maintain the same level ozone. Average production rates Π, given by eqn. (5.23), are $2.3\text{x}10^{-4}$ $\mu g\, m^{-3} s^{-1}$ and $5.3\text{x}10^{-4}$ $\mu g\, m^{-3} s^{-1}$ for the fully optimized and physical models, which correspond to daily productions of 20 and 46 $\mu g\, m^{-3}$, respectively. Thus, the inverse τ relationship is attenuated somewhat by dispersion in the concentration field.

Ozone production from precursors is somewhat smaller than the flux of tropospheric input necessary to maintain the 40 $\mu g\, m^{-3} s^{-1}$ background level. Assuming that the model time constants govern the lifetime of background ozone, the physical and fully optimized models require 107 and 31 $\mu g\, m^{-3}$ per day to achieve a local balance. Precursor production is only 30 and 39% of total daily ozone flux for the two models, consistent with the predicted background level which is $\sim \frac{2}{3}$ of modeled ozone concentrations.

Additional model improvement is undoubtedly possible through the use of spatially variant parameters. Whereas the numerical model is designed to accomodate parameter variation, the analytical model requires constant parameter values to calculate source-receptor relationships (though they may differ for individual pairings). There is no simple algorithm for exploring parameter variation even though there are good physical justifications. Time constraints placed on this study preclude such an exploration, but future work should address the effects of inhomogeneous meteorological and production parameters.

The significance of the high background parameter in the three ozone models cannot be overemphasized; it accounts for over half of the predicted concentrations. Thus the models predict that production from anthropogenic precursors accounts for less than half of boundary layer ozone levels. There is little distinction between the optimized solutions, which predict marginal precursor dependence, and the physical model which relies on intuitive arguments. Average residuals are about 10 $\mu g\,m^{-3}$, a significant fraction of the total continental ozone variation of 14 and 24 $\mu g\,m^{-3}$ for the optimized and physical models, respectively. Clearly, the information provided by the measurements is noisy. Inadequacies in the monitoring network may be obscuring the true pattern of regional ozone.

The conservative opinion of the author is that the fully optimized model is preferable because it is most consistent with the measured data. The flat contour patterns calculated by the models agree with the lack of spatial gradients in observed ozone (Fig. 2.32). The critical issue to address is the appropriateness of the measurement network. Unequal spatial coverage and a monitoring emphasis of urban areas limit confidence in the regional representativeness of the observed data. The results indicate that monitor location is important. A difference between urban and rural monitors is evident from model predictions which overestimate the former and underpredict the latter. Thus, to be representative, the network must reflect average conditions integrated across the region.

Monitoring sites are uniquely affected by proximate source conditions. Locations free from the nearby influence of anthropogenic sources are likely to be a better ground level surrogate for the air column as a whole. Consequently, some researchers have painstakingly identified sites which are free from the influence of anthropogenic sources. There are, however, two problems with their approach. First, these pristine sites may be affected by unusual biogenic emissions which render them equally nonrepresentative. Second, the basic premise of the superiority of remote sites may be ill-founded. A large part of eastern North America is urban (or at least suburban) in nature and the effects of local sources are inescapable. The mix of conditions which characterize regional ozone is not obvious. One of the most useful (and perhaps necessary) goals of future research should be an extensive set of measurements which attempt to characterize regional ozone in the tropospheric boundary layer.

5.4 Model Implications

The models predict seasonal, time-averaged ozone concentrations. Ozone regulation emphasizes exceedance of the federal standard. In general, higher average levels can be anticipated to correspond to a larger number of exceedances. However, average and peak ozone levels do not correlate well (Fig. 2.37) which makes it unlikely that the number of exceedances correlates reliably with seasonal averages. Thus, the averaged model is of limited usefulness to current regulatory efforts.

The effort to establish a secondary ozone standard continues to gain momentum. The impetus for further ozone regulation stems largely from economic costs associated with reduced crop yields and forest damage. If enacted, the standard is apt to be a measure of exposure such as average concentration or growing season average. The time-averaged ozone models are an appropriate analysis tool for estimating these variables. Thus, the models may gain in importance in the future.

The results of the transport models, if representative of regional ozone in eastern North America, have serious implications for controlling average ozone levels. Foremost is the high background level which the fully optimized model predicts as the major component of tropospheric ozone. The background probably results from the balance of tropospheric transport into the boundary layer and natural atmospheric destruction. The level of background ozone is an important natural lower limit as even an abolition of precursor emissions cannot reduce ambient concentrations any further.

This section applies the long range models to three simple scenarios to examine the effects of precursor emission reductions on average ambient ozone levels. The control schemes are purely hypothetical and used solely for instructive purposes. The first example assumes that anthropogenic NO_x emissions are reduced by 50% uniformly across North America. The long range transport solution for NO_x is exactly one-half of the concentration field portrayed in Fig. 4.7, a consequence of the linear model. The second scenario proposes a 50% cut in anthropogenic VOCs emissions. Biogenic sources are assumed constant. The long range transport solution, shown in Fig. 5.44, is very similar to that of the total VOCs solution (Fig. 4.32) because biogenic emissions are the dominant contributor over most of the region. Fig. 5.45, which plots the ratio of reduced to total VOCs, further illustrates the effect of biogenic VOCs. The 50% change in anthropogenic VOCs emissions translates to only a 10-20% change in ambient average VOCs levels. Metropolitan areas, locuses of urban emissions, are influenced the most. The presence of biogenic sources means that reductions in anthropogenic emissions will not result in proportional decreases in ambient concentrations. The results in Fig. 5.45 imply the effect will be especially small at rural sites. The third and final scenario is a simple combination of the previous two cases: a 50% reduction in both anthropgenic VOCs and NO_x emissions.

Because of the uncertainty in ozone comparisons both the fully optimized and physical models are exercised. The two models embody very different source production dependencies and thus provide a measure of the sensitivity of average ozone levels to model formulation as well as precursor changes. The results of the ozone transport solutions are presented as contour maps which have been normalized by the full emission solutions (Figs. 5.14 and 5.28). Regional distributions can range from 0 to 1; a value of 0.8 indicates a 20% decrease in average ambient ozone levels.

Figs. 5.46-5.48 depict changes in seasonally averaged ozone as predicted by the fully optimized model. The solutions are relatively insensitive to precursor emission changes. The largest decreases correspond to the highest regions of predicted ozone. A 50% decrease in VOCs produces an insignificant 1% reduction in average ozone (Fig. 5.46). A 50% NO_x emission rollback results in a 3-5% average ozone decrement (Fig. 5.47). The combined effect is essentially a superposition. Fig. 5.48 suggests that a 50% reduction of both NO_x and VOCs emissions produces a 3-6% decrease in seasonally averaged ozone across eastern North America.

Figs. 5.49-5.51 plot the changes estimated by the physical model. The decrements are larger than those of the fully optimized model because the source function has a greater precursor dependence. Fig. 5.49 plots relative contours for a 50% reduction in VOCs alone. Seasonally averaged ozone levels decrease from 1-6% with the greatest gain occuring over the dense emission region of northern New Jersey and New York City. The response to NO_x reductions is somewhat more significant; a 50% reduction lowers average ozone levels by as much as 17% in the peak region over Pennsylvania (Fig. 5.50). A rollback of 50% each of NO_x and VOCs results in peak decrements of 18% (Fig. 5.51) with typical reductions of 10% or more in seasonal average ozone levels over much of eastern North America.

The models predict relatively small reductions in average ozone levels for large decreases in precursor emissions. The limited response of ozone concentrations is a combination of several factors. Decreases in anthropogenic VOCs translate into modest reductions in total VOCs due to the large biogenic component. Ozone is more sensitive to changes in NO_x than to manmade VOCs because the latter reductions are diluted by natural sources. The ozone source function smoothes the effect of the precursor inputs as the fractional powers P_N and P_V. The optimized models are particularly insensitive. The most significant factor, however, is the high background value which accounts for more than half of modeled ozone concentrations. Changes in the photolytic component are small compared to the background term.

The discussion of the precursor reduction scenarios is limited to the average seasonal models. Peak ozone concentrations, unlike average levels, are significantly higher than the background component. They quite possibly are more sensitive to changes in VOCs and NO_x levels. Further research is necessary to address the relationship between average levels and exceedances and their respective sensitivities to precursor concentrations.

Rate Constant	Value
k_1^*	$1\text{x}10^{-3}$ s^{-1}
k_2	$4\text{x}10^{-4}$ $ppb^{-1}s^{-1}$
k_3	$2\text{x}10^{-1}$ $ppb^{-1}s^{-1}$

Table 5.1: Reaction Rate Constants

Parameter	Model		
	Physically Based	Source Optimized	Fully Optimized
v_ϕ $(\mathrm{m\,s^{-1}})$ (at 40° N)	4.42	4.42	6.85
v_θ $(\mathrm{m\,s^{-1}})$	2.35	2.35	1.87
D $(\mathrm{km^2 s^{-1}})$	0.93	0.93	2.70
τ_r (s) $= (\tau_c^{-1} + \tau_d^{-1} + \tau_w^{-1})^{-1}$	$3.3\text{x}10^4$	$3.3\text{x}10^4$	$1.1\text{x}10^5$
h (m)	550	550	550
P_N	0.75	0.25	0.21
P_V	0.50	0.25	0.23
κ $(\mu\mathrm{g\,m^{-3}})^{1-P_N-P_V}\mathrm{s}^{-1}$	$3.0\text{x}10^{-5}$	$2.0\text{x}10^{-4}$	$9.1\text{x}10^{-5}$
$[O_3]_{\mathrm{background}}$ $(\mu\mathrm{g\,m^{-3}})$	40	40	40

Table 5.2: Model Parameters

Units: Π, Φ: $\mu g\, m^{-3} s^{-1}$ $\quad \kappa$: $(\mu g\, m^{-3})^{1-P_N-P_V} s^{-1}$

$\mathcal{E}_o$ r_o Π Φ $\mathcal{E}_b$ r_b	P_V				
	0	$\frac{1}{4}$	$\frac{1}{2}$	$\frac{3}{4}$	1
P_N	0.161	0.157	0.157	0.158	0.161
	-	0.238	0.225	0.213	0.201
0	6.25x10^{-4}	6.12x10^{-4}	5.95x10^{-4}	5.77x10^{-4}	5.58x10^{-4}
	6.25x10^{-4}	7.08x10^{-4}	7.90x10^{-4}	8.70x10^{-4}	9.51x10^{-4}
	0.130	0.123	0.122	0.124	0.128
	-	0.390	0.362	0.335	0.310
	0.158	0.158	0.160	0.163	0.166
	0.194	0.209	0.207	0.201	0.195
$\frac{1}{4}$	6.07x10^{-4}	5.92x10^{-4}	5.75x10^{-4}	5.57x10^{-4}	5.39x10^{-4}
	7.53x10^{-4}	8.43x10^{-4}	9.32x10^{-4}	1.02x10^{-3}	1.11x10^{-3}
	0.120	0.120	0.123	0.127	0.133
	0.413	0.418	0.397	0.374	0.351
	0.164	0.166	0.169	0.172	0.175
	0.176	0.183	0.184	0.183	0.180
$\frac{1}{2}$	5.84x10^{-4}	5.69x10^{-4}	5.52x10^{-4}	5.35x10^{-4}	5.18x10^{-4}
	8.87x10^{-4}	9.84x10^{-3}	1.08x10^{-3}	1.18x10^{-3}	1.27x10^{-3}
	0.125	0.128	0.132	0.137	0.142
	0.394	0.394	0.384	0.370	0.355
	0.174	0.177	0.179	0.183	0.186
	0.162	0.166	0.167	0.167	0.166
$\frac{3}{4}$	5.60x10^{-4}	5.45x10^{-4}	5.29x10^{-4}	5.12x10^{-4}	4.97x10^{-4}
	1.03x10^{-3}	1.13x10^{-3}	1.23x10^{-3}	1.34x10^{-3}	1.44x10^{-3}
	0.138	0.141	0.145	0.149	0.153
	0.376	0.375	0.368	0.359	0.350
	0.186	0.188	0.191	0.195	0.198
	0.150	0.152	0.154	0.154	0.154
1	5.35x10^{-4}	5.21x10^{-4}	5.06x10^{-4}	4.91x10^{-4}	4.76x10^{-4}
	1.17x10^{-3}	1.28x10^{-3}	1.39x10^{-3}	1.50x10^{-3}	1.62x10^{-3}
	0.152	0.155	0.158	0.161	0.165
	0.360	0.358	0.354	0.348	0.342

Table 5.3: Ozone Statistics: Overall and Box Average Data

Units: Π, Φ:$\mu g\, m^{-3} s^{-1}$ κ:$(\mu g\, m^{-3})^{1-P_N-P_V} s^{-1}$

$\mathcal{E}_r$ r_r κ $\mathcal{E}_m$ r_m	P_V				
	0	$\frac{1}{4}$	$\frac{1}{2}$	$\frac{3}{4}$	1
P_N 0	0.163 - $6.250\text{x}10^{-4}$ 0.126 -	0.158 0.326 $3.981\text{x}10^{-4}$ 0.129 -0.072	0.157 0.296 $2.497\text{x}10^{-4}$ 0.134 -0.066	0.158 0.271 $1.548\text{x}10^{-4}$ 0.140 -0.064	0.160 0.252 $9.509\text{x}10^{-5}$ 0.146 -0.065
$\frac{1}{4}$	0.158 0.317 $3.217\text{x}10^{-4}$ 0.132 0.048	0.157 0.327 $2.026\text{x}10^{-4}$ 0.137 -0.007	0.158 0.311 $1.259\text{x}10^{-4}$ 0.143 -0.030	0.160 0.294 $7.749\text{x}10^{-5}$ 0.149 -0.043	0.163 0.278 $4.734\text{x}10^{-5}$ 0.155 -0.052
$\frac{1}{2}$	0.161 0.301 $1.620\text{x}10^{-4}$ 0.142 0.024	0.162 0.307 $1.010\text{x}10^{-4}$ 0.148 -0.008	0.163 0.301 $6.234\text{x}10^{-5}$ 0.154 -0.029	0.166 0.293 $3.816\text{x}10^{-5}$ 0.160 -0.043	0.169 0.285 $2.320\text{x}10^{-5}$ 0.165 -0.054
$\frac{3}{4}$	0.168 0.289 $8.013\text{x}10^{-5}$ 0.154 0.005	0.169 0.292 $4.960\text{x}10^{-5}$ 0.160 -0.019	0.171 0.291 $3.044\text{x}10^{-5}$ 0.165 -0.037	0.173 0.288 $1.855\text{x}10^{-5}$ 0.170 -0.050	0.176 0.210 $1.123\text{x}10^{-5}$ 0.175 -0.062
1	0.177 0.278 $3.908\text{x}10^{-5}$ 0.166 -0.013	0.178 0.281 $2.405\text{x}10^{-5}$ 0.171 -0.032	0.180 0.282 $1.469\text{x}10^{-5}$ 0.176 -0.047	0.182 0.282 $8.918\text{x}10^{-6}$ 0.181 -0.059	0.185 0.282 $5.385\text{x}10^{-6}$ 0.185 -0.071

Table 5.4: Ozone Statistics: Rural and Meyer Subgroups

Model	L_{v-D} (km)	L_{v-t} (km)	L_{t-D} (km)
Physical	186	166	554
Fully Optimized	380	781	545

Table 5.5: Comparison of Model Length Scales

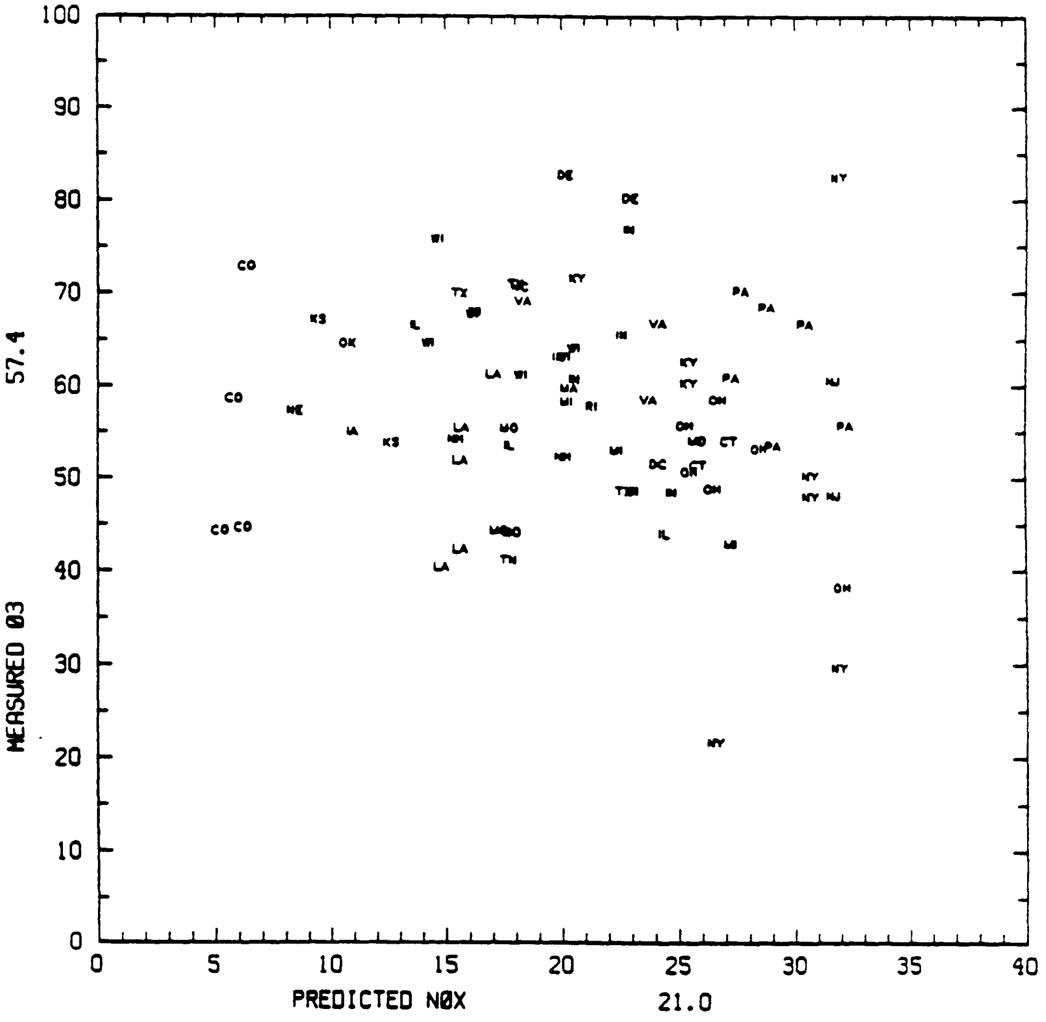

Fig. 5.1 Measured $[O_3]$ vs. modeled NO_x concentrations at urban monitoring sites. Units are $\mu g\ m^{-3}$. 1985 data; average seasonal concentrations. Mean values indicated in axes legends. Correlation coefficient r=-0.14.

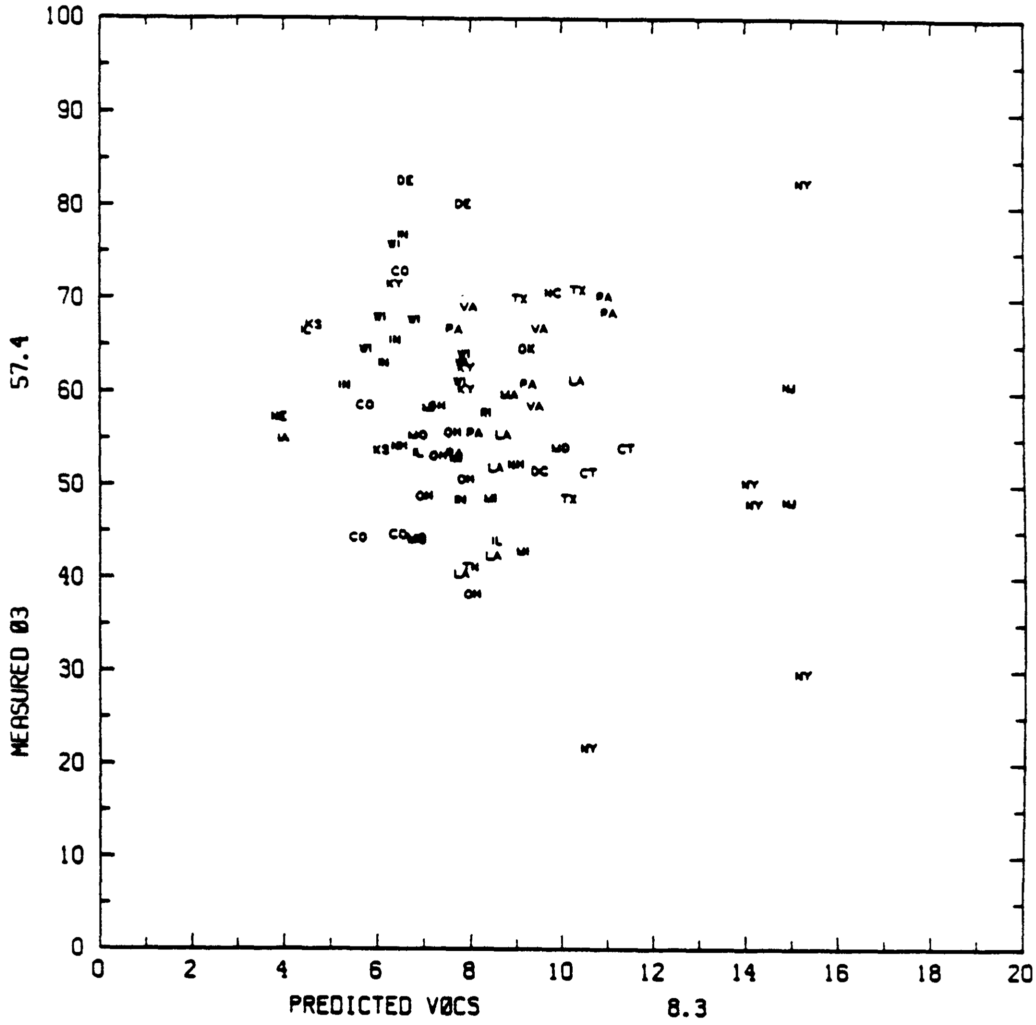

Fig. 5.2 Measured $[O_3]$ vs. modeled VOCs concentrations at urban monitoring sites. Units are $\mu g\,m^{-3}$. 1985 data; average seasonal concentrations. Mean values indicated in axes legends. Correlation coefficient r=-0.16.

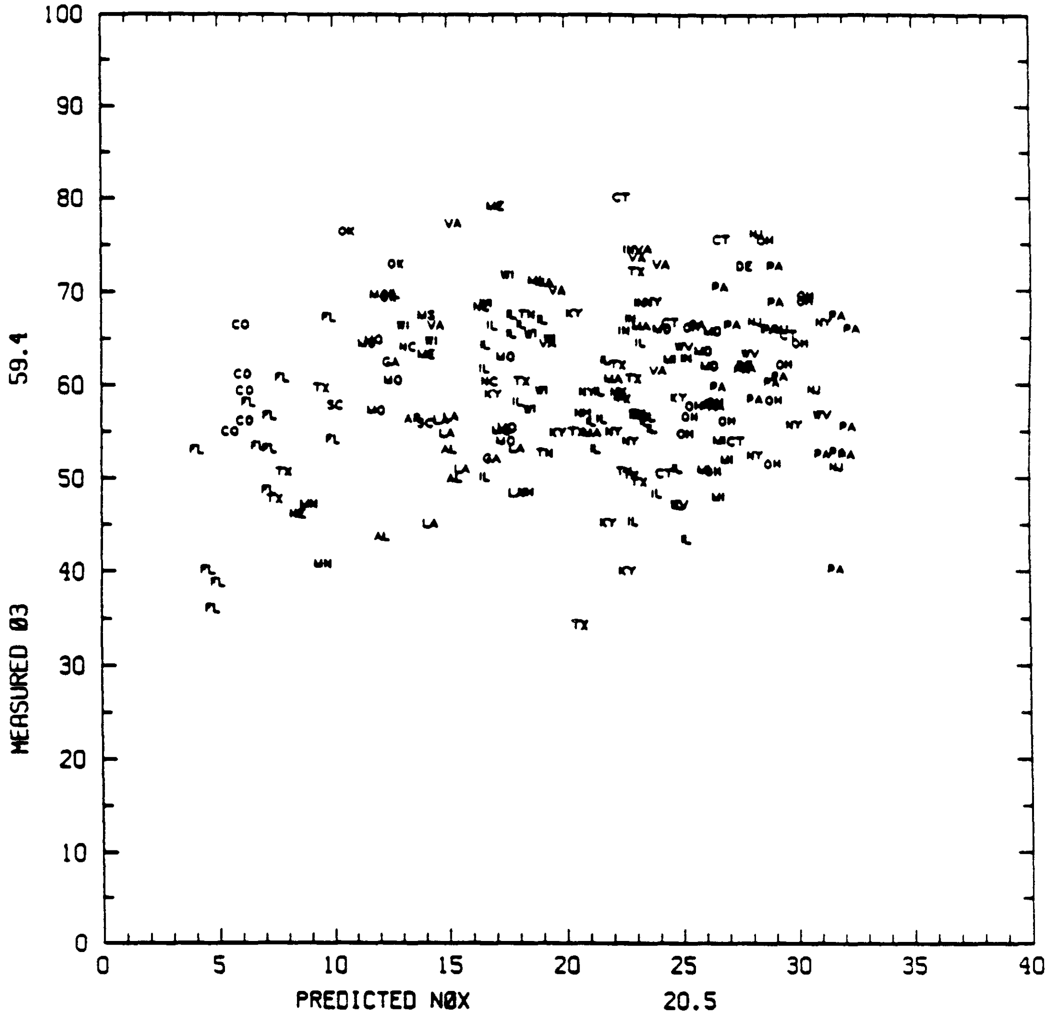

Fig. 5.3 Measured $[O_3]$ vs. modeled NO_x concentrations at suburban monitoring sites. Units are $\mu g\,m^{-3}$. 1985 data; average seasonal concentrations. Mean values indicated in axes legends. Correlation coefficient r=0.17.

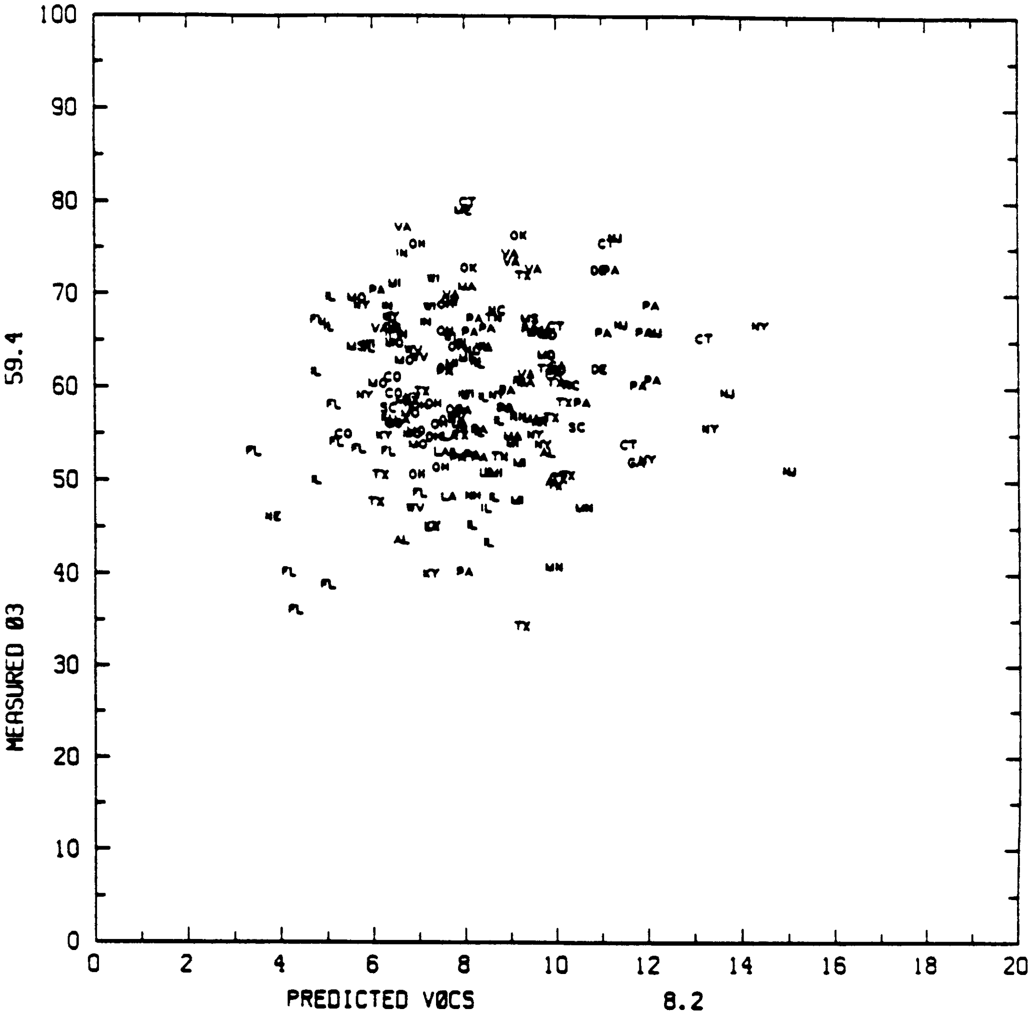

Fig. 5.4 Measured $[O_3]$ vs. modeled VOCs concentrations at suburban monitoring sites. Units are $\mu g\,m^{-3}$. 1985 data; average seasonal concentrations. Mean values indicated in axes legends. Correlation coefficient r=0.08.

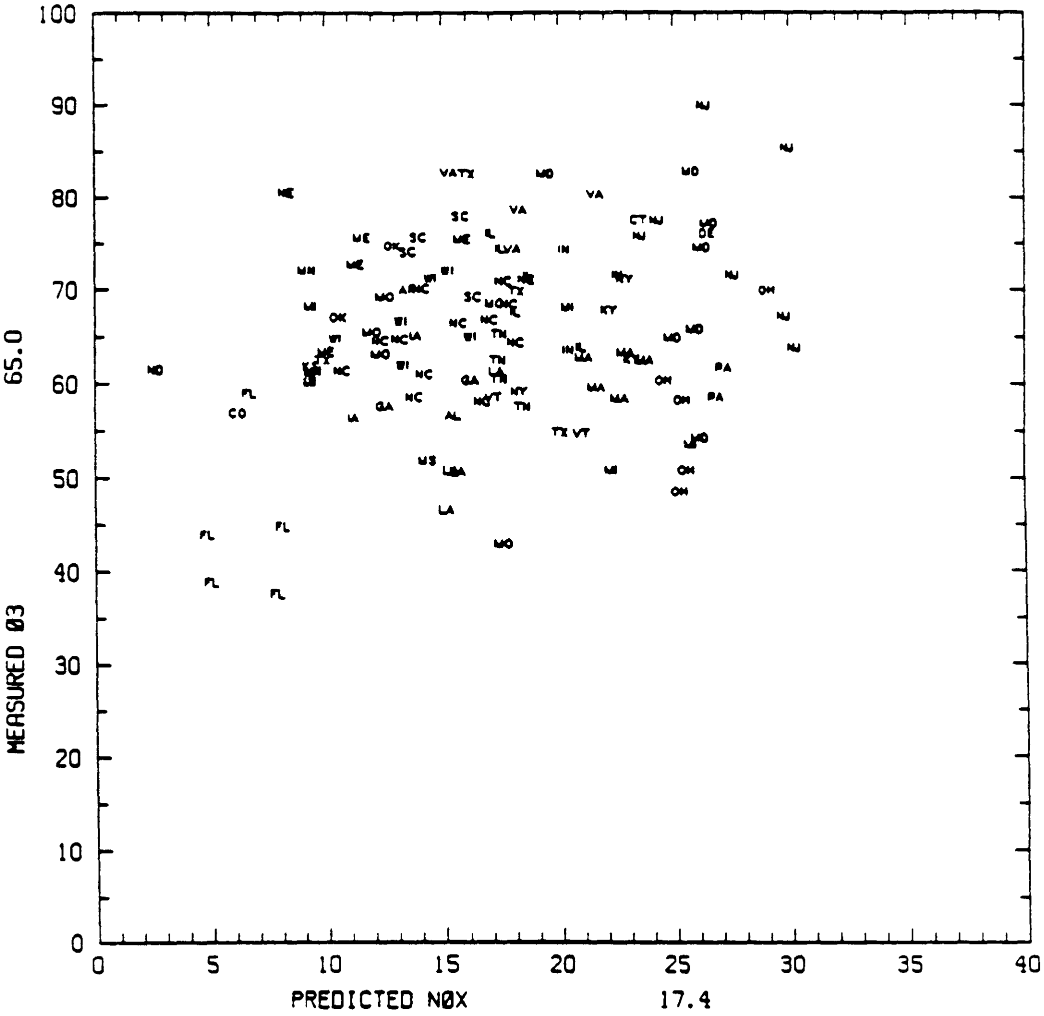

Fig. 5.5 **Measured $[O_3]$ vs. modeled NO_x concentrations at rural monitoring sites. Units are $\mu g\,m^{-3}$. 1985 data; average seasonal concentrations. Mean values indicated in axes legends. Correlation coefficient r=0.25.**

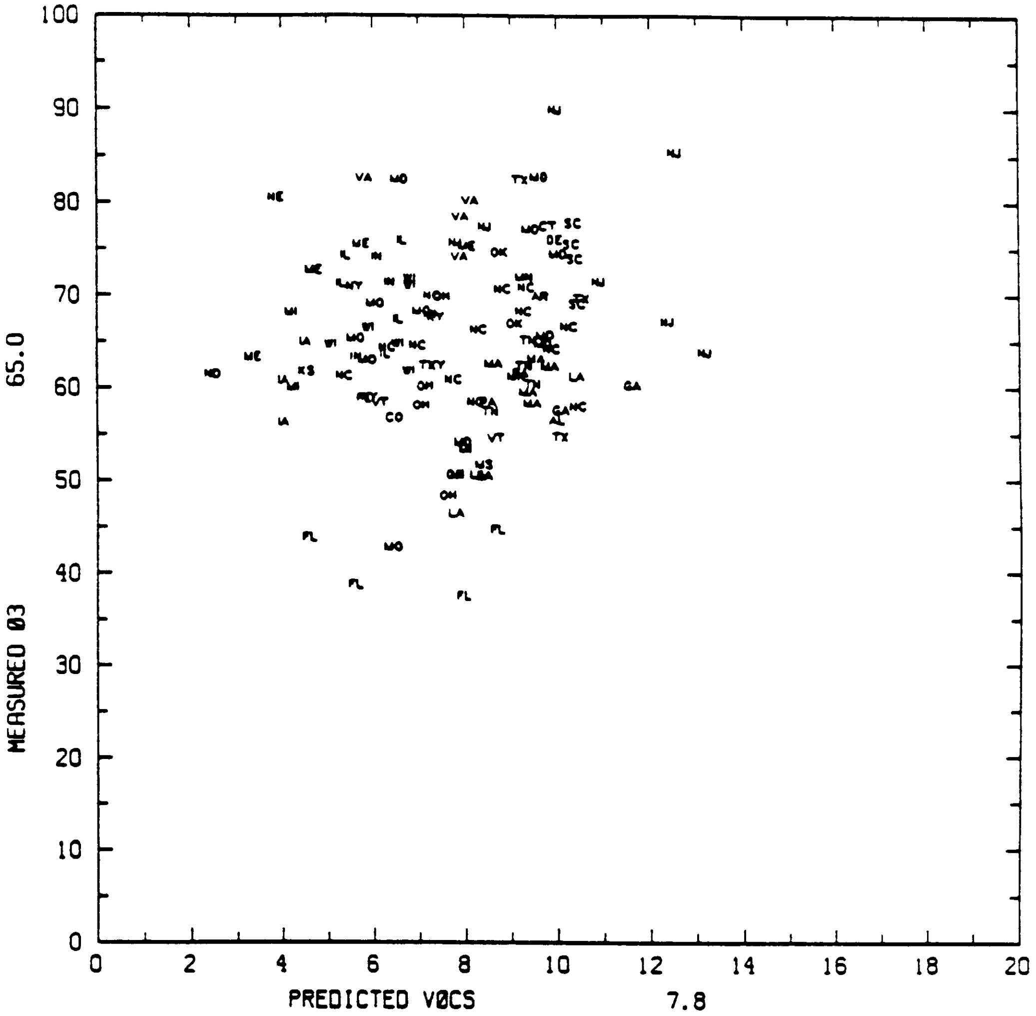

Fig. 5.6 Measured $[O_3]$ vs. modeled VOCs concentrations at rural monitoring sites. Units are $\mu g\, m^{-3}$. 1985 data; average seasonal concentrations. Mean values indicated in axes legends. Correlation coefficient r=0.13.

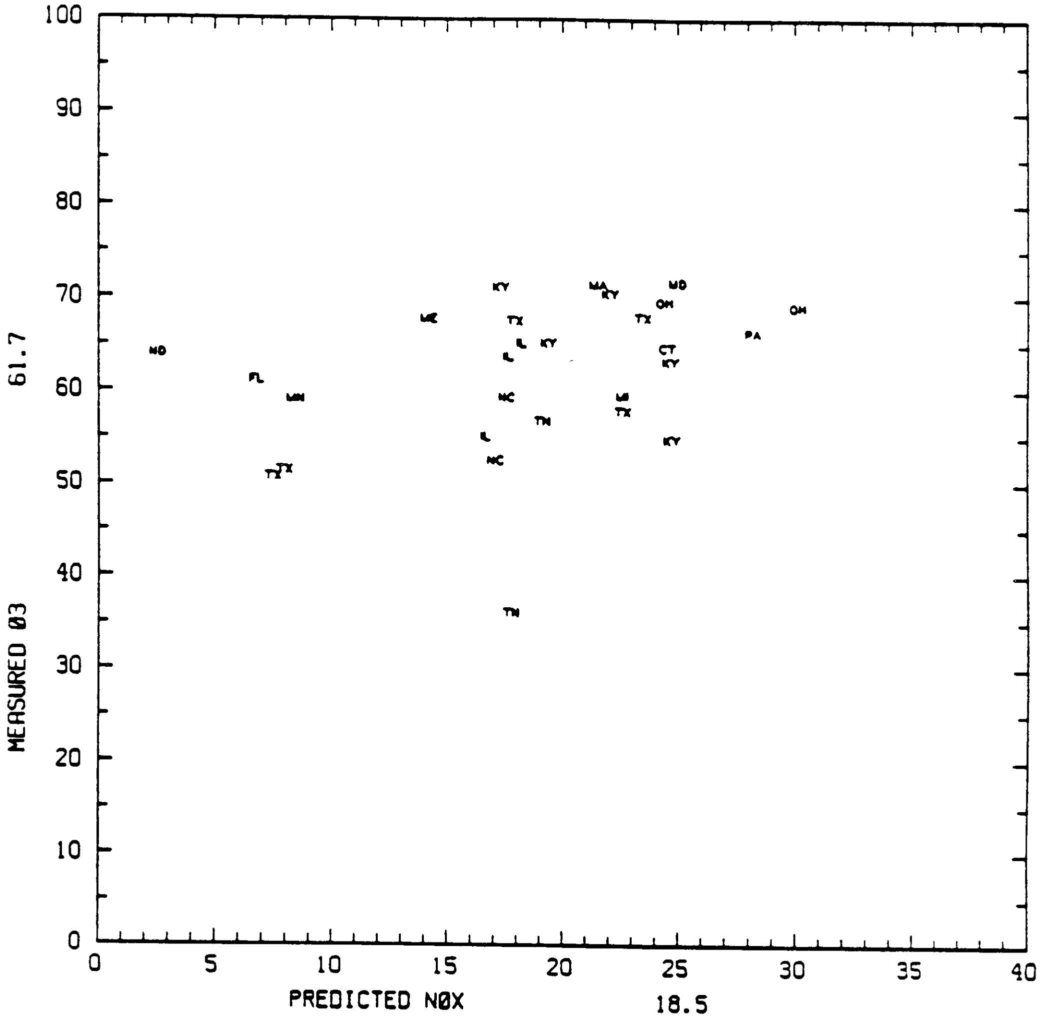

Fig. 5.7 Measured $[O_3]$ vs. modeled NO_x concentrations at unclassified monitoring sites. Units are $\mu g\,m^{-3}$. 1985 data; average seasonal concentrations. Mean values indicated in axes legends. Correlation coefficient r=0.35.

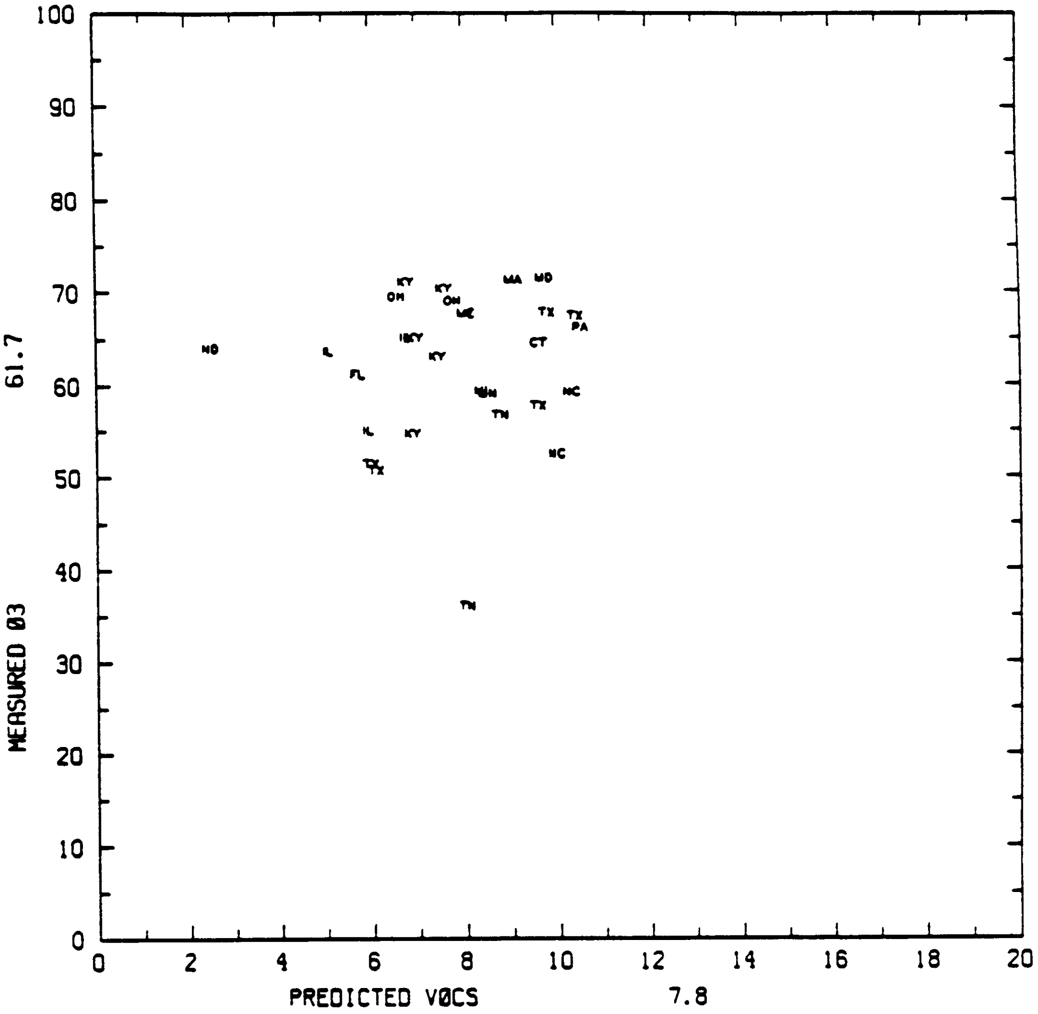

Fig. 5.8 Measured $[O_3]$ vs. modeled VOCs concentrations at unclassified monitoring sites. Units are $\mu g\,m^{-3}$. 1985 data; average seasonal concentrations. Mean values indicated in axes legends. Correlation coefficient r=0.10.

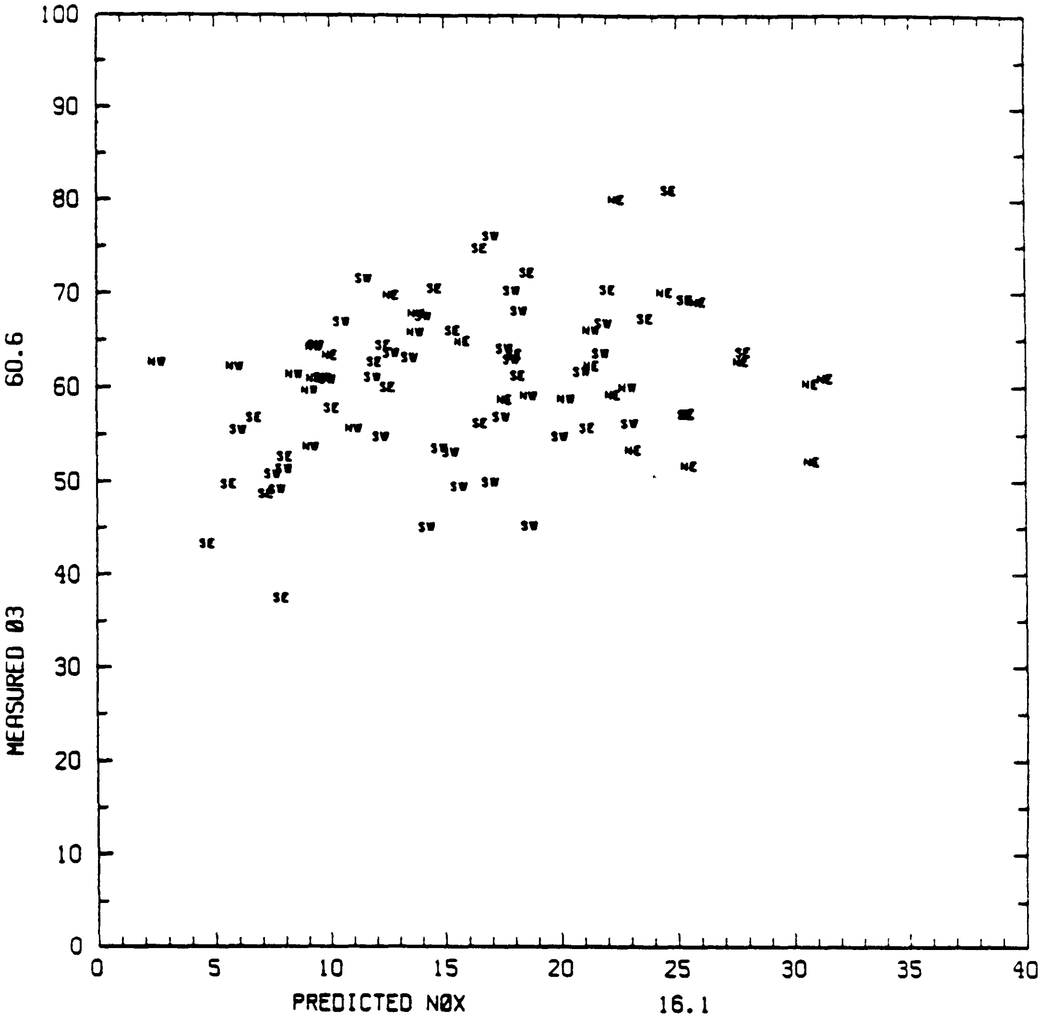

Fig. 5.9 Measured $[O_3]$ vs. modeled NO_x concentrations at box averaged sites (Fig. 5.32). Units are $\mu g\, m^{-3}$. 1985 data; average seasonal concentrations. Mean values indicated in axes legends. Correlation coefficient r=0.28.

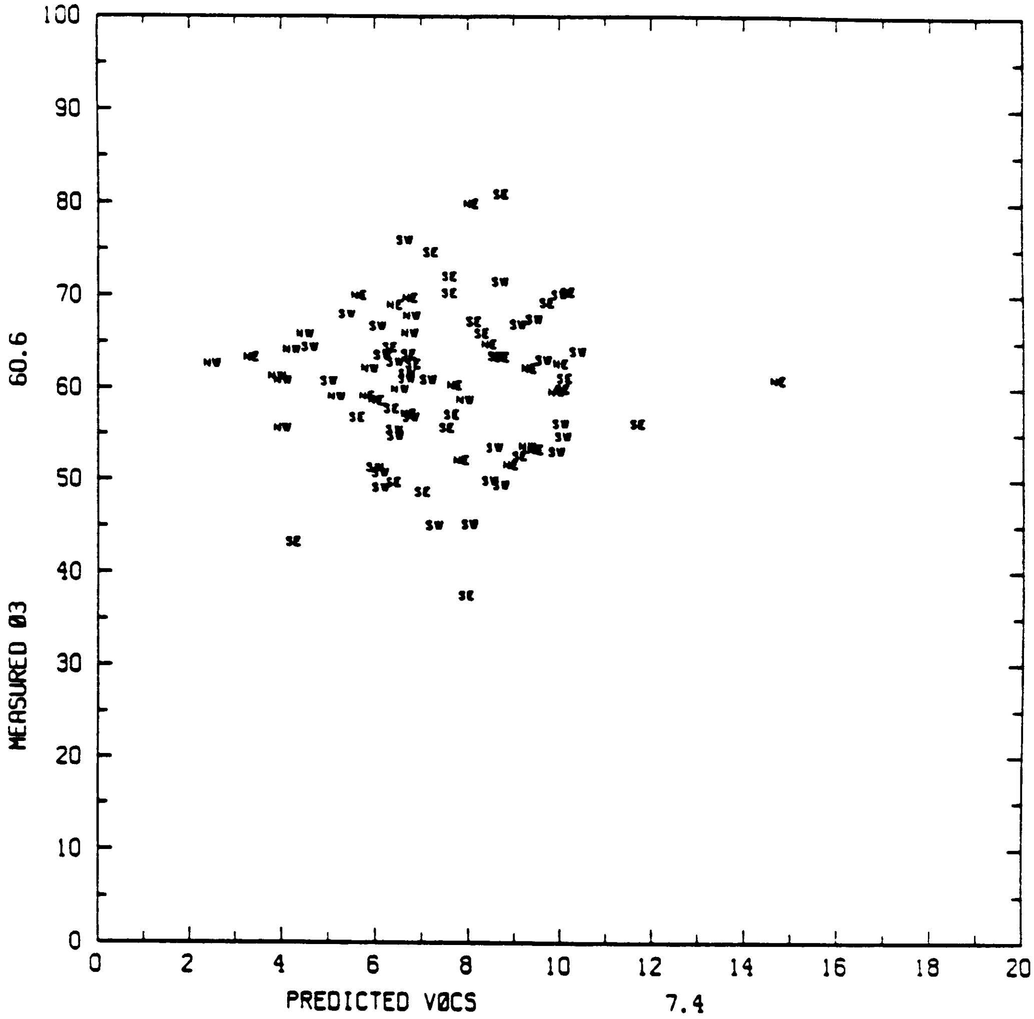

Fig. 5.10 Measured [O_3] vs. modeled VOCs concentrations at box averaged sites (Fig. 5.32). Units are $\mu g\, m^{-3}$. 1985 data; average seasonal concentrations. Mean values indicated in axes legends. Correlation coefficient r=0.02.

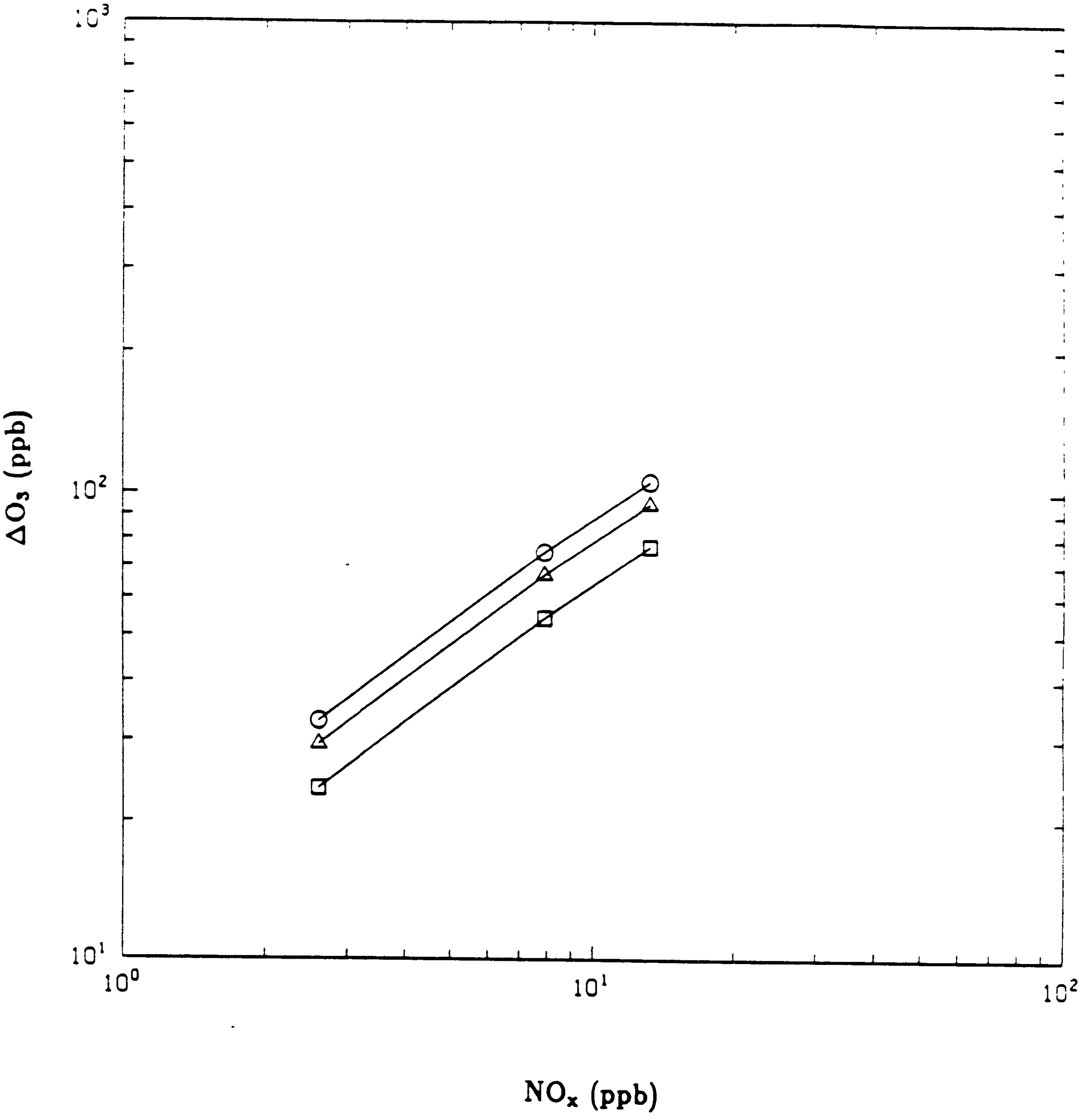

Fig. 5.11 Incremental ozone production, ΔO_3, vs. NO_x. Units are parts per billion (ppb). Square, triangle and circle symbols correspond to differing RO_2 concentrations of 0.027, 0.040 and 0.050 ppb.

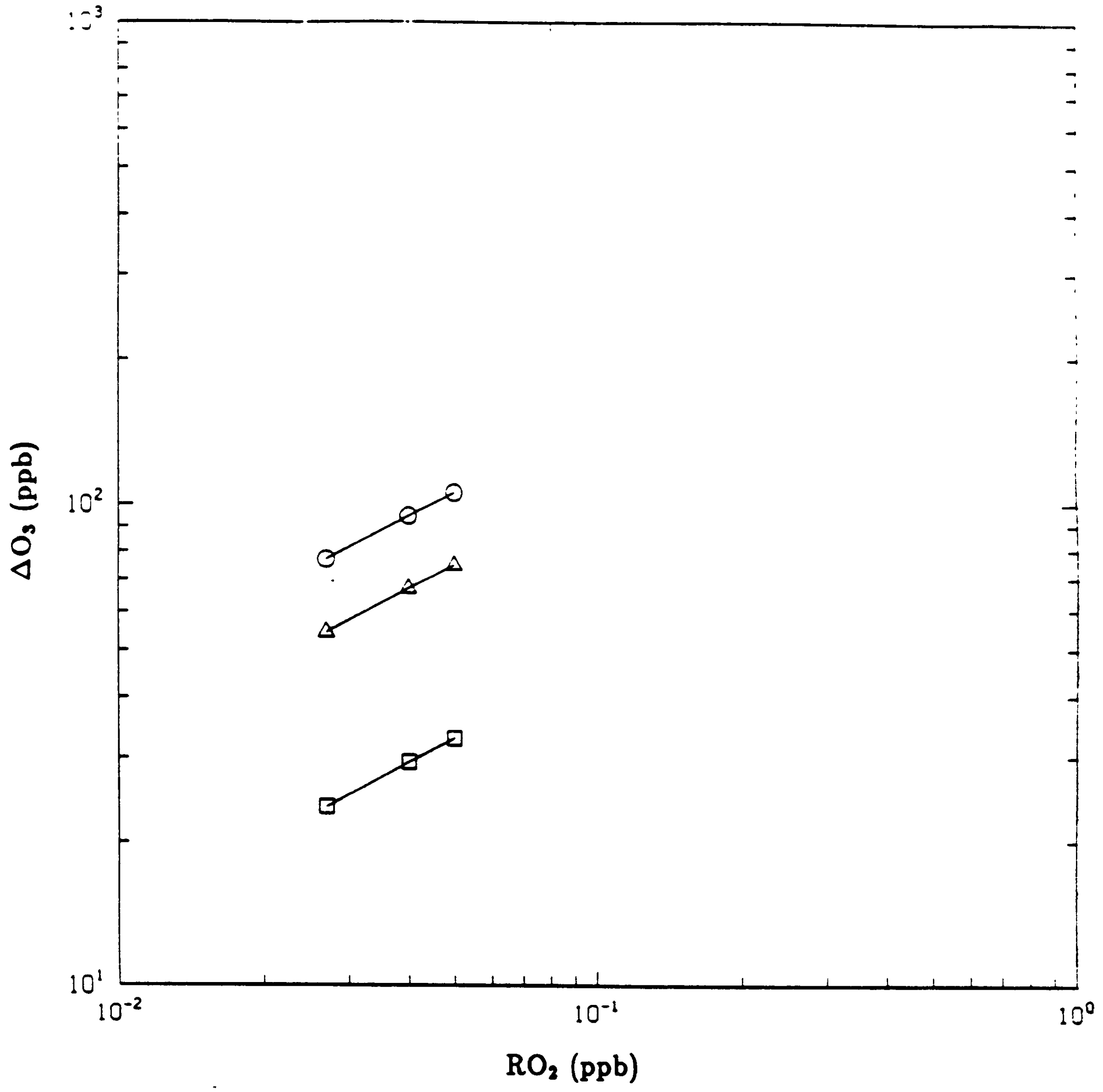

Fig. 5.12 Incremental ozone production, ΔO_3, vs. RO_2 concentration. Units are parts per billion (ppb). Square, triangle and circle symbols correspond to differing NO_x concentrations of 2.6, 7.9 and 13.2 ppb.

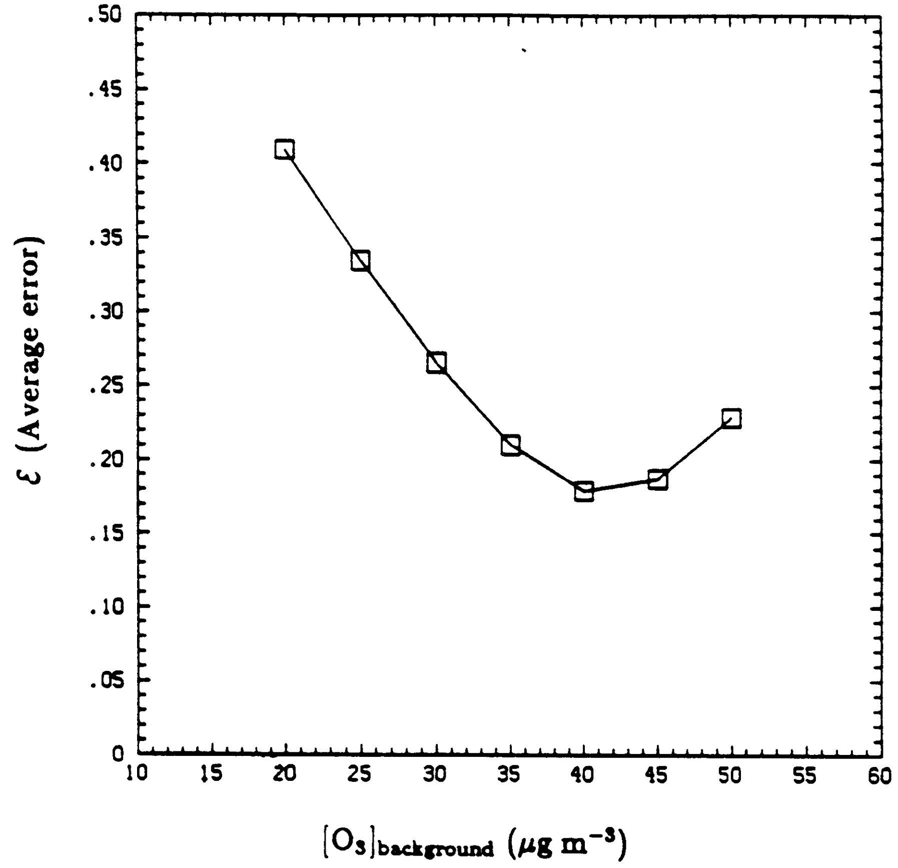

Fig. 5.13 Average error, $\mathcal{E}$, vs. background ozone concentration, $[O_3]_{background}$. Each point incorporates the ozone production rate which minimizes the sum of physical model residuals over the measurement network for the given $[O_3]_{background}$ concentration. $\mathcal{E}_{min} = 17.9\%$ at $[O_3]_{background} = 40\ \mu g\ m^{-3}$.

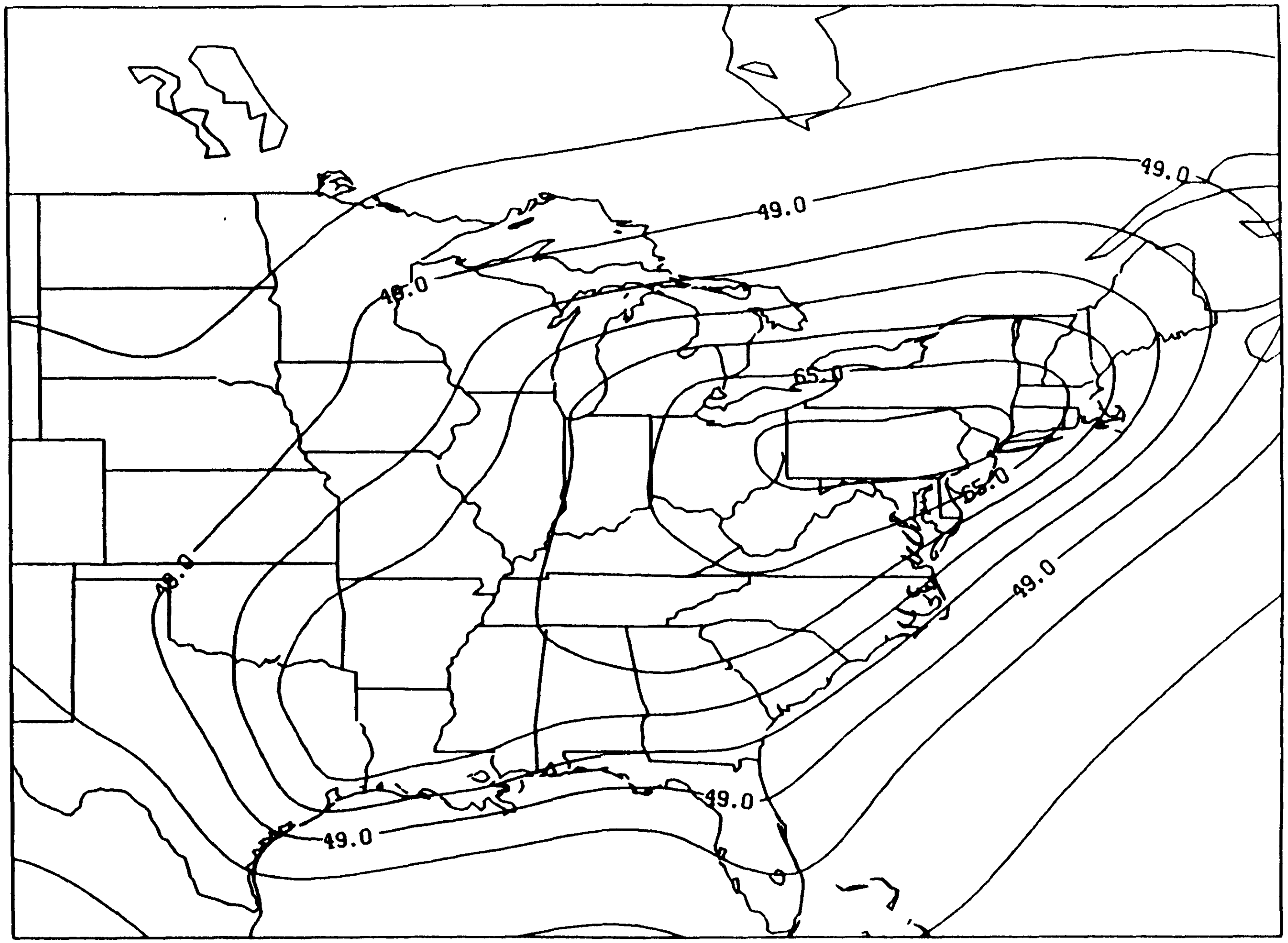

Fig. 5.14 Seasonal average ozone concentrations (μg m^{-3}) predicted by the physical model. Contours from 41 to 69 μg m^{-3} by 4 μg m^{-3}. Outer solution is shown in Fig. VIII.1.

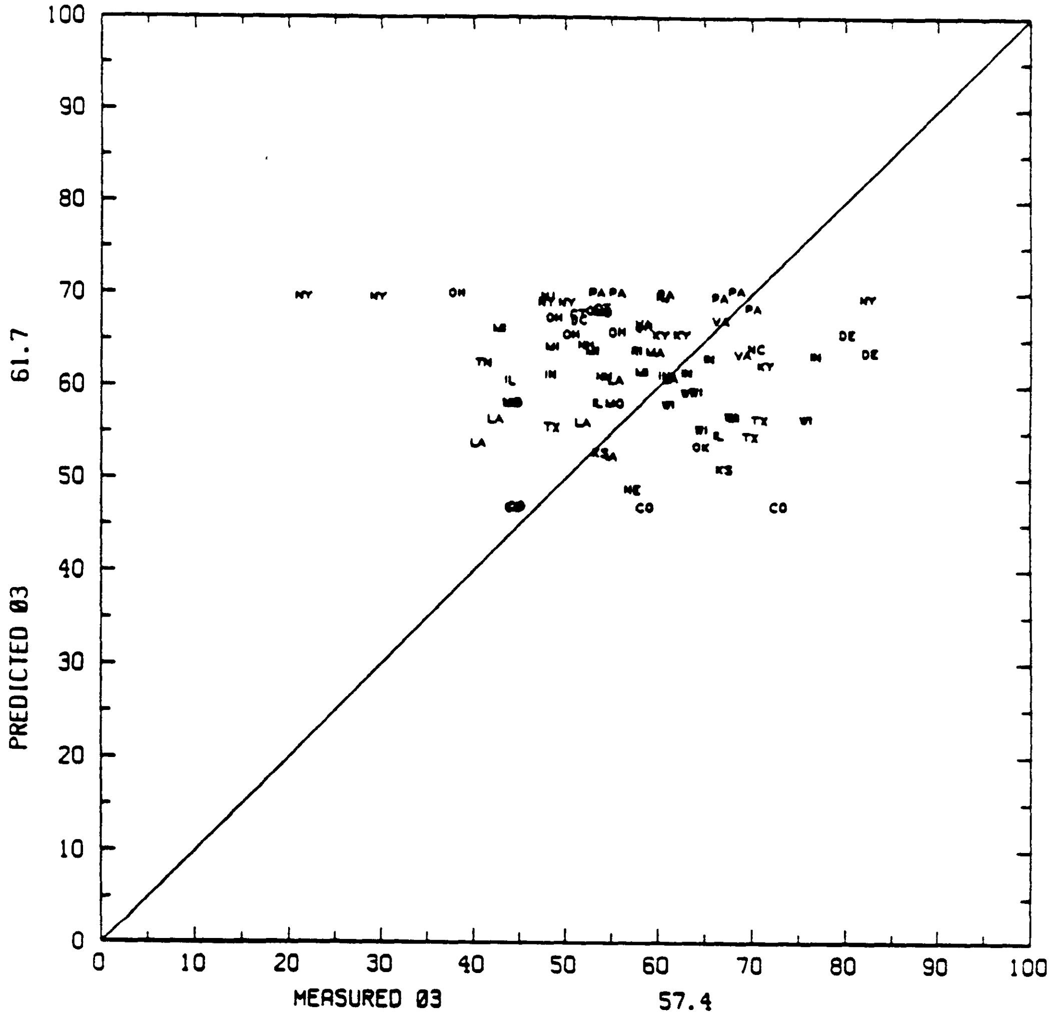

Fig. 5.15 Predicted vs. measured average seasonal ozone concentrations at urban monitors. Physical model; 1985 data. Two letter abbreviations designate the location of each site. Mean values indicated in axes legends. Correlation coefficient r=-0.08.

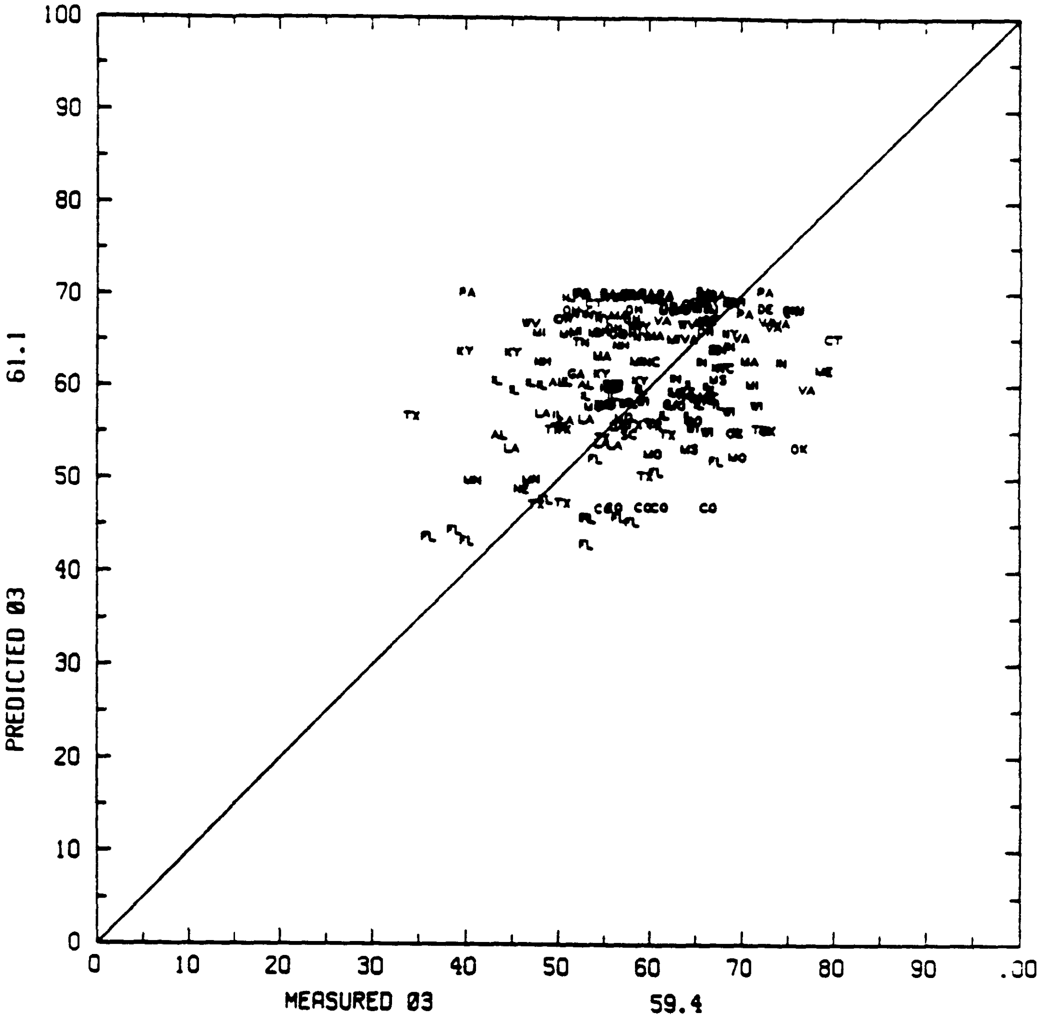

Fig. 5.16 Predicted vs. measured average seasonal ozone concentrations at suburban monitors. Physical model; 1985 data. Two letter abbreviations designate the location of each site. Mean values indicated in axes legends. Correlation coefficient r=0.28.

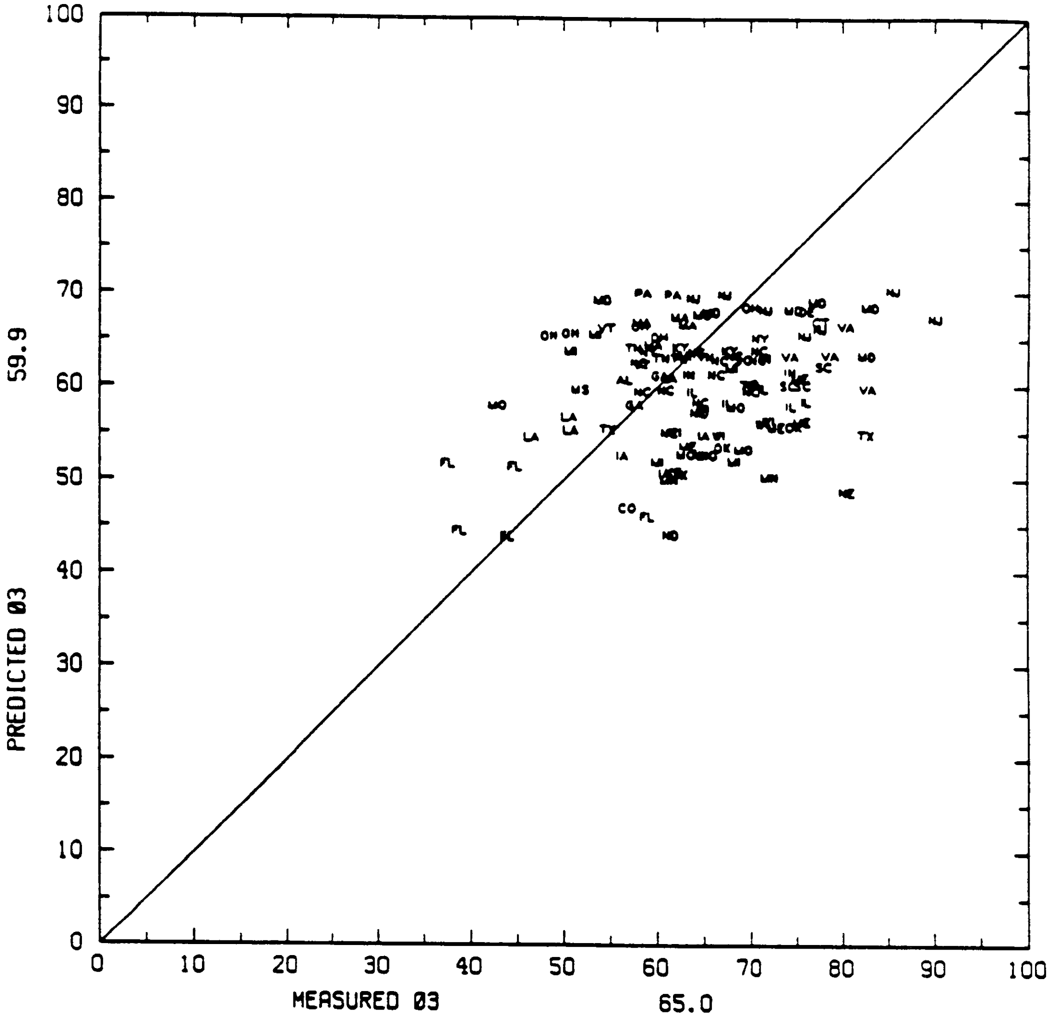

Fig. 5.17 Predicted vs. measured average seasonal ozone concentrations at rural monitors. Physical model; 1985 data. Two letter abbreviations designate the location of each site. Mean values indicated in axes legends. Correlation coefficient r=0.29.

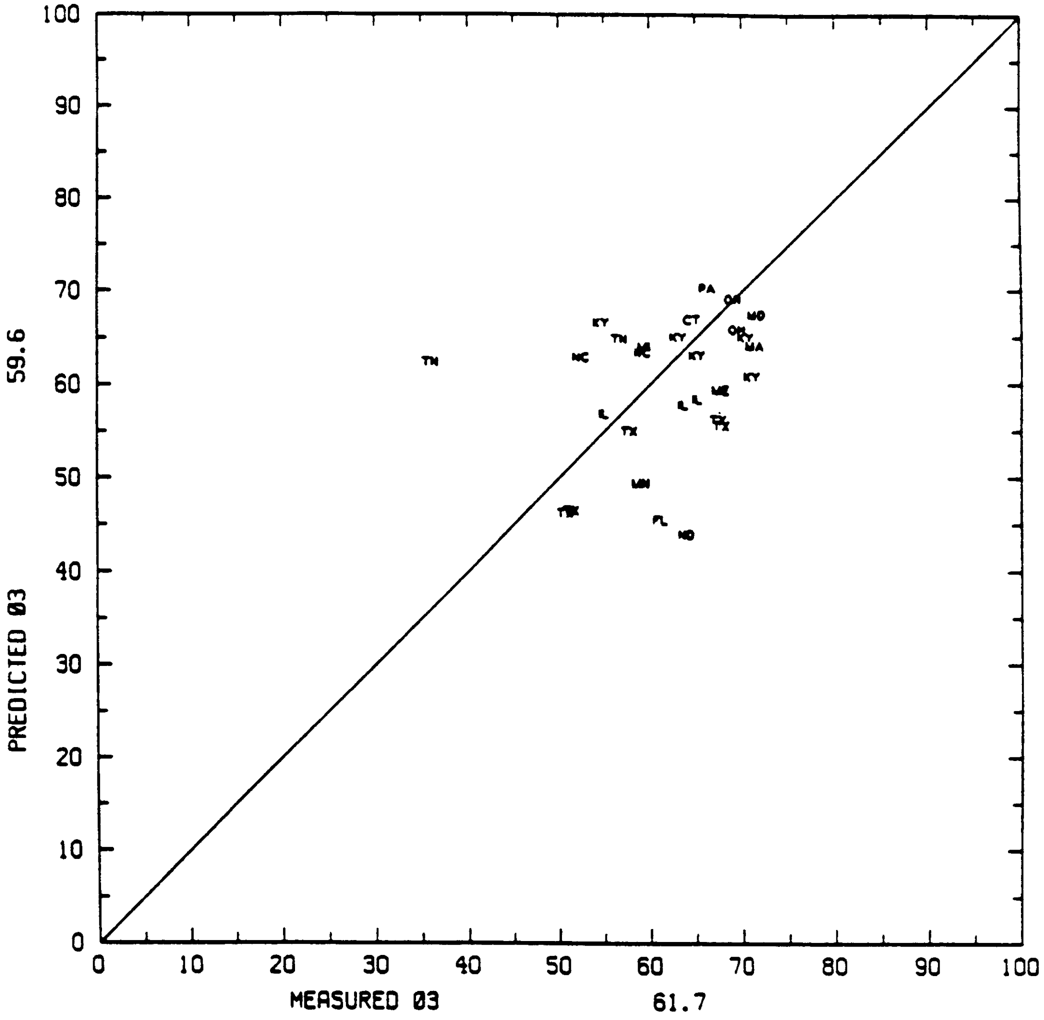

Fig. 5.18 Predicted vs. measured average seasonal ozone concentrations at unclassified monitors. Physical model; 1985 data. Two letter abbreviations designate the location of each site. Mean values indicated in axes legends. Correlation coefficient r=0.27.

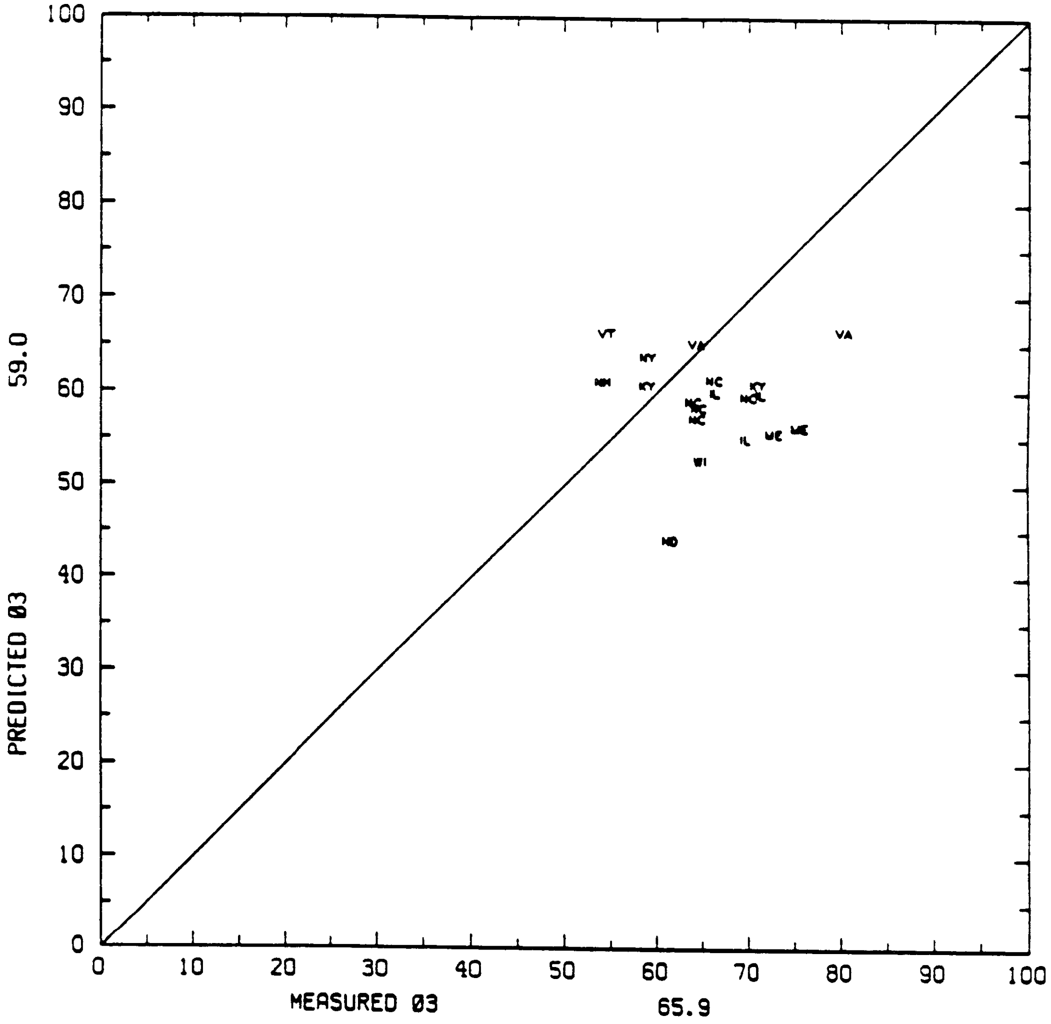

Fig. 5.19 Predicted vs. measured average seasonal ozone concentrations at remote monitors as determined by Meyer [28]. Physical model; 1985 data. Two letter abbreviations designate the location of each site. Mean values indicated in axes legends. Correlation coefficient r=-0.04.

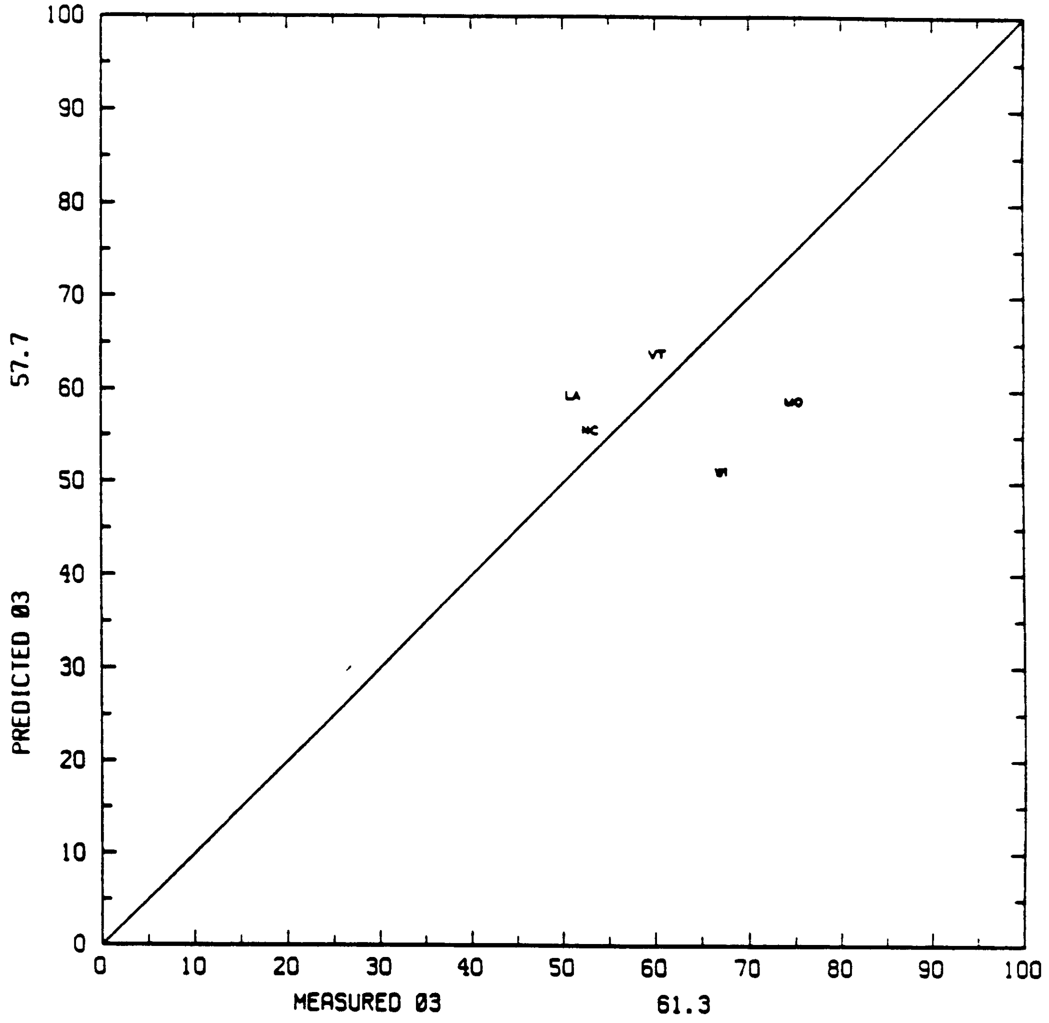

Fig. 5.20 Predicted vs. measured ozone concentrations at remote national park sites [30]. Physical model; 1985 data. Predictions are seasonal averages; observations are annual averages. Two letter abbreviations designate the location of each site. Mean values indicated in axes legends. Correlation coefficient r=-0.16.

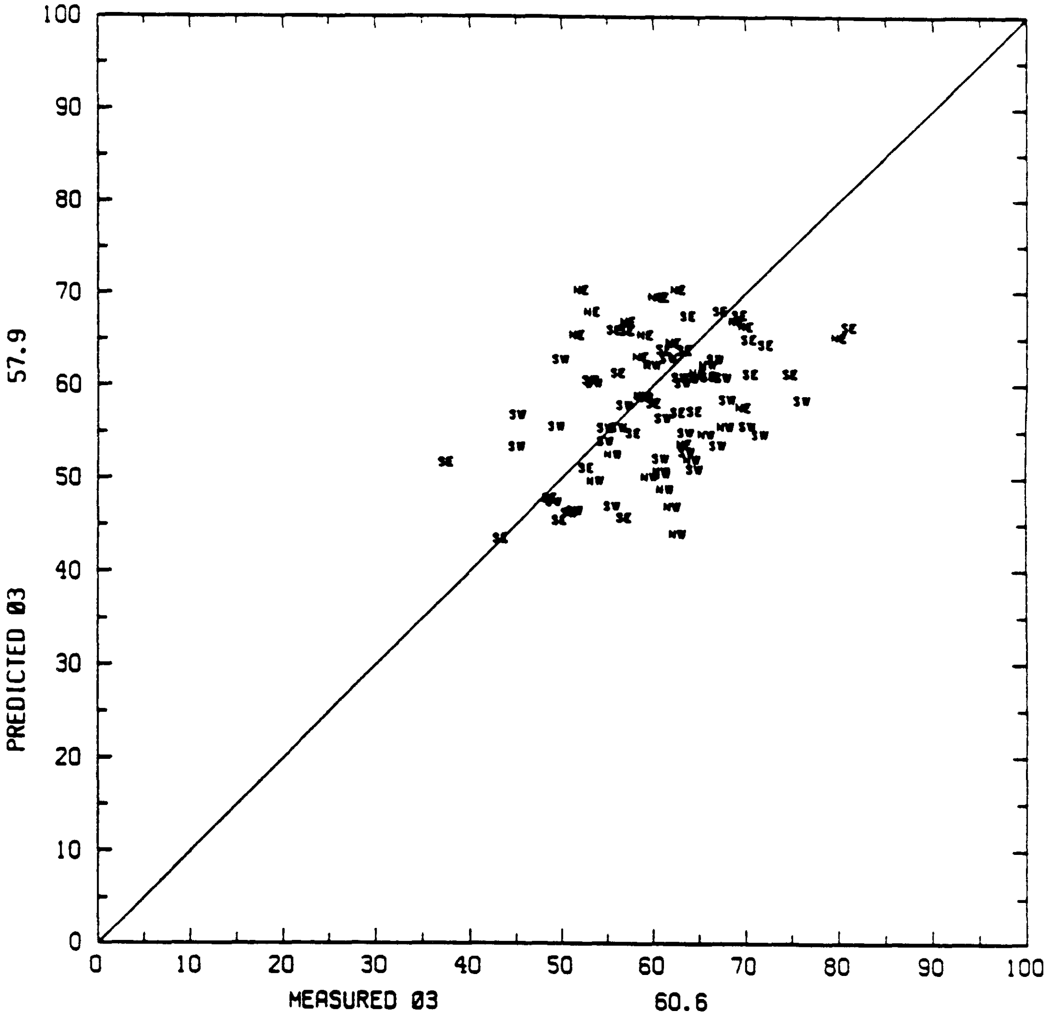

Fig. 5.21 Predicted vs. measured ozone concentrations at box averaged sites (Fig. 2.32). 1985 data; seasonally averaged physical model. Two letter abbreviations designate quadrants of eastern North America. Mean values indicated in axes legends. Correlation coefficient r=-0.16.

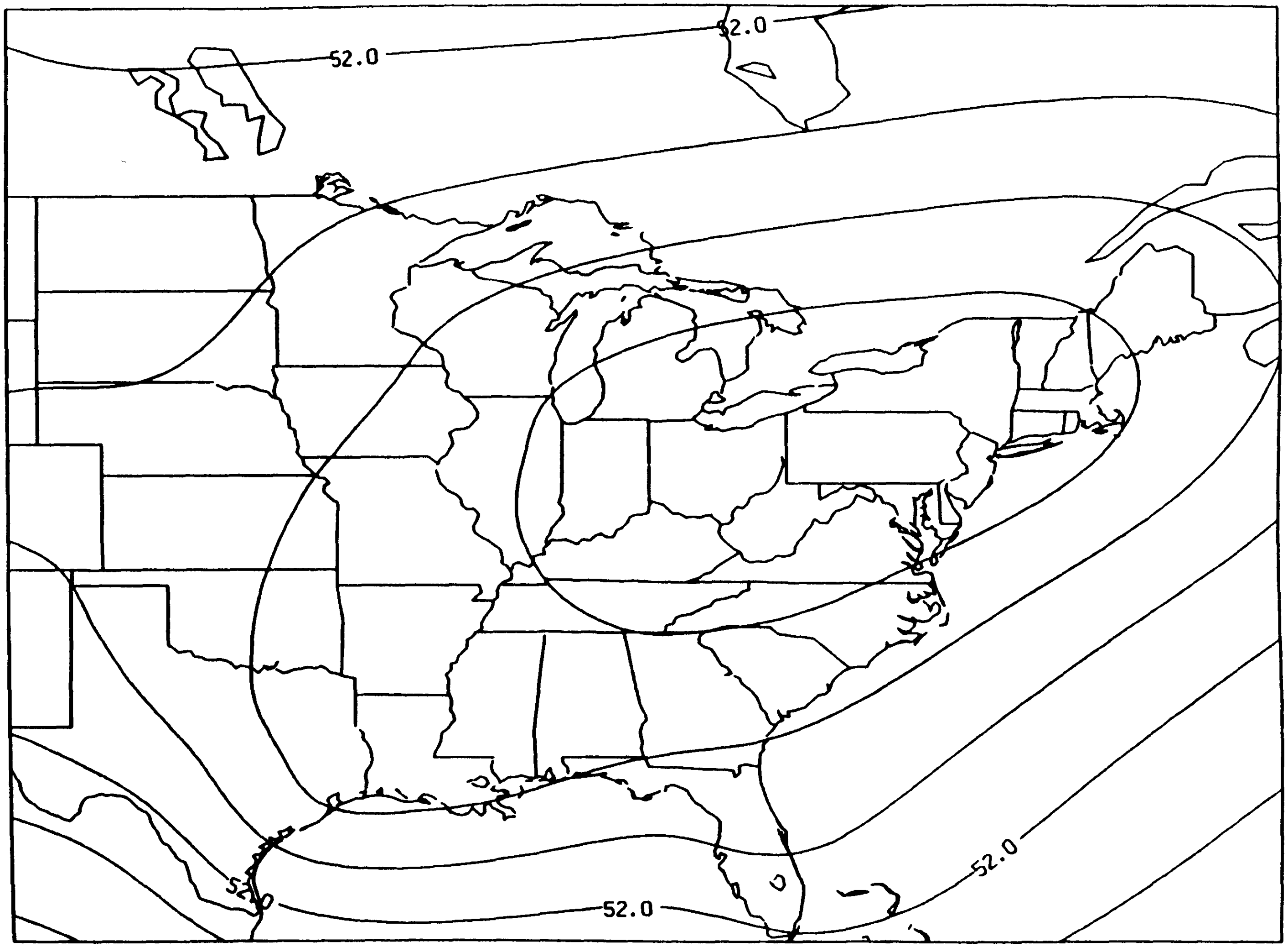

Fig. 5.22 Seasonal average ozone concentrations ($\mu g\,m^{-3}$) predicted by a solely NO_x dependent model. Contours from 49 to 61 $\mu g\,m^{-3}$ by 3 $\mu g\,m^{-3}$. Outer solution is shown in Fig. VIII.2.

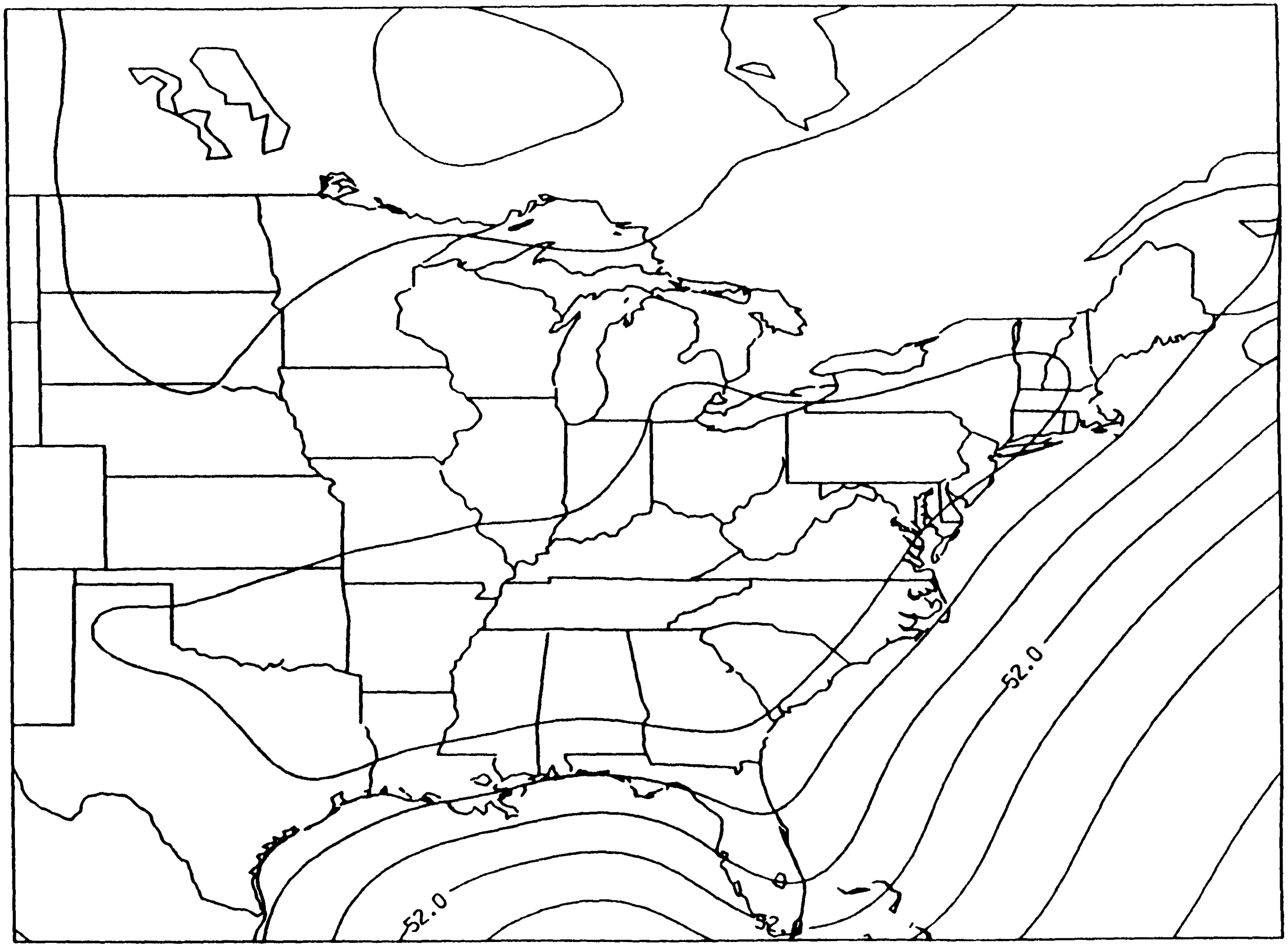

Fig. 5.23 Seasonal average ozone concentrations ($\mu\mathrm{g\,m^{-3}}$) predicted by a solely VOCs dependent model. Contours from 43 to 61 $\mu\mathrm{g\,m^{-3}}$ by 3 $\mu\mathrm{g\,m^{-3}}$. Outer solution is shown in Fig. VIII.3.

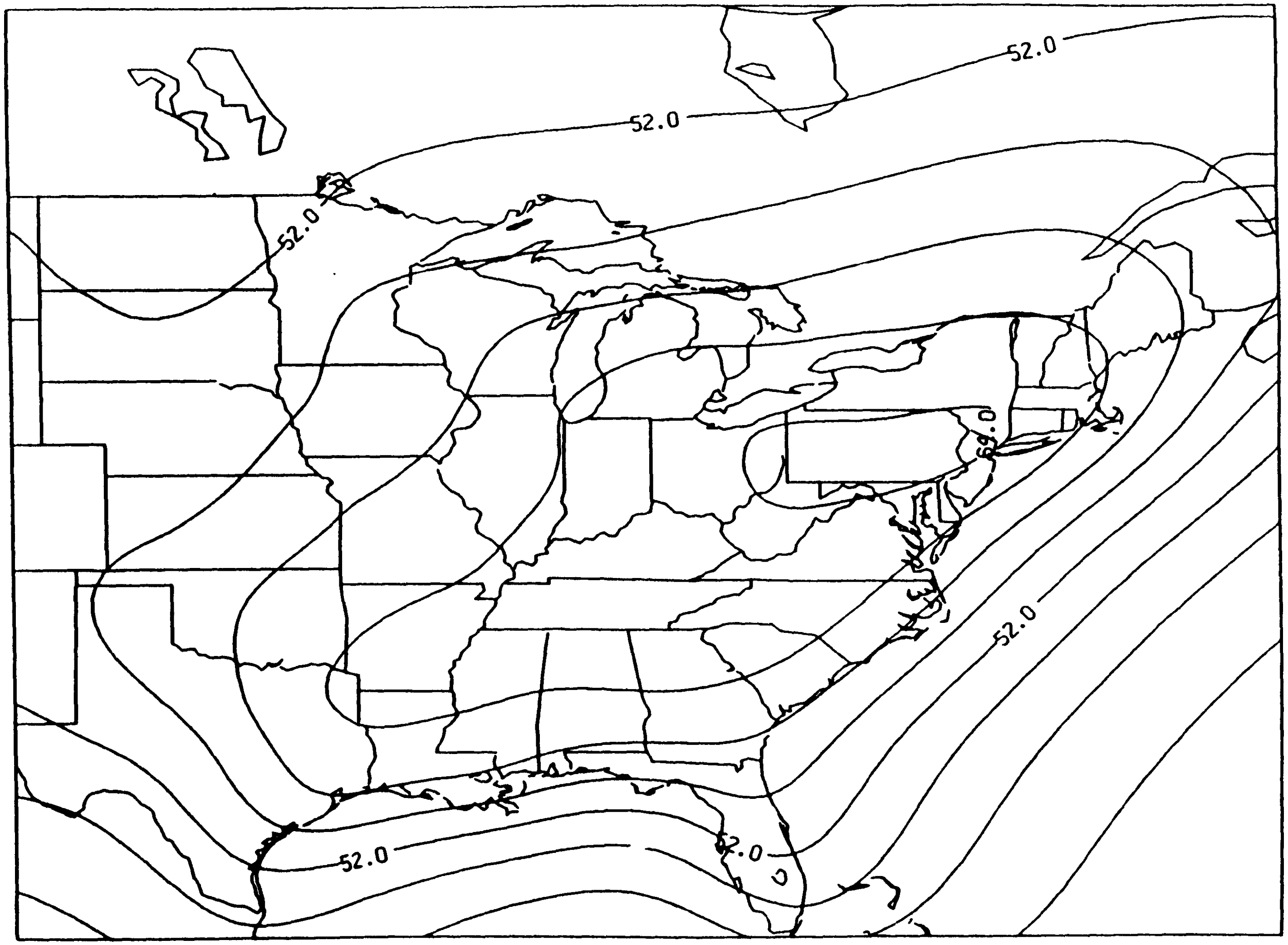

Fig. 5.24 Seasonal average ozone concentrations ($\mu g\ m^{-3}$) predicted by the optimized source model. Contours from 43 to 64 $\mu g\ m^{-3}$ by 3 $\mu g\ m^{-3}$. Outer solution is shown in Fig. VIII.4.

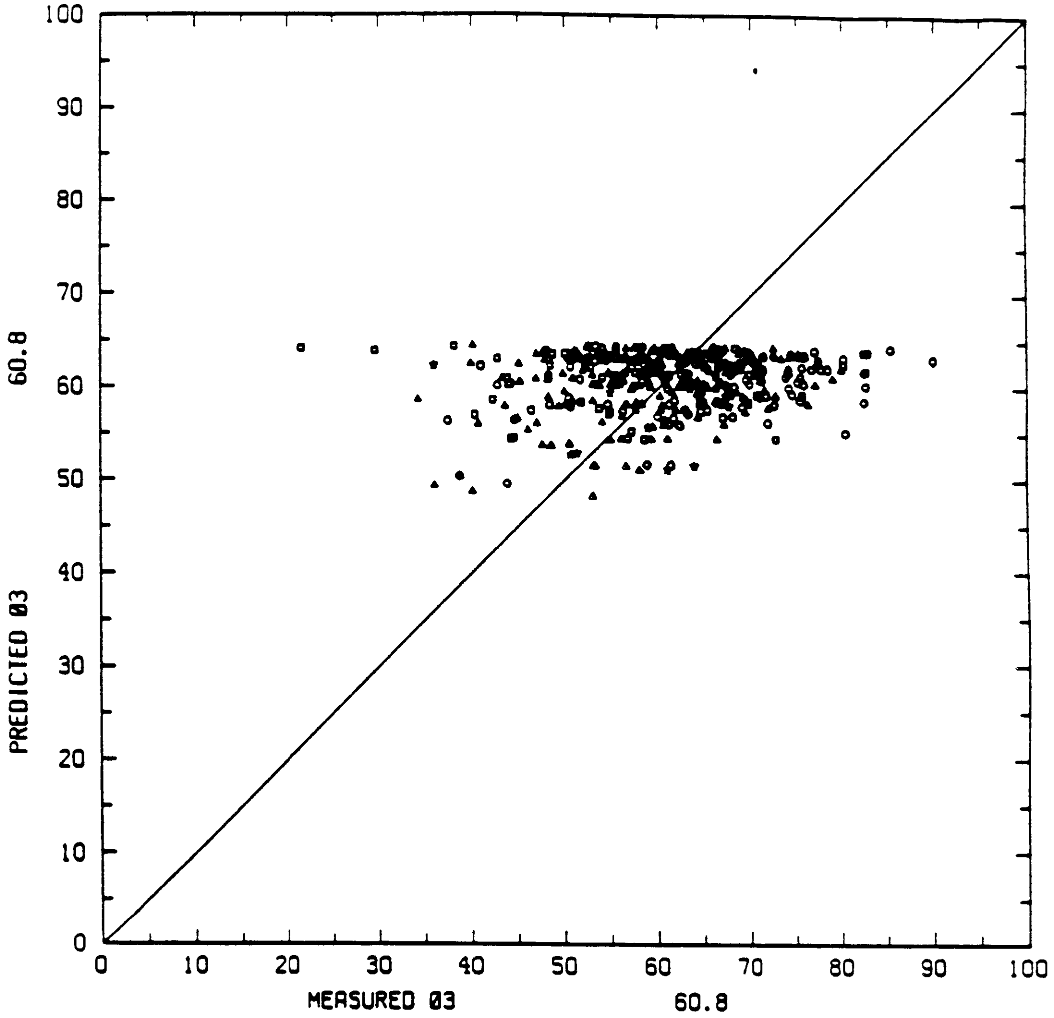

Fig. 5.25 Predicted vs. measured average seasonal ozone concentrations. 1985 data; source optimized model. Square, triangle, circle and star symbols refer to urban, suburban, rural and unclassified monitoring categories. Mean values indicated in axes legends. Correlation coefficient r=0.21. Companion plot to Fig. 5.26.

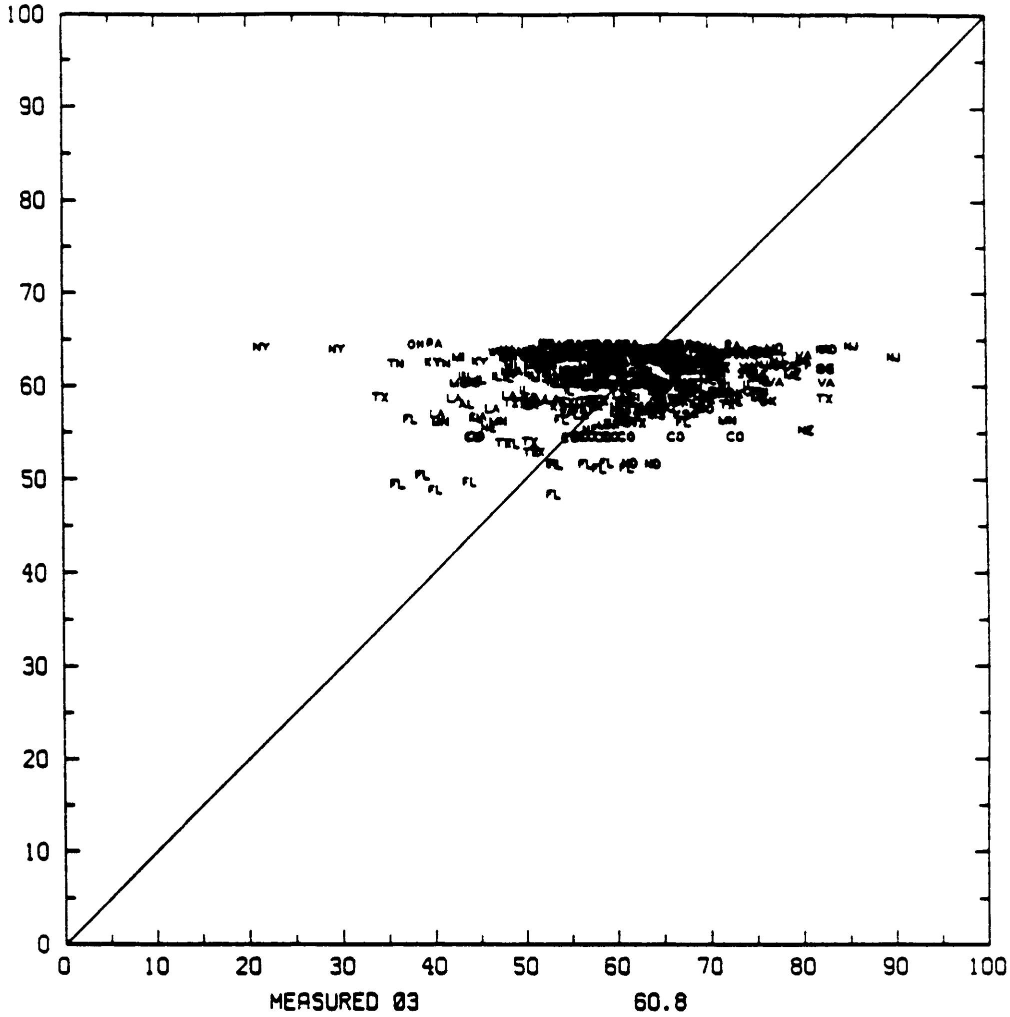

Fig. 5.26 Predicted vs. measured average seasonal ozone concentrations. 1985 data; source optimized model. Two letter abbreviations designate the location of each site. Mean values indicated in axes legends. Correlation coefficient r=0.21. Companion plot to Fig. 5.25.

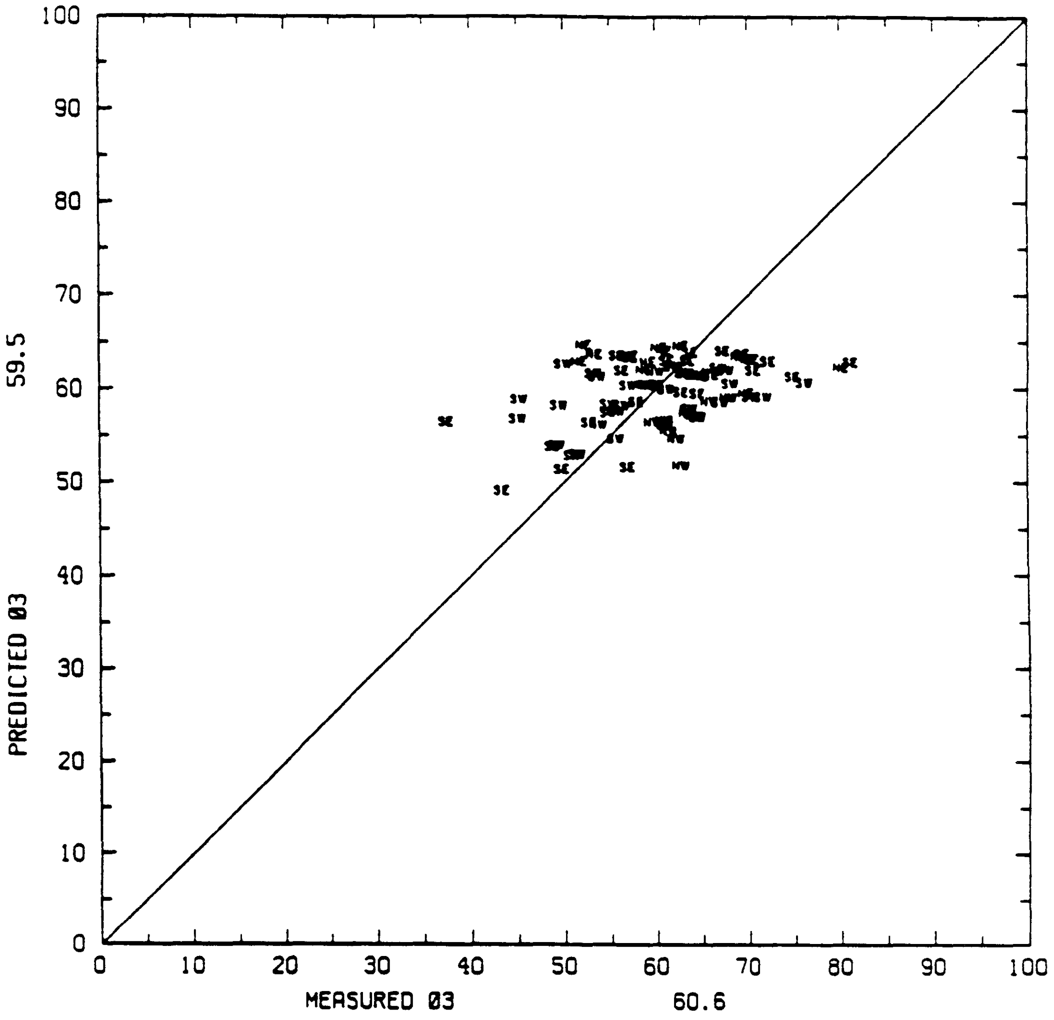

Fig. 5.27 Predicted vs. measured ozone concentrations at box averaged sites (Fig. 2.32). 1985 data; seasonally averaged source optimized model. Two letter abbreviations designate quadrants of eastern North America. Mean values indicated in axes legends. Correlation coefficient r=0.42.

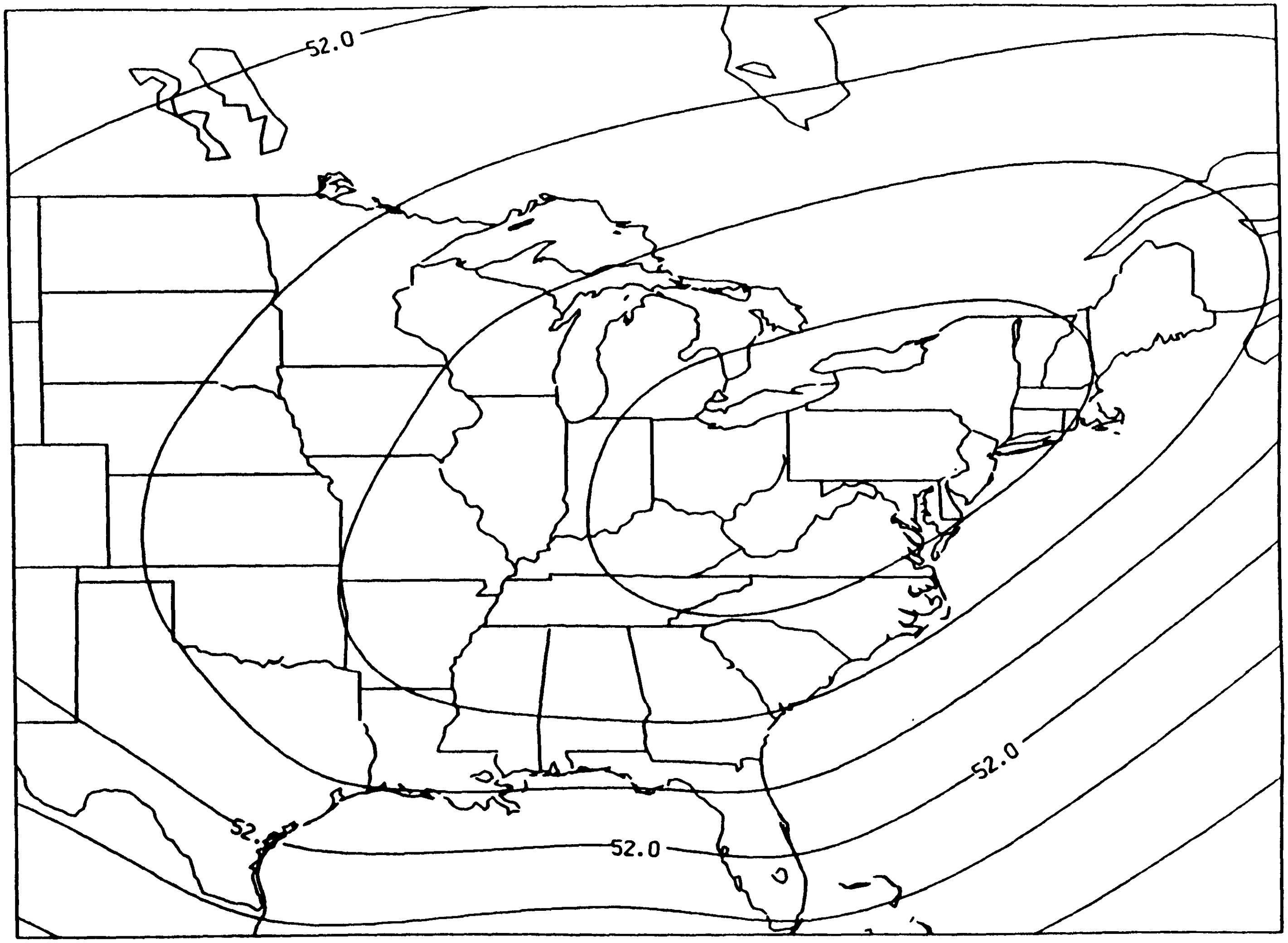

Fig. 5.28 Seasonal average ozone concentrations (μg m^{-3}) predicted by the fully optimized model. Contours from 46 to 61 μg m^{-3} by 3 μg m^{-3}. Outer solution is shown in Fig. VIII.5.

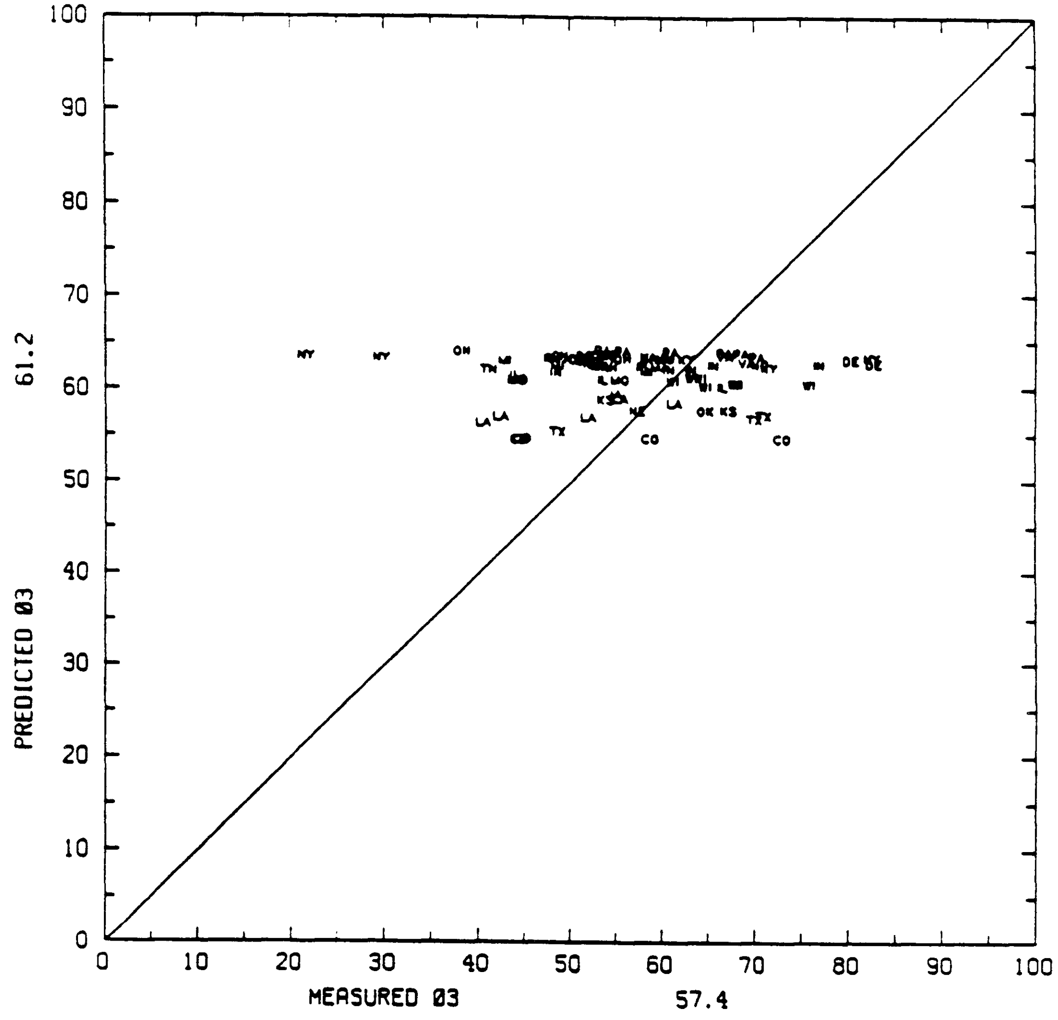

Fig. 5.29 **Predicted vs. measured average seasonal ozone concentrations at urban monitors. Fully optimized model; 1985 data. Two letter abbreviations designate the location of each site. Mean values indicated in axes legends. Correlation coefficient r=0.01.**

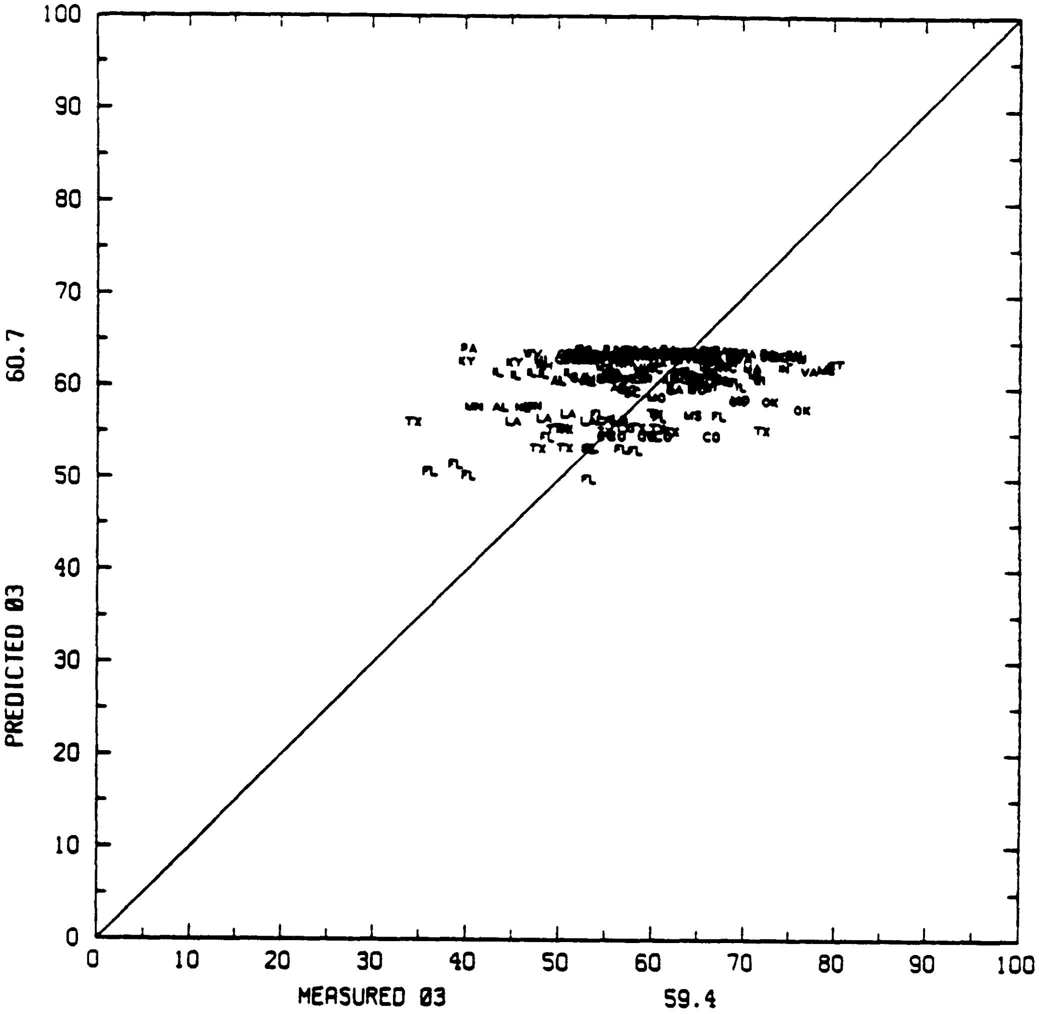

Fig. 5.30 Predicted vs. measured average seasonal ozone concentrations at suburban monitors. Fully optimized model; 1985 data. Two letter abbreviations designate the location of each site. Mean values indicated in axes legends. Correlation coefficient r=0.34.

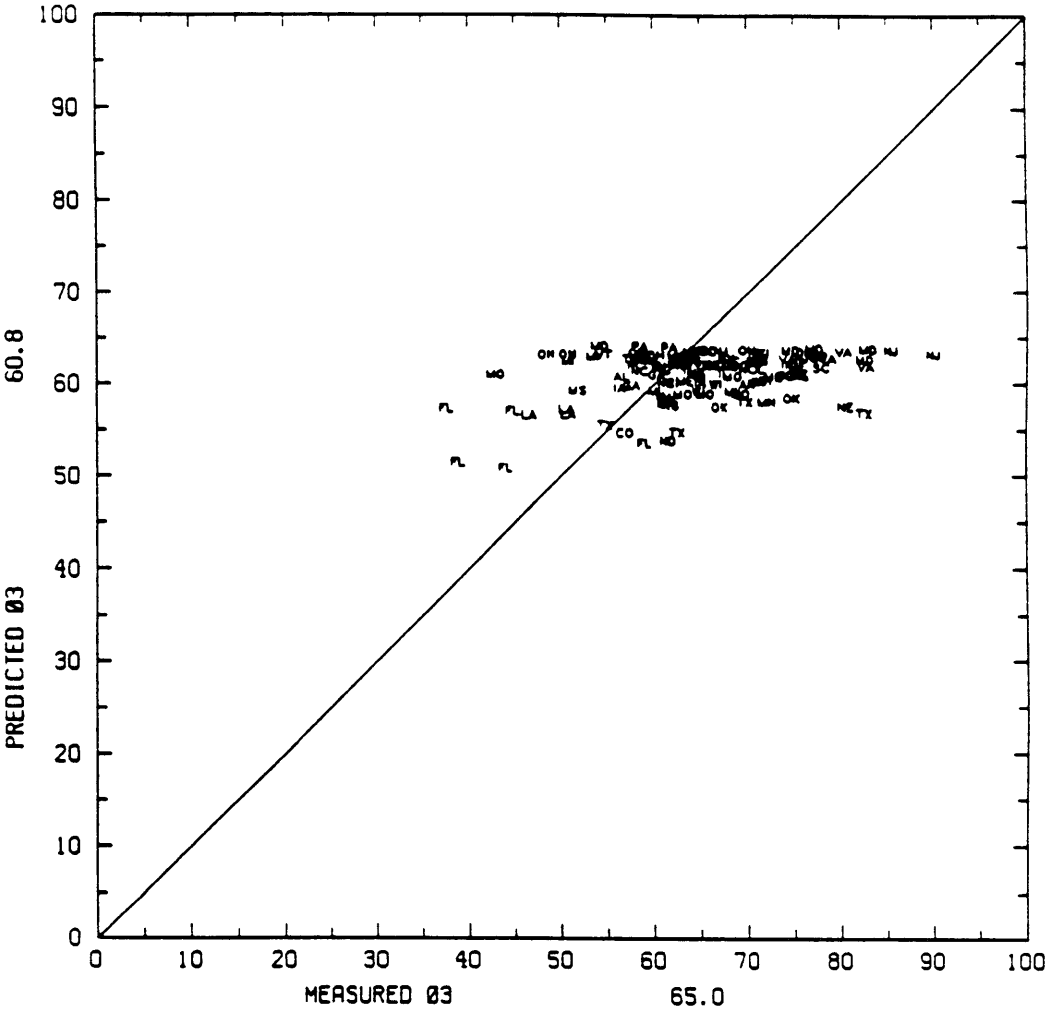

Fig. 5.31 Predicted vs. measured average seasonal ozone concentrations at rural monitors. Fully optimized model; 1985 data. Two letter abbreviations designate the location of each site. Mean values indicated in axes legends. Correlation coefficient r=0.38.

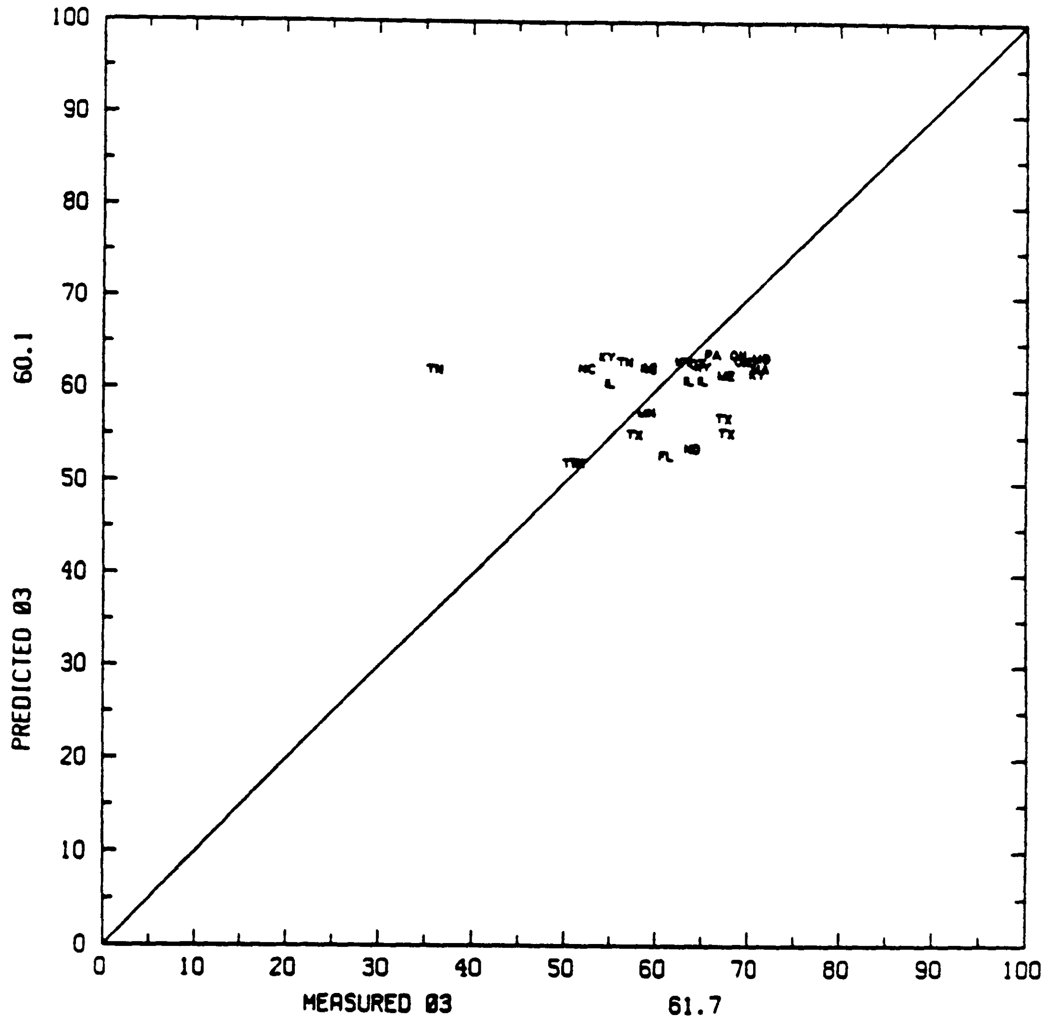

Fig. 5.32 Predicted vs. measured average seasonal ozone concentrations at unclassified monitors. Fully optimized model; 1985 data. Two letter abbreviations designate the location of each site. Mean values indicated in axes legends. Correlation coefficient r=0.25.

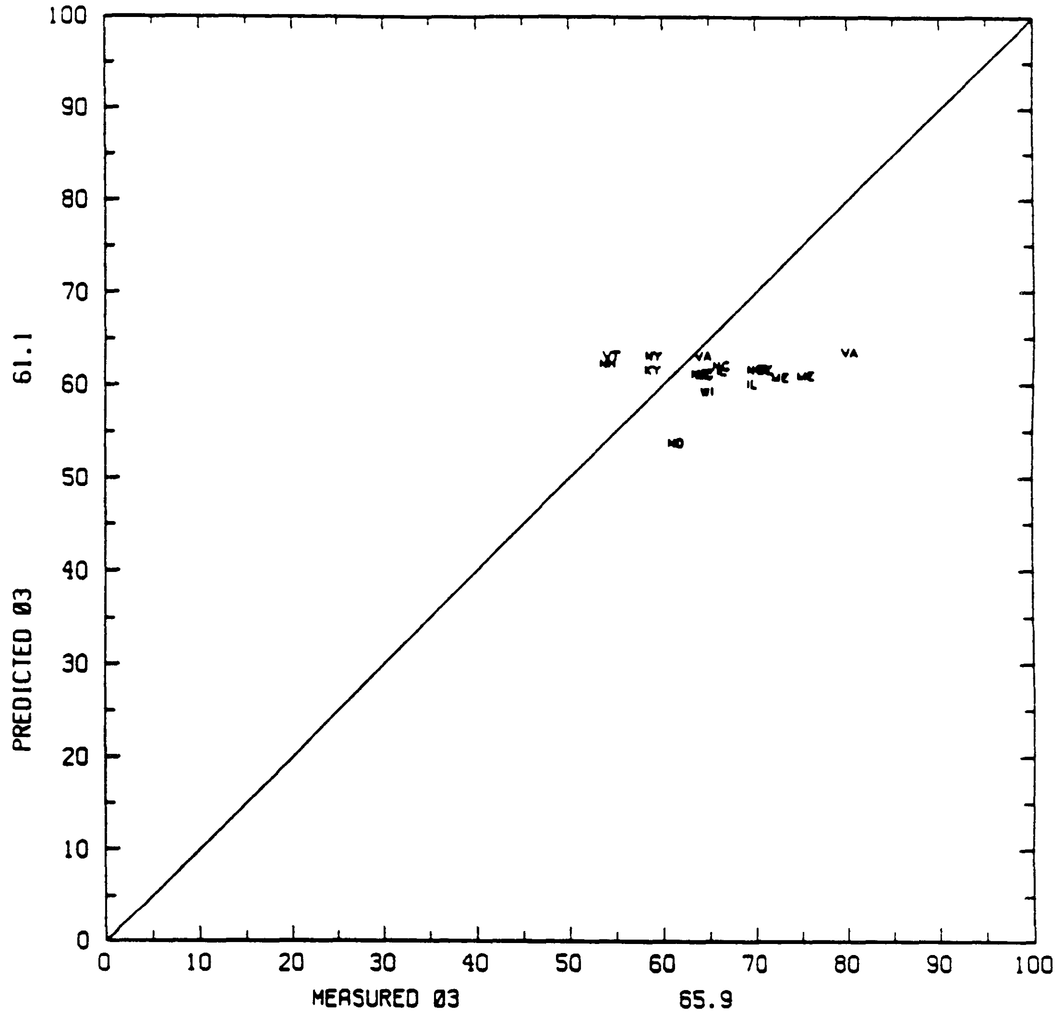

Fig. 5.33 **Predicted vs. measured average seasonal ozone concentrations at remote monitors as determined by Meyer [28]. Fully optimized model; 1985 data. Two letter abbreviations designate the location of each site. Mean values indicated in axes legends. Correlation coefficient r=0.05.**

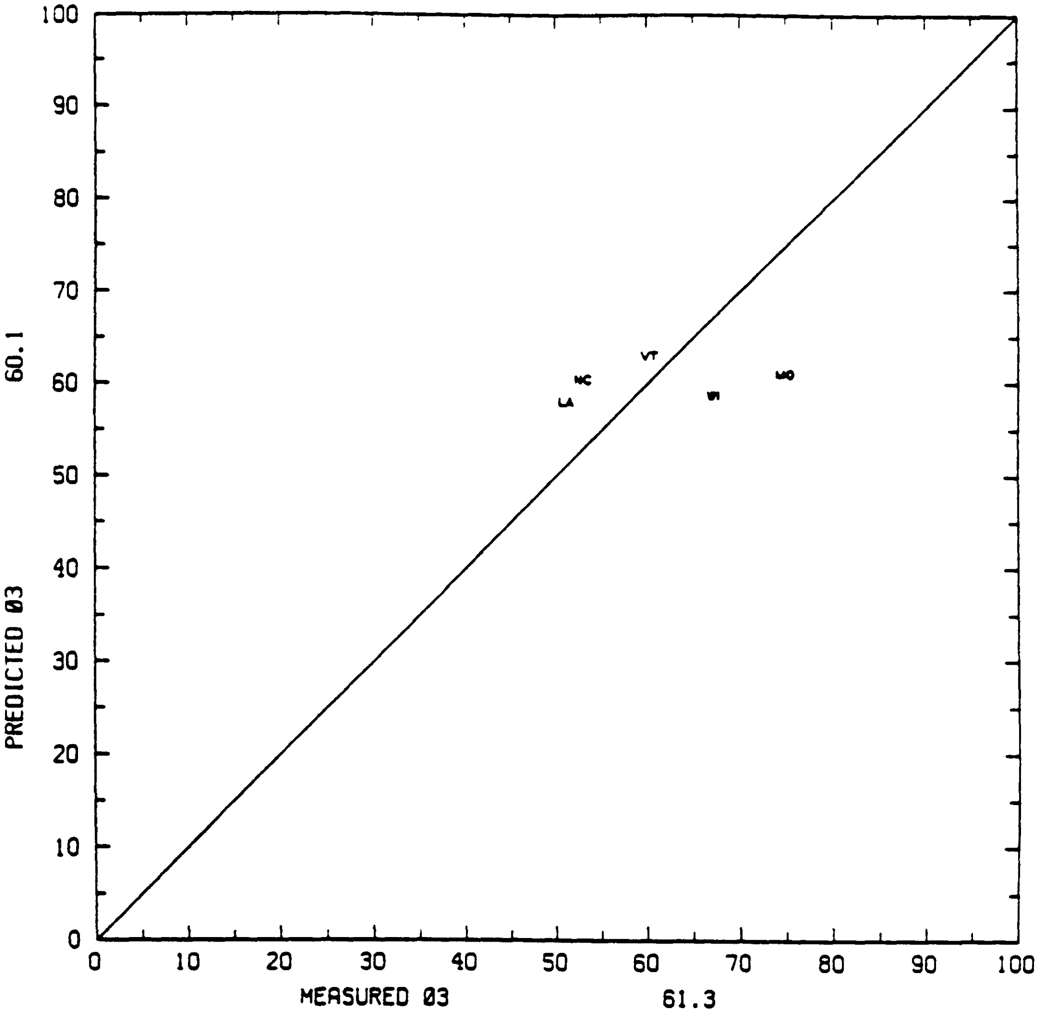

Fig. 5.34 Predicted vs. measured ozone concentrations at remote national park sites [30]. Fully optimized model; 1985 data. Predictions are seasonal averages; observations are annual averages. Two letter abbreviations designate the location of each site. Mean values indicated in axes legends. Correlation coefficient r=0.25.

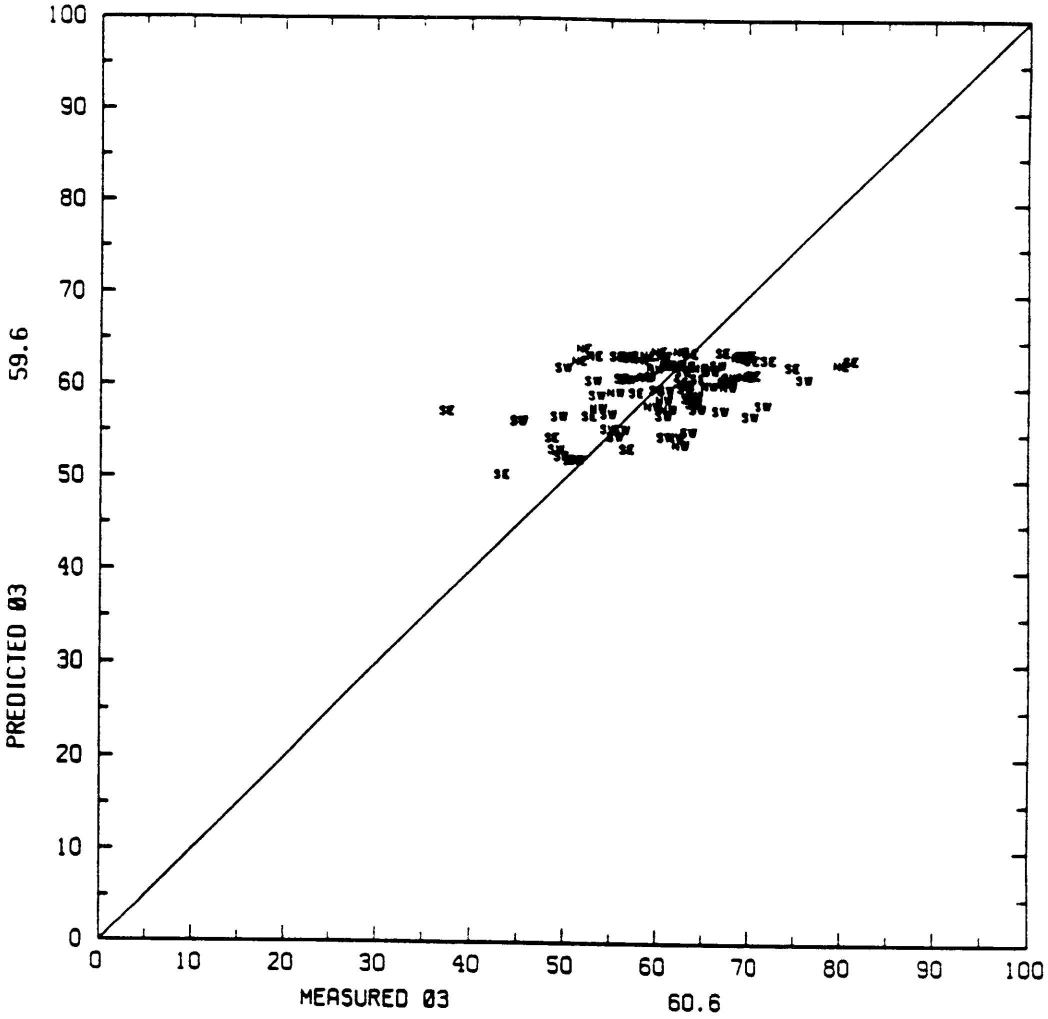

Fig. 5.35 Predicted vs. measured ozone concentrations at box averaged sites (Fig. 2.32). 1985 data; seasonally averaged fully optimized model. Two letter abbreviations designate quadrants of eastern North America. Mean values indicated in axes legends. Correlation coefficient r=0.47.

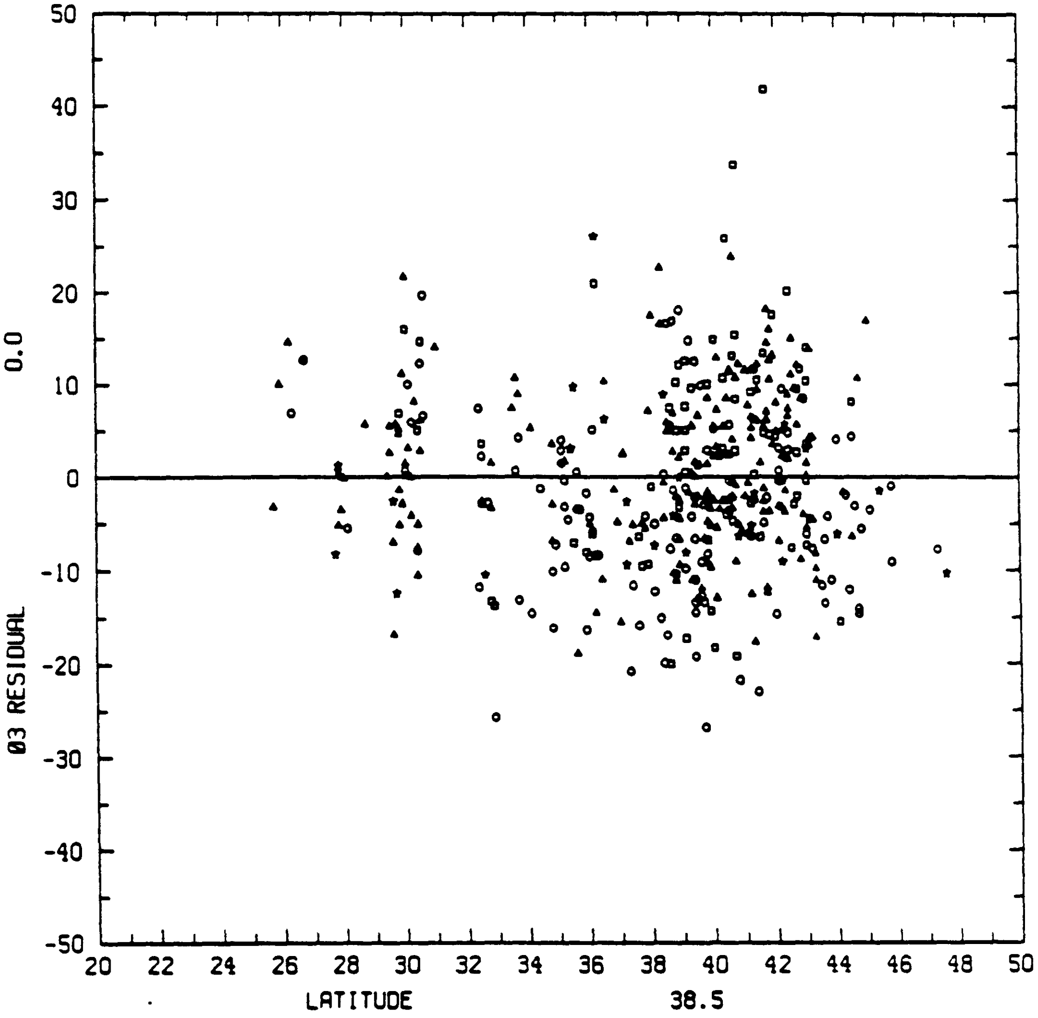

Fig. 5.36 $[O_3]_{residual}$ ($\mu g\ m^{-3}$) vs. latitude (° N). 1985 data; fully optimized model. Square, triangle, circle and star symbols differentiate urban, suburban, rural and unclassified monitors. Companion plot to Fig. 5.37.

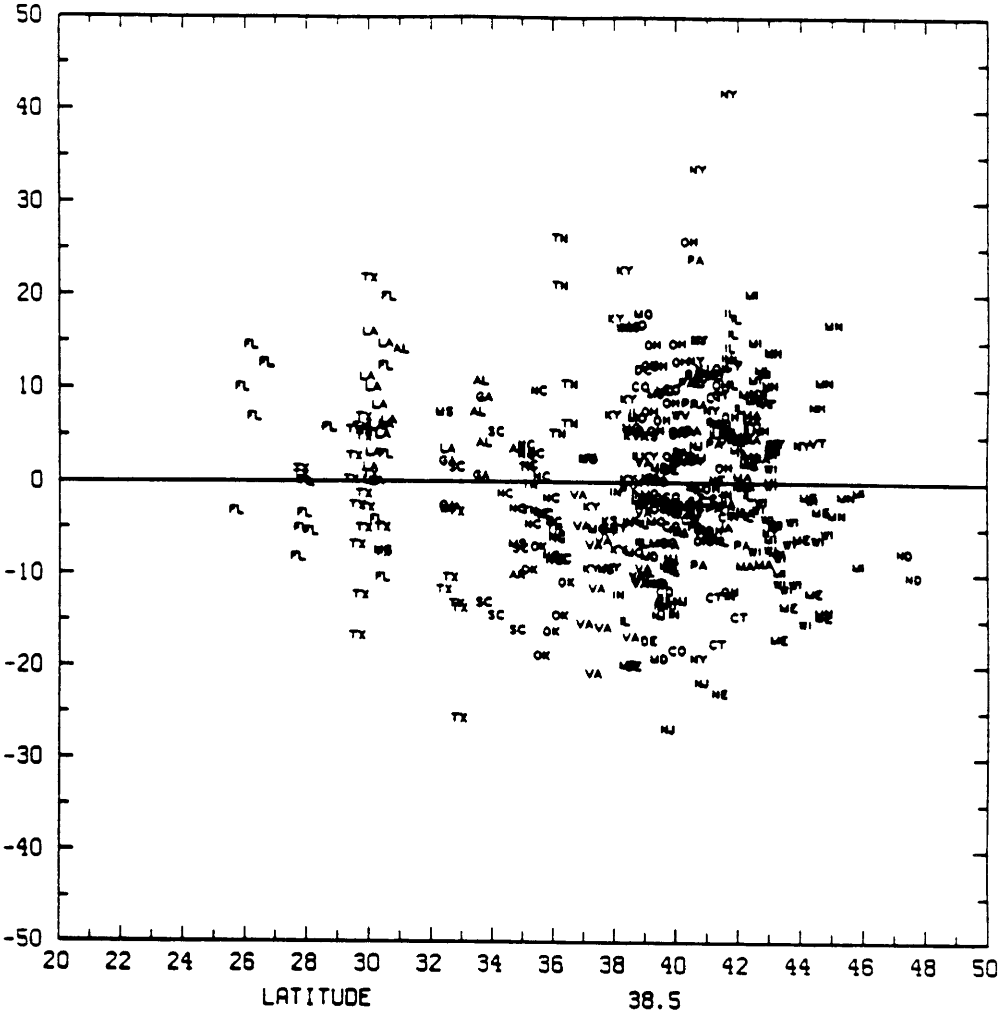

Fig. 5.37 $[O_3]_{\text{residual}}$ ($\mu g\, m^{-3}$) vs. latitude (° N). 1985 data; fully optimized model. Two letter state abbreviations indicate the location of each monitor. Companion plot to Fig. 5.36.

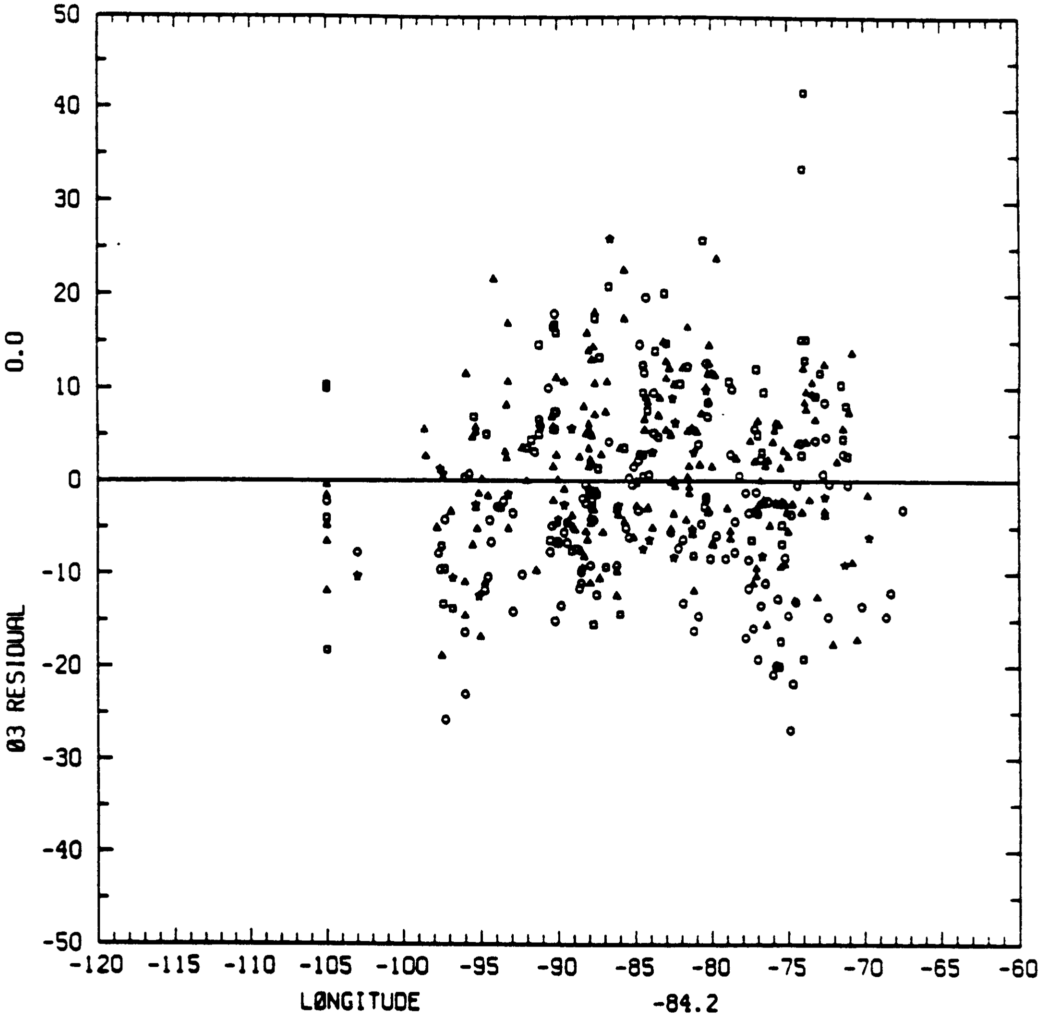

Fig. 5.38 $[O_3]_{\mathrm{residual}}$ ($\mu g\,m^{-3}$) vs. longitude (° W). 1985 data; fully optimized model. Square, triangle, circle and star symbols differentiate urban, suburban, rural and unclassified monitors. Companion plot to Fig. 5.39.

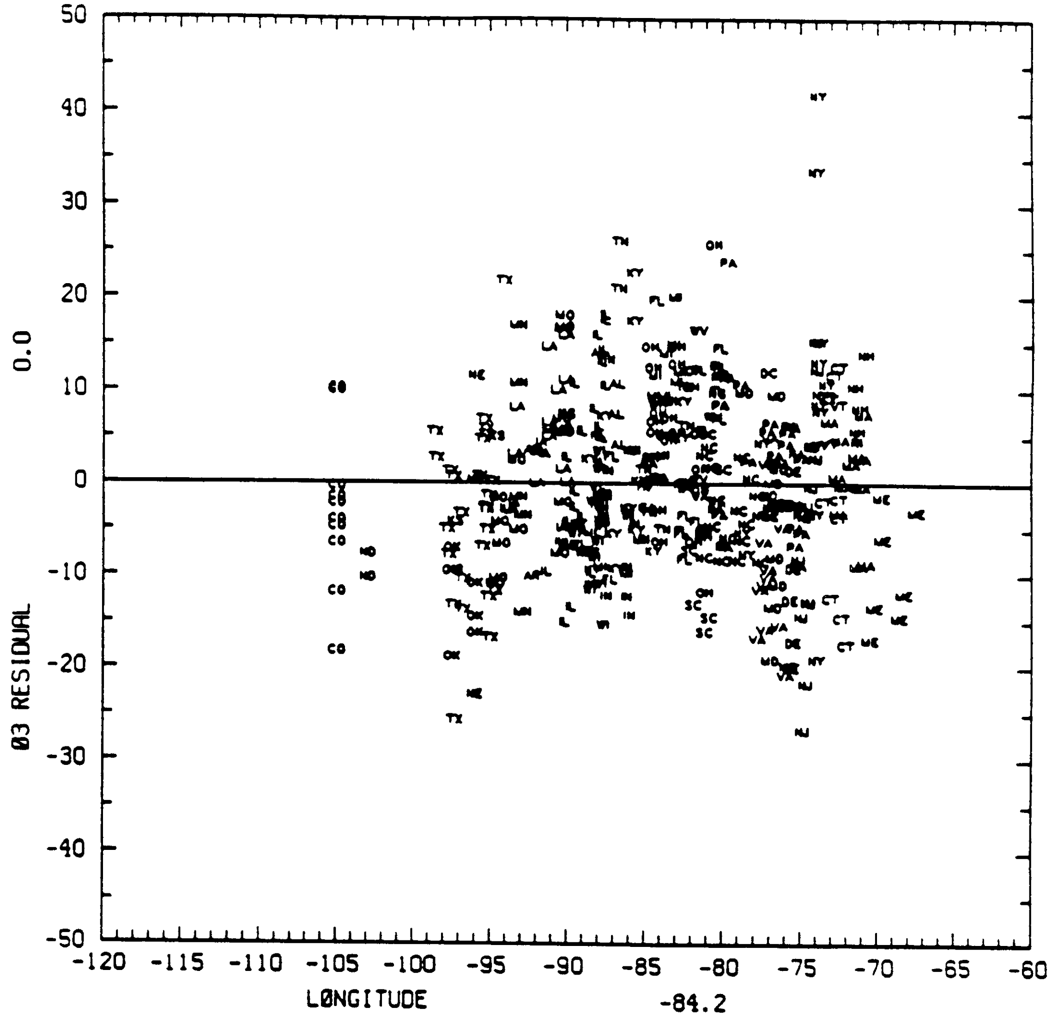

Fig. 5.39 $[O_3]_{\text{residual}}$ ($\mu g\, m^{-3}$) vs. longitude (° W). 1985 data; fully optimized model. Two letter state abbreviations indicate the location of each monitor. Companion plot to Fig. 5.38.

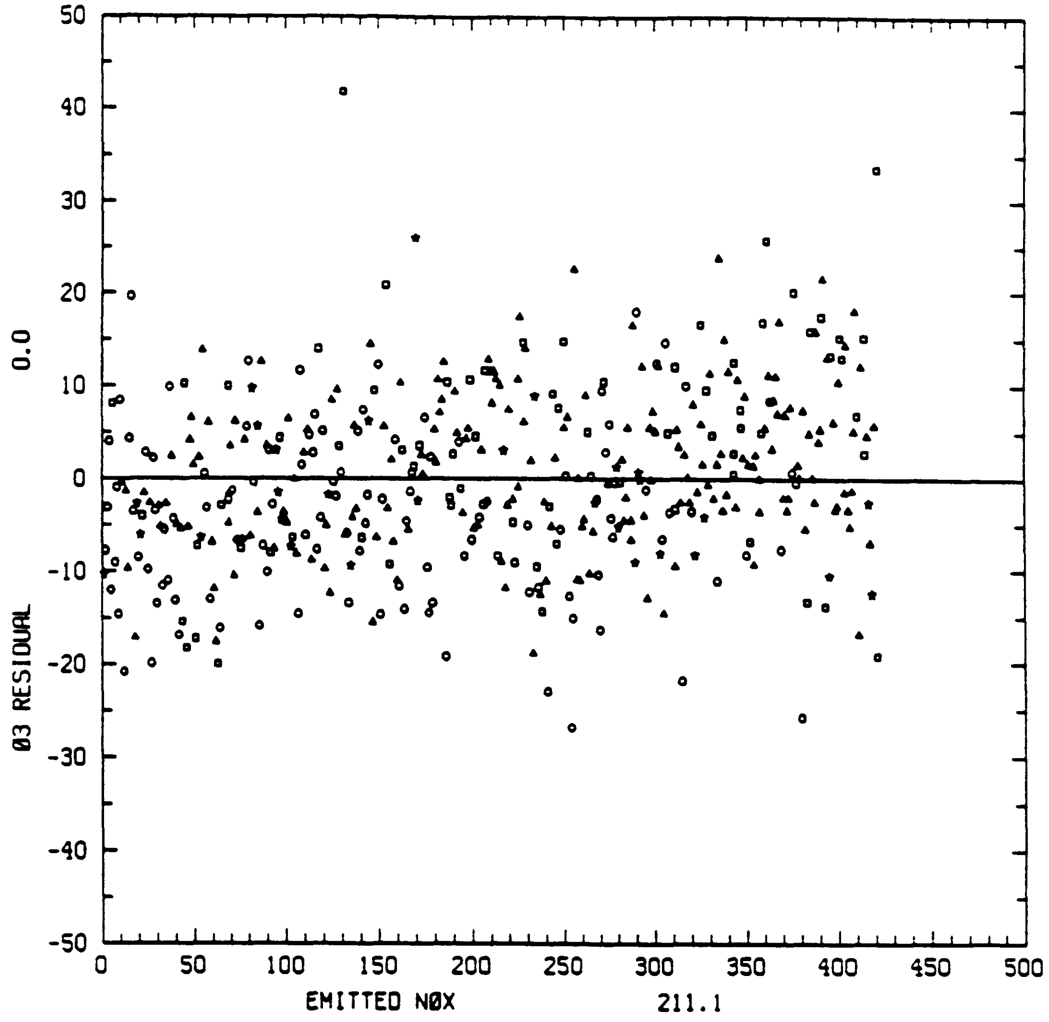

Fig. 5.40 $[O_3]_{residual}$ ($\mu g\, m^{-3}$) vs. relative NO_x emissions. Sites are rank ordered according to the level of local proximate emissions. 1985 data; fully optimized model. Square, triangle, circle and star symbols differentiate urban, suburban, rural and unclassified monitors. Companion plot to Fig. 5.41.

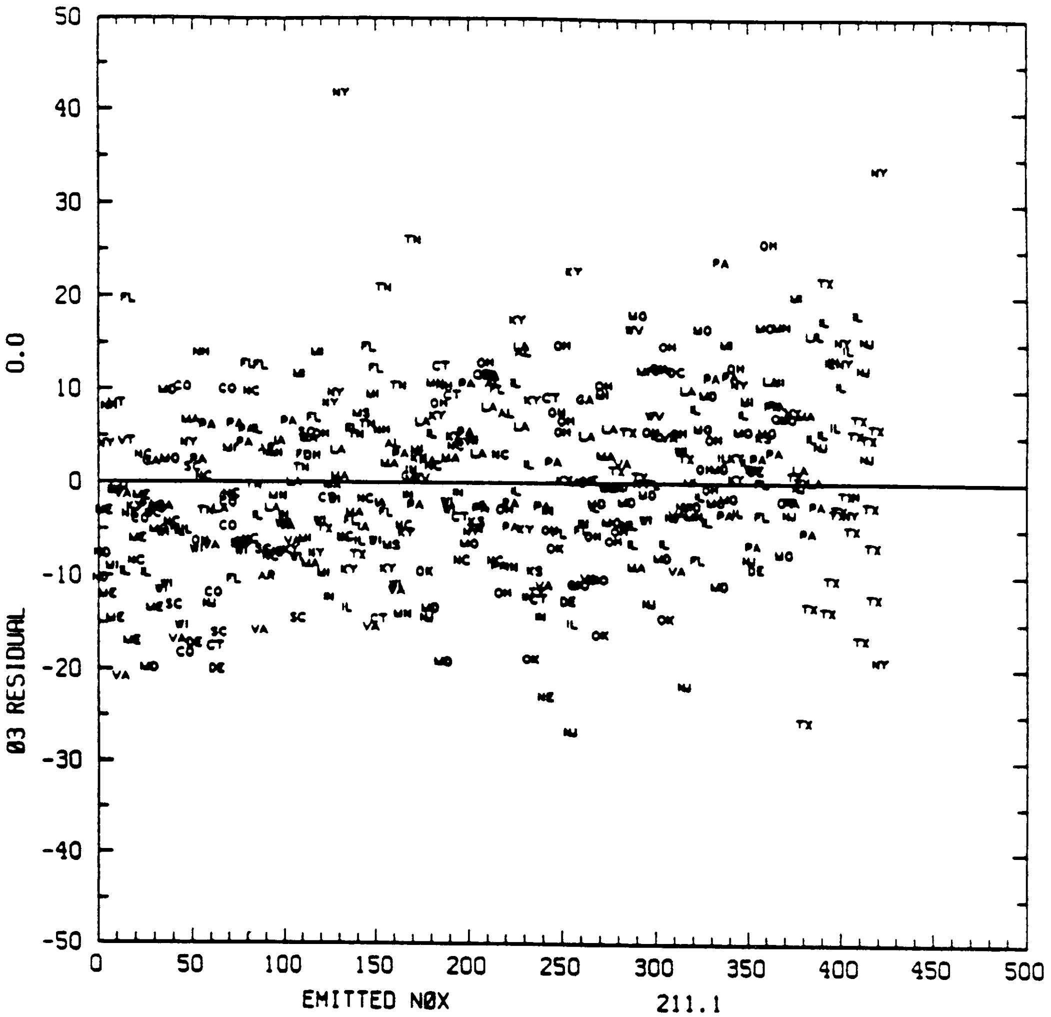

Fig. 5.41 $[O_3]_{\text{residual}}$ ($\mu g\, m^{-3}$) vs. relative NO_x emissions. Sites are rank ordered according to the level of local proximate emissions. 1985 data; fully optimized model. Two letter state abbreviations indicate the location of each monitor. Companion plot to Fig. 5.40.

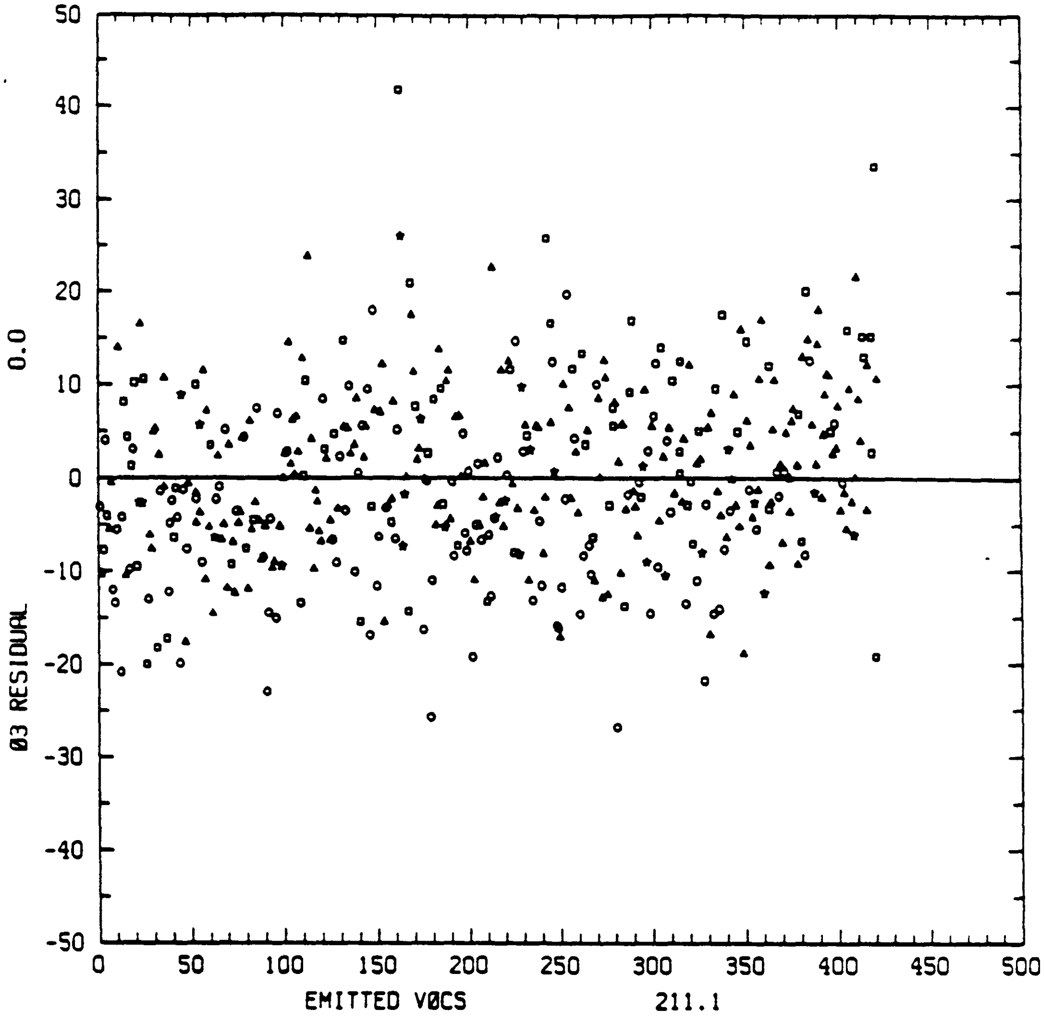

Fig. 5.42 $[O_3]_{residual}$ ($\mu g\,m^{-3}$) vs. relative VOCs emissions. Sites are rank ordered according to the level of local proximate emissions. 1985 data; fully optimized model. Square, triangle, circle and star symbols differentiate urban, suburban, rural and unclassified monitors. Companion plot to Fig. 5.43.

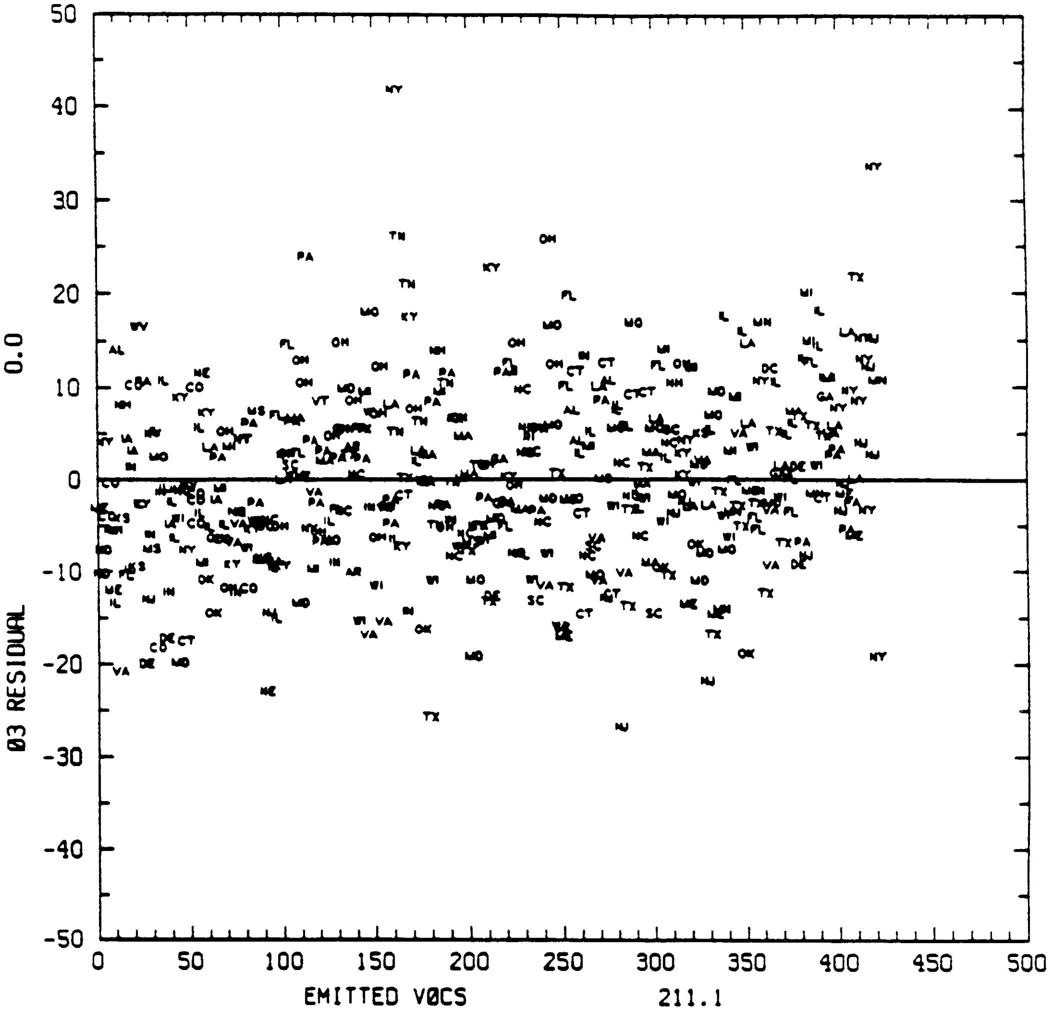

Fig. 5.43 $[O_3]_{\text{residual}}$ ($\mu g\, m^{-3}$) vs. relative VOCs emissions. Sites are rank ordered according to the level of local proximate emissions. 1985 data; fully optimized model. Two letter state abbreviations indicate the location of each monitor. Companion plot to Fig. 5.42.

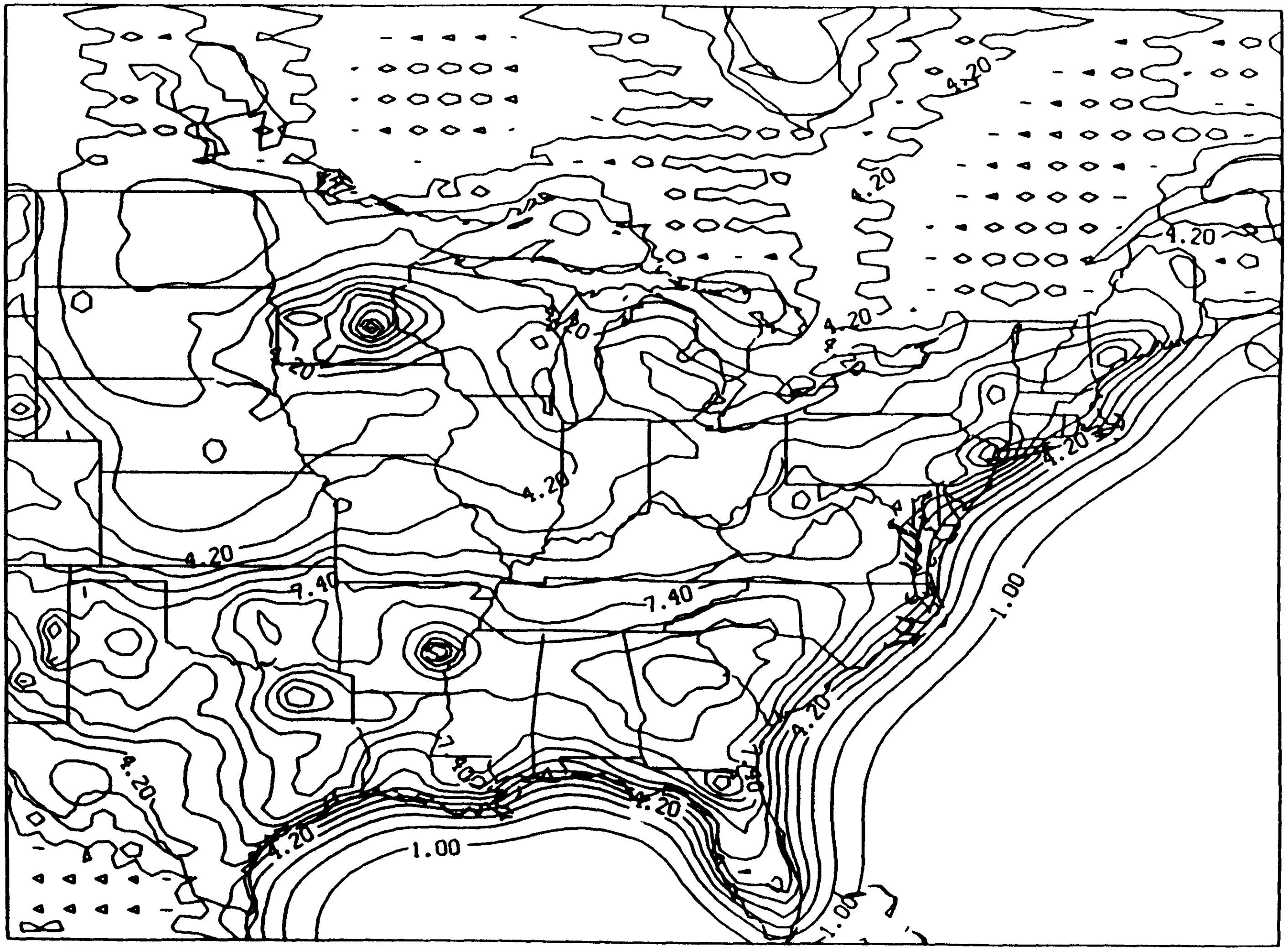

Fig. 5.44 Total modeled VOCs concentrations (μg m^{-3}) assuming a 50% reduction in manmade emissions. Seasonal levels are a superposition of biogenic VOCs (Fig. 4.31) and 30% of anthropogenic VOCs (Fig. 4.29). Inner solution contours from 1.0 to 13.8 μg m^{-3} by 0.8 μg m^{-3}.

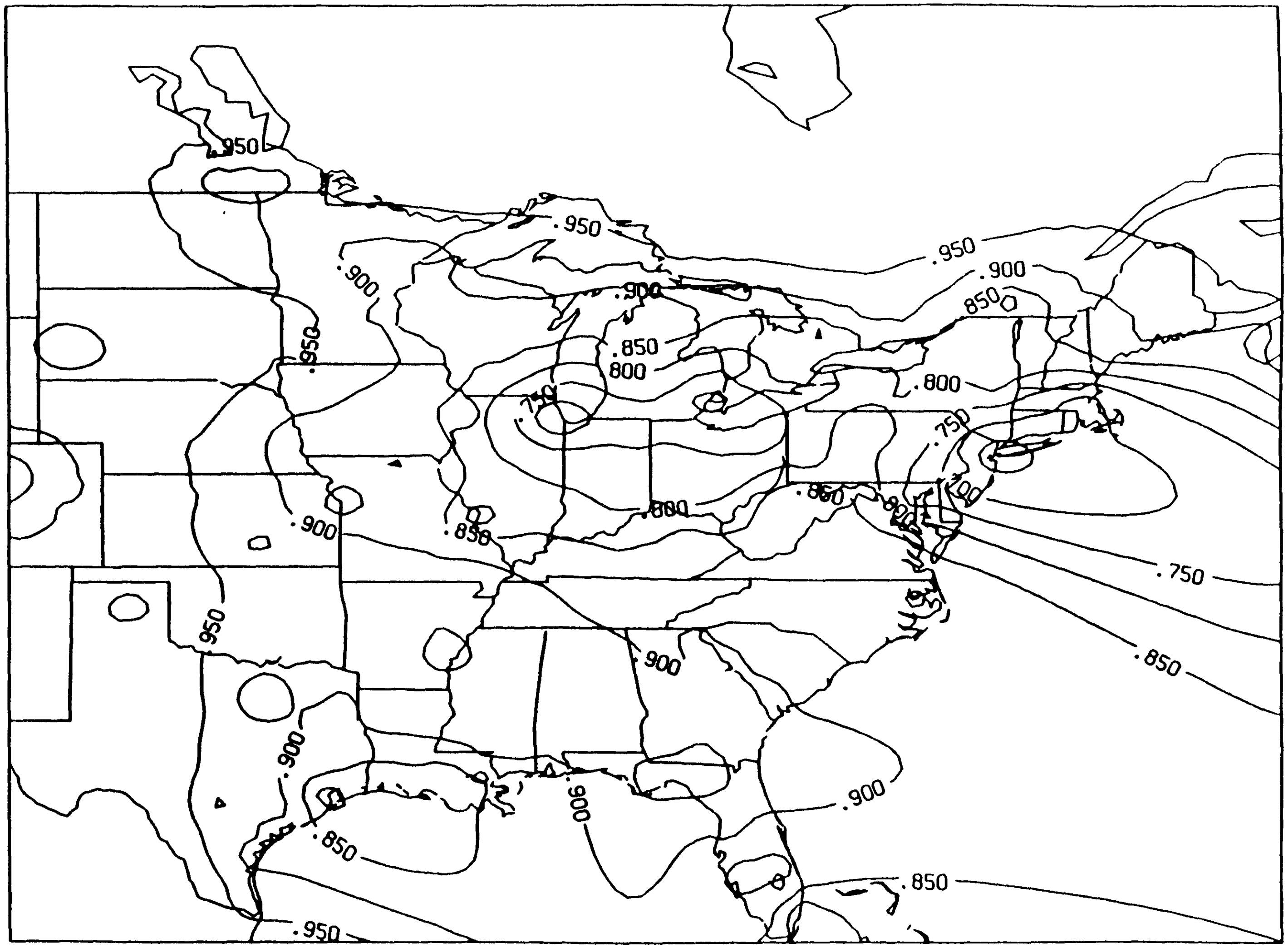

Fig. 5.45 The ratio of total VOCs embodying a 50% reduction in manmade emissions to total VOCs with no reduction. Ratios are constructed by dividing the results in Fig. 5.44 by the total average seasonal VOCs solution in Fig. 4.32. Contours range from 0.65 to 0.95 by 0.05.

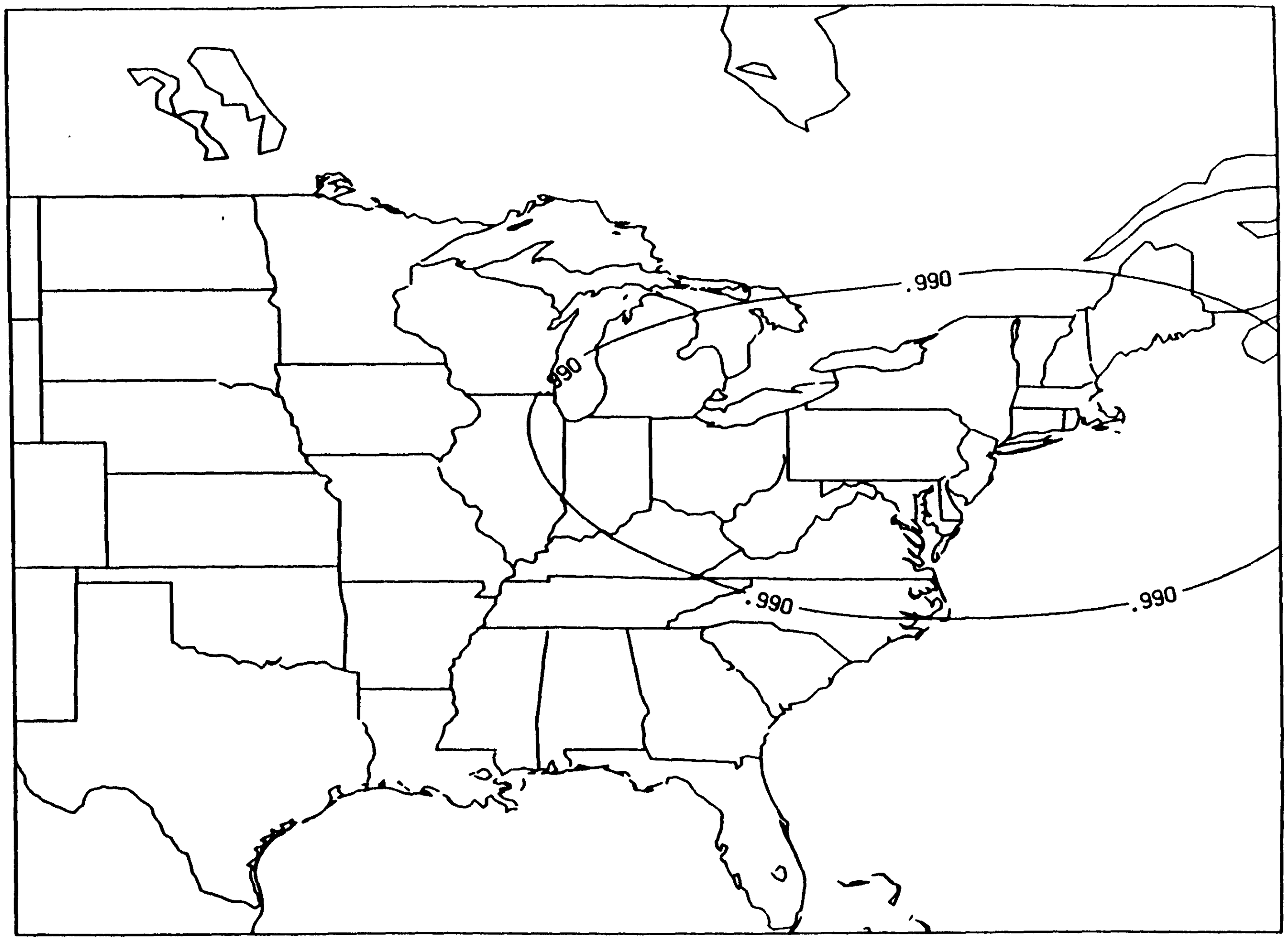

Fig. 5.46 The ratio of reduced seasonal average ozone to base case ozone concentrations using the fully optimized model and assuming a 50% manmade VOCs reduction. Ozone concentrations are normalized by the seasonal average solution shown in Fig. 5.28. Single contour is 0.99.

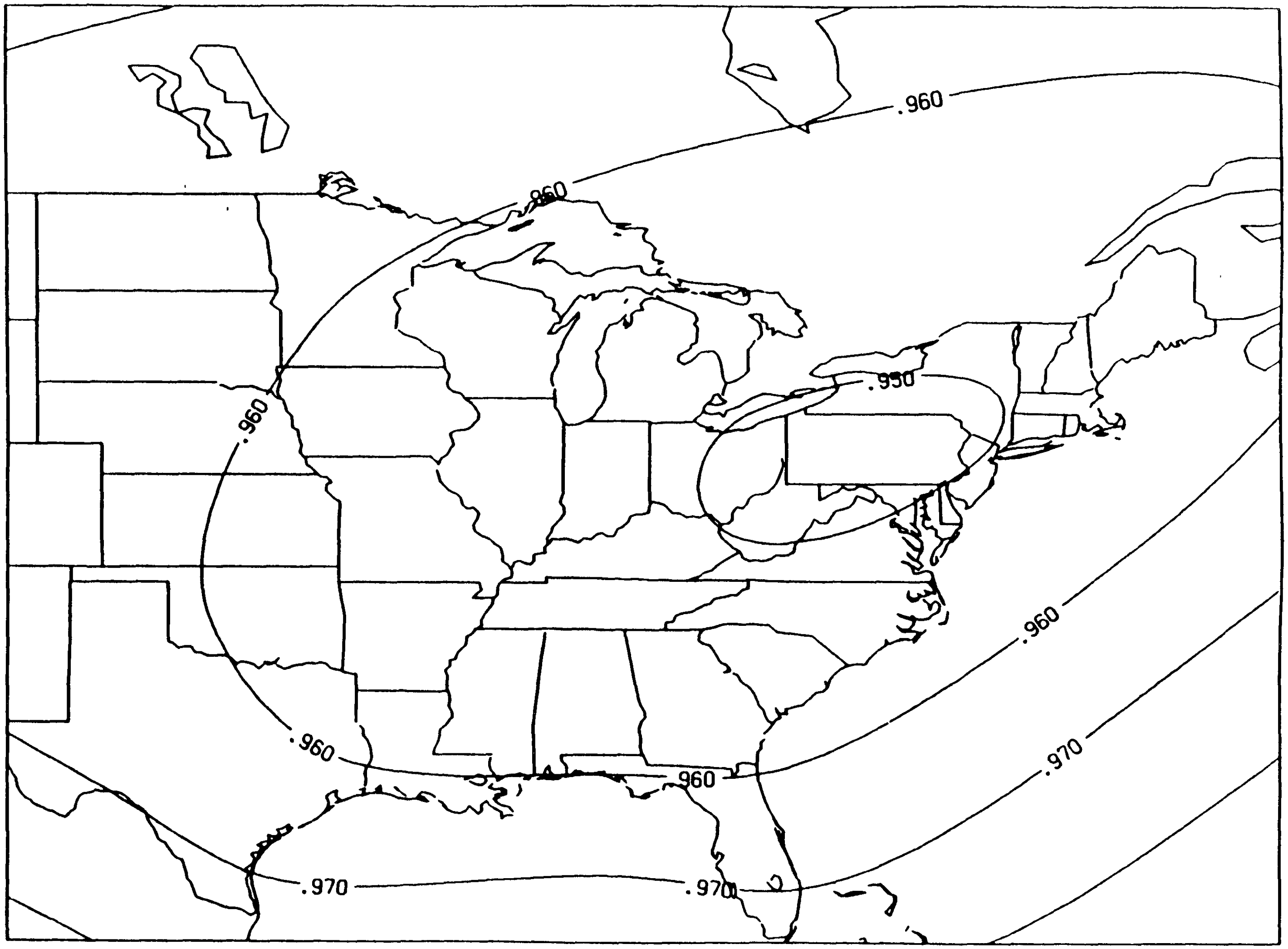

Fig. 5.47 The ratio of reduced seasonal average ozone to base case ozone concentrations using the fully optimized model and assuming a 50% manmade NO_x reduction. Ozone concentrations are normalized by the seasonal average solution shown in Fig. 5.28. Contours range from 0.95 to 0.98 by 0.01.

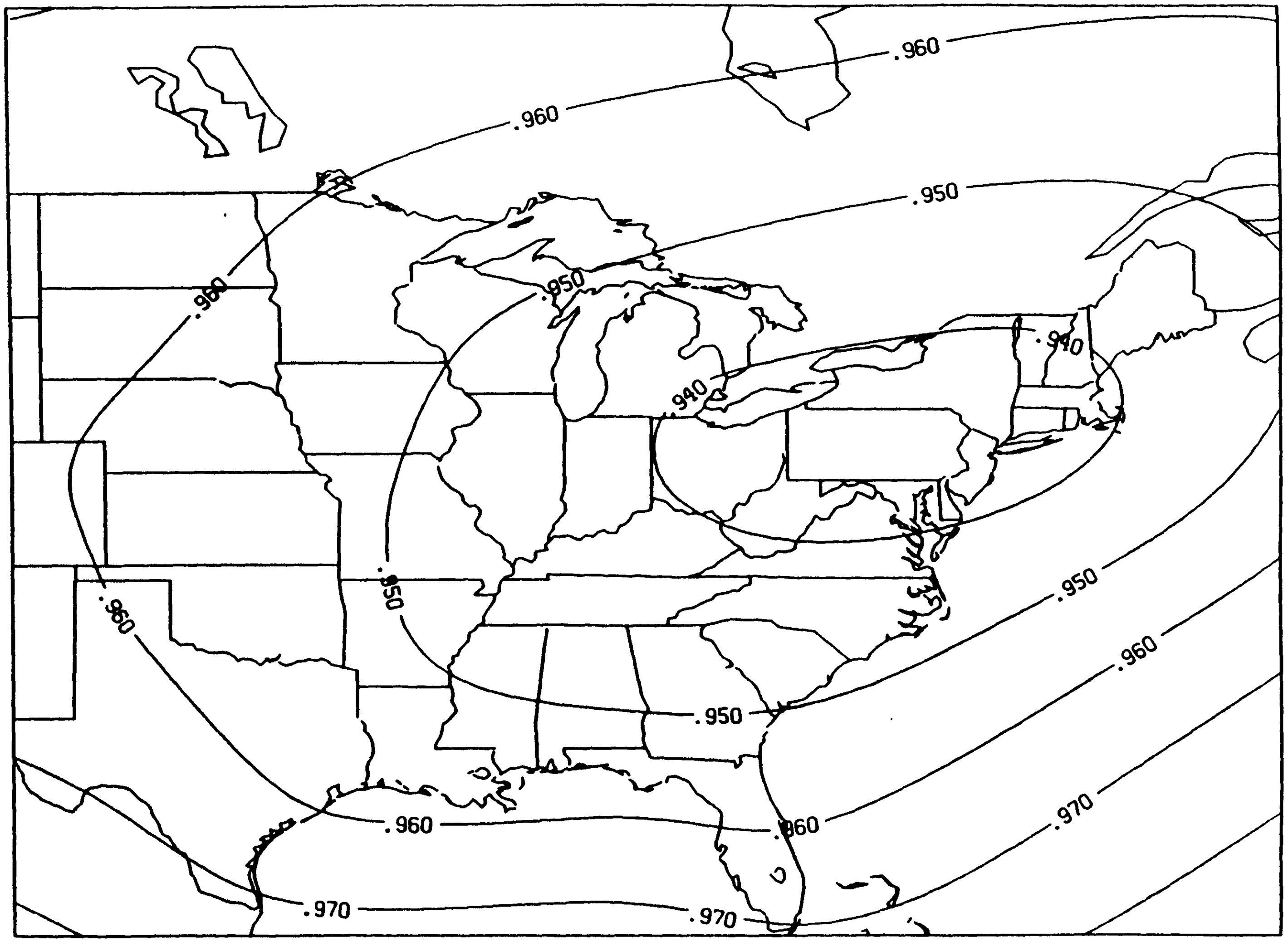

Fig. 5.48 The ratio of reduced seasonal average ozone to base case ozone using the fully optimized model and assuming 50% reductions in both manmade VOCs and NO_x emissions. Ozone concentrations are normalized by the seasonal average solution shown in Fig. 5.28. Contours range from 0.94 to 0.98 by 0.01.

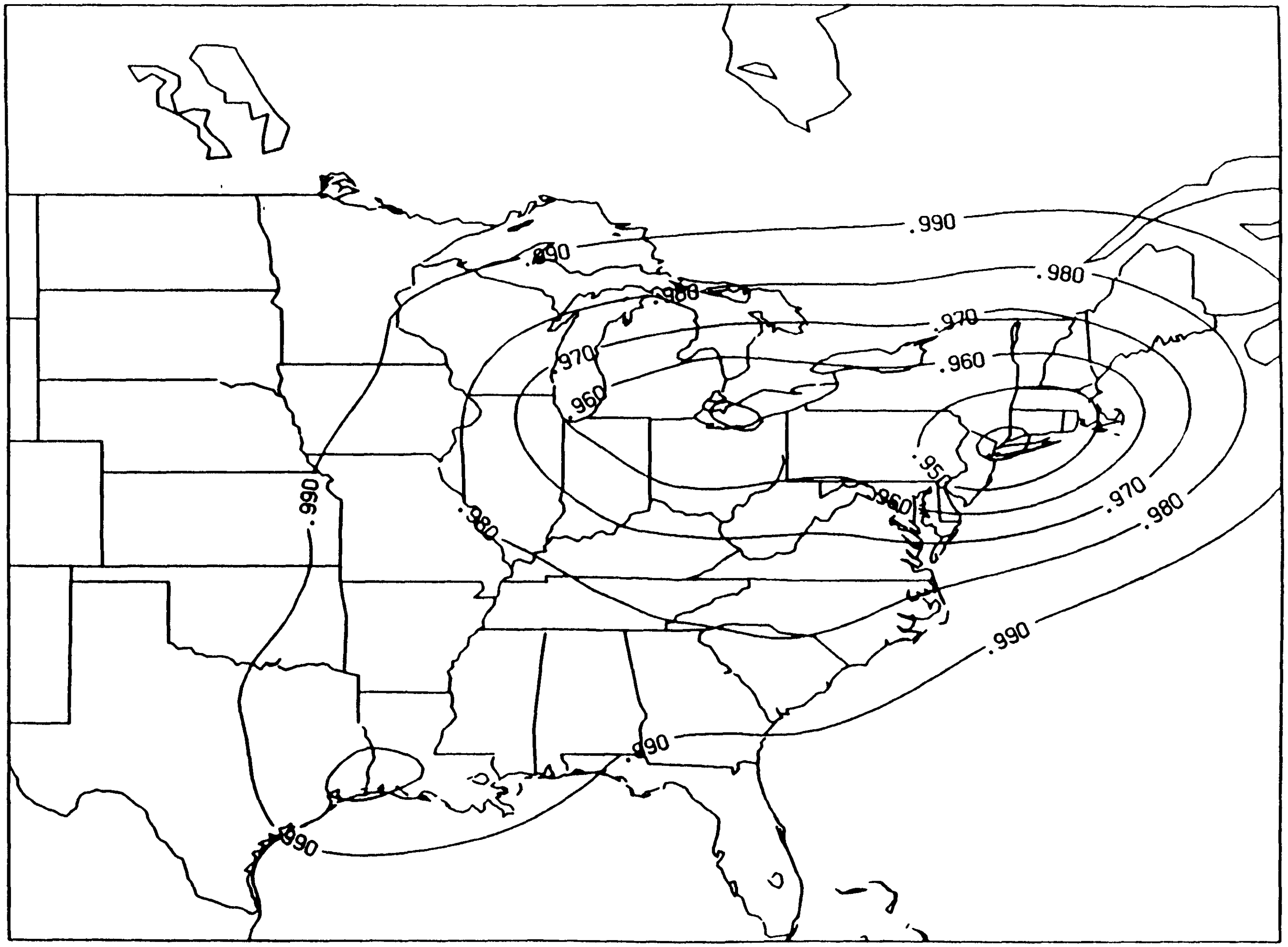

Fig. 5.49 The ratio of reduced seasonal average ozone to base case ozone concentrations using the physical model and assuming a 50% manmade VOCs reduction. Ozone concentrations are normalized by the seasonal average solution shown in Fig. 5.14. Contours range from 0.94 to 0.99 by 0.01.

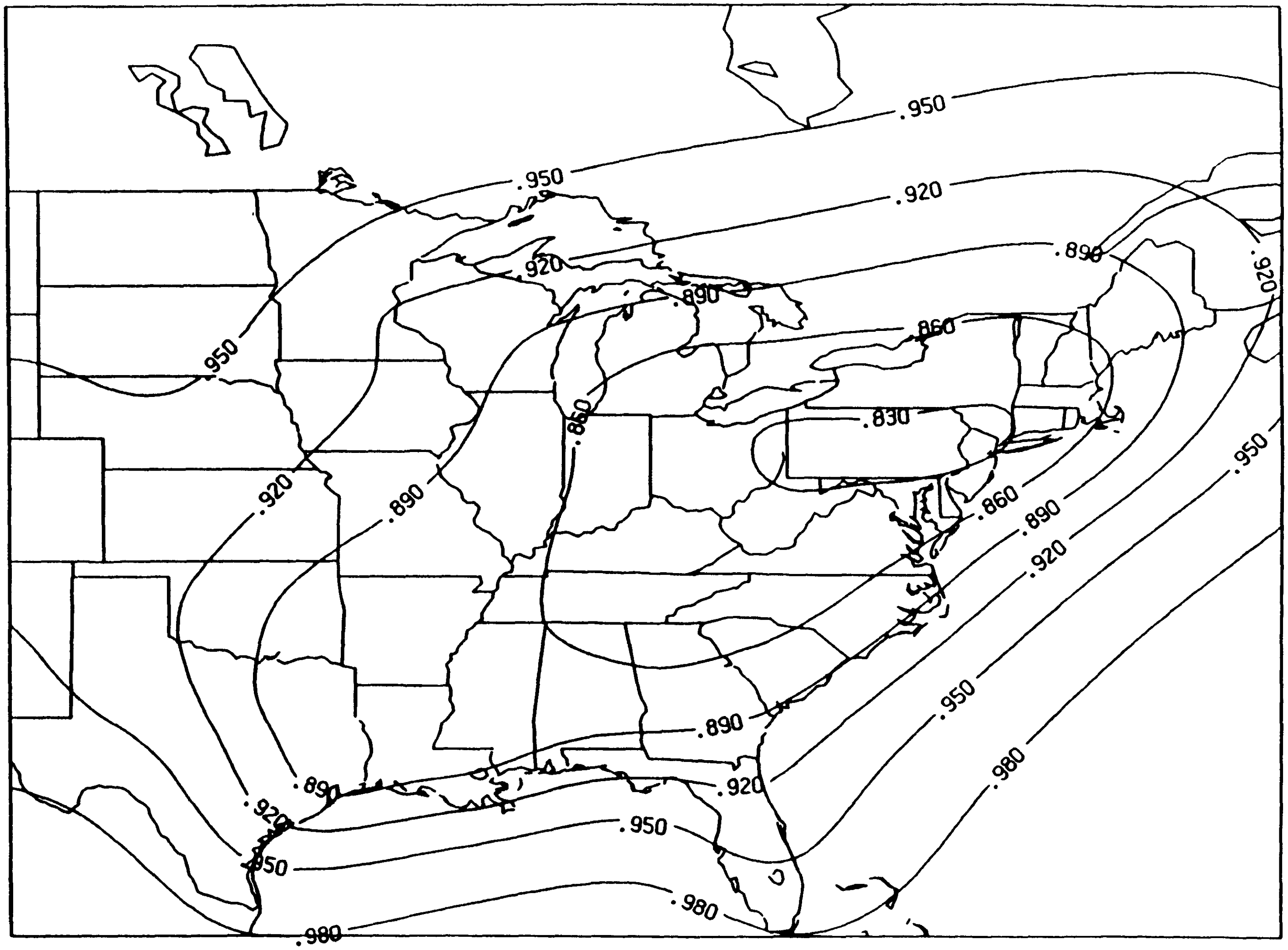

Fig. 5.50 The ratio of reduced seasonal average ozone to base case ozone concentrations using the physical model and assuming a 50% manmade NO_x reduction. Ozone concentrations are normalized by the seasonal average solution shown in Fig. 5.14. Contours range from 0.83 to 0.98 by 0.03.

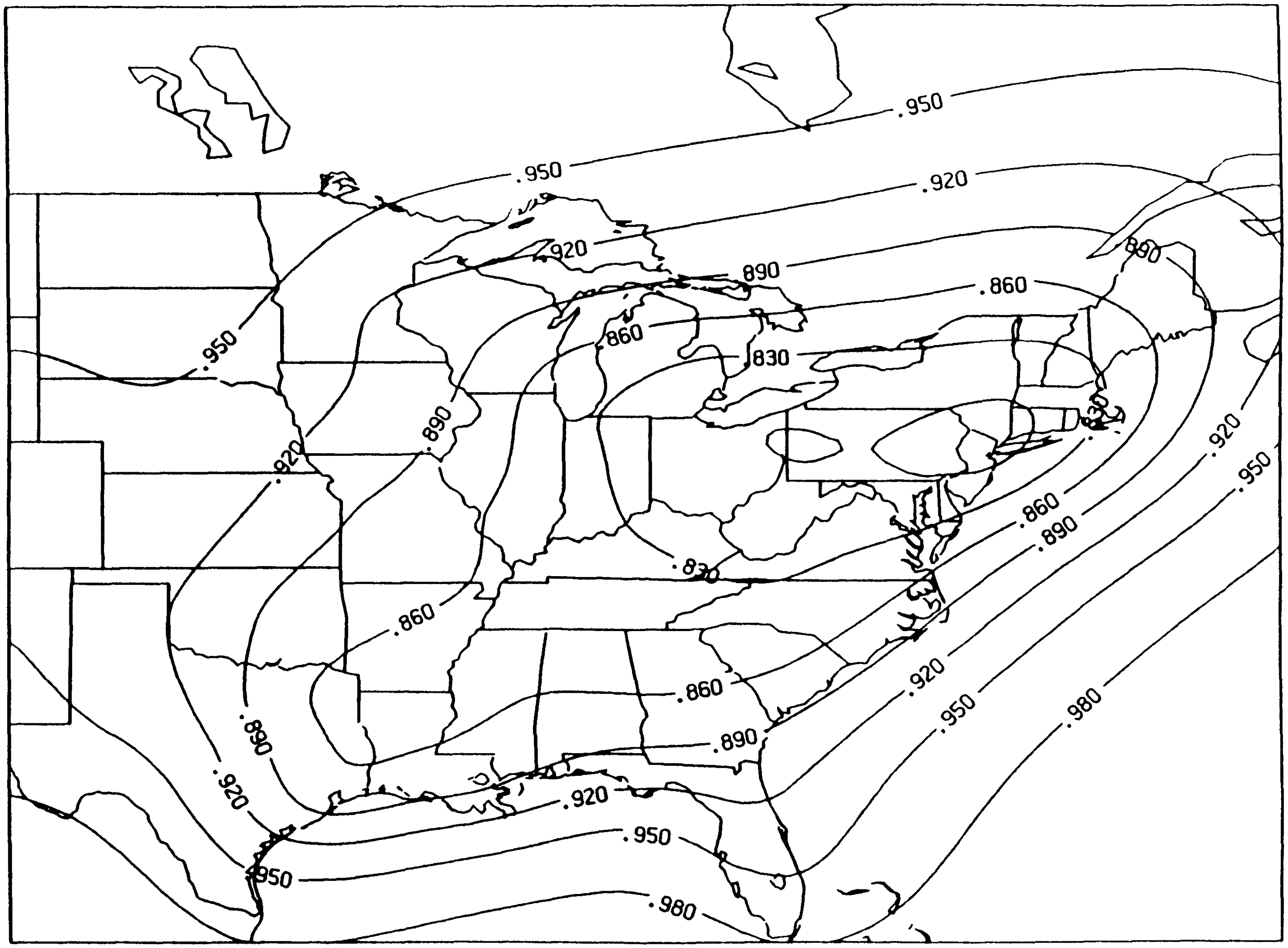

Fig. 5.51 The ratio of reduced seasonal average ozone to base case ozone concentrations using the physical model and assuming 50% reductions in both manmade VOCs and NO_x emissions. Ozone concentrations are normalized by the seasonal average solution shown in Fig. 5.14. Contours range from 0.80 to 0.98 by 0.03.

Chapter 6

Conclusions

The overall goal of developing a regional model of seasonally averaged ozone is accomplished through the sequence of research detailed in the previous five chapters. The numerous findings that evolved through the course of this analysis are summarized in this chapter. The comments are partitioned as a convenience, but the interdependent nature of this study requires consideration of all sections to properly assess the ozone model.

6.1 Measurements

Ground level observations of NO_2 and ozone are essential to this study as they are used to estimate key model parameters. Data is collected at irregularly spaced monitors through eastern North America (ENA). Concentrations differ significantly between site locations. Variations are present on urban scale lengths of 20 km or less (see Appendix VIII). Similar differences occur between measurements in neighboring grid cells. The long range transport approach estimates concentrations on a grid cell dimension of 40 km and thus cannot resolve the fine scale features of the data. Instead, the long range model is designed to predict variations over a scale length of the order of 100 km.

Box averaging of proximate measurements is an appropriate method to identify larger scale trends in the data which are more suitable for model comparison. The averaged spatial pattern of seasonal NO_x concentrations exhibits significant regional variation. Generally, the highest observed NO_x concentrations are located near dense emission regions. Similar comments do not apply to spatial patterns of seasonal ozone concentrations. Consistent regional gradients are not apparent in observed ozone levels except for a N-S decrease in Florida. Elsewhere, ozone concentrations vary locally but suggest no overall pattern.

Although this study is primarily concerned with seasonal averages, NO_2 and ozone concentrations are measured on an hourly basis. The photolytic cycle produces diurnal variation in each species. Additionally, meteorological cycles introduce variation in average daily levels. Seasonal averages are generally constructed over a wide range of unevenly distributed values. Standard deviations are a significant fraction of the mean concentration; in a few unusual cases the standard deviation actually exceeds the seasonal average. Many factors influence ozone production on a local basis; perhaps some of them (e.g., insolation, storm tracks, etc.) vary in a systematic regional fashion. It is conceivable that variables not considered in this thesis may provide information about regional ozone levels.

Monitors are classified by a land use criterion into urban, suburban, and rural subgroups. Sites are not uniformly distributed throughout the region. Careful examination of their locations shows that most are either in or near metropolitan areas. The distinction between categories is not absolute and the presence of proximate sources is not considered as a differentiating criterion. The NO_x and ozone models suggest that there are categorical differences on average, but that the individual nature of each site is important.

6.2 Precursor Models

6.2.1 NO_x Modeling

A long range transport model is constructed which predicts NO_x concentrations in ENA. Model parameters are chosen such that predictions are consistent with rural measurements of both ambient airborne NO_2 concentrations and wet nitrate depositions. Comparisons with observations reveal a serious model deficiency; concentrations at many urban and suburban monitors are significantly underpredicted. An analysis of site locations with respect to NO_x emissions shows that on average urban and suburban monitors have greater proximate sources and as a whole are distinguished from the rural class.

The long range formulation improperly models the near-source region in which concentrations can be expected to decline inversely with distance away from a point source. Local models to properly handle nearby sources are developed. Measurements of all categories are successfully explained as the sum of a long range component from distant sources and a local contribution from proximate emissions. The correlation is not perfect, however, and the scatter emphasizes the uniqueness of individual monitors. The modeled long range component constitutes more than 80% of total NO_x over a large portion of ENA. However, the opposite is true in densely emitting urban areas where the local contribution can reach 80% of the total.

6.2.2 VOCs Modeling

The atmospheric chemistry of VOCs oxidation is not completely understood and seasonally averaged measurements of VOCs species do not exist. The VOCs model represents an initial attempt to estimate regional concentrations of the species involved in ozone production. Although the results cannot be verified without proper measurements, the model is conservatively constructed to be physically realistic. The meteorological parameters are selected to be consistent with the NO_x model. The species dependent parameters are chosen to be consistent with values in the literature.

Ambient VOCs originate from both anthropogenic and biogenic emissions. The latter source is estimated to contribute about 70% of the mass of species most important to ozone production. The anthropogenic component of modeled VOCs concentrations is typically only 20% of the total over much of ENA. Contributions are higher in urban areas where the model attributes half of ambient VOCs levels to manmade emissions.

6.3 Ozone Modeling

The ozone model is designed to predict average seasonal concentrations. Regulatory efforts presently focus on peak hourly ozone levels. The EPA compiles ozone statistics using only the single hourly maximum concentration from each day. A rough but correlative relationship exists between the overall mean and the average of the daily maxima. Therefore, the results of the ozone model can generally be extrapolated to estimate average peak levels, though the relationship at any particular monitor may differ somewhat. An empirical correlation also suggests that seasonal averages may be used to predict growing season averages. However, seasonal averages do not correlate with the mean of the three highest seasonal values. This implies that extrapolating seasonal averages to predict exceedances is not likely to provide reliable estimates.

Measurements of seasonally averaged ozone do not seem to be related to local precursor levels. Plots comparing observed ozone with modeled NO_x and VOCs concentrations show no significant correlation. Additionally, a scatter plot of NO_x and ozone measured at the same monitors is uncorrelated.

The failure for ozone to correlate with precursor concentrations does not mean that ozone production is unrelated as well. The latter relationship is difficult to measure; integrations of simple chemical mechanism suggests a power law dependence of ozone production on NO_x and VOCs concentrations. Several combinations of parameters are explored to find the most satisfactory model of seasonal ozone. A "physical" model embodies meteorological parameters from the precursor models and source parameters suggested by the chemical mechanism integrations. An alternate "fully optimized" model allows measurements to determine the parameters such that residuals are minimzed. The two models differ principally in their sensitivity to precursor concentrations. The fully optimized level is only weakly dependent on NO_x and VOCs while the physical model is moderately dependent on each precursor.

Both models use measurement comparison to determine optimal values of the production coefficient and the background ozone level. The latter parameter is found to be 40 $\mu g\ m^{-3}$ by both models. The fully optimized model produces smaller average error with respect to observations but the improvement over the physical model is much smaller than the average residual. The physical model shows a larger continental gradient than does the fully optimized model, a consequence of its higher precursor dependence. Scatter plots show a larger range of measured concentrations than either model predicts.

The flat contour pattern of spatially averaged measurements is somewhat more consistent with the fully optimized model. Siting irregularity and emphasis on urban measurements cast doubt upon the regional representativeness of the monitoring network. The models tend to underpredict observations at rural sites and overpredict those at urban sites. The appropriateness of the network is not determinable; it depends on whether or not the mix and distribution of sites reflects the true regional ozone pattern.

The background level represents $\frac{2}{3}$ of the average seasonal ambient concentration. Control measures can only affect the photochemical increment above background, thus the model implies that the largest improvement possible is a 33% reduction in ambient levels of average seasonal ozone. The background is the most critical ozone model parameter. Its high value is consistent with published estimates [44] and it is an important component of the model.

Hypothetical control strategies in which anthropogenic VOCs and NO_x emissions are reduced by half demonstrates the difference between the two ozone models. Under this scenario, the fully optimized model predicts that the highest levels of seasonally averaged ozone would be reduced by about 3-6%; the physical model 2-18%. Decreases in VOCs emissions are less effective than NO_x in reducing ozone because of the fixed biogenic component which damps the relative changes in VOCs.

The large background component is a serious consideration for all modelers and policymakers. The fraction of seasonally averaged ozone that can be reduced with control programs is relatively small. Ozone is generated locally from precursors and is transported in the boundary layer. Model time constants for the physical and fully optimized models are 9 and 31 hours, respectively, permitting ozone to disperse downwind from its point of generation. Long range ozone transport is significant and should be included in regional models. The fully optimized ozone model estimates precursor ozone production to average 20 $\mu g\ m^{-3}$ of ozone per day. The physical model, possessing a higher rate of destruction, requires a 46 $\mu g\ m^{-3}$ daily ozone production to compare with measured ambient ozone levels. The level of tropospheric input into the boundary layer needed to maintain a constant ozone background of 40 $\mu g\ m^{-3}$ is 31 and 107 $\mu g\ m^{-3}$ per day, respectively, for the fully optimized and physical models. This corresponds to precursor production of only 39 and 30% of total ozone introduced to the boundary layer. Ozone generation is not limited to areas of precursor emission. Because ozone originates from transported NO_x and VOCs significant production occurs throughout the modeling region (even over water!).

6.4 Recommendations for Future Work

Exceedances of the federal ozone standard are likely to continue despite reductions in precursor emissions. The ineffectiveness of past control programs suggests that the current understanding of ozone is insufficient. Additional research is necessary to decipher the ozone puzzle. Although the seasonally averaged model is not the proper tool to address the problem of peak ozone episodes, it can be used to estimate average levels which may be of future importance in designing control strategies to reduce crop losses and forest damage.

Models of the type developed in this study are able to incorporate the essential physical processes in a simple and straightforward manner. They are cost effective and provide quick assessments which can suggest directions for more extensive research. Although it is able to predict a concentration pattern consistent with observed ozone in ENA, the ozone model in its present form contains too many uncertainties to be confidently used to predict future ozone scenarios. However, the simple methodology does identify two areas which need to be investigated more thoroughly and are of general interest to the ozone problem.

The state of the art understanding of ozone would be tremendously improved by the establishment of a network of monitors geared toward determining representative ozone levels. Researchers are attempting to characterize regional ozone levels with the present array of monitors [46] but the urban emphasis in monitor siting makes the usefulness of their efforts unclear. A representative network could confirm or refute the apparent lack of gradients in ozone levels across ENA. Such knowledge would permit a better evaluation of the background ozone level.

A second area which needs further exploration is VOCs. Relatively little is known about VOCs considering their role as an important ozone precursor. The complex atmospheric chemistry requires further definition. The recent identification of biogenic VOCs has added new complications. The role of both biogenic and anthropogenic emissions needs to be evaluated.

The background level and roles of the precursors are critical inputs to the seasonally averaged ozone model and are of a general and vital interest to all ozone modeling. Future research should provide better estimates of these basic factors. Additional model refinements such as spatially variant parameters may be useful in future efforts, but the high level of uncertainty in the current model limits their usefulness at this stage. The ozone model will be a useful starting point for evaluating regional ozone transport in the future.

References

(1) National Acid Precipitation Assessment Program (NAPAP). Interim Assessment: The Causes and Effects of Acidic Deposition, Vols. I-IV. (Washington, DC: GPO, 1987).

(2) Seinfeld, John. Atmospheric Chemistry and Physics of Air Pollution. (New York: John Wiley & Sons, 1986).

(3) Tilton, Beverley E. "Health effects of tropospheric ozone". Environmental Science and Technology, **23**, no. 3 (1989), pp. 257-263.

(4) Bedi, John F.; Horvath, Steven M.; and Dreschler-Parks, Deborah M. "Adaptation by Older Individuals Repeatedly Exposed to 0.45 Parts per Million Ozone for Two Hours". Journal of the Air & Waste Management Association, **39**, no. 2 (1989), pp. 194-199.

(5) Coffey, Deborah S.; Sprenger, Jeffrey C.; Tingey, David T.; Neely, Grady C.; and McCarty, James C. "National Crop Loss Assessment Program: Quality Assurance Program". Environmental Pollution, **53** (1988), pp. 89-98.

(6) Lee, E. Henry; Tingey, David T.; and Hogsett, William E. "Evaluation of Ozone Exposure Indices in Exposure-Response Modeling". Environmental Pollution, **53** (1988), pp 43-62.

(7) Musselman, Robert C.; McCool, Patrick M.; and Younglove, Theodore. "Selecting Ozone Exposure Statistics for Determining Crop Yield". Environmental Pollution, **53** (1988), pp. 63-78.

(8) Brewer, Patricia F.; Parkhurst, William J.; and Meeks, Timothy K. "Crop Loss Due to Ambient Ozone in the Tennessee Valley". Environmental Pollution, **53** (1988), pp. 273-284.

(9) Adams, R.M.; Hamilton, S.A.; and McCarl, B.A. "The Benefits of Pollution Control: The Case of Ozone and U.S. Agriculture". American Journal of Agricultural Economics, November, 1986, pp. 886-893.

(10) Peterson, David L.; Arbaugh, Michael J.; Wakefield, Victoria A.; and Miller, Paul R. "Evidence of Growth Reduction in Ozone-Injured Jeffrey Pine in Sequoia and Kings Canyon National Parks". Journal of Air Pollution Control and Hazardous Waste Management, **37**, no. 8 (1987), pp. 906-912.

(11) Chock, David P. and Heuss, Jon M. "Urban ozone and its precursors". Environmental Science and Technology, 21, no. 12 (1987), pp. 1146-1153.

(12) Lindsay, Ronald W.; Richardson, Jennifer L.; and Chameides, William L. "Ozone Trends in Atlanta, Georgia: Have Emission Controls Been Effective?". Journal of the Air & Waste Management Association, 39, no. 1 (1989), pp. 40-43.

(13) Liu, S.C.; Trainer, M.; Fehsenfeld, F.C.; Parrish, D.D.; Williams, E.J.; Fahey, D.W.; Hübler, G.; and Murphy, P.C. "Ozone Production in the Rural Troposphere and the Implications for Regional and Global Ozone Distributions". Journal of Geophysical Research, 92, no. D4 (1987), pp. 4191-4207.

(14) Heidorn, Keith C. and Yap, David. "A Synoptic Climatology for Surface Ozone Concentrations in Southern Ontario, 1976-1981". Atmospheric Environment, 20, no. 4 (1986), pp. 695-703.

(15) Jeffries, H.E. and Sexton, K.G. Technical Discussion Related to the Choice of Photolytic Rates for Carbon Bond Mechanisms in OZIPM4/EKMA, EPA-450/4-87-003, February 1987.

(16) Liu, Mei-Kao; Morris, Ralph E.; and Killus, James P. "Development of a Regional Oxidant Model and Application to the Northeastern United States". Atmospheric Environment, 18, no. 6 (1984), pp. 1145-1161.

(17) Schere, Kenneth L. and Fabrick, Allan J. EPA Regional Oxidant Model: Description and Evaluation Plan. Research Triangle Park, NC: U.S. Environmental Protection Agency, August, 1985.

(18) Fay, James A.; Golomb, Dan; and Kumar, Subramanyan. "Source Apportionment of Wet Sulfate Deposition in Eastern North America". Atmospheric Environment, 19, no. 11 (1985), pp 1773-1782.

(19) Fay, James A.; Golomb, Dan; and Kumar, Subramanyan. "Anthropogenic Nitrogen Oxide Transport and Deposition in Eastern North America". Atmospheric Environment, 21, no. 1 (1987), pp 61-68.

(20) Pilotte, James. Private communication. Magnetic tape and Acid Rain Data Base documentation. General Sciences Corporation, Laurel, MD, 1987.

(21) Wagner, Janice K.; Walters, Robert A.; Maiocco, Leslie J.; and Neal, Donald R. Development of the 1980 NAPAP Emissions Inventory. Research Triangle Park, NC: U.S. Environmental Protection Agency, EPA/600/7-86/057a, December 1986.

(22) Heisler, S.L. Interim Emissions Inventory for Regional Air Quality Studies. Palo Alto, CA: Electric Power Research Institute, EPRI EA-6070, November 1988.

(23) Kosteltz, A. Private communication. Computer printout of Canadian SO_x, NO_x and VOCs emissions. Inventory Management Division, Environment Canada, Ottawa, 1987.

(24) Lamb, Brian; Guenther, Alex; Gay, David; and Westberg, Hal. "A National Inventory of Biogenic Hydrocarbon Emissions". Atmospheric Environment, **21**, no. 8 (1987), pp. 1695-1705.

(25) National Air Data Branch, U.S. Environmental Protection Agency, Research Triangle Park, NC.

(26) Hustvedt, Cheryl. Private communication. Magnetic tape containing 1980 quarterly frequency distribution for ozone and NO_2. National Air Data Branch, U.S. Environmental Protection Agency, Research Triangle Park, NC, 1987.

(27) Hustvedt, Cheryl. Private communication. Magnetic tape containing 1985 hourly concentrations of ozone and NO_2. National Air Data Branch, U.S. Environmental Protection Agency, Research Triangle Park, NC, 1988.

(28) Meyer, Edwin L., Jr. Review of Control Strategies for Ozone and their Effects on Other Environmental Issues. Air Management Technology Branch, U.S. Environmental Protection Agency, EPA-450/4-85-011, November, 1986.

(29) Vukovich, Fred M. and Fishman, Jack. "The Climatology of Summertime O_3 and SO_2 (1977-1981)". Atmospheric Environment, **20**, no. 12 (1986), pp. 2423-2433.

(30) Evans, Gary; Finkelstein, Peter; Martin, Barry; Possiel, Norman; and Graves, Maurice. "Ozone Measurements from a Network of Remote Sites". Journal of the Air Pollution Control Association, **33**, no. 4 (1983), pp. 291-296.

(31) Buhr, M.P.; Parrish, D.D.; Williams, E.J.; Fehsenfeld, F.C.; Westberg, H.H.; and Allwine, E.J. "Correlation of ambient levels of O_3, NO_x, and hydrocarbons at a rural eastern U.S. site". EOS, **87** (1986), p. 891.

(32) Patera, A.T. Class notes for M.I.T. course 2.274, Computational Fluid Dynamics, Massachusetts Institute of Technology, Cambridge, MA, 1984.

(33) Kumar, Subramanyam. Modeling of Acid Deposition in Eastern North America. Ph.D. thesis, Massachusetts Institute of Technology, Cambridge, MA, December 1985.

(34) Altshuller, A.P. "The Role of Nitrogen Oxides in Nonurban Ozone Formation in the Planetary Boundary Layer Over N America, W Europe and Adjacent Areas of Ocean". Atmospheric Environment, **20**, no. 2 (1986), pp. 245-268.

(35) Watson, C.R. and Olsen, A.R. Acid Deposition System (ADS) for Statistical Reporting: System Design and User's Code Manual. Research Triangle Park, NC: U.S. Environmental Protection Agency, EPA-600-8-84-023, 1984.

(36) Fay, James A.; Golomb, Dan; and Zemba, Stephen G. "A Regional Model of Average Annual Airborne NOx". Proceedings of The Scientific and Technical Issues Facing Post-1987 Ozone Control Strategies (Hartford, CT, November 1987), pp. 320-330.

(37) Chameides, W.L.; Lindsay, R.W.; Richardson, J.; and Kiang, C.S. "The Role of Biogenic Hydrocarbons in Urban Photochemical Smog: Atlanta as a Case Study". Science, **241**, 16 September 1988, pp. 1473-1475.

(38) Bidleman, Terry F. "Atmospheric processes: Wet and dry deposition of organic compounds are controlled by their vapor partitioning". Environmental Science and Technology, **22**, no. 4 (1988), pp. 361-367.

(39) Hough, Adrian M. and Derwent, Richard G. "Computer Modelling Studies of the Distribution of Photochemical Ozone Production Between Different Hydrocarbons". Atmospheric Environment, **21**, no. 9 (1987), pp. 2015-2033.

(40) Stockwell, William R. "A Homgeneous Gas Phase Mechanism for Use in a Regional Acid Deposition Model", Atmospheric Environment, **20**, no. 8 (1986), pp. 1615-1632.

(41) Golomb, Dan. Personal Communication. Various notes and correspondence, 1988.

(42) Altshuller, A.P. "Estimation of the Natural Background of Ozone Present at Surface Locations". Journal of the Air Pollution Control Association, **37**, no. 12 (1987), pp. 1409-1417.

(43) Wolff, George T.; Lioy, Paul J.; Taylor, Richard S. "The Diurnal Variations of Ozone at Different Altitudes on a Rural Mountain in the Eastern United States". Journal of the Air Pollution Control Association, **37**, no. 1 (1987), pp. 45-48.

(44) Baldocchi, Dennis D.; Hicks, Bruce B.; and Camara, Pamela. "A Canopy Stomatal Resistance Model for Gaseous Deposition to Vegetated Surfaces". Atmospheric Environment, **21**, no. 1 (1987), pp. 91-101.

(45) Walcek, C.J. "A Theoretical Estimate of O_3 and H_2O_2 Dry Deposition Over the Northeast United States". Atmospheric Environment, **21**, no. 12 (1987), pp. 2649-2659.

(46) Lefohn, Allen S. and Pinkerton, John E. "High Resolution Characterization of Ozone Data for Sites Located in Forested Areas of the United States". Journal of Air Pollution Control and Waste Management, **38**, no. 12 (1988), pp. 1504-1511.

(47) *The Princess Bride*, 20th Century Fox Corporation, 1987.

Acknowledgements

The following Acknowledgements are reproduced from the dissertation by S.G. Zemba.

Vizzini, a character in *The Princess Bride* [47] who claimed to be the smartest man in the world, identified two rules to maintain one's well-being. The first is to avoid getting involved in a land war in Asia. The second is to never challenge a Sicilian when death is on the line. Although somewhat less serious in nature, I suggest the addition of a third criterion which warns of the difficulties and frustrations encountered when dealing with atmospheric measurements. (My assertion is based on many hours of experience). There is an important distinction, however. Arrogance and overconfidence cost Vizzini his life in a battle of wits despite his Sicilian heritage. I, however, have fared somewhat better, as attested by this lengthy document.

Many people contributed to my graduate research and I would like to specifically acknowledge a few of them. I am grateful to past and present members of the Fluid Mechanics Lab for both their camaradarie and their inspirational dedication to their work. Thanks also to numerous friends who have helped me to maintain some semblance of sanity. In particular, I thank Virginia Brambilla for the countless "little things" she has helped with over the years. And I thank the 24-Hour Coffeehouse simply for being there.

I am grateful to the Electric Utilities Program of the M.I.T. Energy Laboratory for its financial support. I hope the members will continue to fund worthwhile studies and I urge them to pursue an active leadership role in addressing the critical environmental issues which impact society. I also thank Dr. Mike McCartney of the Woods Hole Oceanographic Institute who, in addition to providing the opportunity to travel to exotic, faraway lands, contributed temporary financial support and an isolated environment almost ideal for the initiation of thesis writing.

I am grateful for the suggestions provided by Profs. Kerry Emanuel and Tony Patera as members of my thesis committee. A special thanks to Dr. Dan Golomb for our many (and usually fruitful) interactions. His comments and propositions stimulated my thinking and also made me aware of several important considerations. And another special thankyou to Prof. James Fay, with whom I have had the pleasure of working of with for the past six years. His assistance and advice were essential to my research. Even more importantly, however, he introduced me to the field of atmospheric science. The opportunity to work in an area that directly benefits humankind is a privilege for which I am extremely grateful.

I have been blessed with opportunities throughout my life. I am fortunate to be part of a family which has encouraged academic efforts. I especially thank my parents, Stephen and Margaret Zemba, for their immeasurable support. Their love and inspiration are responsible for a large part of my success.

Finally, I would like to thank my wife and best friend, Jan Zemba, for her support and for sharing her life with me. I have grown a great deal in the short time I have known her, and I happily anticipate many more years of her companionship.

List of Appendices to Dissertation: